Technische Universität München
TUM School of Engineering and Design

Optimization and data acquisition framework for low-voltage distribution systems in transformation

Soner Candas

Vollständiger Abdruck der von der TUM School of Engineering and Design der Technischen Universität München zur Erlangung eines

Doktors der Ingenieurwissenschaften (Dr. -Ing.)

genehmigten Dissertation.

Vorsitz:

Prof. Dr. Reinaldo Tonkoski Junior

Prüfende der Dissertation:

1. Prof. Dr. Thomas Hamacher
2. Prof. Dr. Tom Brown

Die Dissertation wurde am 07.12.2023 bei der Technischen Universität München eingereicht und durch die TUM School of Engineering and Design am 28.06.2024 angenommen.

Abstract

Decarbonization efforts worldwide will likely involve significant levels of electrification of the heating and mobility demands via the use of heat pumps and battery electric vehicles. Energy affordability and security concerns motivate consumers to adopt solar photovoltaic (PV) systems at a rapid rate, assuming the prosumer role. On the one hand, additional electrical flows caused by these components (so-called DERs) at the distribution grid level push the existing grid assets to unprecedented levels. Grid reinforcement measures may be necessary to accommodate these new loads to the system without endangering the secure grid operation. On the other hand, the flexibilities accompanying these components, e.g., via thermal inertia, storage operation, and intelligent charging, reveal mitigation potentials on the reinforcement requirements. In practice, incentives for flexibility have to be created through effective techno-economic grid relief measures. Wherever grid reinforcement might not be a practical option due to cost volatility and long lead times, the question stands for distribution system operators (DSOs) as to the extent of the flexibilities in their ability to postpone or even prevent the need for reinforcements in a given distribution grid.

This thesis presents a systematic approach to assess the grid reinforcement requirements in low-voltage distribution grids under varying DER penetration levels and the application of various techno-economic relief measures. The scales of DER penetration considered span the expected course of electrification from today until beyond 2050. The relief measures include capacity (peak) pricing, time-variable network tariffs, and DSO-side downregulation of consumption devices (*EnWG § 14a regulation*). Employing a mixed-integer linear programming methodology consisting of multiple steps, the sequential game between the prosumers and the DSO can be represented in the analysis. In order to maintain the traceability of the developed optimization framework for low-voltage grids with realistic sizes, a time series aggregation method is utilized. In order to quantify the grid operation accurately, a post-optimization non-convex power flow step is incorporated into the framework. Each low-voltage distribution system is individual; the grid topologies and demand structures vary significantly. Therefore, a data acquisition suite based largely on open data is developed, allowing the generation of scenarios for a wide selection of regions.

The thesis includes a case study applied to a town in Southern Germany based on real grid data, shedding light on the current state of low-voltage distribution systems and the outlook of their transformation. The main findings from the case study are the following: From cases of medium electrification, i.e., 50% of the buildings adopting DERs, a certain extent of reinforcement becomes necessary throughout all grids investigated. The system peaks that necessitate these reinforcements typically align with the times when heat pumps operate simultaneously during extreme winter periods. As heat pumps operate at almost full load during these periods, room for the flexibility provided by them is small, rendering the grid-relieving potential of economic measures such as capacity or time-variable tariffs low. Nevertheless, the grid reinforcement costs always amounted to less than 3% of the total system costs, deeming them economically acceptable over the long term. If grid reinforcement is infeasible in the short term due to supply shortages and cost volatility, DSO-side downregulation can help keep the peaks in the system under control. However, to ensure social acceptance, this regulation will have to maintain thermal comfort in buildings without discrimination.

The analysis framework presented in this thesis can enhance DSO decision-making, allowing them to estimate the urgency of reinforcing their grids in the course of increased electrification. In avenues where reliable data is lacking, the developed data suite can serve as a foundation for obtaining estimates on the parametrization of the distribution system.

Zusammenfassung

Weltweite Anstregungen zur Dekarbonisierung werden voraussichtlich eine erhebliche Elektrifizierung der Gebäudeheizung und Mobilität durch den Einsatz von Wärmepumpen und batterieelektrischen Fahrzeugen mit sich bringen. Energiekrisen und -sicherheitsbelangen motivieren Verbraucher, die Rolle des Prosumers anzunehmen, indem sie PV-Systeme in einem raschen Tempo zu adoptieren. Einerseits treiben die zusätzlichen elektrischen Lasten, die durch diese Komponenten (sogenannte "DERs" - Distributed Energy Resources) auf der Verteilnetzebene verursacht werden, die Kapazitäten der bestehenden Netzkomponenten auf ein noch nie dagewesenes Niveau. Verstärkungs- und Ausbaumaßnahmen der Verteilnetze könnten notwendig sein, um diese neuen Lasten ins System integrieren zu können, ohne den sicheren Netzbetrieb zu gefährden. Andererseits offenbaren die Flexibilitäten, die mit den DERs einhergehen, z.B. durch thermische Trägheit, Speicherbetrieb und intelligentes Laden, Minderungspotenziale für den Netzausbaubedarf. In der Praxis müssen Flexibilitätsanreize durch effektive technisch-ökonomische Netzentlastungsmaßnahmen geschaffen werden. In Kontexten, in denen eine Netzverstärkung aufgrund von Kostenvolatilität und langen Vorlaufzeiten keine praktische Option sein könnte, steht für Verteilnetzbetreiber (DSOs) die Frage, inwieweit die Flexibilitäten in ihrer Fähigkeit, den Bedarf an Verstärkungen in einem gegebenen Verteilnetz zu verzögern oder sogar zu verhindern, bestehen.

Diese Arbeit stellt einen systematischen Ansatz zur Bewertung der Anforderungen an Netzverstärkungen in Niederspannungsverteilnetzen unter verschiedenen Durchdringungsniveaus von DERs und der Anwendung verschiedener technisch-ökonomischer Netzentlastungsmaßnahmen vor. Die betrachteten Skalen der DER-Durchdringung bilden den erwarteten Verlauf der Elektrifizierung von heute bis über das Jahr 2050 hinaus ab. Zu den Entlastungsmaßnahmen gehören Leistungspreise, zeitvariable Netzwerktarife und die DSO-seitige Abregelung von Verbrauchseinrichtungen (*EnWG § 14a-Regelung*). Unter Verwendung einer mehrstufigen gemischt-ganzzahligen linearen Programmierungsmethodik kann das sequenzielle Spiel zwischen den Prosumern und dem DSO in der Analyse dargestellt werden. Um die Lösbarkeit des entwickelten Optimierungsframeworks für Niederspannungsnetze realistischer Größe zu gewährleisten, wird eine Zeitreihenaggregationsmethode verwendet. Um den Netzbetrieb genau zu quantifizieren, wird ein Postoptimierungsschritt zum nicht-konvexen Lastfluss in das Framework integriert. Jedes Niederspannungsverteilsystem ist individuell; die Netztopologien und Nachfragestrukturen variieren erheblich. Daher wird eine Datenerfassungssuite, die größtenteils auf offenen Daten basiert, entwickelt, die es ermöglicht, Szenarien für eine breite Auswahl von Regionen zu generieren.

Die Arbeit umfasst eine Fallstudie, die auf eine Stadt in Süddeutschland angewendet wird, basierend auf realen Netzdaten, und beleuchtet den aktuellen Zustand der Niederspannungsverteilsysteme sowie gibt den Ausblick auf deren mögliche Transformationspfade. Die wichtigsten Erkenntnisse aus der Fallstudie sind folgende: Ab mittlerem Grad der Elektrifizierung, d.h. wenn 50% der Gebäude die DERs übernehmen, wird ein gewisses Maß an Verstärkung in allen untersuchten Netzen notwendig. Die Lastspitzen in den Systemen, die diese Verstärkungen notwendig machen, stimmen typischerweise mit den Zeiten überein, in denen Wärmepumpen gleichzeitig während extremer Winterperioden betrieben werden. Da Wärmepumpen in diesen Perioden fast voll ausgelastet sind, ist der Spielraum für die Flexibilität, die sie bieten, gering, was das netzentlastende Potenzial wirtschaftlicher Maßnahmen wie Kapazitäts- oder zeitvariabler Tarife gering macht. Dennoch betrugen die Kosten für die Netzverstärkung immer weniger als 3% der Gesamtsystemkosten, was sie langfristig als wirtschaftlich akzeptabel erscheinen lässt. Wenn eine Netzverstärkung kurzfristig aufgrund von Lieferengpässen und Kostenvolatilität nicht machbar ist, kann die DSO-seitige Abregelung helfen, die Spitzen im System in Grenzen zu halten. Um jedoch die soziale Akzeptanz zu gewährleisten, muss diese Regulierung den thermischen Komfort in Gebäuden ohne Diskriminierung aufrechterhalten.

Der in dieser Arbeit vorgestellte Analyserahmen kann die Entscheidungsfindung der DSOs verbessern und ihnen ermöglichen, die Dringlichkeit der Verstärkung ihrer Netze

im Zuge der zunehmenden Elektrifizierung abzuschätzen. In den Gebieten, für die zuverlässige Daten fehlen, kann die entwickelte Datensuite als Grundlage für die Gewinnung erster Schätzungen zur Parametrisierung des Verteilsystems dienen.

Acknowledgments

It has been almost six years since I started my doctoral journey, and now the time has finally come to thank everyone who helped me directly or indirectly in the process that led to the writing of this thesis.

First and foremost, I would like to thank Prof. Dr. Thomas Hamacher for giving me the opportunity to work at the Chair of Renewable and Sustainable Energy Systems (ENS) of the Technical University of Munich on a series of interesting research topics. I thank him for trusting my judgment since day one and letting me be involved in the most diverse set of projects, not to mention our few visits to Singapore. Thanks to his trust, I was able to improve on many aspects of myself. Also, his high interest in my doctoral topic and guidance has been inspiring. I also thank Prof. Dr. Tom Brown for instilling in me the open-source spirit early in my doctoral phase and kindly accepting my wish for him to become an examiner of this thesis.

Next, I would like to thank my mentor Dr. Philipp Kuhn. I could always rely on his very valuable overview of projects and organizational finesse, especially at times when time management gets a bit out of control.

A bunch of thanks goes to my lovely colleagues with whom I had the great pleasure of working in ENS together. With them, work rarely felt like work. I do not even have to mention Anurag Mohapatra and Leonhard Odersky. Your company since the first day and at every phase of this journey made ENS a second home. Thanks to Cristina de la Rúa for simply being one of the best human beings I have ever met. Thanks to Julia Gawlick for her kind soul and for always keeping up the family spirit in ENS. Thanks to Johannes Winklmaier for our enduring friendship and horizon-expanding discussions on the function of science. Thanks to Kay Bareiß for letting me partake in his unique humor. Thanks to Beneharo Reveron Baecker for being not only a great friend but also a sparring partner in research; his critical thinking always pushed the envelope. Thanks to Prashant Pant and Smajil Halilovic for the regular fuel of discipline.

I would like to express my appreciation to my former colleagues in TUM.CREATE in Singapore, which I had the opportunity to visit twice. Thanks to Sebastian Troitzsch, Kai Zhang, and Andrej Trpovski, not only for the scientific exchange but also for their hospitality. It always made me feel at home despite being half a world away.

Special thanks go to all the students I had the honor to supervise and the opportunity to learn from a lot, too: especially Martin Cornejo, Deniz Tepe, and Aparna Justin. Their contributions have been invaluable in developing this body of work.

I would also like to thank all my partners from the eXtremOS, open_MODEX, and STROM projects for their pleasant and productive cooperation. You showed me that success lies in getting out of our offices and working together!

Last but definitely not least, my deepest gratitude goes to my friends and family, to whom I dedicate this work. To all my friends: thanks for your support, especially when times got rough; our friendships are for a lifetime. Thank you, Pavlina, for your endless support and patience in the last two years. Finally, I thank my brother Caner and my parents Figen and Savaş, who trusted me with every decision regardless of the extent, never held back their support, and made it all happen; not only literally but also figuratively.

The journey continues.

Contents

List of Figures

List of Tables

List of Acronyms

1R1C	one resistance and one capacitance
AB	apartment block
AC	alternating current
BDEW	German Federal Association of Energy and Water Industries
BEV	battery electric vehicle
COP	coefficient of performance
DC	direct current
DER	distributed energy resource
DS	distribution system
DSM	demand side management
DSO	distribution system operator
DWD	German Meteorological Service
DHW	domestic hot water
FRT	fixed ratio transformer
gsee	Global Solar Energy Estimator
HEMS	home energy management system
HOODS	holistic optimization of distribution systems
HP	heat pump
HT	high tariff
HV	high voltage
LinDistFlow	linearized distribution flow
LOD	Level of Detail
LT	low tariff
LV	low voltage
LVDS	low voltage distribution system

MBB main busbar

MFH multi-family home

MILP mixed-integer linear programming

MV medium voltage

openmod Open Energy Modelling Initiative

OSM OpenStreetMap

p.u. per unit

P2P peer-to-peer

PF power factor

PV photovoltaics

R Pearson correlation coefficient

SDP semi-definite programming

SFH single-family home

SIA Swiss Society of Engineers and Architects

SLP standard load profile

SOCP second order cone programming

ST standard tariff

TH terrace house

TRY Test Reference Year

tsam Time Series Aggregation Module

VDEW German Association of Electricity Industry

VRDT voltage regulating distribution transformer

WACC weighted average cost of capital

WB wall box

WZ industry branch

Chapter 1

Introduction

1.1 Background and context

Mitigating climate change and handling the highly volatile energy prices influenced by geopolitical factors are two major challenges facing global society. Shifting away from fossil fuels toward renewable resources such as PV and wind energy is vital for reducing emissions in accordance with climate change policy objectives and achieving more stable energy prices. The increasing cost-competitiveness of these technologies further motivates the case for this transition [1]. The transition to renewable energy is well underway at a global scale.

In Germany, various transformation pathways regarding incorporating renewable resources into the national energy system are studied. A comparison study conducted by the German Foundation of Climate Neutrality gives an overview of the possible transformation scenarios. While the actual amounts vary between the studies, commonalities are clear: a significant increase in the electricity supply between 2023 and 2045 (or 2050, for the BMWK scenario) of between 35% and 158% is envisioned, while PV and wind make up a dominating portion of the electricity generation, ranging between 21-39% and 46-64% of the total supply, respectively.

Table 1.1: Long-term electricity supply scenarios for Germany along with the volatile renewable shares, comparison of the "Big Five" studies conducted by the German Foundation of Climate Neutrality [2].

Study	Scenario	Year	Supply in TWh	%PV	%Wind	Source
Present		2023	577	11%	22%	[3]
Agora E.W. (2020)	KNDE2045	2045	1,014	35%	55%	[4]
BDI (2021)	Zielpfad	2045	1,136	21%	64%	[5]
dena (2021)	KN100	2045	899	26%	56%	[6]
BMWK (2022)	TN-Strom	2050	1,207	22%	51%	[7]
	REMIND-Mix	2045	1,154	29%	60%	
Ariadne (2021)	REMod-Mix	2045	1,494	32%	60%	[8]
	TIMES PanEU-Mix	2045	784	39%	46%	

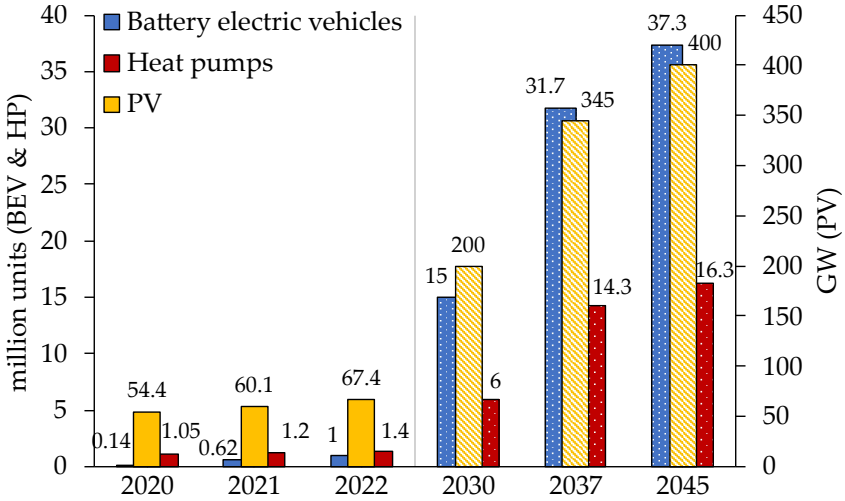

Figure 1.1: Heat pump and battery electric vehicle targets in Germany. The values for 2030 correspond to the targets of the Coalition government, while the values for 2037 and 2045 correspond to the planning benchmark scenario B of the network development plan).

1.1.1 The rise of electrification of demands

The anticipation of this significant increase in electricity supply through scalable renewable technologies is rooted in the endeavor to involve the heating and mobility sectors in decarbonization efforts, possibly through electrification. Electrification has two advantages—first, it makes use of highly efficient technologies such as residential heat pumps (HPs) and BEVs. Second, it creates demand that can be covered by locally scalable renewable generation (such as PV) while reducing dependence on fossil resources. Consequently, these benefits led to many governments setting ambitious targets for adopting these technologies. In particular, as of the date of the writing of this thesis, the German coalition government aims at an increase of BEVs and HPs from respectively 1 and 1.4 million units each in 2022 to 15 [9] and 6 million [10] by 2030. Similarly, the German Network Development Plan (NDP) sets as a planning benchmark an increase of BEV and HPs to as many as 37.3 and 16.3 million units, correspondingly, until 2045 [11]. For PV, an increase from 67 GW in 2022 to 400 GW is expected by 2045 (see Figure 1.1).

To some extent, these adoption rates are driven by political regulation. For instance, the widely debated amendment of the German Building Energy Act (GEG) from April 2023 had established a mandate regarding building heating systems by 2024 [12]. Until its revision, this mandate had required that any retiring building heating system be replaced with cleaner alternatives that run with a minimum of 65% renewable energy–a criterion met by heat pumps. Similarly, as part of the Fit for 55 program, the EU's Environmental Council decided in April 2023 to allow new private vehicles with internal combustion engines only if they support carbon-free fuels by 2035 [13], paving the path for the adoption of more favorable BEVs. For PV, political incentives are currently not necessary. The rising electricity costs combined with the decreasing costs of PV systems (almost 90% decrease in module prices between years 2010 and 2020 [14]) make their installations more attractive than ever before. With an anticipated 9 GW of new installations in 2023, this expansion rate surpasses even those of 2010-2012 (the "peak EEG era"), a time when investments were primarily driven by extraordinarily high feed-in tariff remuneration.

On the other hand, rapid adoption of these technologies–from here on called distributed energy resources (DERs)–means unprecedented stress in the existing electrical system. The majority of this stress will occur at the medium- and low-voltage distribution grids. In Ger-

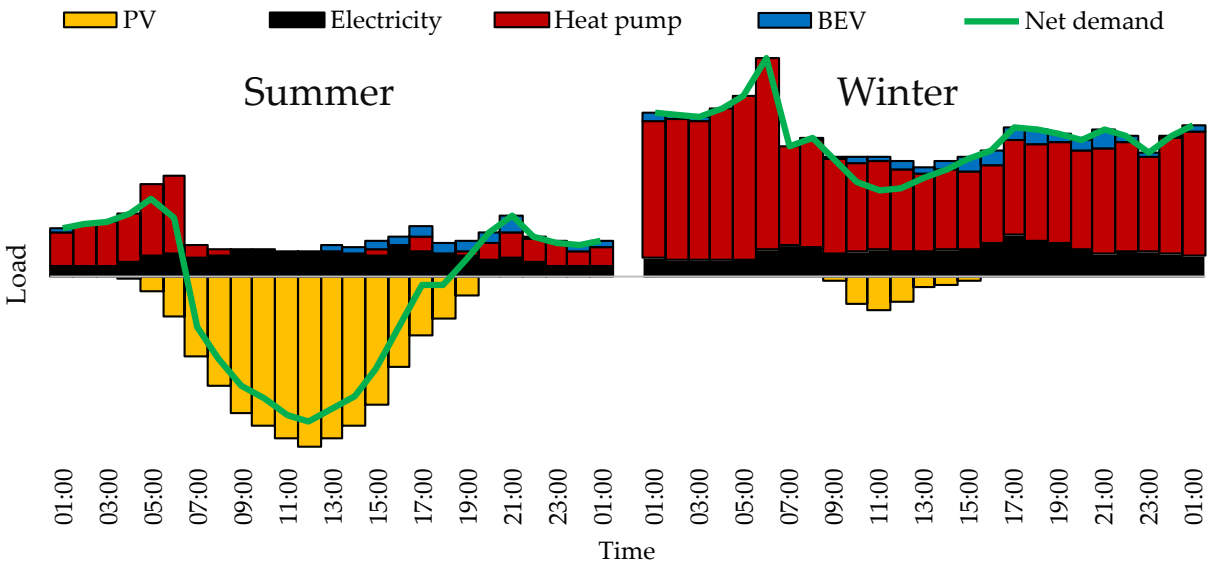

Figure 1.2: A stylized depiction showing the match between various demands and decentralized generation within a fully electrified low-voltage distribution grid.

many, around 70% of the renewable energy unit capacities are connected to the grid at these voltage levels [15]. Likewise, heat pumps and BEV charging stations usually have their grid connections at the voltage distribution level. Despite being over-dimensioned to some extent, the conventional planning guidelines for distribution grids did not account for the amount of electrification required to meet the current decarbonization objectives. Besides the sheer amount of additional electrical demand, the simultaneities of these loads add to the problem. For instance, heating systems exhibit high simultaneities due to their correlation with low ambient temperatures, which can lead to substantial increases in peak electrical demands, especially in winter [16]. For BEV charging, there is a challenge in dealing with the simultaneous return-to-home patterns, resulting in narrow and concurrent charging windows in the late afternoon hours [17]. Conversely, PV feed-in puts stress on the grid by reverse flows. Its generation reaches its peak in summer noon hours when household demands are low, making its utilization to cover as much demand as possible difficult (see Figure 1.2 for a stylized depiction within a 100% electrification setting).

Consequently, there is broad agreement that the widespread adoption of these technologies will necessitate significant reinforcements in the grid capacities, including at the distribution level. According to the Report on the State and Expansion of Distribution Grids published by the German Federal Network Agency in 2021, distribution grid operators have declared grid reinforcement measures summing up to 15.8 billion euros between the years 2021 and 2031 (of which almost 60% dealing with the low-voltage level). This amount is nearly three times higher than in a survey from 2020, i.e., only a year before the report. This discrepancy is not due to a sudden rise in the grid reinforcement costs but rather demonstrates the recency of the assessment of the reinforcement requirements [15]. These requirements could be, however, alleviated by promoting flexible consumer operation.

1.1.2 The rise of prosumers

In the "old" energy world, retail customers for energy were considered as pure *consumers*, whose electrical or fuel demands had to be covered in an on-time manner, charged on a fixed volumetric price per kWh, A fixed retail price gave little reason for consumers to alter their demand behavior. However, the trend towards electrified demands and decentralized generation reveals opportunities for *prosumers* to intelligently shift their loads, with the motivation of reducing their overall energy costs. Hereupon, the capability of prosumers to employ such cost-saving management of their loads and generations will be called *flexibility*. Flexibilities are usually achieved by demand response or using storage systems and can be motivated in various ways, including:

- Unless there is a net-metering scheme in place letting the PV owners sell their excess power at exactly the retail rate, PV generation effectively introduces a new price: the owner either uses electricity from the grid at the retail rate to cover their demand as usual, or she uses the locally generated, zero-marginal-cost PV electricity. This situation consequently motivates her to maximize the *PV self-consumption*, i.e., to use as much of their local generation as possible to take advantage of this marginally free generation (Figure 1.3, left). Most PV systems are sold with battery storage units to facilitate this.

- As it is often not feasible to integrate the PV generation in a building entirely, *local energy market* concepts may serve as a solution to facilitate the exchange of this excess between prosumers [18]. This exchange would settle at a price generally lower than the retail price of electricity but higher than the feed-in tariffs they would receive if they fed the excess back into the grid. Such market concepts would necessitate intelligent decision-making to handle the excess energy in the most cost-efficient manner.

- Non-volumetric or non-uniform pricing schemes are another way to introduce price heterogeneities directly. They motivate the prosumers to shift most of their demands to low-price hours. *Time-of-use retail tariffs* may be offered by the utilities to reflect the variations in the wholesale price of electricity in the retail price better. Historically, lower off-peak prices have been used in countries with high base-load plant capacities, such as Germany, to incentivize households to run their night storage heaters, keeping these base-load plants operational at night. In a setting with a high share of volatile renewable generation, prosumers can be incentivized by *dynamic pricing schemes* to shift their demand to the moments of lower market prices when the generation from renewable resources is high. Similarly, a *time-variable network tariff design* can be made by grid operators to push a portion of the load away from the morning and late afternoon hours where simultaneous loads are high (see Figure 1.3, right). *Capacity tariff* schemes can introduce a "per kW" component to the electricity bill, similarly motivating prosumers to reduce their peak loads.

1.1.3 Interactions between prosumers and the distribution grid operator

A financial interaction exists between DSOs and prosumers, as qualitatively shown in Figure 1.4. The optimal dimensioning of a prosumer's DERs, e.g., the PV units, battery storages, or heat pumps, can be determined by using mixed-integer linear programming-based methods with the goal of minimizing investment costs. Tied to that, the optimal operation of these components is usually governed by home energy management systems (HEMSs), which typically function using rule-based, optimization-based, or data-driven scheduling algorithms to

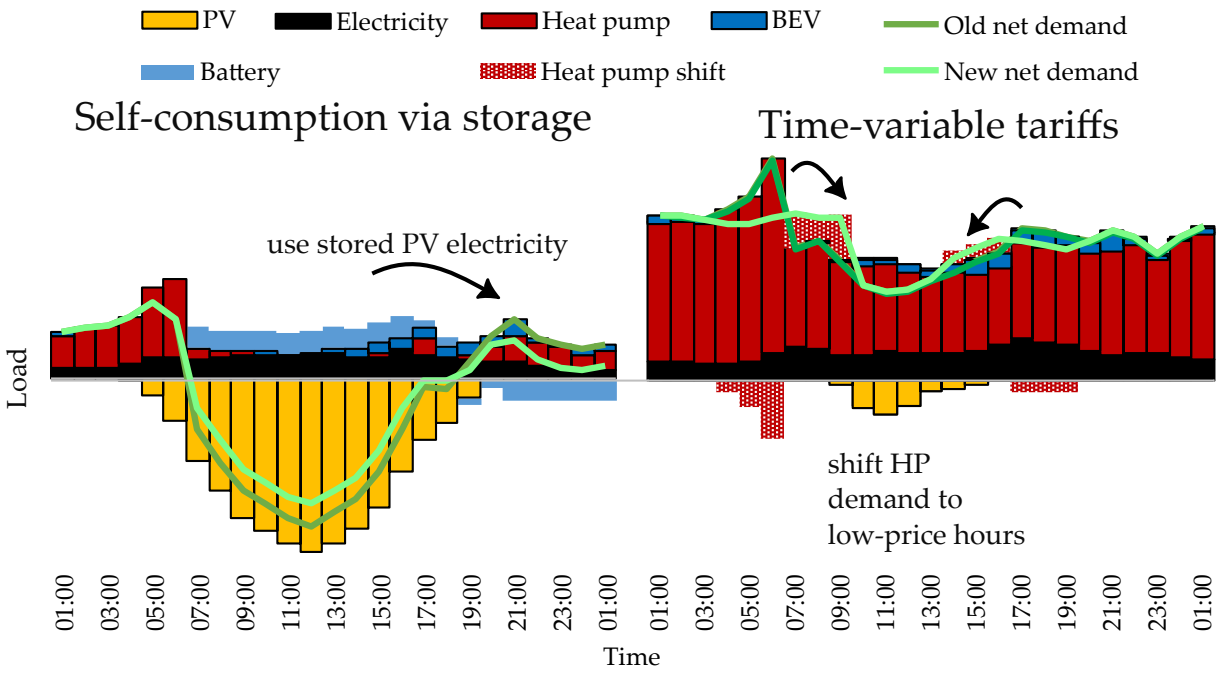

Figure 1.3: Various aspects incentivizing prosumers to employ their flexibilities. The left figure depicts a storage operation integrating excess PV generation into the evening hours. The right figure depicts an adjusted heat pump operation that makes use of time-variable network tariffs.

minimize the running costs, i.e., to save as much energy costs as possible [19]. In this, decision-making is driven solely by the costs seen by the prosumer; the state of the distribution grid is of little concern for her, and the electricity "comes from the socket".

On the other hand, the DSO is responsible for the secure operation of the grid and, wherever necessary, applying grid reinforcement measures. In Germany, the capital expenditure incurred for such grid reinforcement measures is ultimately reflected back to the consumers through the so-called *incentive regulation system*[1], in the form of grid network charges. The incentive regulation system results from the grid operators being natural monopolies, raising the necessity to regulate their revenues. In this system, yearly revenue caps are set for each DSO by considering various factors, including the planned capital expenditures (including for grid reinforcement) and the individual efficiency ranking of the DSO (thereby rewarding the DSOs that implement efficient measures with a higher profit margin). This evaluation is made every five years (regulation periods), and the DSO is then allowed to recover the resultant revenue cap through grid network charges incurred by the consumers, usually through billing by the energy supplier. Essentially, a grid-unaware operation of the DERs by the customers leads to higher network charges in the long term.

Hence, in the larger picture, a non-cooperative game exists between the consumers and DSO through the network tariff dynamics [21]. In an ideal system, prosumers could utilize their flexibilities to reduce their peak consumptions and feed-ins, to be rewarded in turn with lower network charges due to the alleviation of grid expenditures. Yet, the current design of network charges in Germany gives little reason for this in the short term—customers with a yearly consumption of less than 100,000 kWh and without a smart meter system (virtually all household customers) currently receive a constant, volumetric network charge along with a fixed base price. Nevertheless, in many countries, policy adjustments for such incentives are

[1] While a complete description of the incentive regulation system is omitted in this thesis, [20] gives an overview.

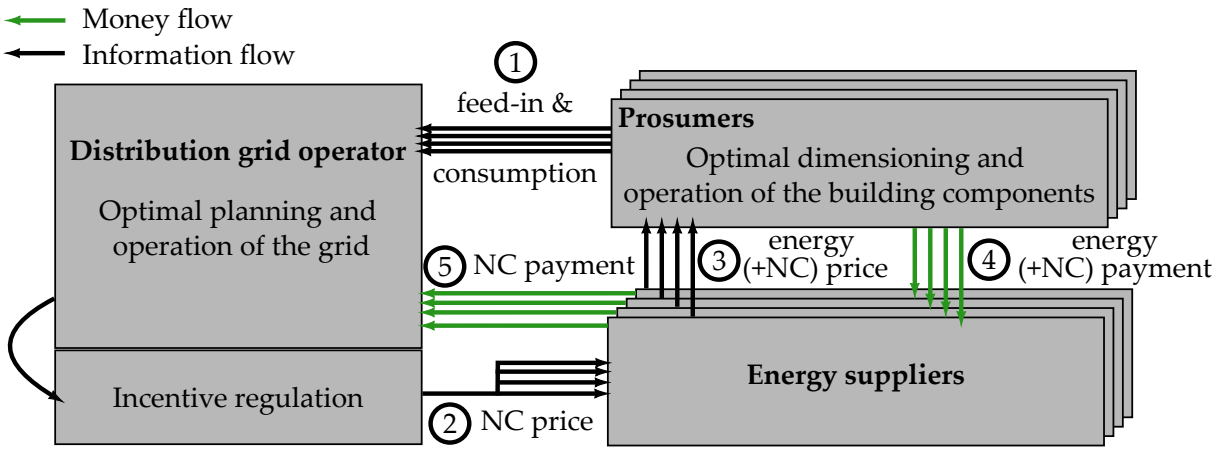

Figure 1.4: Stylized depiction of the conventional interaction between the prosumer and the distribution grid operator. Processes are sequenced with numbers for simplicity for the reader and do not reflect an actual order (NC stands for the network charges).

established or planned in the immediate future:

- The latest draft for an amendment to Section (§) 14a of the German Energy Industry Act plans to levy time-variable network tariffs by 01.01.2024 [22].
- Section (§) 41a of the German Energy Industry Act enforces that, as of 1 January 2022, every energy supplier with more than 100,000 customers has to offer a dynamic pricing tariff for those with a smart meter system. As of 1 January 2025, all energy suppliers will honor this obligation [23].
- Since January 2023, capacity charges make up an obligatory part of retail energy costs in Belgium, set at around 40€/kW per year as of 2023 [24],
- For the cases such financial incentives fail to maintain a secure grid operation, granting the DSOs the authority to occasionally downregulate the consumer DERs remotely is currently planned in Germany as part of § 14a of the German Energy Industry Act.

With these measures, the intention is to resolve the field of tension between prosumers and grid operators, contain the grid violations resulting from the increasing penetration of DERs at moderate levels, and allow DSOs the time to implement the required grid reinforcement measures.

1.2 Objective and scope of this thesis

In the wake of this rapid technical and regulatory transformation of the distribution systems– in particular, the LVDSs where much of the DER adoptions take place [25]–it is of significant importance to investigate various techno-economic aspects which may influence the direction these systems will transform towards. To that end, the research questions tackled in this thesis are as follows:

- How are the load profiles of an optimally dimensioned, highly electrified low-voltage distribution system (LVDS) altered?
- What is the extent of the LV distribution grid reinforcement requirements emerging from deep electrification?
- How much do uncoordinated prosumer optimization paradigms deviate from the global optimum of the LVDS?
- How do the transformation costs (split into the prosumer- and grid-side costs) stand in relation to one another?
- How do the proposed financial incentives and technical measures influence the need for grid reinforcement in the medium and long term?
- Can generalized statements regarding these research questions be derived systematically, or is a case-specific approach necessary?

To answer these research questions, an optimization framework that portrays the planning and operation procedures of prosumers and the responsible DSO under the application of various financial and technical measures is developed in this thesis. This optimization framework is then applied to a case study with different electrification scenarios in regions with diverse characteristics. As data availability is usually scarce and distribution system properties differ significantly, the framework is supplemented by a data acquisition suite that utilizes mostly open data to parametrize the investigated distribution systems.

1.3 Publications

During the author's doctoral studies, the following set of works has been published either as a journal article or a conference contribution. These publications are categorized in their respective themes and listed in anti-chronological order below.

Publications on the modeling of low-voltage distribution systems:

- Candas, Soner; Hamacher, Thomas. **Capacity tariffs and DSO-side down-regulation as grid-relieving measures in future low voltage distribution systems**. *18th IAEE European Conference*, 2023
- Candas, Soner; Reveron Baecker, Beneharo; Mohapatra, Anurag; Hamacher, Thomas. **Optimization-based framework for low-voltage grid reinforcement assessment under various levels of flexibility and coordination**. *Applied Energy 343*, 121147, 2023. DOI: https://doi.org/10.1016/j.apenergy.2023.121147
- Reveron Baecker, Beneharo; Candas, Soner. **Co-optimizing transmission and active distribution grids to assess demand-side flexibilities of a carbon-neutral German energy system**. *Renewable and Sustainable Energy Reviews 163*, 112422, 2022. DOI: https://doi.org/10.1016/j.rser.2022.112422

- Candas, Soner; Zhang, Kai; Hamacher, Thomas. **A comparative study of Benders decomposition and ADMM for decentralized optimal power flow**. *2020 IEEE Power & Energy Society Innovative Smart Grid Technologies Conference (ISGT)*, 1-5, 2020. DOI: https://doi.org/10.1109/ISGT45199.2020.9087777

- Cornejo, Martín; Mohapatra, Anurag; Candas, Soner; Perić, Vedran S. **PHIL implementation of a decentralized online OPF for active distribution grids**. *2022 IEEE Power & Energy Society General Meeting (PESGM)*. 1-5, 2022. DOI: https://doi.org/10.1109/PESGM48719.2022.9916705

- Candas, Soner; Siala, Kais; Hamacher, Thomas. **Sociodynamic modeling of small-scale PV adoption and insights on future expansion without feed-in tariffs**. *Energy Policy 125*, 521-536, 2019. DOI: https://doi.org/10.1016/j.enpol.2018.10.029

Publications on open-source, large-scale energy system modeling:

- Candas, Soner; Muschner, Christoph; Buchholz, Stefanie; Bramstoft, Rasmus; van Ouwerkerk, Jonas; Hainsch, Karlo; Löffler, Konstantin; Günther, Stephan; Berendes, Sarah; Nguyen, Stefanie; Justin, Aparna. **Code exposed: Review of five open-source frameworks for modeling renewable energy systems**. *Renewable and Sustainable Energy Reviews 161*, 112272, 2022. DOI: https://doi.org/10.1016/j.rser.2022.112272

- van Ouwerkerk, Jonas; Hainsch, Karlo; Candas, Soner; Muschner, Christoph; Buchholz, Stefanie; Günther, Stephan; Huyskens, Hendrik; Berendes, Sarah; Löffler, Konstantin; Bußar, Christian; Tardasti, Fateme; von Köckritz, Luja; Bramstoft, Rasmus. **Comparing open source power system models-A case study focusing on fundamental modeling parameters for the German energy transition**. *Renewable and Sustainable Energy Reviews 161*, 112331, 2022. DOI: https://doi.org/10.1016/j.rser.2022.112331

- Berendes, Sarah; Hilpert, Simon; Günther, Stephan; Muschner, Christoph; Candas, Soner; Hainsch, Karlo; van Ouwerkerk, Jonas; Buchholz, Stefanie; Söthe, Martin. **Evaluating the usability of open source frameworks in energy system modeling**. *Renewable and Sustainable Energy Reviews 159*, 112174, 2022. DOI: https://doi.org/10.1016/j.rser.2022.112174

Publications on other topics in energy system modeling:

- Candas, Soner; Dimitropoulos, Nikolaos. **Influence of CO_2 taxation and hydrogen utilization on the cost-optimal development of the German power system by 2050**. *1st IAEE Online Conference 2021*

- Candas, Soner; Guminski, Andrej; Fiedler, Claudia; Pellinger, Christoph; Orthofer, Clara Luisa Orthofer, **Meta-analysis of country-specific energy scenario studies for neighbouring countries of Germany**. *16th IAEE European Conference*, 2019.

1.4 Thesis structure

The structure of the thesis is illustrated in Figure 1.5. Chapter 1 introduced the background, the research questions, and the objective of this thesis. Chapter 2 elaborates on the mathematical formulations of the developed low-voltage distribution system models. Chapter 3 describes the integrated data acquisition workflow, which consists of data sources and data processing tools used to parametrize this thesis's case studies. Chapter 4 presents and discusses the results of the case study. Chapter 5 consists of an essay on methods that can facilitate the extension of the proposed local optimization framework to larger scales. Chapter 6 concludes the thesis, revisiting the research questions, stating the limitations of the work, and providing an outlook for further work.

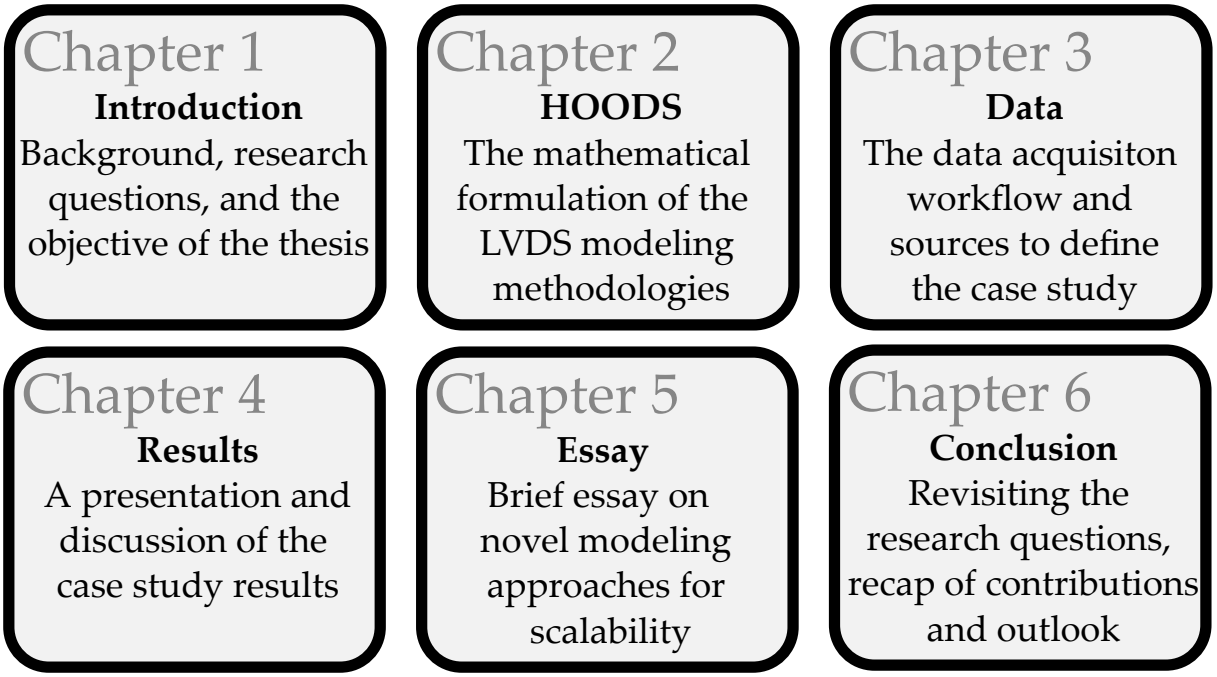

Figure 1.5: The structure of this thesis.

Chapter 2

Holistic optimization of low-voltage distribution systems (HOODS) framework

This Chapter will describe the building blocks of the holistic optimization of distribution systems (HOODS) framework. The Chapter will start with a literature review on low voltage (LV) grid optimization frameworks, continue with the overview of the proposed model structure, followed by the model definitions, the elaboration of various planning paradigms, and the supplementary modules of the framework. For disambiguation, the following definitions are adopted in this Chapter:

- *Distributed energy resources (DERs)* or *building components*: The technical components located at buildings, which serve for the generation, storage, and conversion of energy.
- *Prosumers*, *households* or *buildings*: The agents that demand energy in various forms and operate their building components accordingly. They also have control over the investment decisions of the DERs.
- *Low-voltage (LV) distribution grid*: The part of the electrical power grid where the electrical energy reaches residential consumers. European LV grids usually have a three-phase rated voltage of 400V.
- *Grid components*: The technical components that constitute the electrical network, which transports active and reactive power across the distribution grid. In this framework, they consist of LV transformers (with fixed or variable tap ratios) and distribution (main and service) lines.
- *Distribution system operator (DSO)*: The agent responsible for the coverage of the households' electrical demand without violating the network restrictions. They also decide upon the reinforcement of the grid components to maintain a safe network operation.
- *Low voltage distribution systems (LVDSs)*: The totality of agents involved in the energy supply at the LV grid level. The low voltage distribution system (LVDS) consists of all prosumers in the LV grid and the distribution grid operator.
- *Model*: The mathematical representation of the operation and planning of the LVDS. Along with a cost function, the model can be formulated as an *optimization problem* that can be solved by an optimization *solver* to obtain a cost-optimal LVDS configuration.

- *Paradigm*: A specific variation on the model characterized by different degrees of coordination, flexibility, or the application of techno-economic measures in the LVDS planning and operation.

2.1 Literature review on LVDS optimization

2.1.1 Methods to analyze grid reinforcement requirements under electrification of heating and mobility

An extensive collection of research addresses the issue of reinforcing distribution grids to cater to the increased demand due to electric heating and transportation, as summarized by Thormann et al. [26]. These findings motivate the development of systematic approaches to tackle the non-convex optimization problem that describes the cost-optimal planning and operation of distribution systems.

There is a diverse set of options for relieving stress on a grid, which includes voltage regulators, devices for reactive power compensation, additional parallel cables, managing power feed-in, and altering the configuration of the grid. Each of these options helps prevent the grid from violating voltage and loading limits in different ways. However, choosing the best combination of these options is mathematically challenging due to the large number of choices and the complex, non-linear nature of the electrical grid. The situation gets even more complicated with distributed energy resources (DERs) as they bring new, complex elements to the grid operation.

Sedghi et al. [27] offer a thorough review of different heuristic algorithms for optimizing distribution grid planning, especially when new electrical loads are introduced. The research by Saboori et al. [28] and Koopmann et al. [29] shows how particle swarm optimization and genetic algorithms can be particularly useful for distribution grid expansion. Bakken et al. [30] put forward a grid planning algorithm that considers distinct choices, inspired by the voltage issues arising from an increasing number of photovoltaics (PV) systems in low-voltage grids.

There is also a rich body of literature on using convex optimization or mixed-integer linear programming (MILP) to solve grid reinforcement issues. These methods need some simplifications in the grid model, but they have the advantage of being compatible with efficient solving algorithms. This compatibility makes it easier to find the best solution while giving more flexibility in the system, including decisions about investments and operations for additional assets beyond just the grid. Lopez et al.'s work [31] is an example that showcases the practicality of such convex formulations.

Co-optimizing various assets besides the grid also allows the analysis of the complex interactions between different sectors. This includes understanding the trade-offs between using more electric household appliances and the need to expand the grid, as well as how flexible use of household appliances can reduce the need for grid reinforcement. Morvaj et al. [32], [33] built a framework based on MILP with the help of a genetic algorithm to study how DERs influence the need for grid reinforcement, considering both electricity and heating at the district level. Mashayekh et al. [34] expanded on this by considering cooling demands and minimizing network losses.

Another group of studies primarily looks at how flexible solutions can prevent the need for significant grid upgrades. These solutions focus on managing demand to reduce peak loads and storing electricity and heat. For example, Spiliotis et al. [35] developed a model for a market mechanism that looks at how flexible demand can avoid the need for expanding distribution grids. Using grid simulations, Resch et al. [36] compared different control mech-

anisms for managing flexibility through photovoltaics and batteries. These studies provide valuable insights into how non-grid assets can offer flexibility. Still, they do not fully address the interactions between grid capacity and flexibility options since they do not optimize the whole system.

2.1.2 Contribution of the presented framework over the literature

Expanding on this literature, this thesis presents an optimization framework based on a mixed-integer linear programming approach, incorporating a combined grid reinforcement model. This setup facilitates a globally optimal solution for the entire system, achieved by simultaneously optimizing LV distribution grid reinforcement and flexibility strategies. Within this framework, each building is designated as an "energy hub," [37] where the flexible fulfillment of all energy needs, including electricity, heating, and mobility, as well as their interactions, is considered.

For grid planning, a mixed-integer model is developed that supports the co-optimization of 1) discrete preventive reinforcement actions like transformer upgrades and parallel cabling, and 2) curative strategies such as remote PV feed-in curtailment or downregulation of controllable loads. Through this method, the distribution system operator (DSO) can identify the most cost-effective combination of various available measures. Additionally, a post-optimization non-convex power flow simulation step is conducted to validate the feasibility of the electrical flows and voltages. This step not only guarantees that the planning is physically viable but also provides a detailed quantification of network losses.

This process is anchored in a MILP approach, which can optimally achieve a single, unified strategy, assuming complete cooperation among all active participants - prosumers and the DSO - within the system. However, such a holistic, cooperative approach is typically far removed from the reality of existing regulatory structures. As such, this framework aims to bring these results into the context of more realistic, albeit not necessarily optimal, planning paradigms. This comparison aims to determine the potential of the flexibility components, wide-scale cooperation within future low-voltage distribution grids, and various price schemes for reducing system costs and alleviating grid reinforcement needs. This way, the welfare losses suffered in practical system operation, where the flexibilities may not be exploited to their fullest potential due to a lack of coordination, can be quantified. While comparable studies have been performed before, as seen in the work of Grimm et al. [38], this framework expands upon previous research by incorporating heating and mobility demands and enabling endogenous investments across all assets. To the best of the author's knowledge, this is the first framework that combines: (i) a multi-modal system model at the distribution grid level, (ii) an analysis of the needs for various grid reinforcement strategies, (iii) the consideration of different levels of flexibility and coordination, (iv) under application of a diverse set of techno-economic grid-relieving measures.

2.2 Overview on the HOODS framework

Figure 2.1 gives an overview of the construction blocks of the HOODS framework.

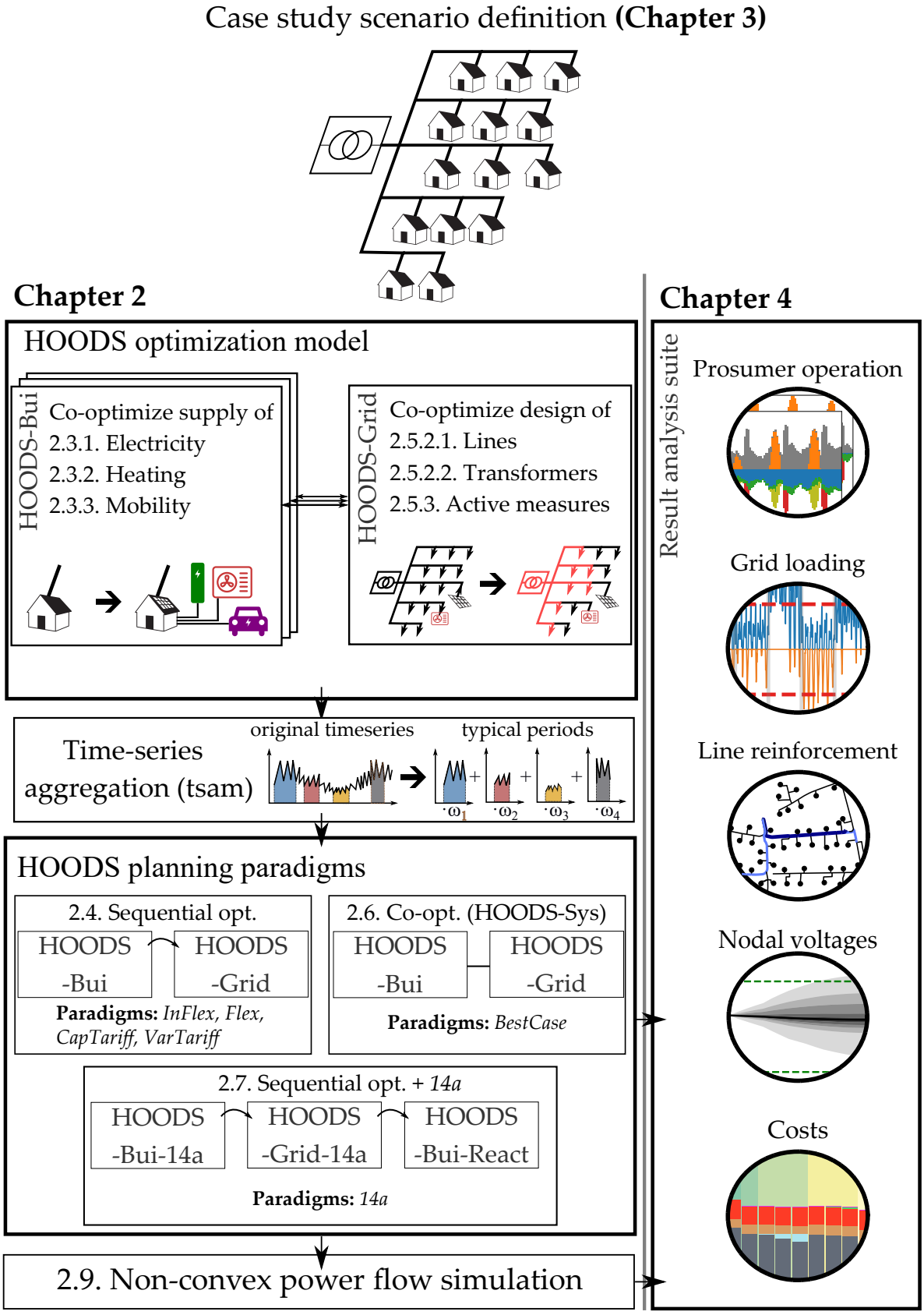

Figure 2.1: Building blocks of the holistic optimization of distribution system (HOODS) framework.

In the HOODS framework, the residential LV distribution systems consist of two levels: the buildings and the distribution grid. Correspondingly, the optimization problem includes the submodules of

1. HOODS-Bui for the optimal dimensioning and operation of the multi-energy supply and storage components in buildings and

2. HOODS-Grid for the optimal sizing and operation of the electrical LV grid components and the utilization of active measures for grid relief.

The *HOODS submodules* consist of respective model variables, parameters, and constraints governing the design and operation of the building and grid components. Building on these, two types of system planning paradigms are developed: a) the *co-optimization* paradigm, which assumes full-coordination and sets a benchmark for the most cost-optimal operation, and b) *the sequential paradigm*, which separates the prosumers and the grid operator as distinct decision making entities.

Thanks to an *aggregation of the model time series*, the tractability of the model is maintained for representative sizes of LV distribution systems with adequate temporal resolution. After the optimization, *a non-convex power flow simulation step* validates the accuracy of the electrical flows and voltages in the LVDS, not only ensuring physically feasible planning but also quantifying the network losses in detail. *The scenario definition* deals with the parametrization of the LVDS with regard to the considered model region and technology options, and the *result analysis suite* provides insights on the model results by investigating the optimal LVDS dimensioning and operation, loading of the transformer and lines, the nodal voltages, and the costs.

The model i) enables both a holistic and uncoordinated optimization of the building and grid components, ii) allows simultaneous formulations for the expansion and the yearly operation, and iii) keeps a tractable MILP formulation. The corresponding optimization problem is formulated and implemented by extending the open-source energy system modeling framework *urbs*[1].

Discussion on the co-optimization and sequential optimization of the LVDS While the presented co-optimization framework provides a computationally tractable formulation for common LV grid sizes, an issue lies in its supposition of a single entity that

- has access to all of the information at the distribution grid level (e.g., the exact building stock, the energy consumption profiles) and

- has authority over the integrated planning of all system components, the ensuing operation thereof, and the local energy exchange between households.

These suppositions are far from the current reality. The adoption of DERs at a building level is highly motivated by individual interests rather than system benefits. Moreover, the exchange of PV electricity between buildings in times of excess to increase its overall integration, as this framework allows, requires advanced local markets, which are not an established practice yet (despite examples of peer-to-peer (P2P) markets as described in [39]). Barring pilot projects, most distribution grids, even in developed countries such as Germany, lack the communication protocols, measurement instruments, and regulatory framework necessary for an intelligent operation that would approximate the social optimum [40].

[1] GitHub repository: `https://github.com/tum-ens/urbs`.

Therefore, the co-optimization paradigm results are considered a benchmark for the best-case planning and operation of the whole distribution system. To be compared with this benchmark, more realistic, sequential variations are also implemented. In game theory terms, a Stackelberg game [41] is formed within the LVDS where the prosumers are considered *leaders*, whereas the DSO is considered the *follower*. Thus, the decision-making of the prosumers regarding the dimensioning and the operation of their DERs is made first (HOODS-Bui), followed by the reaction of the DSO to this to maintain a safe grid operation (HOODS-Grid). Here, a perfect information flow between the agents is assumed, i.e., the operation of the prosumers at the grid interface is monitored completely by the DSO.

The sequential optimization approach has various implications. Unlike holistic optimization, a bi-directional information flow between the prosumers and the DSO does not exist. Hence, grid-relieving DER operation is not stimulated unless the prosumer receives a direct financial benefit through such behavior. For instance, a smoothened battery electric vehicle (BEV) charging is incentivized only if the prosumers are penalized for high peak behavior via financial measures such as capacity pricing (see Section 2.3.4).

The following Sections will elaborate on the building blocks of the HOODS framework, starting with each of its submodules, HOODS-Bui and HOODS-Grid, followed by the paradigm variations, and concluding with the methodology of the time series aggregation and the post-optimization non-convex power flow.

2.3 HOODS-Bui: Modeling of building components

The HOODS-Bui model deals with the optimal dimensioning and operation of the DERs and are defined for each building within a given grid. Buildings can be located at a subset $\mathcal{I}^b$ of the given set of network nodes $\mathcal{I}$ within the LV distribution grid (building $i \in \mathcal{I}^b \subseteq \mathcal{I}$). For each building, respective electricity, space heating, domestic hot water (DHW), and mobility demands $d_{i,t}^{\{...\}}$ have to be covered for each time step $t \in \mathcal{T}$, specifically on an hourly basis. If no building is located in a given network bus, $d_{i,t}^{\{...\}} = 0$. These demands can be covered by a set of technologies as depicted in Table 2.1. In covering these demands, temporal flexibility options exist: electrical and heat can be stored in the form of batteries and buffer storage units, allowing shifting the demand across time from the hours of scarcity (or high prices) into those with excess generation (or lower prices). Additionally, flexibility in space heating supply can be achieved by using the thermal inertia of the building. Similarly, the charging of BEVs can be scheduled flexibly to cater to technical restrictions or to take advantage of price fluctuations. The corresponding reference energy system in Figure 2.2 illustrates the energetic interactions within each building. Here, each vertical line represents various energy commodities, each block a DER, and each arrow a commodity flow.

Table 2.1: Building components defined for each energy demand.

Energy demand	Supply	Flexibility
Electricity	Solar PV, grid electricity	Battery storage
Space heating	Heat pump	Heat storage, thermal inertia of building
Domestic hot water	Heat pump	Heat storage
Mobility	Wall box	Smart charging

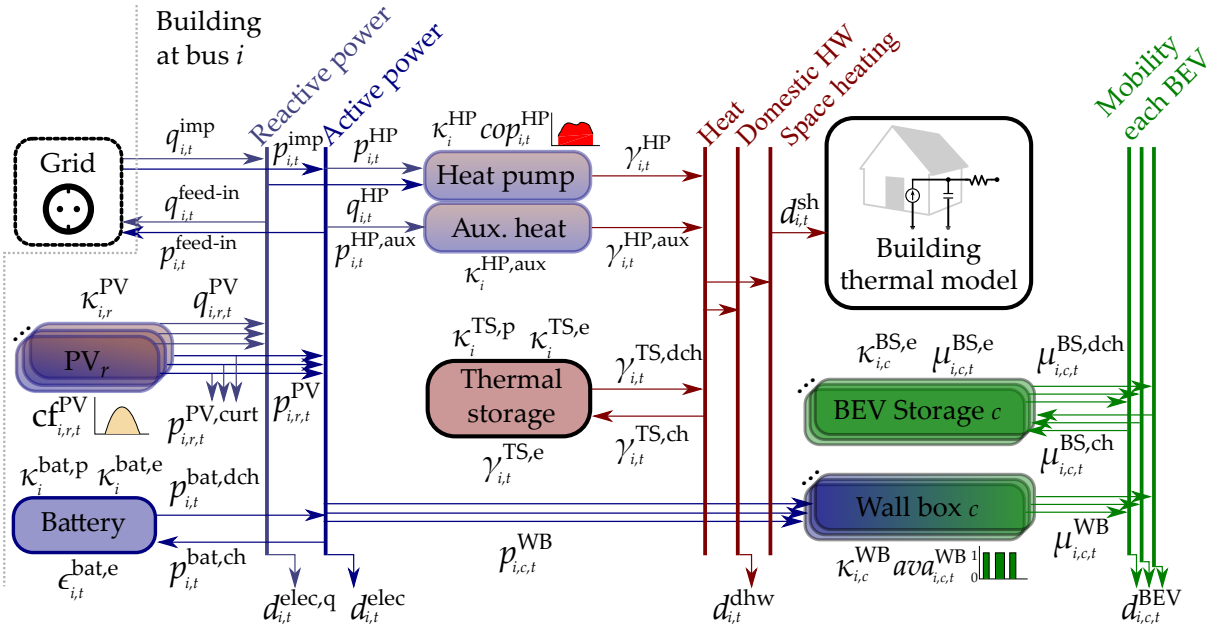

Figure 2.2: Sector-coupled reference energy system for a fully-electrified building and the corresponding energetic flows.

2.3.1 Electricity side

Building components dealing with the local generation and storage of electrical energy consist of PV units and household batteries, respectively.

2.3.1.1 Solar photovoltaics (PV)

A portion of the electrical demand of a building can be covered by rooftop solar photovoltaic (PV) systems. These can be installed on each roof section $r \in \mathcal{R}^i$ of a building i.

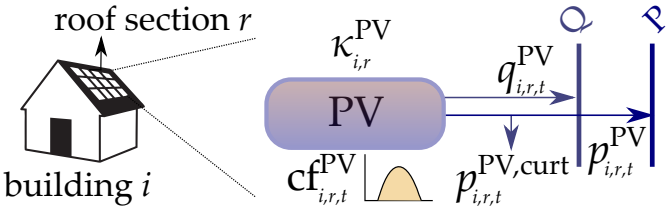

Figure 2.3: Reference energy representation for solar photovoltaics (PV) units.

A weather-dependent, linear modeling of the electricity generation from PV units at each roof section $r \in \mathcal{R}^i$ of a given building at $i \in \mathcal{I}^b$ in a given modeled hour $t \in \mathcal{T}_m$ is given via the following constraint:

$$p^{\mathrm{PV}}_{i,r,t} + p^{\mathrm{PVcurt}}_{i,r,t} = \kappa^{\mathrm{PV}}_{i} \cdot cf^{\mathrm{PV}}_{i,r,t}, \qquad \forall t \in \mathcal{T}_m \quad \forall r \in \mathcal{R}^i \tag{2.1}$$

$$p^{\mathrm{PV}}_{i,r,t}, p^{\mathrm{PVcurt}}_{i,r,t} \geq 0, \qquad \forall t \in \mathcal{T}_m \quad \forall r \in \mathcal{R}^i \tag{2.2}$$

where $p^{\mathrm{PV}}_{i,r,t}$ is the hourly active power generation from the PV unit, $\kappa^{\mathrm{PV}}_{i,r}$ is the capacity of PV built on the roof section r, and $cf^{\mathrm{PV}}_{i,r,t}$ is the unitless capacity factor at the given hour (e.g. a capacity factor of 0.5 for a 10 kW PV unit would yield a total of 5 kWh/h during the given hour). If the production comes at an excess that cannot be used or stored, a portion of the active power generation may be curtailed by an amount of $p^{\mathrm{PVcurt}}_{i,r,t}$ for grid relief purposes. Active power curtailment (APC) is achieved by driving the inverter voltage away from the maximum

power point (MPP). While curtailment is considered an inefficient practice that leads to the direct loss of otherwise useful, zero-marginal cost electricity, it is a reliable measure for dealing with grid congestion issues [42]. Correspondingly, most PV owners are obligated to allow the distribution system operator to curtail their excess production in times of high grid loading (source Germany). While PV owners lack financial motivation for voluntary curtailment, new tariff structures such as capacity-based grid surcharges or electricity tariffs might also introduce a financial case for it in the future.

$\cos\phi^{\mathrm{PV}}_{\mathrm{min}}$ is the minimum power factor that the PV inverter can operate at. For instance, the German VDE-AR-N 4105 norm sets a mandatory minimum power factor of up to $\cos\phi^{\mathrm{PV}}_{\mathrm{min}} = 0.95$ for units between 3.68 kVA and 13.8 kVA, and $\cos\phi^{\mathrm{PV}}_{\mathrm{min}} = 0.9$ for a module capacity larger than 13.8 kVA. By injecting reactive power within this range, PV inverters can support the grid against voltage drops. The mentioned $\cos\phi^{\mathrm{PV}}_{\mathrm{min}}$ guideline, however, ties the reactive power supply requirement to the times when active power generation is also generated. PV inverters, on the other hand, can provide reactive power even in hours of low irradiation. Yet, in many countries, including Germany, no remuneration mechanism for reactive power is in place at the low voltage level. Hence, the incentive for the PV owners to support the grid with reactive power at those times is missing [43]. Additional costs usually prevent a voluntary over-dimensioning of the PV inverters for the purpose of increasing their reactive power supply capacities.

The reactive power provision from PV at a given time is assumed not to reduce the active power capability. Moreover, it is assumed that the PV inverter generating the reactive power has adequate capacity to accommodate the additional apparent power.

$$-\tan\left(\phi^{\mathrm{PV}}_{\mathrm{min}}\right)\cdot p^{\mathrm{PV}}_{i,r,t} \leq q^{\mathrm{PV}}_{i,r,t} \leq \tan\left(\phi^{\mathrm{PV}}_{\mathrm{min}}\right)\cdot p^{\mathrm{PV}}_{i,r,t}. \qquad \forall t \in \mathcal{T}_m \qquad \forall r \in \mathcal{R}^i \tag{2.3}$$

The capacity expansion of PV is restricted by the area of each roof section $A_{i,r}$, with a roof area usage factor of U_A (given in kW/m^2):

$$0 \leq \kappa^{\mathrm{PV}}_{i,r} \leq U_A \cdot A_{i,r} \cdot \beta^{\mathrm{PV}}_{i,r}, \qquad \forall r \in \mathcal{R}^i \tag{2.4}$$

where $\beta^{\mathrm{PV}}_{i,r} \in \{0,1\}$ is the binary variable representing the decision to install a PV module on the roof section r of the building i.

2.3.1.2 Battery storage

In Germany, the tariffs for the feed-in of the excess PV electricity to the outside grid are significantly lower than the retail electricity price (8.6 ct/kWh[2] compared to an average of 40 ct/kWh as of 2023). Thus, maximizing the PV self-consumption gains high economic importance. The overproduction of PV electricity at each building can be integrated through the intelligent operation of battery storage units. Figure 2.4 depicts the battery storage operation.

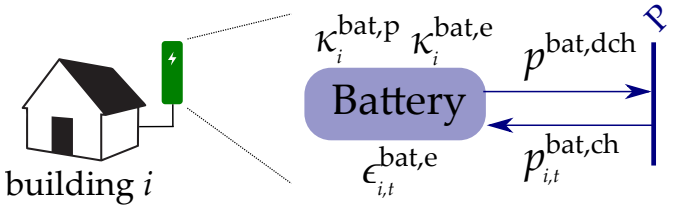

Figure 2.4: Reference energy representation for battery storage units.

[2]German Law for the expansion of renewable energies ("Gesetz für den Ausbau erneuerbarer Energien (Erneuerbare-Energien-Gesetz - EEG 2023)") § 48 Solar energy (Solare Strahlungsenergie): https://www.gesetze-im-internet.de/eeg_2014/__48.html

The eqs. (2.5a) to (2.5f) govern the operation of a battery:

$$\epsilon_{i,t}^{\text{bat,e}} = \epsilon_{i,t-1}^{\text{bat,e}} + \eta^{\text{bat,ch}} \cdot p_{i,t}^{\text{bat,ch}} - \frac{p_{i,t}^{\text{bat,dch}}}{\eta^{\text{bat,dch}}}, \qquad \forall t \in \mathcal{T}_m \tag{2.5a}$$

$$0 \leq p_{i,t}^{\text{bat,dch}} \leq \kappa_i^{\text{bat,p}}, \qquad \forall t \in \mathcal{T}_m \tag{2.5b}$$

$$0 \leq p_{i,t}^{\text{bat,ch}} \leq \kappa_i^{\text{bat,p}}, \qquad \forall t \in \mathcal{T}_m \tag{2.5c}$$

$$0 \leq \epsilon_{i,t}^{\text{bat,e}} \leq \kappa_i^{\text{bat,e}}, \qquad \forall t \in \mathcal{T}_m \tag{2.5d}$$

$$\epsilon_{i,0}^{\text{bat,e}} = \epsilon_{i,T_{\text{end}}}^{\text{bat,e}}, \tag{2.5e}$$

$$\kappa_i^{\text{bat,e}} = \kappa_i^{\text{bat,p}} \cdot etp^{\text{bat}}, \tag{2.5f}$$

where the variable $\epsilon_{i,t}^{\text{bat,e}}$ expresses the energy content of the battery unit at a given time, $p_{i,t}^{\text{bat,ch}}, p_{i,t}^{\text{bat,dch}}$ are the hourly charged and discharged amounts of active power, and $\kappa_i^{\text{bat,p}}, \kappa_i^{\text{bat,e}}$ are the power and energy capacities of the battery unit. The constraint (2.5a) governs the state-of-charge of the battery subject to the charging and discharging efficiencies of $\eta^{\text{bat,ch}}, \eta^{\text{bat,dch}}$. The eqs. (2.5b) to (2.5d) restrict the battery operation and the state-of-charge with their respective capacities, the equation (2.5e) enforces the cyclic operation of the battery, and the equation (2.5f) ties the power and energy capacities of the battery by a preset energy-to-power ratio of etp^{bat}. No reactive power capabilities are defined for the battery inverters, as no norms currently prescribe such a requirement. Operational nonlinearities regarding current, voltage, self-discharge, or cell aging are neglected in the linear modeling of the household battery at the energy level. Due to its computational advantages, such "generic" storage modeling has been common practice, as also adopted by most energy system modeling frameworks [44].

2.3.1.3 Electricity balance

At each timestep $t \in \mathcal{T}_m$, the energy balance for active and reactive power is maintained by the following constraints for a given node $i \in \mathcal{I}$:

$$\sum_{r \in \mathcal{R}^i} p_{i,r,t}^{\text{PV}} + p_{i,t}^{\text{bat,dch}} + p_{i,t}^{\text{imp}} = d_{i,t}^{\text{elec}} + p_{i,t}^{\text{bat,ch}} + \sum_{c \in \mathcal{C}^i} p_{i,c,t}^{\text{WB}} + p_{i,t}^{\text{HP}} + p_{i,t}^{\text{feed-in}}, \qquad \forall t \in \mathcal{T}_m \tag{2.6a}$$

$$\sum_{r \in \mathcal{R}^i} q_{i,r,t}^{\text{PV}} + q_{i,t}^{\text{imp}} = d_{i,t}^{\text{elec,q}} + q_{i,t}^{\text{HP}} + q_{i,t}^{\text{feed-in}}, \qquad \forall t \in \mathcal{T}_m \tag{2.6b}$$

where the terms $(p,q)_{i,t}^{\text{imp}} \geq 0$ and $(p,q)_{i,t}^{\text{feed-in}} \geq 0$ stand for the power withdrawn from or injected into the grid at a given time step, respectively. $p_{i,t}^{\text{BEV}}$ is the active power consumption of the wall box (see Section 2.3.3), $(p,q)_{i,t}^{\text{HP}}$ are the active and reactive power consumption of the heat pump (see Section 2.3.2), and $d_{i,t}^{\text{elec}}, d_{i,t}^{\text{elec,q}}$ are the exogenously provided time series for the active and reactive power demand of the electrical appliances in the building. In the basic sense, the electrical gain terms on the left-hand side are balanced by the loss terms on the right-hand side.

2.3.2 Heat side

2.3.2.1 Heat demand

Within each building, thermal energy has to be generated to satisfy the demand of space heating $d_{i,t}^{\text{sh}}$ and domestic hot water (DHW) $d_{i,t}^{\text{DHW}}$. Space heating refers to the heating of the living spaces of a building to maintain a comfortable temperature, whereas DHW is used for various occupant activities such as cooking, cleaning, bathing, or showering.

1R1C building model for space heat demand The space heating and DHW demands can be defined as exogenous parameters in case they are present, possibly through prior activity-based building heat demand simulation models such as *EnergyPlus* [45], *UrbanHeatPro* [46], or *CityEnergyAnalyst* [47]). Alternatively, the space heating demand can be optimized endogenously using a lumped parameter model such as one resistance and one capacitance (1R1C), analogously to the formulation implemented in the *UrbanHeatPro* tool[3] which is based on the calculation method proposed by TABULA [48]. Despite its simplicity, the 1R1C model has been found sufficiently accurate to capture the essential thermal behavior of buildings [49], [50]. It strikes a good balance between computational complexity and acceptable accuracy to be applied in an optimization environment. In practice, the challenge lies in finding accurate values for the lumped parameters, which can be identified by utilizing measurement data as described in [49]. If measurement data is lacking, one can match the building in question with the suitable average building from the TABULA typology [51].

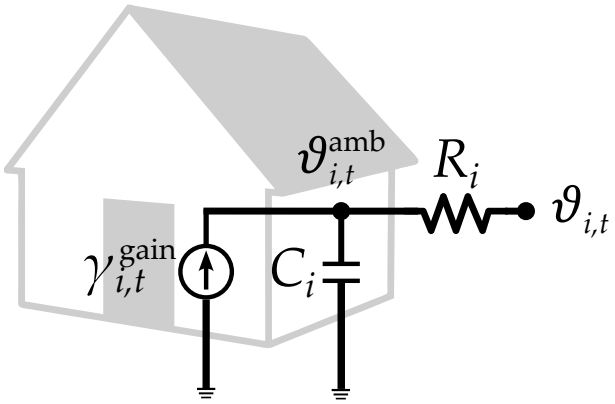

Figure 2.5: 1R1C model of a building to simulate thermal behavior.

The basic 1R1C model assumes a single temperature zone within the building envelope and lumps all the thermal properties of the building into the single thermal resistance and thermal capacitance parameters (see Figure 2.5). The equivalent thermal resistance of a building R_i (in K/W) represents the overall inverse conductivity of all the interfaces (e.g., walls, roof, windows, floor) through which heat transfer (in the form of transmission and ventilation) into and out of the building envelope takes place. A higher thermal resistance leads to lower heat loss or gains across the boundaries of the building, which is a characteristic of a well-insulated building. The equivalent resistance R_i consists of the inverse of the transmission and ventilation conductance components U_i and V_i, respectively:

$$R_i = \frac{1}{U_i + V_i}. \tag{2.7}$$

Transmission losses typically occur across surfaces of four types in a building, i.e., walls, windows, roof, and floor. Therefore, the overall transmission conductance U_i (the inverse

[3] https://github.com/tum-ens/UrbanHeatPro

resistance) of a building is constituted as the sum over all these surfaces:

$$U_i = U_i^{\text{wall}} \cdot A_i^{\text{wall}} + U_i^{\text{window}} \cdot A_i^{\text{window}} + U_i^{\text{roof}} \cdot A_i^{\text{roof}} + U_i^{\text{floor}} \cdot A_i^{\text{floor}}, \tag{2.8}$$

where $U_i^{\cdots}$ and $A_i^{\cdots}$ stand for the U-value in $\text{W/m}^2\cdot\text{K}$ and the total area of a given surface type in m^2, respectively. The U-value, or the surface heat transfer coefficient, depends on various factors such as the used material, configuration, and surface thickness.

Ventilation losses occur due to air recirculation due to building use (e.g. opening of windows or doors) and infiltration through unintentional openings, and the corresponding thermal resistance is calculated as follows:

$$V_i = c_p^{\text{air}} \cdot (n_i^{air,use} + n_i^{air,inf}) \cdot v_i, \tag{2.9}$$

where $n_i^{air,use}$ and $n_i^{air,inf}$ are the air change rates in 1/h due to building use and infiltration, v_i is the volume of the building envelope in m^3, and c_p^{air} is the volumetric heat capacity of air in $Wh/(m^3 \cdot K)$.

On the other hand, the thermal capacitance C_i in J/K quantifies the amount of heat that can be stored by all the building elements the building envelope contains. A higher thermal capacitance leads to higher thermal inertia, e.g., slower response to ambient temperature changes or heat gains. Similar to the transmission resistance, the elements of the roof, walls, and floor constitute a thermal capacitance:

$$C_i = m_i^{\text{roof}} \cdot c^{\text{roof}} + m_i^{\text{wall}} \cdot c^{\text{wall}} + m_i^{\text{floor}} \cdot c^{\text{floor}}, \tag{2.10}$$

where $m_i^{\cdots}$ and $c_i^{\cdots}$ stand for the respective building element's mass and specific heat capacity.

Consequently, the thermal circuit diagram for the 1R1C model is depicted in Figure 2.5. Here, $\vartheta_{i,t}$ stands for the uniform temperature of a building i, ϑ_t^{amb} is the ambient temperature, and $\gamma_{i,t}^{\text{gain}}$ the total heat gain of the building, each at a given time t. The following differential equation thus describes the thermal behavior of the building:

$$C_i \cdot \frac{d\vartheta_i}{dt} + \frac{1}{R_i} \cdot (\vartheta_i - \vartheta^{\text{amb}}) = \gamma_{i,t}^{\text{gain}}. \tag{2.11}$$

Assuming a discretization time step of Δt, the discrete backward Euler form of this equation then yields:

$$C_i \cdot \frac{\vartheta_{i,t} - \vartheta_{i,t-1}}{\Delta t} + \frac{1}{R_i} \cdot (\vartheta_{i,t} - \vartheta_t^{\text{amb}}) = \gamma_{i,t}^{\text{gain}}. \tag{2.12}$$

The total heat gains consist of

- the internal gains $\gamma_{i,t}^{\text{int}}$ from occupant activity inside the building,
- solar gains $\gamma_{i,t}^{\text{sol}}$ from the incident global solar radiation, and
- the heat generation $\gamma_{i,t}^{\text{sh,gen}}$ by the heating system in the building:

$$\gamma_{i,t}^{\text{gain}} = \gamma_{i,t}^{\text{int}} + \gamma_{i,t}^{\text{sol}} + \gamma_{i,t}^{\text{gen}}. \qquad \forall t \in \mathcal{T}_m \tag{2.13}$$

Then, solving (2.12) for $\gamma_{i,t}^{\text{sh,gen}}$ yields the heat production necessary to reach a building temperature of $\vartheta_{i,t}$ at a given time:

$$d_{i,t}^{\text{sh}} := \gamma_{i,t}^{\text{sh,gen}} = C_i \cdot \frac{\vartheta_{i,t} - \vartheta_{i,t-1}}{\Delta t} + \frac{1}{R_i} \cdot (\vartheta_{i,t} - \vartheta_t^{\text{amb}}) - \gamma_{i,t}^{\text{int}} - \gamma_{i,t}^{\text{sol}}. \qquad \forall t \in \mathcal{T}_m \tag{2.14}$$

Finally, maintenance of a comfortable range of building temperatures $[\vartheta_{i,t}^{\min}, \vartheta_{i,t}^{\max}]$ can be enforced at each model time step through the following inequalities:

$$\vartheta_{i,t}^{\min} \leq \vartheta_{i,t} \leq \vartheta_{i,t}^{\max}. \qquad \forall t \in \mathcal{T}_m \tag{2.15}$$

2.3.2.2 Heat pumps with an auxiliary heating unit

In the context of electrified heating, heat pumps (HPs) are deemed a highly efficient technology for building heat supply. In particular, air-source HPs have been selected over ground and gas-source variants in the model. Despite having efficiency disadvantages in very low ambient temperatures, air-source HPs are the most used type in Europe [52]. They can be employed independent of the access to groundwater and have significantly lower installation costs than the ground-source HPs. Moreover, they may have a low-emission operation as the electricity mix becomes decarbonized in the future, unlike the gas-source HPs, which require natural gas to operate.

Most heat pumps are equipped with an auxiliary, direct electric heating unit that can be deployed at times of peak demands, primarily due to extreme cold weather or high coincidence in domestic hot water demanding activities. Naturally, since these supplementary heating systems have an energy efficiency of only around one, their operating costs are much higher than the regular heat pump operation with a coefficient of performance (COP) of around in the heating periods [53]. However, they are significantly less costly to install, making the case for an operation at low-frequency time intervals with high peaks, i.e., a low number of full load hours.

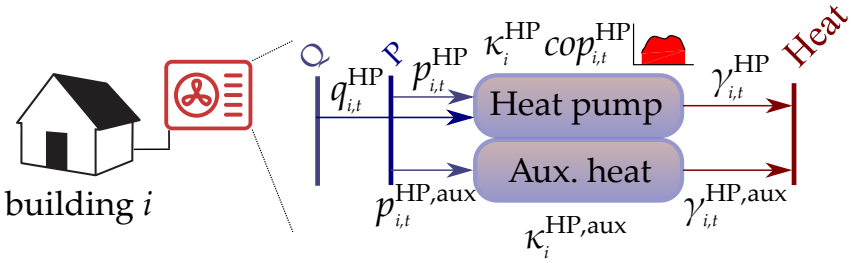

Figure 2.6: Reference energy representation for heat pumps with auxiliary heating units.

Figure 2.6 depicts the operation of the heat pump system. The eqs. (2.16a) to (2.16e) define the power consumption and the capacity restriction of the heat pump along with its auxiliary unit:

$$\gamma_{i,t}^{\mathrm{HP}} = p_{i,t}^{\mathrm{HP}} \cdot cop_{i,t}^{\mathrm{HP}}, \qquad \forall t \in \mathcal{T}_m \tag{2.16a}$$

$$q_{i,t}^{\mathrm{HP}} \cdot = p_{i,t}^{\mathrm{HP}} \cdot \tan(\phi^{\mathrm{HP}}), \qquad \forall t \in \mathcal{T}_m \tag{2.16b}$$

$$0 \leq p_{i,t}^{\mathrm{HP}} \leq \kappa_i^{\mathrm{HP}}, \qquad \forall t \in \mathcal{T}_m \tag{2.16c}$$

$$\gamma_{i,t}^{\mathrm{HP,aux}} = p_{i,t}^{\mathrm{HP,aux}} \cdot \eta^{\mathrm{HP,aux}}, \qquad \forall t \in \mathcal{T}_m \tag{2.16d}$$

$$0 \leq p_{i,t}^{\mathrm{HP,aux}} \leq \kappa_i^{\mathrm{HP,aux}}, \qquad \forall t \in \mathcal{T}_m \tag{2.16e}$$

where $\gamma_{i,t}^{\mathrm{HP}}$ is the heat output from the heat pump, $cop_{i,t}^{\mathrm{HP}}$ is the exogenously defined coefficient of performance (COP), and κ_i^{HP} is the electrical capacity, and $\tan(\phi)^{\mathrm{HP}}$ is the Q/P ratio of the heat pump. Likewise, $\gamma_{i,t}^{\mathrm{HP,aux}}$, $\eta^{\mathrm{HP,aux}}$ and $\kappa_{i,t}^{\mathrm{HP}}$ denote the heat output, the efficiency and the capacity of the auxiliary heating unit.

Distinct values for each hour can be used to factor in the COP variations depending on the ambient temperature. Here, a continuous operation of the heat pump between zero and the full load (complete modulation) is allowed in the model without any influence on the COP.

In contrast, most commercial single-stage heat pumps may only operate at full load in their current state of maturity. Although this representation is most suitable for the new generation of inverter-driven heat pumps with flexible operation ranges, this is also a valid formulation for single-load units. The modeled heat pump can be operated at full load for only a fraction of the hour, followed by a shutdown for the remaining period, thereby meeting a continuous range of total heat production $\gamma_{i,t}^{\mathrm{HP}}$ within an hour. Similar to PV, decision variables for heat pump installations $\beta_i^{\mathrm{HP}}, \beta_i^{\mathrm{HP,aux}}$ are modeled using the following equation:

$$0 \leq \kappa_i^{\mathrm{HP}} \leq M \cdot \beta_i^{\mathrm{HP}}, \tag{2.17}$$

$$0 \leq \kappa_i^{\mathrm{HP,aux}} \leq M \cdot \beta_i^{\mathrm{HP,aux}}, \tag{2.18}$$

where M is a large-valued parameter.

2.3.2.3 Sensible thermal storage

In addition to the thermal inertia of the building, flexibility in the heat supply can be achieved through sensible thermal storage systems typical for domestic use.

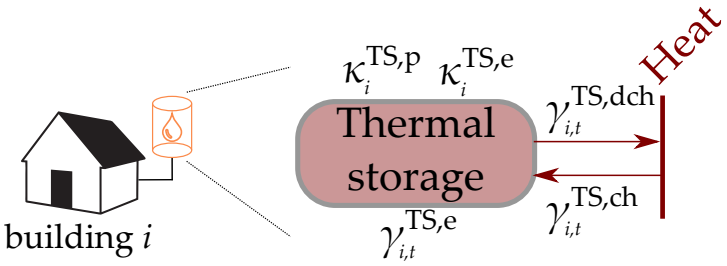

Figure 2.7: Reference energy representation for the thermal storage units.

Figure 2.7 depicts the operation of the thermal storage system. Analogous to the battery model (eqs. (2.5a) to (2.5e)), the thermal storage is modelled as follows:

$$\gamma_{i,t}^{\mathrm{TS,e}} = \gamma_{i,t-1}^{\mathrm{TS,e}} + \eta^{\mathrm{TS,ch}} \cdot \gamma_{i,t}^{\mathrm{TS,ch}} - \frac{\gamma_{i,t}^{\mathrm{TS,dch}}}{\eta^{\mathrm{TS,dch}}}, \qquad \forall t \in \mathcal{T}_m \tag{2.19a}$$

$$0 \leq \gamma_{i,t}^{\mathrm{TS,dch}} \leq \kappa_i^{\mathrm{TS,p}}, \qquad \forall t \in \mathcal{T}_m \tag{2.19b}$$

$$0 \leq \gamma_{i,t}^{\mathrm{TS,ch}} \leq \kappa_i^{\mathrm{TS,p}}, \qquad \forall t \in \mathcal{T}_m \tag{2.19c}$$

$$0 \leq \gamma_{i,t}^{\mathrm{TS,e}} \leq \kappa_i^{\mathrm{TS,e}}, \qquad \forall t \in \mathcal{T}_m \tag{2.19d}$$

$$\gamma_{i,0}^{\mathrm{TS,e}} = \gamma_{i,T_{\mathrm{end}}}^{\mathrm{TS,e}}, \tag{2.19e}$$

where the variable $\gamma_{i,t}^{\mathrm{TS,e}}$ expresses the energy content of the thermal storage unit at a given time, $\gamma_{i,t}^{\mathrm{TS}}, \gamma_{i,t}^{\mathrm{TS,dch}}$ are the hourly charged and discharged amounts of heat, and $\kappa_i^{\mathrm{TS,e}}, \kappa_i^{\mathrm{TS,p}}$ are the energy content and charge/discharge capacities of the storage unit, respectively.

2.3.2.4 Heat balance

The coverage of the hourly space and water heating demands $d_{i,t}^{\mathrm{sh}} + d_{i,t}^{\mathrm{dhw}}$ is maintained by the energetic heat balance equation (2.20):

$$\gamma_{i,t}^{\mathrm{HP}} + \gamma_{i,t}^{\mathrm{TS,dch}} = \gamma_{i,t}^{\mathrm{TS,ch}} + d_{i,t}^{\mathrm{sh}} + d_{i,t}^{\mathrm{dhw}} + \gamma_{i,t}^{\mathrm{vent}}, \qquad \forall t \in \mathcal{T}_m \tag{2.20}$$

where the space heating demand $d_{i,t}^{\mathrm{sh}}$ is determined by the thermal behavior of the building as per equation 2.14 and the domestic hot water demand $d_{i,t}^{\mathrm{dhw}}$ is provided exogenously. The variable $\gamma_{i,t}^{\mathrm{vent}}$ stands for the quantity of heat voluntarily expelled from the building via ventilation.

2.3.3 Mobility side

In addition to the conventional electrical appliances and heating, domestic charging demands for battery electric vehicles (BEVs) $d_{i,c}^{\text{mob}}$ are defined for each car $c \in \mathcal{C}^i$ that belongs to the occupants of each building i. A one-to-one correspondence between each BEV and wall box (WB) is assumed to avoid high modeling complexity brought by WB sharing between cars. In other words, there is precisely one wall box for each vehicle, and each charging station serves exactly one car.

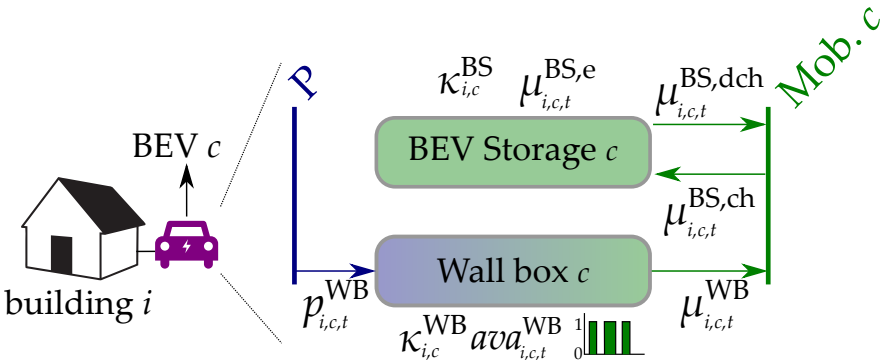

Figure 2.8: Reference energy representation for the battery electric vehicle (BEV) charging and storage units.

Figure 2.8 represents the energetic interactions of a given BEV. Each BEV system consists of a charging and a storage unit. Through the charging unit (the wall box), the electricity is converted into an electrical mobility commodity, for which the domestic charging demand $d_{i,c}^{\text{mob}}$ is defined. Since only the portion of the charging that takes place at home is considered, the charging is limited to when the corresponding BEV is present at its respective building. For each BEV, this information is provided exogenously as a time-variable binary parameter $ava_{i,c,t}^{\text{CS}}$. Assuming a conversion efficiency $\eta_{i,c}^{\text{CS}}$ and a rated power of $\kappa_{i,c}^{\text{WB}}$ per wall box, the respective operation is then governed by the following equation:

$$\mu_{i,c,t}^{\text{WB}} = ava_{i,c,t}^{\text{WB}} \cdot \eta_{i,c}^{\text{WB}} \cdot p_{i,c,t}^{\text{WB}}, \qquad \forall t \in \mathcal{T}_m \qquad \forall c \in \mathcal{C}^i \tag{2.21}$$

$$p_{i,c,t}^{\text{WB}} \leq \kappa_{i,c}^{\text{WB}}, \qquad \forall t \in \mathcal{T}_m \qquad \forall c \in \mathcal{C}^i \tag{2.22}$$

where $p_{i,c,t}^{\text{WB}}$ electrical input to the wall box, $\mu_{i,c,t}^{\text{WB}}$ is the electrical energy transferred to the BEV at a given time, and $\kappa_{i,c}^{\text{WB}}$ is the charging capacity of the wall box.

Although the hourly domestic charging demands are provided as set values for each time step, these demands can be satisfied flexibly in practice through intelligent charging. For instance, a daily demand of 5 kWh can be covered within the first hour of the BEV arrival at home or shifted to multiple evening hours to reduce grid loading or take advantage of variable electricity tariffs. To allow such flexible charging behavior, the battery of the BEV is incorporated into the model as a separate storage unit (the BEV storage)[4]. The BEV storage is modeled as a lossless storage unit with no self-discharge, a battery capacity of $\kappa_{i,c}^{\text{BS}}$, its

[4]The analogy between the storage unit and the flexible operation can be inferred by comparing the summation of (2.23a) for all time steps $\{0, \ldots, T_{\text{end}}\}$ with the equation (2.23e), leading to the following balance: $\sum_{t \in \mathcal{T}} \mu_{i,t}^{\text{BS,dch}} = \sum_{t \in \mathcal{T}} \mu_{i,t}^{\text{BS,ch}}$.

maximum rate of (dis)charging restricted by the wall box capacity $\kappa_{i,c}^{\text{WB}}$:

$$\mu_{i,c,t}^{\text{BS,e}} = \mu_{i,c,t-1}^{\text{BS,e}} + \mu_{i,c,t}^{\text{BS,ch}} - \mu_{i,c,t}^{\text{BS,dch}}, \qquad \forall t \in \mathcal{T}_m \qquad \forall c \in \mathcal{C}^i \tag{2.23a}$$

$$0 \leq \mu_{i,c,t}^{\text{BS,e}} \leq \kappa_{i,c}^{\text{BS}}, \qquad \forall t \in \mathcal{T}_m \qquad \forall c \in \mathcal{C}^i \tag{2.23b}$$

$$0 \leq \mu_{i,c,t}^{\text{BS,dch}} \leq \kappa_{i,c}^{\text{WB}}, \qquad \forall t \in \mathcal{T}_m \qquad \forall c \in \mathcal{C}^i \tag{2.23c}$$

$$0 \leq \mu_{i,c,t}^{\text{BS,ch}} \leq \kappa_{i,c}^{\text{WB}}, \qquad \forall t \in \mathcal{T}_m \qquad \forall c \in \mathcal{C}^i \tag{2.23d}$$

$$\mu_{i,c,0}^{\text{BS,e}} = \mu_{i,c,T_{\text{end}}}^{\text{BS,e}}, \qquad \forall c \in \mathcal{C}^i \tag{2.23e}$$

where $\mu_{i,c,t}^{\text{BS,ch}}$, $\mu_{i,c,t}^{\text{BS,dch}}$ represent the up- and downshift of the domestic charging demand at a given time.

2.3.3.1 Mobility balance

The aforementioned mobility variables are then incorporated into the energy balance of the electrical mobility commodity as follows:

$$\mu_{i,c,t}^{\text{WB}} = d_{i,c,t}^{\text{mob}} + \mu_{i,c,t}^{\text{BS,ch}} - \mu_{i,c,t}^{\text{BS,dch}}, \qquad \forall t \in \mathcal{T}_m \qquad \forall c \in \mathcal{C}^i \tag{2.24}$$

where $d_{i,c,t}^{\text{mob}}$ stands for the mobility demand of a BEV c at a building c at a given time t. This way, the optimization problem solver can decide on the optimal charging schedule while preserving the energy balance.

This concludes the modeling of the building components, their associated flexibilities, and the interactions between them. The following will describe the costs attached to the operation and installation of these components.

2.3.4 Costs for the prosumer

The costs that accrue in each building to be paid by the prosumer are associated with

- the investments in the DERs (PV, heat pump, batteries, and thermal storage)
- the payments for the electricity consumption (possibly including the capacity tariff)
- negative costs through the feed-in of excess PV electricity (in the form of a fixed feed-in tariff)

The mathematical depiction of these costs will be elaborated on in this Section.

PV and heat pump costs For PV and heat pump technologies, the annualized investment costs c_i^{PV} and c_i^{HP} are constituted as

$$\begin{aligned} c_i^{\text{HP}} = \quad & af^{\text{HP}} \cdot \left(c^{\text{HP,inv,fix}} \cdot \beta_i^{\text{HP}} + c^{\text{HP,inv,var}} \cdot \kappa_i^{\text{HP}} \right) \\ + \quad & af^{\text{HP,aux}} \cdot \left(c^{\text{HP,aux,inv,fix}} \cdot \beta_i^{\text{HP,aux}} + c^{\text{HP,aux,inv,var}} \cdot \kappa_i^{\text{HP,aux}} \right) \quad , \end{aligned} \tag{2.25}$$

$$c_i^{\text{PV}} = \sum_{r \in \mathcal{R}_i} af^{\text{PV}} \cdot \left(c^{\text{PV,inv,fix}} \cdot \beta_{i,r}^{\text{PV}} + c^{\text{PV,inv,var}} \cdot \kappa_{i,r}^{\text{PV}} \right), \tag{2.26}$$

where $af^{\{\dots\}}$ stands for the annuity factor for each investment and $c^{\text{PV,inv,fix}}$, $c^{\text{HP,inv,fix}}$, $c^{\text{HP,aux,inv,fix}}$, $c^{\text{PV,inv,var}}$, $c^{\text{HP,inv,var}}$, $c^{\text{HP,aux,inv,fix}}$ represent the investment cost components. The annuity factor

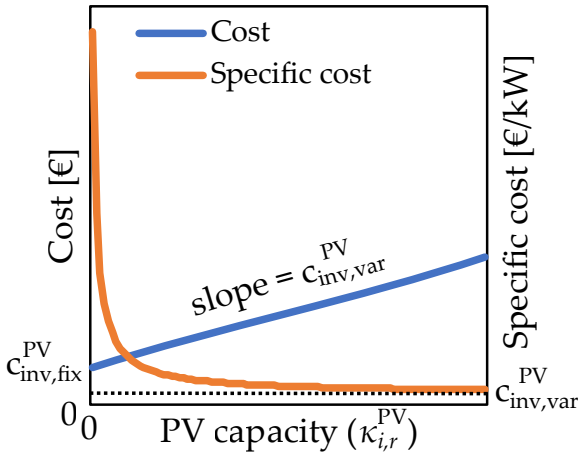

Figure 2.9: The fixed and capacity-dependent cost structure of PV installations.

is used to convert the one-off investment payments into annual installations and is calculated for each component as follows:

$$af = \frac{x \cdot (x+1)^N}{(x+1)^N - 1}, \tag{2.27}$$

where x and N stand for the weighted average cost of capital (WACC) and the economic lifetime of the component, respectively.

The investment costs consist of a fixed ($c^{\text{inv,fix}}$) and a capacity-dependent portion ($c^{\text{inv,var}}$). This way, the economies of scale in the DER installations can be incorporated into the model, as Figure 2.9 depicts in a stylized way for PV.

Storage costs The main costs associated with the storage units consist of capacity-dependent investment costs:

$$c_i^{\text{bat}} = af^{\text{bat}} \cdot c^{\text{bat,inv,var}} \cdot \kappa_i^{\text{bat,e}}, \tag{2.28}$$

$$c_i^{\text{TS}} = af^{\text{TS}} \cdot c^{\text{TS,inv,var}} \cdot \kappa_i^{\text{TS,e}}, \tag{2.29}$$

where $c^{\text{bat,inv,var}}, c^{\text{TS,inv,var}}$ stand for the specific investment costs of the storage units in €/kWh.

In order to prevent the unrealistic behavior of simultaneous charging and discharging of the storages ("unintended storage cycling" [54]), a low variable cost $c^{\text{sto},\epsilon}_{\text{spec}} = 0.001$ €/kW is attached to all storage operation:

$$c_i^{\text{sto},\epsilon} = c^{\text{sto},\epsilon}_{\text{spec}} \cdot \sum_{t \in \mathcal{T}} \omega_t \cdot \left(p_{i,t}^{\text{bat,dch}} + p_{i,t}^{\text{bat,ch}} + \gamma_{i,t}^{\text{TS,dch}} + \gamma_{i,t}^{\text{TS,ch}} + \mu_{i,t}^{\text{VMS,dch}} + \mu_{i,t}^{\text{VMS,ch}} \right), \tag{2.30}$$

where, ω_t is the corresponding weight of a time step t resultant from the time series aggregation (see Section 3.6). While this cost component is too small to significantly influence the optimal operation, it prevents unintended storage cycling without using an integer formulation, avoiding high computational complexity.

Electricity costs For each kWh withdrawn from the distribution grid, prosumers are charged a volumetric price $c^{\text{imp}}_{\text{spec},t}$. While the long-term dynamics between the network charge and the prosumer behavior are not modeled endogenously, a time step-dependent value can be set for this price to simulate time-variable network charges or dynamic prices.

$$c_i^{\text{imp}} = \sum_{t \in \mathcal{T}} \left(\omega_t \cdot c^{\text{imp}}_{\text{spec},t} \cdot p_{i,t}^{\text{imp}} \right). \tag{2.31}$$

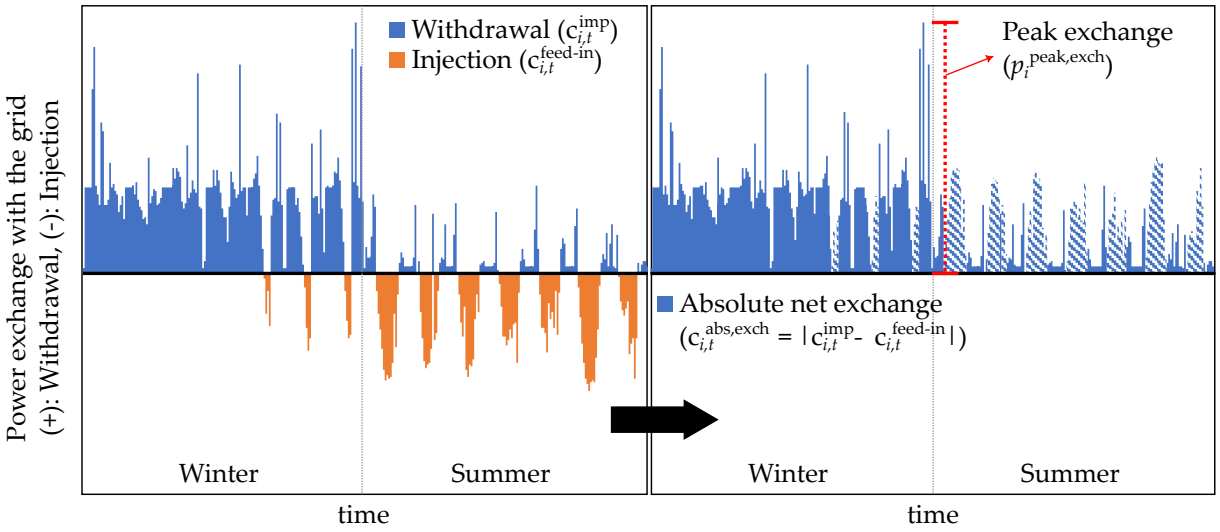

Figure 2.10: An example of a building's power exchange profiles in winter and summer. Winter is dominated by electricity withdrawal from the grid due to high heating demands, and summer is dominated by the injection of excess PV into the grid (left figure). In absolute terms, the net peak injection, corresponding to the capacity pricing, is caused by the short-term, high-power BEV charging on the last day of winter (right figure).

Feed-in revenue Conversely, for each kWh injection (feed-in) of excess PV electricity into the grid, the prosumers are remunerated an amount of $c_{\text{spec}}^{\text{feed-in}}$ (usually denoted as the feed-in tariff):

$$c_i^{\text{feed-in}} = -\sum_{t \in \mathcal{T}} \left(\omega_t \cdot c_{\text{spec}}^{\text{feed-in}} \cdot p_{i,t}^{\text{feed-in}} \right). \tag{2.32}$$

Capacity (peak) pricing Additional to the volumetric energy price as in 2.31, a peak-dependent capacity tariff can also be implemented into the model. Capacity tariffs usually relate to the portion of the network tariffs charged for the peak demand of the prosumer throughout the year, under a specific price set in €/kW each year. In Germany, small-scale customers, which make up most of the prosumers, are not yet charged for their peak behavior, while some countries, such as Belgium, introduced these charges to all grid users in 2023.

To implement capacity tariffs into the model, a peak exchange variable for each prosumer $p_i^{\text{peak,exch}}$ has to be defined. This variable represents the highest net power exchange (withdrawal or injection) of the prosumer with the grid throughout the entire period of the model (see Figure 2.10):

$$p_i^{\text{peak,exch}} = \max\{\max_{t \in \mathcal{T}}(p_{i,t}^{\text{imp}}), \max_{t \in \mathcal{T}}(p_{i,t}^{\text{feed-in}})\}. \tag{2.33}$$

However, *max* operations cannot be used in constraints directly in a MILP problem. As a workaround, an intermediate variable $p_{i,t}^{\text{abs,exch}}$ can be defined, which stands for the absolute value of the net power exchange at a given timestep:

$$p_{i,t}^{\text{abs,exch}} = |p_{i,t}^{\text{imp}} - p_{i,t}^{\text{feed-in}}|, \qquad \forall t \in \mathcal{T}_m \qquad \forall i \in \mathcal{I}^b \tag{2.34}$$

which can replace the right-hand side of (2.33) as follows:

$$p_i^{\text{peak,exch}} = \max_{t \in \mathcal{T}}(p_{i,t}^{\text{abs,exch}}). \tag{2.35}$$

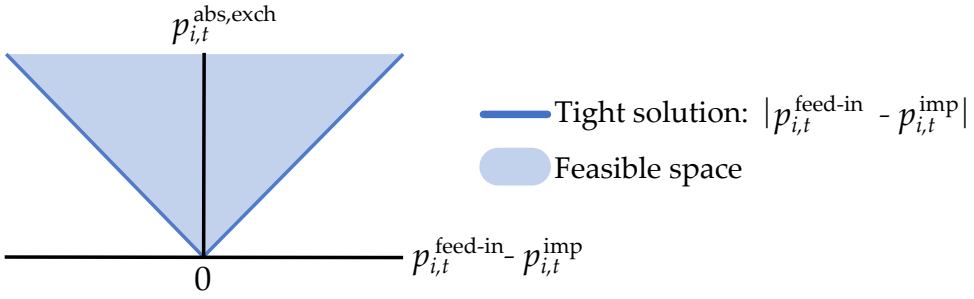

Figure 2.11: Depiction of the solution space formed by the equations (2.36) and (2.37) for defining the absolute net injection for each prosumer. These equations set a lower bound for the absolute net injection (light blue area), which is tightly binding at the optimum (dark blue line) due to the cost minimization.

The absolute value operation in (2.34) can be implemented in a relaxed manner via two inequalities (see Figure 2.11 for the intuition):

$$p_{i,t}^{\text{abs,exch}} \geq \quad p_{i,t}^{\text{imp}} - p_{i,t}^{\text{feed-in}}, \qquad \forall t \in \mathcal{T}_m \qquad \forall i \in \mathcal{I}^b \tag{2.36}$$

$$p_{i,t}^{\text{abs,exch}} \geq -p_{i,t}^{\text{imp}} + p_{i,t}^{\text{feed-in}}, \qquad \forall t \in \mathcal{T}_m \tag{2.37}$$

Indeed, these inequalities rather set the desired absolute value as a lower limit for the variable ($p_{i,t}^{\text{abs,exch}} \geq |p_{i,t}^{\text{feed-in}} - p_{i,t}^{\text{imp}}|$). Nonetheless, its involvement as a cost factor in the optimization problem will lead to a tight result at the solution—as long as the tolerance of the optimization solver is low enough. The peak net injection variable can then be defined as an upper limit for all net absolute injections throughout the year as follows, achieving the desired behavior of (2.35):

$$p_i^{\text{peak,exch}} \geq p_{i,t}^{\text{abs,exch}}, \qquad \forall t \in \mathcal{T}_m \tag{2.38}$$

Payments for the peak net injection are then incurred under a given capacity tariff $c_{\text{spec}}^{\text{CP}}$ as follows:

$$c_i^{\text{cap}} = c_{\text{spec}}^{\text{CP}} \cdot p_i^{\text{peak,exch}}. \tag{2.39}$$

In total, the building-side costs incurred for each prosumer sum up as follows:

$$c_i = c_i^{\text{HP}} + c_i^{\text{PV}} + c_i^{\text{bat}} + c_i^{\text{TS}} + c_i^{\text{sto},\epsilon} + c_i^{\text{imp}} + c_i^{\text{feed-in}} + c_i^{\text{cap}}. \tag{2.40}$$

2.3.5 Formulation of the HOODS-Bui optimization problem

Together with the operational constraints described in Sections 2.3.1 to 2.3.3 and the costs elaborated in Section 2.3.4, the optimal building component dimensioning and operation problem for the prosumer (HOODS-Bui) in a given building i can be established as follows:

HOODS-BUI(i):

$$\begin{aligned}\min_{\boldsymbol{\kappa}_i,\boldsymbol{\epsilon}_i} \quad & c_i = c_i^{\text{HP}} + c_i^{\text{PV}} + c_i^{\text{bat}} + c_i^{\text{TS}} + c_i^{\text{sto},\epsilon} + c_i^{\text{imp}} + c_i^{\text{feed-in}} + c_i^{\text{cap}} \\ \text{s.t.} \quad & (2.1-2.4), (2.5a-2.5f), (2.6a-2.6b), \\ & (2.14-2.15), (2.16a), (2.16b), (2.16c), (2.16d), (2.16e), (2.17-2.18), \\ & (2.19a-2.19e), (2.20), (2.21-2.22), (2.23a-2.23e), (2.24), \\ & (2.25-2.26), (2.28-2.32), (2.36-2.38), (2.39),\end{aligned}$$

where, for brevity, the DER capacity variables are grouped into

$$\boldsymbol{\kappa}_i = \begin{bmatrix} \kappa_{i,r}^{\text{PV}}, \beta_{i,r}^{\text{PV}}, & \forall r \in \mathcal{R}^i \\ \kappa_i^{\text{bat,e}}, \kappa_i^{\text{bat,p}}, \kappa_i^{\text{HP}}, \kappa_i^{\text{HP,aux}}, \beta_i^{\text{HP}}, \kappa_i^{\text{TS,e}}, \kappa_i^{\text{TS,p}} & \end{bmatrix}, \tag{2.41}$$

the operation variables into

$$\boldsymbol{\epsilon}_i = \begin{bmatrix} p_{i,r,t}^{\text{PV}}, q_{i,r,t}^{\text{PV}}, p_{i,r,t}^{\text{PV,curt}}, & \forall t \in \mathcal{T}_m & \forall r \in \mathcal{R}^i \\ p_{i,t}^{\text{HP}}, q_{i,t}^{\text{HP}}, \gamma_{i,t}^{\text{HP}}, \gamma_{i,t}^{\text{HP,aux}}, p_{i,t}^{\text{HP,aux}}, & \forall t \in \mathcal{T}_m & \\ p_{i,t}^{\text{bat,ch}}, p_{i,t}^{\text{bat,dch}}, \epsilon_{i,t}^{\text{bat,e}}, \gamma_{i,t}^{\text{TS,ch}}, \gamma_{i,t}^{\text{TS,dch}} \gamma_{i,t}^{\text{TS,e}}, & \forall t \in \mathcal{T}_m & \\ p_{i,c,t}^{\text{WB}}, \mu_{i,c,t}^{\text{WB}}, \mu_{i,c,t}^{\text{BS,dch}}, \mu_{i,t}^{\text{BS,ch}}, \mu_{i,t}^{\text{BS,e}} & \forall t \in \mathcal{T}_m & \forall c \in \mathcal{C}^i \\ p_{i,t}^{\text{imp}}, q_{i,t}^{\text{imp}}, p_{i,t}^{\text{feed-in}}, q_{i,t}^{\text{feed-in}}, p_{i,t}^{\text{abs,exch}}, & \forall t \in \mathcal{T}_m & \\ p_i^{\text{peak,exch}} & & \end{bmatrix}. \tag{2.42}$$

This is a mixed-integer linear programming problem, which can be solved relatively efficiently with off-the-shelf solvers such as Gurobi or CPLEX. See Appendix A.1 for the complete problem formulation.

2.4 Bridging between HOODS-Bui and HOODS-Grid

As discussed in Section 2.2, the prosumer optimization model HOODS-Bui is tied with the grid operator optimization model HOODS-Grid in a sequential game. On the one hand, this approach simulates the status-quo practice, dropping the assumption of holistic system coordination and replacing it with a two-level process. This allows the simulation of the non-cooperativeness between these agents, reflecting the current reality better. On the other hand, it will enable a highly scalable formulation as the models for solving the building (sub)problems are now independent of each other.

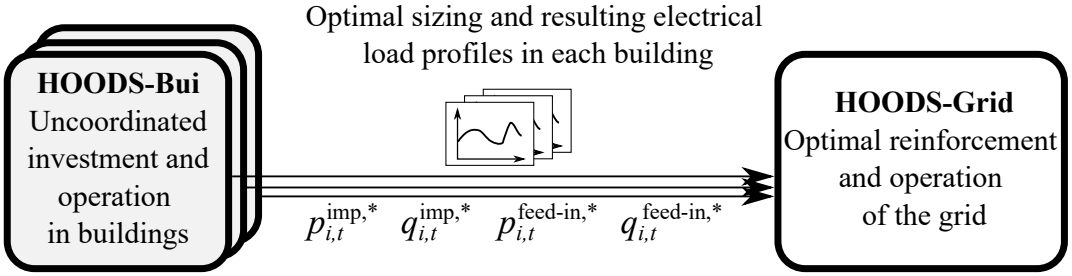

Figure 2.12: The sequential optimization procedure.

The procedure for the sequential approach is illustrated in Figure 2.12 and operates as follows:

1. First, each prosumer $i \in \mathcal{I}^b$ runs their respective, grid-unaware HOODS-Bui subproblem, optimizing their DER capacities and operation with a cost-minimizing goal,

2. Resulting from these subproblems of each prosumer $i \in \mathcal{I}^b$, the grid operator receives the optimized prosumer power withdrawal and feed-in profiles $p_{i,t}^{\text{imp}*}, q_{i,t}^{\text{imp}*}, p_{i,t}^{\text{feed-in}*}$, $q_{i,t}^{\text{feed-in}*}$, $\forall t \in \mathcal{T}_m$ in their respective nodes. The net nodal injections are then fixed at these profiles in the grid problem:

$$p_{i,t}^{\text{net}} = p_{i,t}^{\text{imp}*} - p_{i,t}^{\text{feed-in}*}, \qquad \forall t \in \mathcal{T}_m \qquad \forall i \in \mathcal{I}^b \tag{2.43}$$

$$q_{i,t}^{\text{net}} = q_{i,t}^{\text{imp}*} - q_{i,t}^{\text{feed-in}*}. \qquad \forall t \in \mathcal{T}_m \qquad \forall i \in \mathcal{I}^b \tag{2.44}$$

   In essence, the prosumer operation is externalized into preset time series of positive and negative loads for the grid operator. For the rest of the buses where no buildings or the main busbar (MBB) is located, the net injections are set to zero:

$$p_{i,t}^{\text{net}} = 0, \qquad \forall t \in \mathcal{T}_m \qquad \forall i \in \mathcal{I} \setminus (\mathcal{I}^b \cup \text{MBB}) \tag{2.45}$$

$$q_{i,t}^{\text{net}} = 0. \qquad \forall t \in \mathcal{T}_m \qquad \forall i \in \mathcal{I} \setminus (\mathcal{I}^b \cup \text{MBB}) \tag{2.46}$$

3. Anticipating the emerging load profiles, the DSO has to now decide on the optimal grid planning and operation corresponding to the minimal costs while respecting all grid constraints (this model is denoted by HOODS-Grid).

Note that it is not aimed to simulate a practical planning or market mechanism through this sequential approach. The grid operators usually do not have access to the necessary instrumentation to anticipate the consumer load profiles in such granular detail—intelligent metering systems with communication units are still not widespread in many countries. In Germany, the penetration of these meters is less than 1% as of 2022 [55]. Further, target grid planning does not take place in such an immediate fashion—it is a long-term process usually spanning up to multiple decades and necessitating reliable forecasts and safety factors. Rather, the main goals of implementing this paradigm are

- to analyze the existing grid capacities and the need for reinforcement in non-cooperative (and thus more realistic) system operation, where system-wide flexibilities may not be exploited to their fullest potential due to the impracticality of global optimization and

- to quantify the welfare losses that are suffered in such non-cooperative settings.

2.5 HOODS-Grid: Modeling of the LV grid optimization

This Section deals with the formulation of the above-mentioned LV grid optimization model. It begins with a description of the underlying power flow model *linearized distribution flow (LinDistFlow)*, followed by the modeling of the grid reinforcement and relief measures and the costs attached to these.

2.5.1 *LinDistFlow* power flow model

Power flow within a grid is governed by a system of equations that is non-convex for the system state variables. Therefore, approximations of these non-convex power flow equations have to be made to formulate the load flows within a convex optimization problem. In particular, considering the high model complexity brought by the integer grid reinforcement formulations, a linear model is necessary to achieve a tractable model that can be applied to any LV grid with a respectable size, with simulations spanning a temporal scope large enough to capture the relevant daily and seasonal variations. To this end, the *LinDistFlow* model [56] is employed.

Derivation of the *LinDistFlow* model. Before deriving the *LinDistFlow* formulation along with the necessary assumptions, the balanced alternating current (AC) power flow equations are introduced. By abuse of notation, the temporal indexing of the variables is refrained from for brevity.

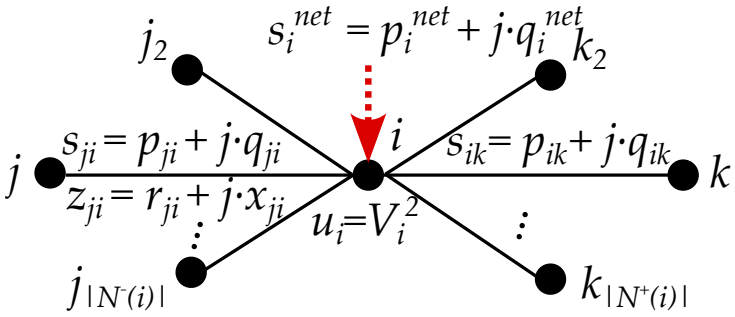

Figure 2.13: Balanced AC power flow into and from a node.

In a balanced system, the *branch flow model* [57] for the AC power flow over a line set of lines interfacing with a given bus i, as illustrated in Figure 2.13, consists of the following equations for each bus $i \in \mathcal{I}$:

$$\text{Ohm's law:} \qquad V_i = V_j - z_{ji} \cdot I_{ji}, \qquad \forall j \in \mathcal{N}^-(i) \quad (2.47a)$$

$$\text{Branch power flow:} \qquad s_{ji} = V_j \cdot (I_{ji})^*, \qquad \forall j \in \mathcal{N}^-(i) \quad (2.47b)$$

$$\text{Bus power balance:}^5 \qquad s_i^{net} + \sum_{j \in N^-(i)} \left(s_{ji} - z_{ji}|I_{ji}|^2\right) = \sum_{k \in N^+(i)} s_{ik}, \quad (2.47c)$$

where V_i and s_i^{net} stand for the complex voltage and net bus injection for a given bus i, while z_{ji}, I_{ji} and s_{ji} denote the complex impedance, current and power flow over a given line ji connecting buses i and j. $N^+(i)$ and $N^-(i)$ represent the sets of the successor and predecessor buses of a given bus i. Multiplying both sides of (2.47a) with their complex conjugates yields:

$$\begin{aligned} V_i \cdot V_i^* &= (V_j - z_{ji} \cdot I_{ji}) \cdot (V_j - z_{ji} \cdot I_{ji})^*, \\ V_i^2 &= V_j^2 - V_j \cdot z_{ji}^* \cdot I_{ji}^* - V_j^* \cdot z_{ji} \cdot I_{ji} + |z_{ji}|^2 \cdot I_{ji}^2, \\ V_i^2 &= V_j^2 - 2 \cdot \mathrm{Re}[z_{ji}^* \cdot V_j \cdot I_{ji}^*] + |z_{ji}|^2 \cdot I_{ji}^2, \\ u_i &= u_j - 2 \cdot r_{ji} \cdot p_{ji} - 2 \cdot x_{ji} \cdot q_{ji} + (r_{ji}^2 + x_{ji}^2) \cdot l_{ji}, \qquad \forall ji \in \mathcal{L} \quad (2.48) \end{aligned}$$

where $u_i = V_i^2$ and $l_{ji} = I_{ji}^2$ denote the squared voltage and current magnitudes respectively. Similarly, taking the magnitude squares in (2.47b) gives:

$$\frac{|s|_{ji}^2}{u_j} = \frac{p_{ji}^2 + q_{ji}^2}{u_i} = l_{ji}. \qquad \forall ji \in \mathcal{L} \quad (2.49)$$

Finally, separating the real and imaginary parts of (2.47c) one gets:

$$p_i^{net} + \sum_{j \in N^-(i)} \left(p_{ji} - r_{ji} \cdot l_{ji}\right) = \sum_{k \in N^+(i)} p_{ik}, \qquad \forall i \in \mathcal{I} \quad \text{(2.50a)}$$

$$q_i^{net} + \sum_{j \in N^-(i)} \left(q_{ji} - x_{ji} \cdot l_{ji}\right) = \sum_{k \in N^+(i)} q_{ik}. \qquad \forall i \in \mathcal{I} \quad \text{(2.50b)}$$

Here, the notation defined earlier for the set of lines $\mathcal{L}$ and buses $\mathcal{I}$ is adopted. Thereby, equations (2.48), (2.49), (2.50a), and (2.50b) form a system of $2 \cdot |\mathcal{L}| + 2 \cdot |\mathcal{I}|$ nonlinear equations, which constitutes the *DistFlow* model. For a known set of power injections $p_i^{net}, q_i^{net} \quad \forall i \in \mathcal{I}$ and substation voltage u_0, one would arrive at a sum of $3 \cdot |\mathcal{L}| + |\mathcal{I}| - 1$ variables (for current, reactive and active power magnitudes over each line and voltages for each non-substation bus). For a radial grid topology, the corresponding graph is a tree, i.e., $|\mathcal{L}| = |\mathcal{I}| - 1$. Thereby, for radial networks, the *DistFlow* model consists of an equal number of equations and variables, leading to a unique power flow solution. These solutions can be effectively calculated using common methods such as Newton's method. Indeed, for meshed grids, additional, nonlinear cycle conditions are needed to ensure a consistent set of voltage angles, increasing the complexity [58]. Nevertheless, most distribution grids in the low-voltage level are configured radially due to the simplicity of design and observation [59].

The case of an *optimal* power flow (OPF), on the other hand, deals with the possibility of choosing the optimal grid operation by defining further degrees of freedom to the system, such as for the power injections. In reaching this optimum, the solution should also respect various system restrictions such as thermal line capacities or voltage limits. Yet, while the set of equations $2|\mathcal{L}| + 2|\mathcal{I}|$ sufficiently describes the state of a balanced grid, its non-convex nature prevents the utilization of efficient optimization algorithms for realistically large systems.

In order to achieve tractability, convex relaxations and approximations are often applied to the original set of equations (a survey of such various methods can be found in [58]). *Relaxations* may operate by turning strict equalities of the non-linear equations into inequalities—such as in the second order cone programming (SOCP) relaxation [60]; or remove the rank-1 constraint of a voltage product matrix $\mathbf{V} \cdot \mathbf{V}^H$—such as in the semi-definite programming (SDP) relaxation [61]. When the relaxed conditions are observed in the solution, a so-called *exactness* is achieved, and a feasible global optimum to the power flow problem is ensured. While these methods are mathematically proven to provide exact results for balanced radial grids, the persisting nonlinearities hurt their scalability as model complexity increases.

Approximations, on the other hand, work by introducing assumptions to the model, usually to simplify the model constraints while only sacrificing a moderate accuracy. Typical examples are the direct current (DC) power flow [62] and *LinDistFlow* formulations. While the DC power flow model is proven to provide efficient and adequately accurate results for transmission system models, it neglects the aspects of reactive power flow and considerable voltage variations between buses, which are prevalent in lower-voltage distribution systems. *LinDistFlow*, on the other hand, strikes a good balance of allowing the consideration of these aspects and high computational efficiency thanks to its linear formulation. It is commonly used in similar studies that deal with balanced AC-OPF in distribution networks (some examples are [63], [64], [65], [66], and [67]).

Assuming relatively smaller losses, the linear formulation of the *LinDistFlow* model is achieved by dropping all terms associated with the losses, i.e., $r \cdot l, x \cdot l$ and $(r_{ji}^2 + x_{ji}^2)$ from the equations (2.48), (2.50a), and (2.50b). This simplification, along with a reduction of the precedent bus set $N^+(i)$ cardinality to 1 resultant of a radial configuration, leads to the following set of equations (now reintroducing the temporal subscripts for completeness):

***LinDistFlow* equations**

$$u_{i,t} = u_{j,t} - 2 \cdot r_{ji} \cdot p_{ji,t} - 2 \cdot x_{ji} \cdot q_{ji,t}, \qquad \forall t \in \mathcal{T}_m \quad \forall ji \in \mathcal{L} \quad (2.51)$$

$$p^{\text{net}}_{i,t} + p_{ji,t} = \sum_{k \in N^+(i)} p_{ik,t}, \qquad \forall t \in \mathcal{T}_m \quad \forall i \in \mathcal{I} \quad (2.52)$$

$$q^{\text{net}}_{i,t} + q_{ji,t} = \sum_{k \in N^+(i)} q_{ik,t}. \qquad \forall t \in \mathcal{T}_m \quad \forall i \in \mathcal{I} \quad (2.53)$$

Note that, by abuse of notation, in equations that are defined for a particular bus i, i.e., (2.52) and (2.53), j denotes the single predecessor node of i in the radial setting. Also note that the equations eqs. (2.51) to (2.53) are equivalent to the active and reactive power balance equations (2.6a) and (2.6b) presented earlier, where the overall net injections $p^{net}_{i,t}$ and $p^{net}_{i,t}$ are constituted by the corresponding operation of the presented building components.

2.5.2 Grid reinforcement measures

Conventional grid planning protocols primarily deal with overloading and voltage challenges by reinforcing the grid components. On rarer occasions, adjustments to the switching mechanism or voltage control might be made. While there is a range of protocols for designing distribution grids, each DSO determines its individual approach based on its history and operational context. Widely used strategies involve upgrading to higher-capacity transformers or parallel cable reinforcement. Another approach is grid reconfiguration or segmentation, possibly through the inclusion of a new transformer [68].

Figure 2.14 illustrates the two types of grid reinforcement measures that are allowed in this model: i) the addition of parallel lines and ii) replacing the conventional, fixed ratio transformer (FRT) with a voltage regulating distribution transformer (VRDT), possibly having a larger capacity. These measures have been assigned high practical relevance for alleviating grids in the rise of PV uptake, as shown in a survey made with ten German grid operators [69]. The other measures mentioned in the survey, such as wide-area control, involve medium voltage (MV)-LV grid interactions, which are not covered by the exclusively LV grid scope of this model. Similarly, local segmentation of the grid was not included as a tractable formulation was not achievable within the proposed MILP formulation.

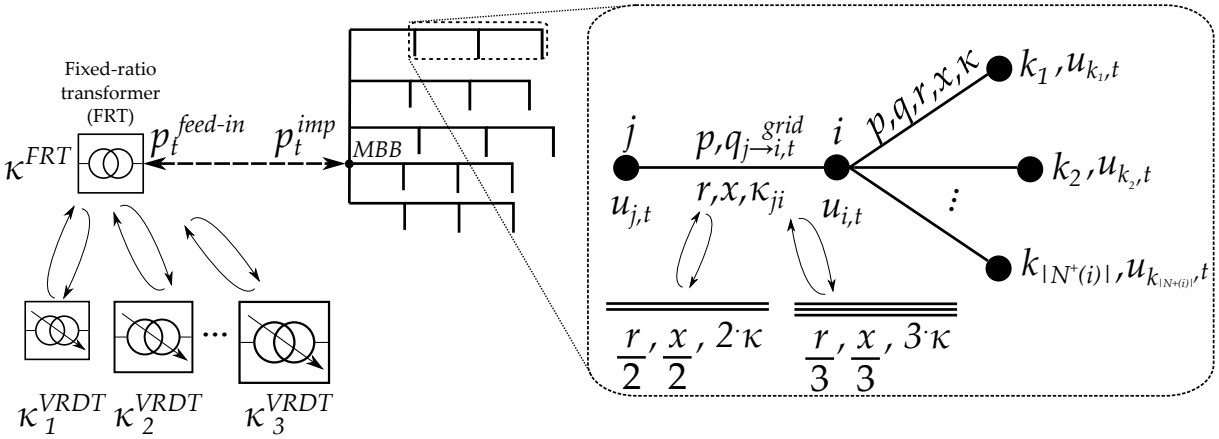

a) Replacement with VRDTs of various capacities b) Reinforcement of connections via parallel cabling

Figure 2.14: Distribution grid reinforcement measures as defined in the model.

2.5.2.1 Parallel line reinforcement

The first grid reinforcement measure considered in the model is parallel line reinforcement. The grid-relieving functions of parallel cable installations are twofold: i) additional parallel lines not only increase the power transfer capacity by increasing the effective conductor area but also ii) the voltage drop for a given loading is reduced thanks to a smaller effective impedance of the line. The reinforcement of the connection $ji \in \mathcal{L}$ between a given pair of buses j, i is realized by installing a second or third parallel cable. The single, double, and triple cable settings for a given cable type are denoted by {I, II, III}. Here, a formulation akin to [31] is employed and, similar to transformers, these cable settings are modeled as discrete, mutually exclusive options $\alpha^{\mathrm{I}}_{ji}, \alpha^{\mathrm{II}}_{ji}, \alpha^{\mathrm{III}}_{ji}$ for each line section ji:

$$\sum_{m \in \{\mathrm{I,II,III}\}} \alpha^{m}_{ji} = 1. \qquad \forall ji \in \mathcal{L} \tag{2.54}$$

The effective power flow between two buses is then given as the sum over all possible cable settings:

$$p_{ji,t} = \sum_{m \in \{\mathrm{I,II,III}\}} p^{m}_{ji,t}, \qquad \forall t \in \mathcal{T}_m \qquad \forall ji \in \mathcal{L} \tag{2.55a}$$

$$q_{ji,t} = \sum_{m \in \{\mathrm{I,II,III}\}} q^{m}_{ji,t}. \qquad \forall t \in \mathcal{T}_m \qquad \forall ji \in \mathcal{L} \tag{2.55b}$$

Assuming a single cable of this type has i) a thermal apparent power capacity of κ^{cable} derived from the maximum allowable current, ii) a reactance of x^{cable}, and iii) a resistance of r^{cable}, the corresponding electrical parameters of each setting can be calculated as follows:

$$\kappa^{\mathrm{I}}_{ji} = \kappa^{\text{cable}}, \qquad r^{\mathrm{I}}_{ji} = r^{\text{cable}}, \qquad x^{\mathrm{I}}_{ji} = x^{\text{cable}}, \tag{2.56a}$$

$$\kappa^{\mathrm{II}}_{ji} = 2 \cdot \kappa^{\text{cable}}, \qquad r^{\mathrm{II}}_{ji} = \frac{r^{\text{cable}}}{2}, \qquad x^{\mathrm{II}}_{ji} = \frac{x^{\text{cable}}}{2}, \tag{2.56b}$$

$$\kappa^{\mathrm{III}}_{ji} = 3 \cdot \kappa^{\text{cable}}, \qquad r^{\mathrm{III}}_{ji} = \frac{r^{\text{cable}}}{3}, \qquad x^{\mathrm{III}}_{ji} = \frac{x^{\text{cable}}}{3}. \tag{2.56c}$$

The thermal apparent power capacities κ^{cable} can be calculated using the thermal current limits I^{max} for each cable as follows:

$$\kappa^{\text{cable}} = \sqrt{3} \cdot V^{\text{rated}} \cdot I^{max}, \tag{2.57}$$

and adjusted according to the German DIN VDE 0276-60 norm with respect to the operational conditions. The line capacities restrict the active and reactive power through the maximum allowable apparent power:

$$\left(p^{m}_{ji,t}\right)^2 + \left(q^{m}_{ji,t}\right)^2 \leq \left(\kappa^{m}_{ji}\right)^2 \cdot \alpha^{m}_{ji}. \qquad \forall ji \in \mathcal{L} \tag{2.58}$$

Mixed-integer problems with convex quadratic constraints such as (2.58) belong to a class known as mixed-integer quadratically constrained problems (MIQCP), and they can be solved by commercial solvers. However, they scale badly in the presence of multi-period models with investment planning. Therefore, the linearized formulation proposed in [70] is adopted, with the angle intervals of $\frac{\pi}{4}$:

$$a_y \cdot p^{m}_{ji,t} + b_y \cdot q^{m}_{ji,t} \leq c_y \cdot \kappa^{m}_{ji} \cdot \alpha^{m}_{ji}, \quad \forall m \in \{\mathrm{I,II,III}\} \;\; \forall y \in \{1, 2, \ldots, 8\} \;\; \forall t \in \mathcal{T}_m \;\; \forall ji \in \mathcal{L} \tag{2.59}$$

Table 2.2: Coefficients for the constraint (2.59).

y	a_y	b_y	c_y
1	1	$\sqrt{2}+1$	$\sqrt{2}+1$
2	1	$\sqrt{2}-1$	1
3	1	$-\sqrt{2}+1$	1
4	-1	$\sqrt{2}+1$	$\sqrt{2}+1$
5	-1	$-\sqrt{2}-1$	$\sqrt{2}+1$
6	-1	$-\sqrt{2}+1$	1
7	-1	$\sqrt{2}-1$	1
8	1	$-\sqrt{2}-1$	$\sqrt{2}+1$

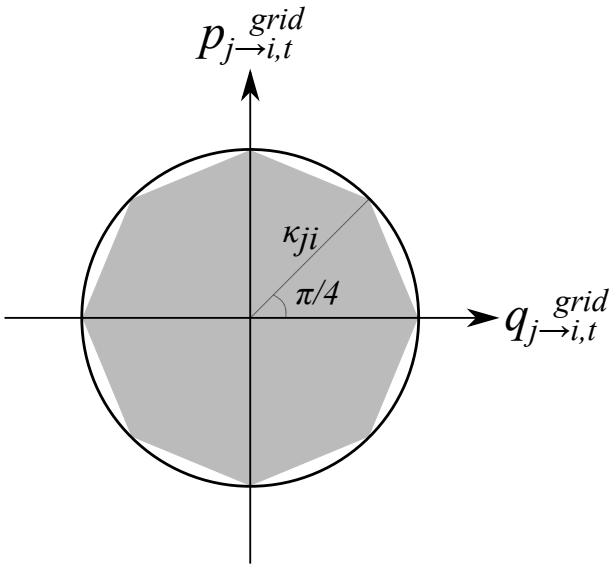

Figure 2.15: Linearized feasible space given a thermal line limit of κ_{ji} and angle steps $\pi/4$.

where $a_y, b_y, c_y \; \forall y \in \{1, 2, \ldots, 8\}$ compose the set of coefficients that define the regular octagon inscribed inside the original feasible space (See Table 2.2 for the set of coefficients and Figure 2.15 for the resultant space).

As each cable setting has a differently scaled impedance, the *LinDistFlow* voltage drop equation (2.54) has to be modified to tie the corresponding voltage drops with all possible cable settings between each bus. As the mutual exclusivity constraint (2.54) allows only a single setting (and hence power flow through that setting) to be built for each cable section, this can be achieved with a sum expression as follows:

$$u_{i,t} = u_{j,t} - 2 \cdot \sum_{m \in \{\mathrm{I,II,III}\}} \left(r^m_{ji} \cdot p^m_{ji,t} + x^m_{ji} \cdot q^m_{ji,t} \right). \qquad \forall t \in \mathcal{T}_m \qquad \forall i \in \mathcal{I} \qquad (2.60)$$

2.5.2.2 Replacement of the FRT with a VRDT

In order to increase the total capacity of a low-voltage distribution system for injecting and absorbing power, another passive measure is to replace its feeding transformer. While on-load tap changing transformers are commonplace for transmission grids, usually fixed ratio transformers (FRTs) are used in low-voltage distribution grids. The tap ratios of FRTs are set during the installation in a static manner to maintain the suitable voltage levels between the medium- and low-voltage grids. Only in rare circumstances that change the load characteristics in a sustained state can the transformer be de-energized to adjust the tap ratio. Thus, they are also called de-energized tap changer transformers [71].

A voltage regulating distribution transformer (VRDT), on the other hand, offers a solution to address the challenges posed by the emerging electrical loads in distribution grids. It incorporates an active controlling element that enables on-load adjustment of the tap ratio. This flexibility allows the VRDT to maintain the voltage quality of the grid, considering the varying loading or feed-in requirements. This capability becomes increasingly crucial due to the growing adoption of new electric loads like heat pumps, electric mobility, and the rising number of PV installations. These factors often push distribution grids to their limits, necessitating a transformer that can adapt to different situations. The added degree of freedom through the variable tap ratios via VRDT effectively increases the allowable range for over- and under-voltages within the grid dynamically. In this, it uses real-time voltage measurements [72]. While an FRT can theoretically be *upgraded* to a VRDT by installing the necessary control elements into the existing transformer, usually incompatibilities exist in terms of the necessary tank structure, volume of oil, and cooling systems, deeming an appropriate conversion impractical. The total replacement of the transformer is often necessary [71].

In order to model the decision of replacing an existing FRT that has a capacity of κ^{FLT}, with a given set of VRDT options $\mathcal{O}$ having capacities of κ_o^{VRDT} for each VRDT $o \in \mathcal{O}$, corresponding binary variables α^{FRT} and α_o^{VRDT} $\forall o \in \mathcal{O}$ are defined first. To ensure the mutual exclusivity of transformer installations, i.e., restricting the planning to choosing a single class o, the following constraint is introduced:

$$\alpha^{\text{FRT}} + \sum_{o \in \mathcal{O}} \alpha_o^{\text{VRDT}} = 1. \tag{2.61}$$

Note that this formulation does not exclude the modeling of parallelly connected VRDTs–this can still be achieved by defining a transformer class o that represents a bundle of VRDTs with the respective collective capacity of κ_o^{VRDT}. However, it restricts the model to having only a single point of connection between the LV and the MV grid.

The power supply from the transformer can be related to the grid injection terms at the main busbar (MBB) of the grid as follows:

$$p^{\text{net}}_{\text{MBB},t} = p^{\text{imp}}_{\text{MBB},t} - p^{\text{feed-in}}_{\text{MBB},t}, \qquad \forall t \in \mathcal{T}_m \tag{2.62}$$

$$q^{\text{net}}_{\text{MBB},t} = q^{\text{comp}}_{\text{MBB},t}, \qquad \forall t \in \mathcal{T}_m \tag{2.63}$$

where $p^{\text{imp}}_{\text{MBB},t}$ and $p^{\text{feed-in}}_{\text{MBB},t}$ stand for the active power withdrawal and injection, and $q^{\text{comp}}_{\text{MBB},t}$ the reactive power supply from the transformer, through the main busbar, into the grid. The capacity of the built transformer to carry this power flow is then tied to the investment decision as follows:

$$a_y \cdot p^{\text{net}}_{\text{MBB},t} + b_y \cdot q^{\text{net}}_{\text{MBB},t} \leq c_y \cdot \left(\alpha^{\text{FRT}} \cdot \kappa^{\text{FLT}} + \sum_{o \in \mathcal{O}} \alpha_o^{\text{VRDT}} \cdot \kappa_o^{\text{VRDT}}\right). \qquad \forall t \in \mathcal{T}_m \qquad \forall y \in \{1, 2, \ldots, 8\} \tag{2.64}$$

Note that, here, the same linearization of the apparent power is used as the one for the thermal line limits (2.59).

Allowable voltage bands. As mentioned above, VRDTs also assist the grid in respecting the over- and under-voltage limits. For instance, in Germany, the DIN EN 50160 norm requires that the grid voltages are kept within the permissible range of $\pm 10\%$ deviations around the rated voltage V_{base} of 400V, at least in 95% of all 10-minute operation intervals, on a weekly basis[6]. However, this range is reserved for the whole medium and low-voltage ensemble. As

[6]For simplicity, this limit is enforced to each model time step separately. Yet, this is a conservative approach and a linear formulation representing the precise regulation is also possible.

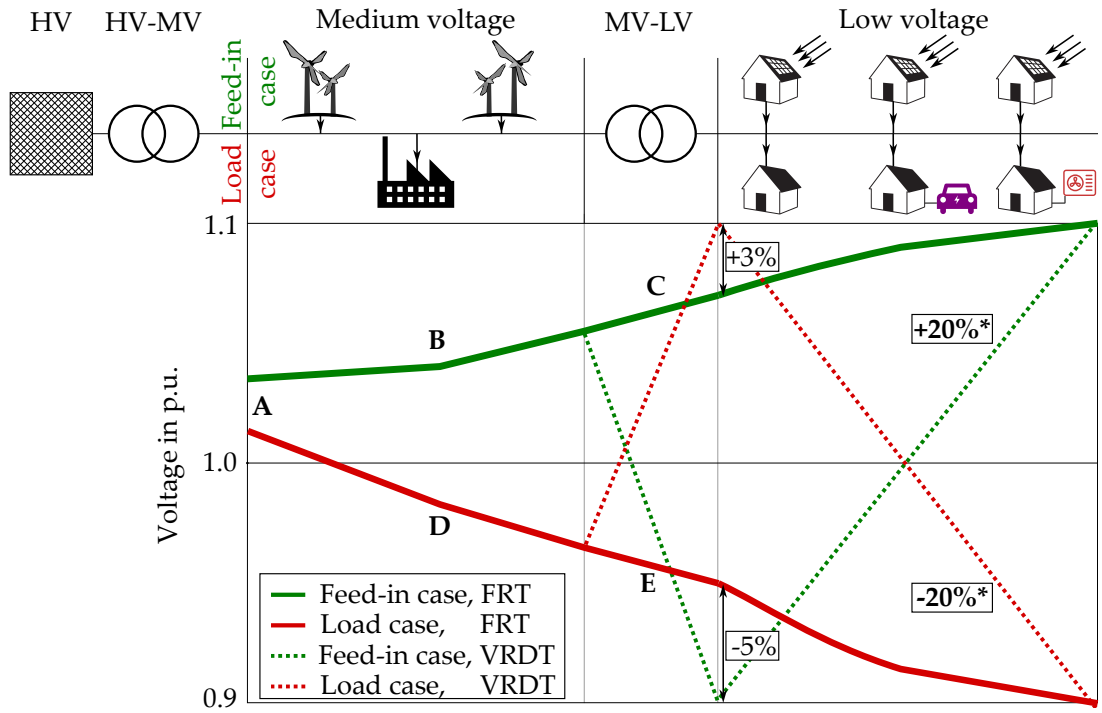

Figure 2.16: Allowable voltage bands for low-voltage distribution grids, with a fixed ratio transformer (FRT) and a voltage regulating distribution transformer (VRDT).
*Discrete tap change steps of VRDTs and further reserve requirements are neglected. Adapted from `ront.info`

.

the voltages between both grid levels are coupled to each other across FRTs, a more conservative band ($[V'_{\text{min}}, V'_{\text{max}}]$) is conventionally allocated to the LV grid alone. This conservative band is defined individually by the responsible distribution grid operator, depending on the individual characteristics of the region in question, such as PV penetration and the average length between consumers [73] [74]. For instance, one might consider the following exemplary distribution of the $\pm 10\%$ band:

- an uncontrollable offset due to the voltage deviations at the high voltage (HV) side, leading to a dead band of up to 2% (typical tap change step of an HV-MV transformer) [74] (line A in Figure 2.16),
- a 2% overvoltage due to decentral generation in MV (line B in Figure 2.16),
- a total of up to 3% over- and under-voltages through the MV-LV transformers, including additional reserves (lines C and E in Figure 2.16), and
- a 5% voltage drop at MV due to loads (line D in Figure 2.16).

This leads to a voltage band between $+3\%$ and -5% per unit (p.u.) that can be allocated to the LV grid level. An identical range has also been proposed by a guideline paper from 2009 for the Association of Bavarian Energy and Water Industry (VBEW) [75], and similar ranges have been reported by various distribution grid operators as summarized in [73].

This voltage band, however, assumes a constant tap ratio through the MV-LV transformer. VRDTs, on the other hand, grant an additional degree of freedom by adjusting the tap ratio of the transformer (and hence the voltage levels at the interface of the LV grid with MV). This decouples the MV and LV grid voltages, allowing them to be set independently. This

way, the LV grid can utilize the entire permissible voltage range of $[V_{\min}, V_{\max}]$. In reality, the discrete nature of the tap change steps or specific requirements from the grid operator may result in further restrictions over the exploitable voltage range [76], [74]. This behavior is not represented in this model due to its necessity for additional integer variables and moderate influence on the operation range.

Table 2.3 illustrates the resulting voltage bands for each case and bus. These limitations are imposed on the corresponding bus voltages $u_{i,t} = (V_{i,t})^2$ via the following constraints:

$$\frac{u_{i,t}}{(V_{\text{base}})^2} \leq \left((V'_{\max})_i^2 + \sum_{o \in \mathcal{O}} \alpha_o^{\text{VRDT}} \cdot \left((V_{\max})_i^2 - (V'_{\max})_i^2 \right) \right), \qquad \forall t \in \mathcal{T}_m \qquad \forall i \in \mathcal{I} \tag{2.65a}$$

$$\frac{u_{i,t}}{(V_{\text{base}})^2} \geq \left((V'_{\min})_i^2 + \sum_{o \in \mathcal{O}} \alpha_o^{\text{VRDT}} \cdot \left((V_{\min})_i^2 - (V'_{\min})_i^2 \right) \right). \qquad \forall t \in \mathcal{T}_m \qquad \forall i \in \mathcal{I} \tag{2.65b}$$

Table 2.3: Example permissible voltage bands in the LV grid (per V_{base}).

	Buses →	MBB	1	2	...	n	...	$\mathcal{N}$
Without VRDT	$(V'_{\min})_i$	1	0.95					
	$(V'_{\max})_i$	1	1.03					
With VRDT	$(V_{\min})_i$	0.9	0.9					
	$(V_{\max})_i$	1.1	1.1					

2.5.3 Curative (active) grid-relieving measures

Aside from the preventive (passive) reinforcement measures described in the preceding Section[7], the DSO also has curative (active) measures in its disposal for achieving grid-relieving behavior and energy balance. The active measures considered in the model are:

- reactive power compensation,
- DSO-side remote PV curtailment, and
- DSO-side remote curtailment of heat pumps and wall boxes (§ 14a) (introduced later in Section 2.7).

2.5.3.1 Reactive power compensation

For satisfying the reactive power demand of the electrical household appliances and the heat pumps, the LV grid can be additionally supplied reactive power $q^{\text{comp}}_{\text{MBB,t}}$ from the overlying grid. Reactive power can be mostly sourced through systems such as capacitor banks, static VAR, or synchronous compensators [77], under a specific cost per kVAr compensated:

$$q^{\text{net}}_{\text{MBB},t} = q^{\text{comp}}_{\text{MBB},t}. \qquad \forall t \in \mathcal{T}_m \tag{2.63}$$

2.5.3.2 DSO-side remote PV curtailment

While the curtailment of PV generation was defined as a decision variable for the prosumers in their respective subproblems, financial motivation usually lacks for them to use this option and forgo feed-in tariff payments (barring the capacity tariff costs as described by (2.39)).

[7]Usage of VRDT can be considered a semi-passive measure, as it involves dynamic adjustment of the tap-ratio depending on the voltage situation in the grid

Instead, it might be in the interest of the DSO to remotely curtail an amount of excess PV feed-in that prosumers intend to feed into the grid as an active grid-relieving measure in addition to grid reinforcement.

Due to the prohibitively high implementation costs involved in dynamically managing the output for hundreds of thousands of small-scale PV units, Germany had previously adopted a uniform restriction that capped these units at 70% of their rated capacity. This regulation remained in effect until the Renewable Energy Act underwent revision in 2023 [78]. While this cap is abolished as of 2023, and PV systems smaller than <25 kW are currently out of the scope of a remote curtailment regulation, this option is included as an active measure that may allow DSOs to alleviate grid reinforcement requirements in LV grids in the future.

The remote curtailment of the PV feed-in by the DSO effectively reduces the net feed-in from a building node by the curtailed amount. This corresponds to a modification of the equation (2.52) as follows:

$$p_{i,t}^{\text{net}} - p_{i,t}^{\text{PV,DSOcurt}} + p_{ji,t} = \sum_{k \in N^+(i)} p_{ik,t}, \qquad \forall t \in \mathcal{T}_m \qquad \forall i \in \mathcal{I}^b \tag{2.66}$$

where $p_{i,t}^{\text{PV,DSOcurt}}$ corresponds to the total amount of curtailed PV generation by the DSO across all PV units installed on a building ($\forall c \in \mathcal{C}^i$). To ensure that the DSO-side curtailment can only be conducted in a feed-in case and does not exceed the intended feed-in amount, the following constraint is set:

$$0 \leq p_{i,t}^{\text{PV,DSOcurt}} \leq p_{i,t}^{\text{feed-in}*}. \qquad \forall t \in \mathcal{T}_m \qquad \forall i \in \mathcal{I}^b \tag{2.67}$$

For nodes where no buildings are located, the power flow equation stays unmodified:

$$p_{i,t}^{\text{net}} + p_{ji,t} = \sum_{k \in N^+(i)} p_{ik,t}. \qquad \forall t \in \mathcal{T}_m \qquad \forall i \in \mathcal{I} \setminus \mathcal{I}^b \tag{2.68}$$

This concludes the modeling of the grid reinforcement options, along with the respective operational constraints and the power flow formulation. Together, these define the solution space for the HOODS-Grid model, which can be formulated into an optimization problem for minimizing the total costs associated with all grid-side measures.

2.5.4 Costs for the DSO

Grid costs incurred for the DSO, which are considered in the optimization problem, are the following:

- costs for voltage regulating distribution transformer (VRDT) installations
- costs for parallel line installations
- costs for reactive power supply
- costs for DSO-side curtailment of PV feed-in
- marginal costs for DSO-side downregulation (introduced later in the § 14a paradigm, see Section 2.7)

2.5.4.1 VRDT costs

Distinct unit costs are defined for each size class $o \in \mathcal{O}$ of VRDTs. The resultant costs can be represented as the sum product of these unit costs with the installation decision variables α_o:

$$c_{\text{DSO}}^{\text{VRDT}} = \sum_{o \in \mathcal{O}} \left((af^{\text{VRDT}} \cdot c_o^{\text{VRDT,inv}} + c_o^{\text{VRDT,O\&M}}) \cdot \alpha_o^{\text{VRDT}} \right), \tag{2.69}$$

where the investment costs $c_o^{\text{VRDT,inv}}$ include the cost of the transformer, building a new transformer station if necessary, the secondary units (e.g. controllers), and the installation of the transformer; and $c_o^{\text{VRDT,O\&M}}$ represents the annual operation and maintenance costs of the VRDT.

2.5.4.2 Parallel line costs

Similarly, the total costs for parallel cable installations can be represented as a sum product of the section-specific cabling costs $c_{ji,\text{spec}}^{\text{line},m}$ and the cable reinforcement decision variables α_{ji}^{m}, over a combination of all possible line sections in the grid, for the installation of double and triple cable settings in these:

$$c_{\text{DSO}}^{\text{line}} = \sum_{ji \in \mathcal{L}} \left(\sum_{m \in \{\text{II,III}\}} \left(af^{\text{VRDT}} \cdot c_{ji,\text{spec}}^{\text{line},m} \cdot \alpha_{ji}^{m} \right) \right), \tag{2.70}$$

The $c_{ji,\text{spec}}^{\text{line},m}$ stands for the line section-specific cabling costs, which are defined as follows:

$$c_{ji,\text{spec}}^{\text{line,II}} = l_{ji} \cdot (c_{\text{ins}} + c_{\text{mat}}), \tag{2.71a}$$

$$c_{ji,\text{spec}}^{\text{line,III}} = l_{ji} \cdot (c_{\text{ins}} + 2 \cdot c_{\text{mat}}), \tag{2.71b}$$

where l_{ji} is the length of the line section, c_{mat} the material costs per line length, and c_{ins} the line installation costs per length.

2.5.4.3 Reactive power compensation costs

For each kVAr reactive power compensation supplied by the DSO, a variable cost of $c_{\text{spec}}^{\text{Qcomp}}$ incurred. While the contracts between grid operators and reactive power suppliers lack systematic transparency, an average price can be set at 1€/MVAr.h from the example prices given in the report of the German Federal Energy Agency [79]. The corresponding costs sum up throughout the entire year as follows:

$$c_{\text{DSO}}^{\text{Qcomp}} = c_{\text{spec}}^{\text{Qcomp}} \cdot \sum_{t \in \mathcal{T}_m} \left(\omega_t \cdot q_{\text{MBB},t}^{\text{comp}} \right). \tag{2.72}$$

2.5.4.4 DSO-side curtailment costs

In return for the DSO-side curtailment of excess PV feed-in, they have to compensate the affected households with the usual feed-in tariff per curtailed amount of electricity:

$$c_{\text{DSO}}^{\text{PVcurt}} = c_{\text{spec}}^{\text{feed-in}} \cdot \sum_{t \in \mathcal{T}_m} \cdot \sum_{i \in \mathcal{I}^b} \left(\omega_t \cdot p_{i,t}^{\text{PV,DSOcurt}} \right). \tag{2.73}$$

All these costs combined, the total grid-side costs to be paid by the DSO can be formulated as follows:

$$c_{\text{DSO}} = c_{\text{DSO}}^{\text{VRDT}} + c_{\text{DSO}}^{\text{line}} + c_{\text{DSO}}^{\text{Qcomp}} + c_{\text{DSO}}^{\text{PVcurt}}. \tag{2.74}$$

Thus, to reach the optimum, the grid operator has to strike a balance between passive reinforcement measures of transformer and cable installations and the active measures of reactive power compensation and PV curtailment.

Post-optimization loss compensation costs While the aforementioned cost terms are represented in the optimization problem as part of its objective function, additional costs manifest during actual grid operation. These costs correspond to the compensation of the power losses within the grid, which are not depicted in the optimization model as the *LinDistFlow* model neglects these losses. These can, however, be evaluated after conducting the non-convex power flow simulation post-optimization (See Section 2.9). The loss compensation terms come in two:

- *Costs due to active power loss compensation:* To keep the balance of supply and demand in the grid, compensation for the transport losses of electricity is procured and paid by the grid operator in Germany [80]. DSOs usually pay a lower price than the retail electricity price for procuring this compensation energy. This price is set to 0.1€/kWh, which corresponds to the average between the reference prices reported by the German Federal Network Agency for years 2022 and 2023 [81].
- *Costs due to reactive power loss compensation*: Due to reactive power losses, the actual reactive power that has to be compensated by the grid operator is higher than depicted by the linear model. These have to be additionally accounted for by the DSO.

2.5.5 Formulation of the HOODS-Grid optimization problem

Bringing the operational restrictions and the cost terms outlined in the previous Sections together, the optimal reinforcement and operation problem for the distribution grid operator (HOODS-Grid) can be formulated as follows:

HOODS-Grid:

$$\begin{aligned}
\min_{\boldsymbol{\alpha}, \boldsymbol{f}} \quad & c_{\text{DSO}} = c_{\text{DSO}}^{\text{VRDT}} + c_{\text{DSO}}^{\text{line}} + c_{\text{DSO}}^{\text{Qcomp}} + c_{\text{DSO}}^{\text{PVcurt}} \\
\text{s.t.} \quad & (2.43), (2.44), (2.45), (2.46), (2.51), (2.66), (2.53), (2.54), (2.55a - 2.55b), \\
& (2.59), (2.60), (2.61), (2.62), (2.63), (2.64), (2.65a - 2.65b), \\
& (2.67), (2.68), (2.69), (2.70), (2.72), (2.73)
\end{aligned}$$

where, for brevity, the grid expansion variables are grouped into

$$\boldsymbol{\alpha} = \begin{bmatrix} \alpha_{ji}^{m} & \forall ji \in \mathcal{L} & \forall m \in \{\text{I,II,III}\} \\ \alpha^{\text{FRT}} & & \\ \alpha_{o}^{\text{VRDT}} & \forall o \in \mathcal{O} & \end{bmatrix} \tag{2.75}$$

and the grid operation variables into

$$\boldsymbol{f} = \begin{bmatrix} u_{i,t} & \forall i \in \mathcal{I} & \forall t \in \mathcal{T} & \\ p_{ji,t}^{m}, q_{ji,t}^{m} & \forall ji \in \mathcal{L} & \forall m \in \{\text{I,II,III}\} & \forall t \in \mathcal{T} \\ p_{\text{MBB},t}^{\text{imp}}, p_{\text{MBB},t}^{\text{feed-in}}, q_{\text{MBB},t}^{\text{comp}} & \forall t \in \mathcal{T} & & \\ p_{i,t}^{\text{PV,DSOcurt}} & \forall t \in \mathcal{T} & \forall i \in \mathcal{I}^{b} & \end{bmatrix}. \tag{2.76}$$

See Appendix A.2 for the complete problem formulation.

2.6 HOODS-Sys: Co-optimization model

The previous Sections dealt with the building and grid subproblems, which can be solved sequentially as mentioned. These models can be fused into a single problem for the whole system, denoted as HOODS-Sys from here on, where the decisions of the prosumers and the DSO are optimized with a single hand, i.e., by a hypothetical *central planner* (see Figure 2.17). In contrast to the prosumers and DSO, this central planner would be able to

- set the building- and grid-side costs into relation directly with each other to decide where the highest saving potentials exist, and
- manage the excess PV electricity to share it between prosumers, maximizing the system-wide self-consumption.

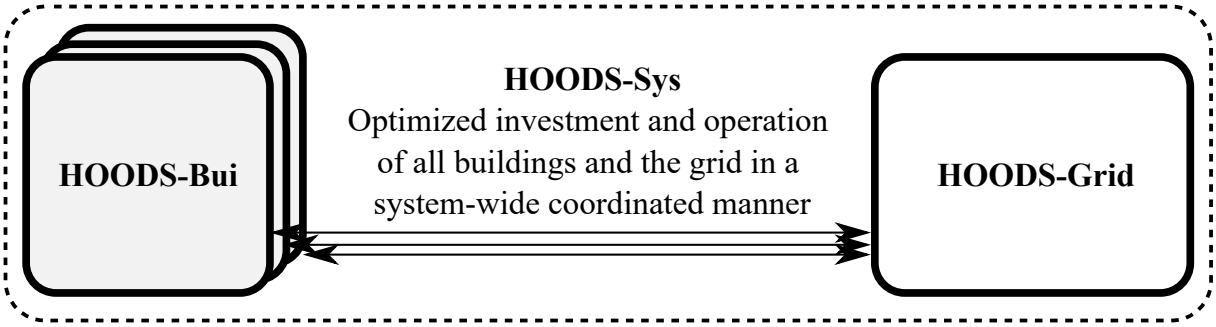

Figure 2.17: The co-optimization procedure.

This way, it can reveal an optimum not reachable by a sequential approach due to the lack of system-wide coordination. This optimum, however, can not be achieved in a practical sense due to the lack of communication and conflicts of interest between the actors. Therefore, it will instead serve as a benchmark for the best possible transformation of the LV distribution system. Against this benchmark, various sequential paradigms with different techno-economic measures will be compared. This way, one can evaluate the potential of these measures to improve the system costs against the welfare losses that are inevitably suffered by the lack of coordination.

Drawing on the submodel formulations presented in Sections 2.3.5 and 2.5.5, the HOODS-Sys can be formulated by merging the submodel variables and constraints with minor adjustments.

HOODS-SYS:

$$\min_{\boldsymbol{\kappa},\boldsymbol{\epsilon},\boldsymbol{\alpha},\boldsymbol{f}} \quad c_{\text{sys}} = \sum_{i\in\mathcal{I}^b}\left(c_i^{\text{HP}} + c_i^{\text{PV}} + c_i^{\text{bat}} + c_i^{\text{TS}} + c_i^{\text{sto},\epsilon}\right) + c_{\text{DSO}}^{\text{VRDT}} + c_{\text{DSO}}^{\text{line}} + c_{\text{DSO}}^{\text{Qcomp}} + \sum_{t\in\mathcal{T}}\omega_t\left(c_{\text{spec},t}^{\text{imp}}\cdot p_{\text{MBB},t}^{\text{imp}} - \cdot c_{\text{spec}}^{\text{feed-in}}\cdot p_{\text{MBB},t}^{\text{feed-in}}\right) \tag{2.77}$$

$$\text{s.t.}\Big\{(2.1-2.4),(2.5a-2.5f),(2.6a-2.6b),(2.14-2.15),(2.16a-2.18),(2.19a-2.19e),(2.20)(2.21-2.22),(2.23a-2.23e),(2.24),(2.25-2.26),(2.28-2.32)\qquad\forall i\in\mathcal{I}^b\Big\}$$

$$p_{i,t}^{\text{net}} = p_{i,t}^{\text{imp}} - p_{i,t}^{\text{feed-in}} \qquad \forall t\in\mathcal{T}_m \qquad \forall i\in\mathcal{I}^b \tag{2.78}$$

$$q_{i,t}^{\text{net}} = q_{i,t}^{\text{imp}} - q_{i,t}^{\text{feed-in}} \qquad \forall t\in\mathcal{T}_m \qquad \forall i\in\mathcal{I}^b \tag{2.79}$$

$$(2.51),(2.52),(2.53),(2.54),(2.55a-2.55b),(2.59),(2.60),(2.61),(2.62),(2.63),(2.64),(2.65a-2.65b),(2.67),(2.69),(2.70),(2.72),(2.73)$$

See Appendix A.3 for the complete problem formulation.

In the above co-optimization model formulation, the adjustments made beyond the sole fusion of the prosumer and grid submodels are as follows:

- As the capacity tariff payments paid by the prosumers are collected by the DSO, the net costs for the prosumer-DSO ensemble are zero. Therefore, the corresponding cost term c_i^{cap} and the constraints (2.39, 2.36, and 2.37) are omitted,
- As the payments for remote PV curtailment made by the DSOs are collected by the prosumers, the corresponding cost term $c_{\text{DSO}}^{\text{PVcurt}}$ is omitted,
- As the system-wide import and feed-in of electricity is managed across the main busbar of the grid, the prosumer-specific import and feed-in cost terms ($c_i^{\text{imp}}, c_i^{\text{feed-in}}$) are replaced with their aggregated variant in the cost function,
- The net grid injections of the prosumers are not fixed and are instead endogenously optimized. Therefore, the equations (2.43) and (2.44) are replaced with their relaxed counterparts (2.78) and (2.79),
- As the PV curtailment decision can be taken in the prosumer level through the equation (2.1), no explicit DSO-side curtailment formulation is necessary. Therefore, the nodal power balance equations (2.66) and (2.68) are replaced by (2.52).

2.7 EnWG § 14a regulation: DSO-side remote curtailment of heat pumps and wall boxes

In addition to the sequential and co-optimization approaches, another model variant is developed. This variant incorporates the supplementary grid relief measure of DSO-led curtailment of controllable consumption devices, in line with the current German government's plans. Although this variant also employs a sequential approach, it necessitates more comprehensive model modifications for implementation and, as such, warrants a separate discussion in this Section.

2.7.1 Background of the EnWG § 14a regulation

In order to curb the high peaks resulting from the simultaneous operation of heat pumps and BEVs, which may occur despite the financial grid-relieving incentives for the prosumers, Germany is providing the authority for all DSOs to apply a "grid-oriented regulation of the controllable consumption devices and controllable network connections" which are located in their respective grids. This is declared in Section (§) 14a of the latest edition of the Energy Industry Act in 2023, hence will be shortly denoted as the *§ 14a regulation*. As of writing this thesis, details of this regulation are still taking form in its second consultation phase, however, the concrete implementation is set to come into effect by the beginning of 2024.

While its complete description can be found in the legal paper [22] from 14.06.2023, some major aspects of the planned § 14a regulation will be explained here.

Note that while the final decision of the § 14a regulation, dated 27.11,2023 [82], has been published during the submission of this thesis, the following description of the regulation and its model implementation are based on the paper from 14.06.2023.

- The Act defines the following as *controllable consumption units*:

  1. Charging points for electric vehicles that are not publicly accessible (private wall boxes),
  2. Heat pump systems, including their additional or auxiliary (electric) heating units,
  3. Air-conditioning systems for cooling, and
  4. Battery storage units, when operated in the withdrawal direction (charging),

  which have an electrical capacity higher than 4.2 kW and a direct or indirect connection to the LV distribution grid.

- In essence, the grid operator is obligated to monitor the grid's reliability and safety at all times.

- In the event this reliability and safety are threatened or disrupted due to overloading of the grid components within a specific grid area in particular, the DSO shall be both entitled and obliged to curtail ("reduce") the grid-effective power consumption of these devices in the affected network area to the extent necessary. In particular, this reduction can be applied to a specific limit—each of these devices shall be reserved at least $4.2\ kW$ of consumption capacity at all times.

- The curtailment of each device must be discrimination-free, suitably tailored, and objectively essential to prevent or rectify the threat or disruption.

- The grid operator ascertains the basis for implementing this curtailment through continuous monitoring of the grid state.

- The operators of the devices (the prosumers in this context) have to provide the DSOs with the technical means to facilitate such regulation with the necessary communication and control equipment.

- For the altered consumption behavior induced due to curtailment, no direct compensation will be made to the prosumer. Nevertheless, in the amended Section 14a of the Energy Industry Act, new schemes for reduced network tariffs will be offered to prosumers in turn [83]. Additionally, the right to occasionally curtail these devices strips the DSO of the ability to delay or deny the grid connection of these devices due to the overloading of the grid.

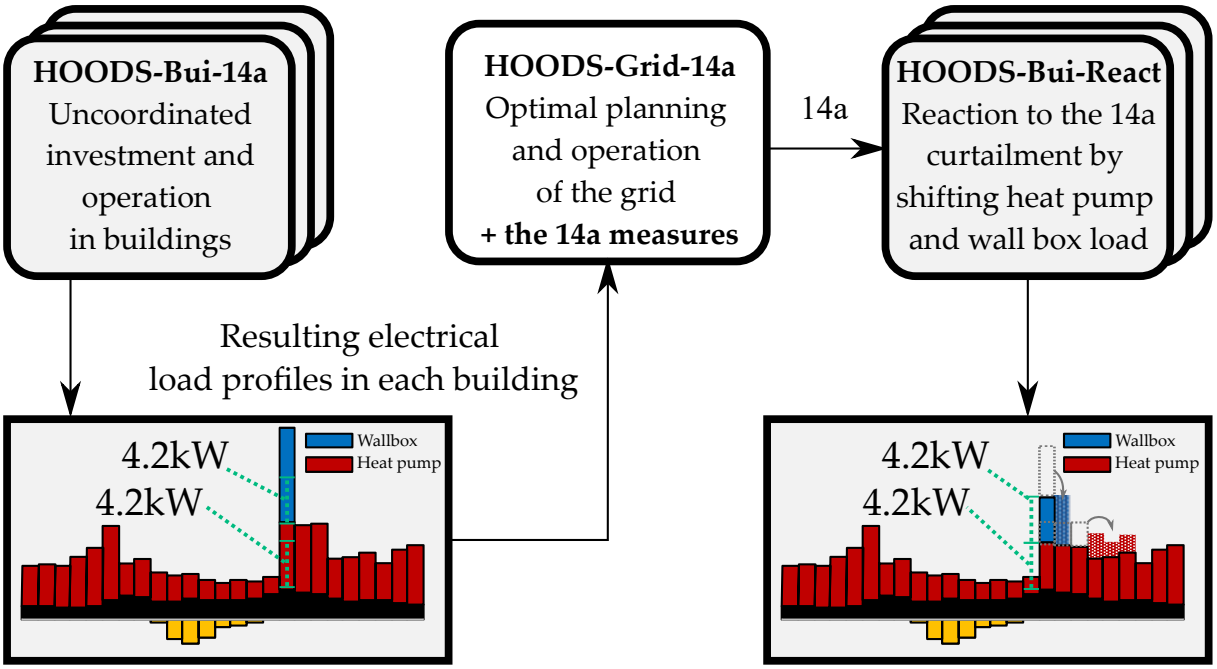

Figure 2.18: The three-level approach of the § 14a regulation modeling.

- The obligation of the DSO for justified grid reinforcement remains permanent and unrestricted. In other words, the DSO shall not treat this regulation as a way to avoid grid reinforcement measures altogether. However, it can and should consider the concrete grid reinforcement requirements by taking these supplementary curtailment options into account.

Especially the last aspect motivates the inclusion of this regulation in the framework, as the optimization approach allows for finding the best combination of passive and active measures that the DSO has at its disposal. Moreover, there are ongoing dialogues concerning the social acceptance of this regulation, given that it entails a compulsory constraint on consumer preferences in satisfying their heating and mobility demands. This renders an examination of its benefits and risks highly interesting.

2.7.2 Modeling approach of the EnWG § 14a regulation

Due to its non-cooperative character, a sequential approach is also adopted for modeling the § 14a regulation within the framework. The process is illustrated in Figure 2.18. In the first step, denoted HOODS-Bui-14a, the prosumers optimize their DER capacities and operation as usual, similarly to HOODS-Bui. Next, the DSO decides on the optimal grid reinforcement and operation in the HOODS-Grid-14a step—now the downregulation as per § 14a is included as an additional active measure. The curtailment signals are then sent to the prosumers in a third step, where they react to the restricted heat pump and wall box operations by shifting their corresponding demands (HOODS-Bui-React). In this third step, the under-satisfaction of the building temperature maintenance and the mobility demand is introduced in a penalized way in order to assess the loss of comfort resulting from the curtailment in the buildings.

In the following Sections, each of these building blocks will be described, focusing on the contrasts between them and their counterparts from Sections 2.3.5 and 2.5.5.

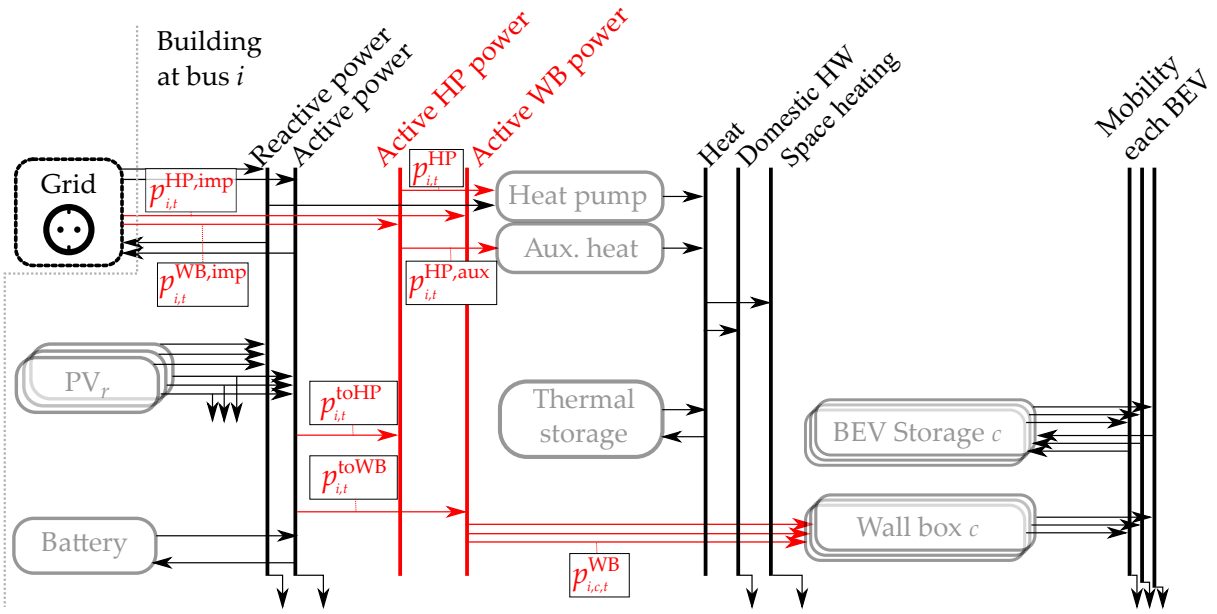

Figure 2.19: The modified reference energy system for the § 14a regulation implementation, where the introduced flow variables are depicted in red.

2.7.2.1 HOODS-Bui-14a

In order to determine their curtailment capabilities, the DSO has to distinguish between the portions of the withdrawn electricity consumed by the heat pumps and the wall boxes. Yet, in the regular form of HOODS-Bui, only aggregated import amounts $p^{\text{import}}_{i,t}$ are communicated to the DSO. Therefore, in HOODS-Bui-14a, two additional commodities are introduced:

- active heat pump (HP) power, which serves as the input commodity of the heat pump and its auxiliary unit, and
- active wall box (WB) power, which serves as the input commodity of the wall boxes.

These device-specific electrical commodities will be collectively called § 14a commodities for simplicity. Figure 2.19 illustrates the modified reference energy system. Correspondingly, these amounts can also be withdrawn, under the same price as regular electricity, from the grid (the imported portions denoted as $p^{\text{HP,imp}}_{i,t}$ and $p^{\text{WB,imp}}_{i,t}$). The § 14a regulation does not disallow prosumers from using locally generated electricity for operating these devices. Therefore, any portion of the electricity supplied to the building can be converted into their respective § 14a commodities, these amounts denoted as $p^{\text{toHP}}_{i,t}$ and $p^{\text{toWB}}_{i,t}$. To prevent the model from importing the regular electricity commodity for the purpose of being converted directly into the § 14a commodities and consumed by these devices, a small variable cost $c^{\text{conv}}_{\text{spec}}$ is attached to this conversion process. This way, when power from the grid is required to operate these devices, the prosumer will always prefer its respective § 14a commodity.

Ultimately, the introduction of the § 14a commodities to the model entails two additional commodity balance equations, a modification of the electricity balance equation, and an ad-

justment of the prosumer import costs:

$$p_{i,t}^{\text{HP,imp}} + p_{i,t}^{\text{toHP}} = p_{i,t}^{\text{HP}} + p_{i,t}^{\text{HP,aux}}, \qquad \forall t \in \mathcal{T}_m \qquad \forall i \in \mathcal{I}^b \tag{2.80}$$

$$p_{i,t}^{\text{WB,imp}} + p_{i,t}^{\text{toWB}} = \sum_{c \in \mathcal{C}^i} p_{i,c,t}^{\text{WB}}, \qquad \forall t \in \mathcal{T}_m \qquad \forall i \in \mathcal{I}^b \tag{2.81}$$

$$\sum_{r \in \mathcal{R}^i} p_{i,r,t}^{\text{PV}} + p_{i,t}^{\text{bat,dch}} + p_{i,t}^{\text{imp}} = d_{i,t}^{\text{elec}} + p_{i,t}^{\text{bat,ch}} + p_{i,t}^{\text{toWB}} + p_{i,t}^{\text{toHP}} + p_{i,t}^{\text{feed-in}}, \qquad \forall t \in \mathcal{T}_m \qquad \forall i \in \mathcal{I}^b \tag{2.82}$$

$$c_i^{\text{imp}} = \sum_{t \in \mathcal{T}} \left(\omega_t \cdot c_{\text{spec},t}^{\text{imp}} \cdot (p_{i,t}^{\text{imp}} + p_{i,t}^{\text{HP,imp}} + p_{i,t}^{\text{WB,imp}}) \right). \qquad \forall i \in \mathcal{I}^b \tag{2.83}$$

The resulting model formulation is as follows:

HOODS-Bui-14a(i):

$$\min_{\substack{\boldsymbol{\kappa}_i, \boldsymbol{\epsilon}_i, \\ \boldsymbol{p}_{i,t}^{\text{imp,HP}}, \boldsymbol{p}_{i,t}^{\text{imp,WB}}, \\ \boldsymbol{p}_{i,t}^{\text{toHP}}, \boldsymbol{p}_{i,t}^{\text{toWB}}}} \quad c_i = c_i^{\text{HP}} + c_i^{\text{PV}} + c_i^{\text{bat}} + c_i^{\text{TS}} + c_i^{\text{sto},\epsilon} + c_i^{\text{imp}} + c_i^{\text{feed-in}} + c_i^{\text{cap}} + \underline{c_{\text{spec}}^{\text{conv}} \cdot \sum_{t \in \mathcal{T}} \omega_t \left(p_{i,t}^{\text{toHP}} + p_{i,t}^{\text{toWB}} \right)}$$

s.t. $(2.1 - 2.4)$, $(2.5a - 2.5f)$, ~~$(2.6a)$~~, $(2.6b)$,
$(2.14 - 2.15)$, $(2.16a)$, $(2.16b)$, $(2.16c)$, $(2.16d)$, $(2.16e)$, $(2.17 - 2.18)$,
$(2.19a - 2.19e)$, (2.20), $(2.21 - 2.22)$, $(2.23a - 2.23e)$, (2.24),
$(2.25 - 2.26)$, $(2.28 - 2.30)$, ~~$(2.31$~~ $- 2.32)$, $(2.36 - 2.38)$, (2.39),
$\underline{(2.80), (2.81), (2.82), (2.83)}$

where the additions over the HOODS-Bui model are denoted with an underline, and the removals with a ~~strikethrough~~. See Appendix A.4 for the complete problem formulation.

2.7.2.2 HOODS-Grid-14a

In the § 14a variant of the HOODS-Grid problem, all grid active power injection terms (2.43) are modified, now incorporating the withdrawal of the § 14a commodities distinctly:

$$p_{i,t}^{\text{net}} = p_{i,t}^{\text{imp}*} + p_{i,t}^{\text{HP}*} + p_{i,t}^{\text{WB}*} - p_{i,t}^{\text{feed-in}*}, \qquad \forall t \in \mathcal{T}_m \qquad \forall i \in \mathcal{I}^b \tag{2.84}$$

The demand in each node can now be down-regulated by an amount of $p_{i,t}^{\text{HP,14a}}$ and $p_{i,t}^{\text{WB,14a}}$ for each heat pump and wall box in a building bus, respectively. This leads to the following modified form of (2.66):

$$p_{i,t}^{\text{net}} - p_{i,t}^{\text{PV,DSOcurt}} + p_{ji,t} = \sum_{k \in N^+(i)} p_{ik,t} - p_{i,t}^{\text{HP,14a}} - p_{i,t}^{\text{WB,14a}}. \qquad \forall t \in \mathcal{T}_m \qquad \forall i \in \mathcal{I}^b \tag{2.85}$$

The down-regulation has to ensure that a free capacity of 4.2 kW per device is maintained. This condition is maintained with the following constraints:

$$0 \leq p_{i,t}^{\text{HP,14a}} \leq \begin{cases} p_{i,t}^{\text{HP,imp}*} - 4.2 \text{ kW} & \text{if } p_{i,t}^{\text{HP,imp}*} \geq 4.2 \text{ kW} \\ 0 & \text{if } p_{i,t}^{\text{HP,imp}*} < 4.2 \text{ kW} \end{cases} \qquad \forall t \in \mathcal{T}_m \; \forall i \in \mathcal{I}^b \tag{2.86}$$

$$0 \leq p_{i,t}^{\text{WB,14a}} \leq \begin{cases} p_{i,t}^{\text{WB,imp}*} - 4.2 \text{ kW} \cdot |\mathcal{C}^i| & \text{if } p_{i,t}^{\text{WB,imp}*} \geq 4.2 \text{ kW} \cdot |\mathcal{C}^i| \\ 0 & \text{if } p_{i,t}^{\text{WB,imp}*} < 4.2 \text{ kW} \cdot |\mathcal{C}^i| \end{cases} \qquad \forall t \in \mathcal{T}_m \; \forall i \in \mathcal{I}^b \tag{2.87}$$

Note that for the sake of simplicity, in buildings that contain multiple wall boxes, the aggregated wall box behavior is communicated with the DSO. This way, curtailment is only permitted when the total charging surpasses an average of 4.2 kW per wall box. For example, in instances where two wall boxes are in place, charging of a minimum of 8.4 kW will always be ensured. This corresponds to an assumed simultaneity factor of 1 between these devices.

For each kWh of down-regulated consumption, attaching a very low variable cost c_{spec}^{14a} ensures that the DSO only applies these measures if it leads to savings in other avenues, i.e., grid reinforcement.

With these definitions, the HOODS-Grid-14a model can be formulated as follows:

HOODS-Grid-14a:

$$\min_{\substack{\boldsymbol{\alpha},\boldsymbol{f}\\ \boldsymbol{p}^{\text{HP,DSOcurt}}\\ \boldsymbol{p}^{\text{WB,DSOcurt}}}} \quad c_{\text{DSO}} = c_{\text{DSO}}^{\text{VRDT}} + c_{\text{DSO}}^{\text{line}} + c_{\text{DSO}}^{\text{Qcomp}} + c_{\text{DSO}}^{\text{PVcurt}} + \underline{c_{\text{spec}}^{14a} \cdot \sum_{t\in\mathcal{T}} \omega_t \left(p_{i,t}^{\text{HP,14a}} + p_{i,t}^{\text{WB,14a}}\right)}$$

$$\text{s.t.} \ \underline{\text{(2.43)}}, (2.44), (2.45), (2.46), (2.51), (2.53), (2.54), (2.55a - 2.55b),$$
$$(2.59), (2.60), (2.61), (2.62), (2.63), (2.64), (2.65a - 2.65b),$$
$$\underline{\text{(2.66)}}, (2.67), (2.68), (2.69), (2.70), (2.72), (2.73)$$
$$\underline{(2.84), (2.85), (2.86), (2.87)},$$

where the additions over the HOODS-Grid model are denoted with an underline, and the removals with a strikethrough. See Appendix A.5 for the complete problem formulation.

2.7.2.3 HOODS-Bui-React

After receiving the curtailment signals from the DSO, the prosumers re-evaluate the optimal DER operation under the restrictions caused by the downregulation. The goal of this step is to assess the capacity of the prosumer to shift the consumption of their controllable consumption devices to avoid unmet demand and the loss of comfort to the best of their ability. In this step, it is assumed that the DER capacity planning has already taken place in the first step (HOODS-Bui-14a) so that the corresponding capacity variables are fixed to their optimal values:

$$\boldsymbol{\kappa_i} = \boldsymbol{\kappa_i^*} \tag{2.88}$$

and they are not optimized again. The restrictions caused by the downregulation are implemented by reducing the heat pump and wall box capacity constraints correspondingly at the times curtailment occurs. The following will describe this restriction procedure.

Restriction of the heat pump consumption through § 14a The § 14a regulation applies to the whole heat pump system, including the auxiliary heating unit. Here, it is assumed that the ensured capacity will be reserved for the main heat pump unit due to its lower running costs. In other words, the curtailment will affect the auxiliary unit first. Only if the downregulation amount decided by the DSO (denoted with a star as $p_{i,t}^{\text{HP,14a}^*}$) is higher than the initially intended consumption of the auxiliary unit, the curtailment will reach the main heat pump unit too. Therefore, in order to set these restrictions for each part of the heat pump system, several case distinctions have to be made. These relate to the capacities of the main heat pump and the auxiliary heating unit (see Figure 2.20):

- **Main unit capacity being smaller than 4.2 kW (Case 1)**: no restriction of the main unit through a § 14a curtailment has been possible (the normal capacity limit (2.16c) holds)

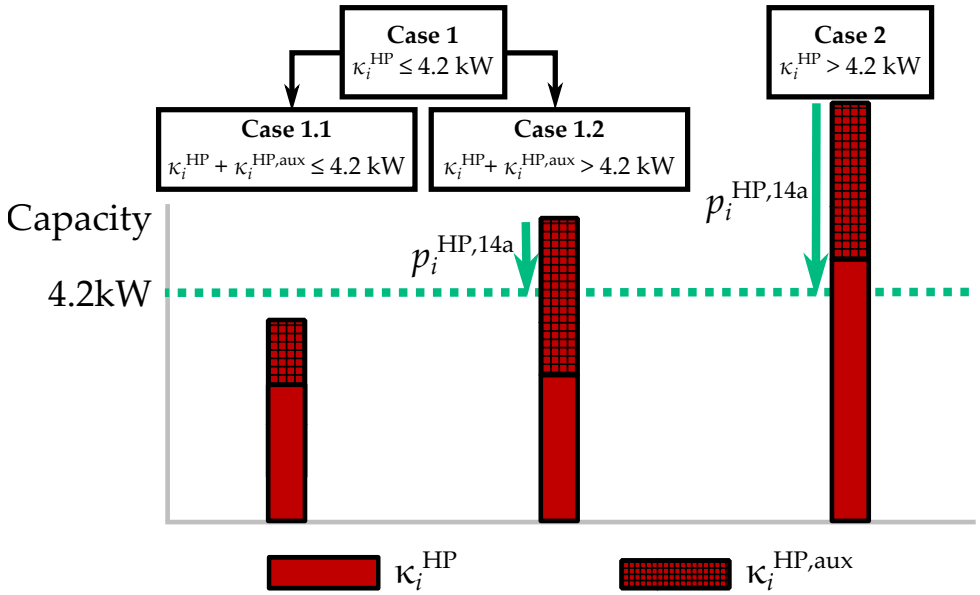

Figure 2.20: Case distinctions for determining the heat pump capacity restriction through the § 14a downregulation. The green arrows illustrate the maximum down-regulation that can be applied by the DSO.

- **Total heat pump system capacity being smaller than 4.2 kW (Case 1.1)**: likewise, no downregulation may be applied on the auxiliary unit either (the normal capacity limit (2.16e) holds),

- **Total heat pump system capacity being larger than 4.2 kW (Case 1.2)**: only the auxiliary heating unit may be downregulated. Thus its normal capacity limit (2.16e) is replaced by the following:

$$0 \leq p_{i,t}^{HP,aux} \leq \begin{cases} p_{i,t}^{HP,aux*} - p_{i,t}^{HP,14a*} & \text{if } p_{i,t}^{HP,14a*} \geq 0 \ \wedge \ \kappa_{i,t}^{HP,aux*} + \kappa_{i,t}^{HP*} \geq 4.2 \text{ kW} \\ \kappa_{i,t}^{HP,aux*} & \text{if } p_{i,t}^{HP,14a*} = 0 \ \wedge \ \kappa_{i,t}^{HP,aux*} + \kappa_{i,t}^{HP*} \geq 4.2 \text{ kW} \end{cases} \quad \forall t \in \mathcal{T}_m \tag{2.89}$$

- **Main unit capacity being larger than 4.2 kW (Case 2)**: depending on the level of down-regulation the DSO decides for, both the main and the auxiliary unit may be met. Thus, the normal capacity limits (2.16c, 2.16e) are replaced by the following:

$$0 \leq p_{i,t}^{HP} \leq \begin{cases} p_{i,t}^{HP*} - (p_{i,t}^{HP,14a*} + p_{i,t}^{HP,aux*}) & \text{if } \quad p_{i,t}^{HP,14a*} \geq p_{i,t}^{HP,aux*} \ \wedge \ \kappa_{i,t}^{HP*} \geq 4.2 \text{ kW} \\ \kappa_{i,t}^{HP} & \text{if } 0 \leq p_{i,t}^{HP,14a*} \leq p_{i,t}^{HP,aux*} \ \wedge \ \kappa_{i,t}^{HP*} \geq 4.2 \text{ kW} \end{cases} \quad \forall t \in \mathcal{T}_m \tag{2.90}$$

$$0 \leq p_{i,t}^{\mathrm{HP,aux}} \leq \begin{cases} 0 & \text{if } p_{i,t}^{\mathrm{HP,14a*}} \geq p_{i,t}^{\mathrm{HP,aux*}} \ \wedge \ \kappa_{i,t}^{\mathrm{HP*}} \geq 4.2 \text{ kW} \\ p_{i,t}^{\mathrm{HP,aux*}} - p_{i,t}^{\mathrm{HP,14a*}} & \text{if } p_{i,t}^{\mathrm{HP,14a*}} \leq p_{i,t}^{\mathrm{HP,aux*}} \ \wedge \ \kappa_{i,t}^{\mathrm{HP*}} \geq 4.2 \text{ kW} \\ \kappa_{i,t}^{\mathrm{HP,aux*}} & \text{if } p_{i,t}^{\mathrm{HP,14a*}} = 0 \ \wedge \ \kappa_{i,t}^{\mathrm{HP*}} \geq 4.2 \text{ kW} \end{cases} \quad \forall t \in \mathcal{T}_m \tag{2.91}$$

Simply put, these constraints together achieve the desired effect: the heat pump components are only restricted if their collective capacity exceeds 4.2 kW, and the auxiliary heating unit is affected first. The case definition relates to already calculated values from the previous steps and not to variables endogenous to this step, thus it can be included in the optimization problem.

Restriction of the wall box consumption through § 14a The restriction of the wall box operation is achieved in a more straightforward manner than the heat pump system. Indeed, multiple wall boxes may be present in a given building bus. It is assumed, however, that the DSO does not discriminate between these when applying the downregulation. This leads to an equal allocation of the allowed capacities among each wall box $c \in \mathcal{C}^i$:

$$0 \leq p_{i,c,t}^{\mathrm{WB}} \leq \begin{cases} \dfrac{\sum_{c \in \mathcal{C}^i} \left(p_{i,c,t}^{\mathrm{WB*}} \right) - p_{i,t}^{\mathrm{WB,14a*}}}{|\mathcal{C}^i|} & \text{if } p_{i,t}^{\mathrm{WB,14a*}} \geq 0 \\ \kappa_{i,c,t}^{\mathrm{WB}} & \text{if } p_{i,t}^{\mathrm{WB,14a*}} = 0 \end{cases} \quad \forall t \in \mathcal{T}_m \quad \forall c \in \mathcal{C}^i \tag{2.92}$$

Unfulfillment of the heating demand Note that these restrictions are applied to the device operations directly in the model for simplicity. Indeed, this contrasts with the proposed regulation, where the restrictions are intended to be applied to the net power withdrawal of the device from the external grid instead. This would let the downregulated devices still be operated by locally supplied electricity, such as from PV generation or discharge from batteries. Thereby, the prosumers would have additional options for utilizing their flexibilities at times of down-regulation. Yet, the potential of this leeway is expected to be low in scenarios with high heat-pump penetration, as the DSO would require downregulation the most in cold winter weeks, where the electricity generation from PV generation is low.

The need for load shifting arises from these restrictions, which can be achieved by other flexibility sources present in the system. For mobility, the expected loss of comfort is low–the curtailed wall boxes can be operated during the preceding or subsequent hours while the BEV is still at the premises. BEV battery and wall box capacities are usually large enough compared to the daily consumption to allow enough room for such shifting. The curtailed heat pump can be operated aside the hours of downregulation, storing the excess heat in the thermal storage system or preheating the building by exploiting its thermal inertia. However, in contrast to wall boxes, the heat pump utilization ratios are high, especially in winter times. Thus, the additional operation in the non-curtailed hours might not be sufficient to compensate for the reduced operation. To investigate the cases where, or how often, the flexibility options fail to satisfy the heating demand, a relaxation of the constraints responsible for the temperature maintenance (2.15) and the heat balance (2.20) is made:

$$\vartheta_{i,t}^{\min} - \vartheta_{i,t}^{\mathrm{slack}} \leq \vartheta_{i,t} \leq \vartheta_{i,t}^{\max}, \qquad \forall t \in \mathcal{T}_m \tag{2.93}$$

$$\gamma_{i,t}^{\mathrm{HP}} + \gamma_{i,t}^{\mathrm{TS,dch}} + \gamma_{i,t}^{\mathrm{slack}} = \gamma_{i,t}^{\mathrm{TS,ch}} + d_{i,t}^{\mathrm{sh}} + d_{i,t}^{\mathrm{dhw}} + \gamma_{i,t}^{\mathrm{vent}}, \qquad \forall t \in \mathcal{T}_m \tag{2.94}$$

where the terms introduced in bold $\boldsymbol{\vartheta}^{\text{slack}}_{i,t}, \boldsymbol{\gamma}^{\text{slack}}_{i,t}$ are the slack variables for the violation of the temperature maintenance and the unfulfillment of the heating balance, respectively. To ensure that these slack variables are used as a last resort, they are incorporated into the cost function as very largely-valued penalty terms with coefficients $c^{\vartheta,\text{slack}}_{\text{spec}}$ and $c^{\gamma,\text{slack}}_{\text{spec}}$. This means using these slack variables comes at a high cost, steering the optimization process to avoid their usage unless absolutely necessary. Note that using only one slack variable, that is, for temperature maintenance, is not sufficient to prevent an infeasible solution—the cases where the domestic hot water demand cannot be met have to be taken into account. The penalty coefficients have to be set in a relation, such that the model decides to cool down the building rather than violate the heat balance. This will allow for quantifying the loss of temperature comfort later in the result analysis.

With the introduced restriction constraints and slack variables, the HOODS-Bui-React model can be formulated as follows:

HOODS-Bui-React(i):

$$
\begin{aligned}
\min_{\substack{\boldsymbol{\kappa}_i, \boldsymbol{\epsilon}_i, \\ \boldsymbol{p}^{\text{imp,HP}}_{i,t}, \boldsymbol{p}^{\text{imp,WB}}_{i,t}, \\ \boldsymbol{p}^{\text{toHP}}_{i,t}, \boldsymbol{p}^{\text{toWB}}_{i,t}, \\ \boldsymbol{\vartheta}^{\text{slack}}_{i,t}, \boldsymbol{\gamma}^{\text{slack}}_{i,t}}} \quad & c_i = c_i^{\text{HP}} + c_i^{\text{PV}} + c_i^{\text{bat}} + c_i^{\text{TS}} + c_i^{\text{sto},\epsilon} + c_i^{\text{imp}} + c_i^{\text{feed-in}} + c_i^{\text{cap}} \\
& \quad + c^{\text{conv}}_{\text{spec}} \cdot \sum_{t \in \mathcal{T}} \omega_t \left(p^{\text{toHP}}_{i,t} + p^{\text{toWB}}_{i,t} \right) \\
& \quad + \sum_{t \in \mathcal{T}} \omega_t \left(c^{\vartheta,\text{slack}}_{\text{spec}} \cdot \vartheta^{\text{slack}}_{i,t} + c^{\gamma,\text{slack}}_{\text{spec}} \cdot \gamma^{\text{slack}}_{i,t} \right) \\
\text{s.t.} \quad & (2.1 - 2.4), (2.5a - 2.5f), (2.6b), \\
& (2.14 - \cancel{2.15}), (2.16a), (2.16b), \cancel{(2.16c)}, (2.16d), \cancel{(2.16e)}, (2.17 - 2.18), \\
& (2.19a - 2.19e), (\cancel{2.20}), (2.21 - 2.22), (2.23a - 2.23e), (2.24), \\
& (2.25 - 2.26), (2.28 - 2.30), (2.32), (2.36 - 2.38), (2.39), \\
& (2.80), (2.81), (2.82), (2.83) \\
& \text{if } \kappa_i^{\text{HP}*} \leq 4.2 \text{ kW}: \quad \underline{(2.16c)} \\
& \quad \text{if } \kappa_i^{\text{HP}*} + \kappa_i^{\text{HP,aux}*} \leq 4.2 \text{ kW}: \quad \underline{(2.16e)} \\
& \quad \text{else}: \quad \underline{(2.89)} \\
& \text{else}: \quad \underline{(2.90), (2.91)} \\
& \underline{(2.92), (2.93), (2.94)} \\
& \boldsymbol{\kappa}_i = \boldsymbol{\kappa}_i^*
\end{aligned}
$$

where the additions over the HOODS-Bui-14a model are denoted with an underline, and the removals with a ~~strikethrough~~. See Appendix A.6 for the complete problem formulation.

2.8 Discussion on the modeling assumptions

Some assumptions were made to constitute the HOODS problems in the presented MILP model formulation. The major model assumptions are summarized below:

- the single-year modeling approach, while grid planning usually takes multi-year periods into account,
- a balanced distribution grid with a radial structure,
- a perfect forecast for the flexibility supply in the home energy management system (HEMS) operation. Most HEMSs work with either rule-based or, at most, model predic-

tive control algorithms with limited and imperfect forecasts in practice. Nevertheless, discrepancies are limited due to the short-term (daily) operation of the storage units in buildings, as they are mainly utilized to integrate the daily fluctuations of PV electricity.

- no consideration of stochasticity in model parameters such as demands, component costs, and PV availability.
- the limitation of the grid reinforcement measures to those elaborated,
- the linear modeling of the model components as described.

This concludes the optimization problem formulations employed in this framework.

2.9 Post-optimization non-convex AC power flow simulation using *pandapower*

To maintain the tractability of the optimization problem, a simplified power flow formulation, *LinDistFlow*, was used for the HOODS framework grid model. As mentioned, this formulation drops the terms related to losses in the power flow and voltage drop equations, which might lead to approximation errors. Therefore, after the system planning is finalized, a non-convex AC power flow simulation is conducted with the reinforced grid components and the resultant nodal injections. The subsequent power flow simulation serves two concrete purposes:

- *Calculating the power losses in the system:* The non-convex power flow re-introduces the power loss terms, yielding the physically accurate energy flows and import amounts
- *Re-calculating the resultant bus voltages and line loadings:* The satisfaction of the corresponding grid restrictions is validated by recalculating the voltages and loadings.

The power flow calculation is based on the Newton-Raphson method and is conducted using the *pandapower* [84] library. The *LinDistFlow* approach will be validated in Section 4.1.2 through its comparison with the non-convex AC power flow results.

This concludes the Chapter regarding the methodology around the HOODS framework. The next Chapter will elaborate on the scenario definition made for the case study of this thesis.

Chapter 3

Definition of the case study

3.1 Goal of the case study

The goal of the case study in this thesis is to conduct a comprehensive analysis of the transformation of low voltage distribution systems (LVDSs) under a diverse set of operational and planning paradigms. As a toolkit to address the research questions of this dissertation, the optimization framework elaborated in the previous Chapter is developed. This Chapter will describe the case study of this thesis to which the optimization framework is applied. The case study deals with four LV distribution grids with varying characteristics to enhance the informativeness of the analysis. The following Sections will start with an overview of the scenario structure, followed by a definition of the case study regions, where each data acquisition step will be elaborated on.

3.2 Overview of the case study scenarios

Figure 3.1 gives an overview of the scenario space investigated in this case study. The scenarios are composed of three dimensions, as illustrated in Figure 3.1. These are:

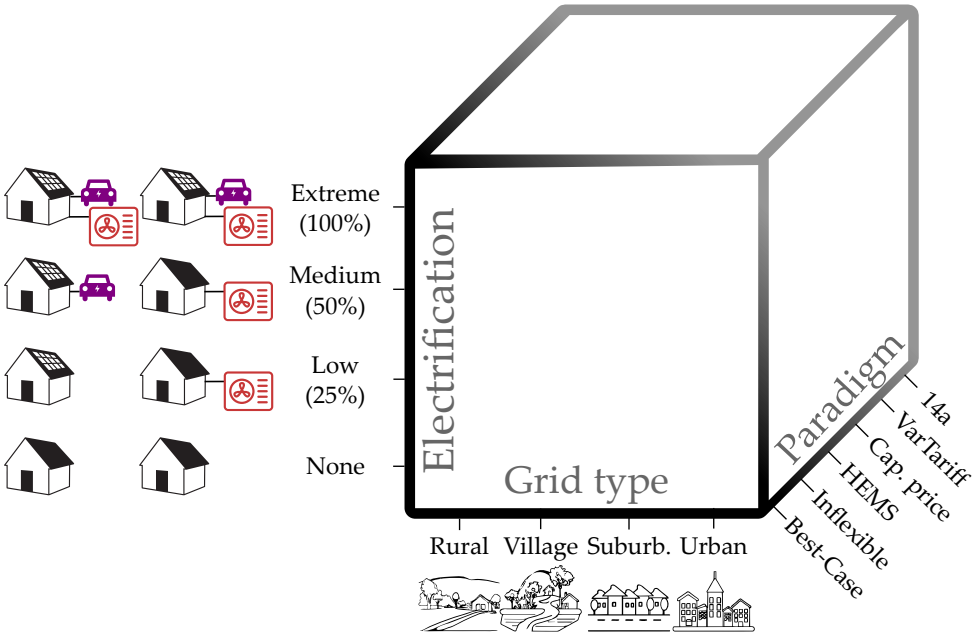

Figure 3.1: The scenario space of the case study.

- **Grid type:** A variation between LV distribution grids supplying various kinds of regions is made. These consist of a *rural*, a *village-type*, a *suburban*, and an *urban* grid.
- **Rate of electrification:** Various adoption rates for photovoltaics (PV), heat pumps, and BEVs are investigated. This consists of a zero-electrification scenario followed by a low, medium, and extreme electrification rate.
- **Planning paradigm:** This dimension deals with the different means of how the system planning and operation is conducted. It includes a *best-case* paradigm assuming total system coordination by a single decision-maker (HOODS-Sys), followed by the various uncoordinated paradigms where each prosumer and the grid operator optimize their respective systems to minimize their costs. The usage of flexibilities is varied between the *inflexible* and *HEMS* paradigms, while the *14a*, *capacity price*, and *variable tariff* paradigms investigate the influence of various technical and financial measures to alleviate the grid reinforcement needs.

3.3 Dimension 1: data to define a distribution system

To derive robust statements from the case study, realistic data is essential. The dataset developed in the study consists of the following types:

- Distribution grid topologies and capacities,
- Building stock,
- Weather data,
- Demands for electricity, heating, and mobility; and
- Techno-economic technology data.

To develop a realistic case study, consistency between these data has to be achieved. For example, the building stock should align with the load buses in the distribution grid. Likewise, the energy demands of each building have to be defined consistently with the building stock. Figure 3.2 illustrates the data concept implemented for this case study. In this figure, blocks in orange represent the open-source tools employed for data conversion and computation. The data sources are depicted in blue. The labels with asterisks indicate proprietary data, while the remaining ones are open.

This Section will delineate the steps undertaken to curate this coherent, integrated data set suitable for analysis.

3.3.1 Distribution grid models

In academia, working with realistic distribution grid data is a challenge. Since there are numerous factors that grid operators consider during planning, grid structures differ significantly from one another and cannot be generally reduced to a few representative models. Adding to this, the availability of real data is low, and digital models of distribution grids are usually not available in Germany. Some of them are still being expanded without systematic archiving. The distribution grid operators, who archive their networks digitally, do not publish these models due to the lack of financial or regulatory incentives. Concerns regarding data privacy and the security of critical infrastructure further contribute to the lack of transparency.

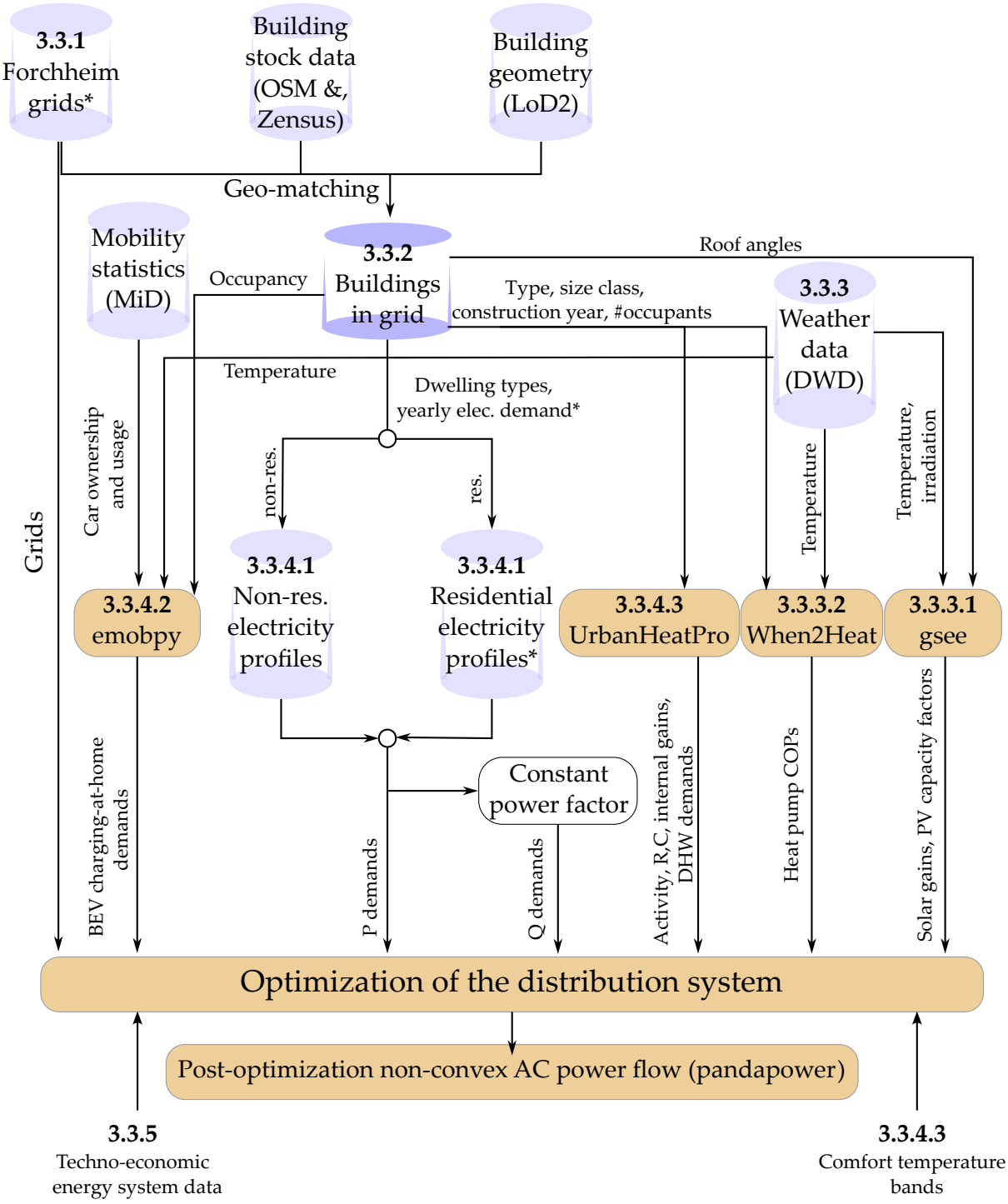

Figure 3.2: The integrated data concept developed for the case study of this thesis. The numbers for a given data source or tool represent the number of the corresponding Subsections where these are elaborated.

Compared to distribution grids, grid data for transmission networks can be procured more reliably. The overhead lines with pylons are visible in aerial photographs. Thus, they can be relatively easily identified. For instance, most high- and medium-voltage conductors and substations were subsequently marked in OpenStreetMap (OSM). Projects such as SciGRID, in particular, have tapped into this data source to model the transmission grids for Germany and then for Europe [85]. The same does not apply to distribution networks. The predominance of cables and geographical dispersion prevent such an automated approach. For economic reasons, many low-voltage networks are designed based on experience and are usually not monitored. Most of them are not archived or captured in digital models as part of distribution system operator (DSO) operations.

To tackle the low availability of distribution grid data, work has been done mainly in two avenues: i) deriving *benchmark grids* from a set of available grid data and ii) generating *synthetic grids* from the spatial configuration of buildings. The former deals with using usually publicly inaccessible datasets and applying aggregation methods on these to provide representative grid benchmark models (as described in [86, 87, 88]). Some of these models have also been integrated into open-access software packages, such as *pandapower* [84], facilitating ease of access to these models. While these benchmark models describe the typical topologies for various contexts, they also have limitations. They combine grids with varying characteristics into a single model, meaning specific local conditions cannot be accounted for. Hence, they come up short to be part of the integrated data set mentioned above. The *grid synthesis methods*, on the other hand, use local data such as building configuration and street topologies to emulate the grid planning process, yielding a probable distribution grid design tailored for a given area. In this, they use scalable methods such as the hierarchical clustering of load areas to define the bounding areas of each LV distribution grid [89], and minimum spanning tree algorithms to estimate the grid topologies [90]. While these methods allow flexible use, thorough validation is necessary, as the synthesized grid design may deviate significantly from real grids in the region. The low availability of actual grid data renders this validation difficult, if not impossible.

Due to these shortcomings of representative and synthetic grids, real grid data available to the author has been used in this case study. Within the scope of the research project *STROM*, the distribution grid for the city of Forchheim and the annual electricity consumption at each bus has been made available for research uses by the city utility (*de: Stadtwerke Forchheim*). Forchheim is a town in Upper Franconia, in the federal state Bavaria of Germany. It spans an area of 44.95 km^2, and as of 2021, it has a population of 32,433 occupants. In the RegioSTaR spatial topology standard developed by the German Federal Ministry of Transport and Digital Infrastructure [91], Forchheim is classified as a small-town village-type area in a regiopolitan urban region. Thereby, it contains both rural and urban characteristics.

The Forchheim grid dataset comprises numerous low-voltage distribution grids fed by 183 medium voltage (MV)/low voltage (LV) transformers. However, due to the limited computational resources and scope of the thesis, a few grids that represent diverse characteristics must be selected. In line with the classification made by Kerber [86], one grid for each of the following region types has been chosen: i) rural, ii) village-type (in short *village*), iii) suburban, and iv) urban. Analogous to their definition, a selection was made as a result of a pre-screening of the grids in terms of their number of loads and average distance to neighbors (higher the former and smaller the latter, one gets a denser, more "urban" grid).

The main characteristics of the selected grids are given in Table 3.1. They contain different numbers of buildings (load buses) for each grid, between 13 (for the rural grid) and 84 (for the urban grid). While the grid data also includes yearly electricity consumption for the preceding three years, the maximum values of the three years for each load are assumed for

a worst-case consideration. As a result, the yearly consumption varies from 90 MWh/year in the rural grid to 1,570 MWh/year in the urban grid. This translates to an average load per building of about 19 kWh/year in the urban grid, compared to a range of 7-10 kWh/year in the other grids. The higher value in the urban grid is due to the larger number of multi-family and non-residential buildings, whereas the other grids mainly consist of single-family houses. The prominent cable types for the main section of the grids are overhead lines for the rural grid and underground cables of 150 and 185 mm^2 cross section for the other grids. The building service lines have slightly larger capacities for the rural and village grids (with 50 mm^2) than the suburban and urban grids (with 35 mm^2). For the considered grids, a positive relationship between the load levels and the transformer capacities was also not observed–the rural and urban grids were fed by a transformer of 630 kVA, and the village and suburban grids by a transformer of 400 kVA.

Table 3.1: Key figures of the investigated low-voltage distribution grids. *The data set for the grid includes information on yearly electricity consumption for individual consumers over three years: 2019, 2020, and 2021. In this analysis, the year with the maximum electricity consumption is chosen for each consumer to evaluate a worst-case scenario.

		Grids			
Parameters	Unit	Rural	Village	Suburban	Urban
Number of buses	-	33	79	196	211
... of which load buses	-	13	28	81	84
Total load*	MWh/a	90	228	692	1,580
Total cable length	m	670	2,100	2,943	4,137
Prominent cable, main	-	15-AL1/3-ST1A0.4	NAYY 4x185SE	NAYY 4x185SE	NYY-J 3x150SM
Prominent cable, service	-	NAYY-J 4x50	NAYY-J 4x50	NYY-J 4x35	NYY-J 4x35
Transformer size	kVA	630	400	400	630

3.3.2 Building stock

Reliable building stock data is essential to characterize the energetic demands in a given distribution system. For the *building geometry*, the Level of Detail (LOD)2 database[1] provided as part of the open data initiative of the Bavarian surveying authority is used. This dataset was curated by intersecting the building floor plans using data from a recent airborne laser scanning survey, ALKIS-3D building measurement, or the aerial image-based digital surface model (latest data from 2021). In doing this, each building is assigned one or more roof shapes from a catalog of standard roof shapes. Compared to LOD1, which represents each building as a rectangular block, LOD2 also incorporates the shapes of multiple roof sections for each building (Figure 3.3). Thereby, not only the *floor area* and *height* for space heating calculations, but also a more refined calculation of the rooftop PV potentials can be made with a set of roof sections $r \in \mathcal{R}^i$ for each building i using their individual angles (See Section 3.3.3.1).

The buildings to be considered are filtered through the geographic intersection of the load buses defined in the grid data with the LOD2 building data (See Figure 3.4 for the set of buildings within every grid region). *The number of floors* and the *number of dwellings* for each of these buildings are then made through direct visual inspection. With this inspection, the uses of the buildings were also identified. The identified non-residential buildings include public buildings such as churches and schools or commercial buildings such as restaurants, offices, or shops. For mixed-use buildings, which consist not only of residential units but also

[1] https://geodaten.bayern.de/opengeodata/OpenDataDetail.html?pn=lod2

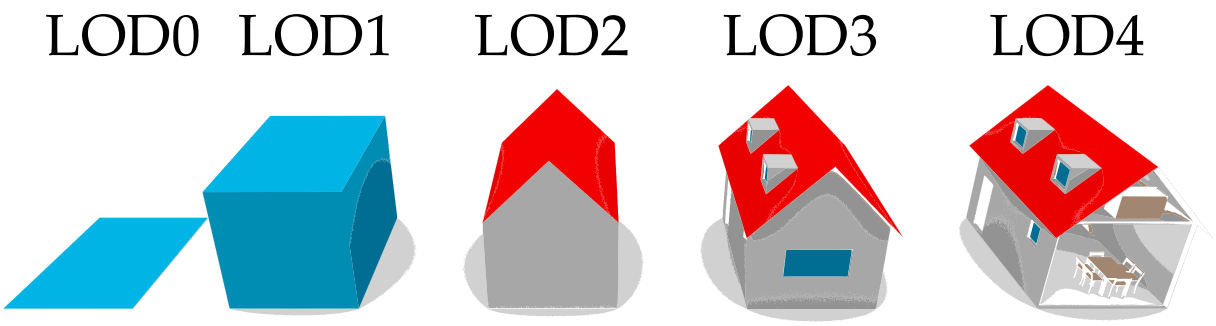

Figure 3.3: Various levels of detail (LOD) for building geometry data. Adopted from [92]

of non-residential units usually on the ground floor, the distribution of the units was likewise made. The *size class* of the residential buildings has been determined by the following logic:

- *terrace house (TH)* if a building has less than four free walls and is part of a connected group of at least three buildings,
- *multi-family home (MFH)* if a building does not have a TH characteristic and consists of more than two dwellings, and
- *single-family home (SFH)* if a building does not have a TH characteristic and consists of less than two dwellings.

No building with a size class of *apartment block (AB)* was observed in the investigated regions.

In order to classify each building in one of the TABULA topologies to estimate their thermal characteristics (see Section 2.3.2), one requires the *construction year of each residential building* besides the size class. While no building-specific construction year data is available publicly, aggregate information is provided by a census made in 2011[2]. In this census, information was collected from each residential unit regarding the number of occupants and the ranges of construction years for each building, which was then published in an aggregated form (sums for each 100m * 100m grid block) for anonymity reasons. To obtain building-specific values, a random distribution of the construction years is made into the buildings contained by each grid block (see Figure 3.5). Likewise, the total number of occupants is distributed to each building, where more occupants are allocated to buildings with a larger dwelling area.

The thermal resistance and capacitance (R and C) values (to be used as formulated in Section 2.3.2) of each building are calculated using the *UrbanHeatPro* tool, which is based on the methodology provided by TABULA. Here, the refurbishment state "usual refurbishment" is selected for each building. For the considered subset of the buildings, this approach yields a space heating demand per square meter representative of the national averages (150 kWh/m^2.year).

Table 3.2 gives a general overview of the building stock obtained via the process above. A notable observation from the table is that the buildings in the rural and urban areas exhibit relatively larger $U + V$ (lower R) values on average than those in the village and suburban areas. In the case of the urban grid, this can be attributed to the combination of an aging building stock and a large average footprint area. Expansive non-residential buildings such as a school and a church significantly contribute to this. Similarly, the rural region is characterized by an older building stock compared to village and suburban grids, contributing to its larger average $U + V$ value.

It has to be noted that this analysis deals with the current state of the building stock and assumes that no refurbishment takes place in the considered grid regions. Indeed, this leads

[2] https://atlas.zensus2011.de/

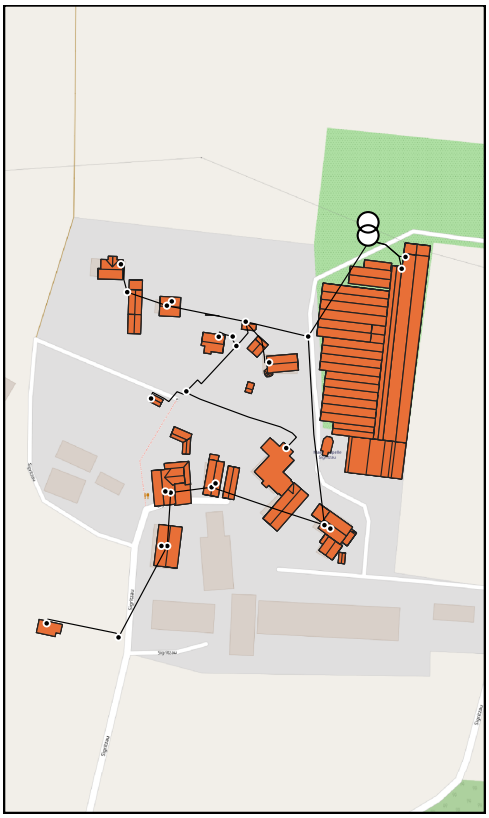

(a) Rural

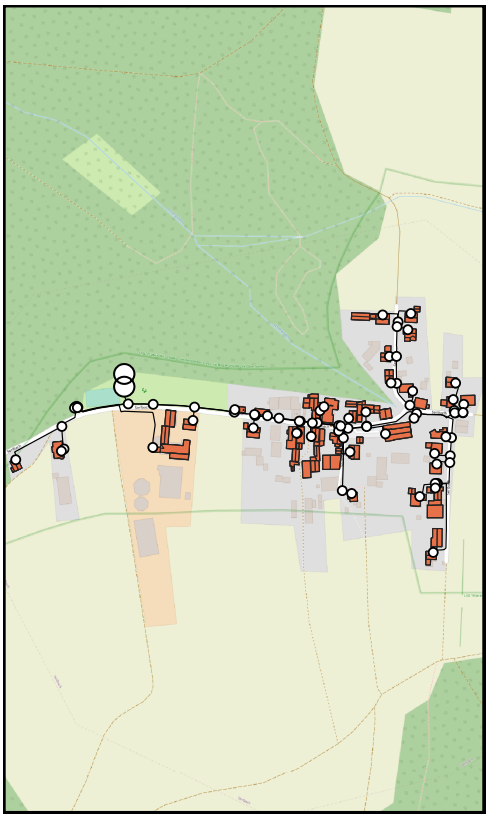

(b) Village

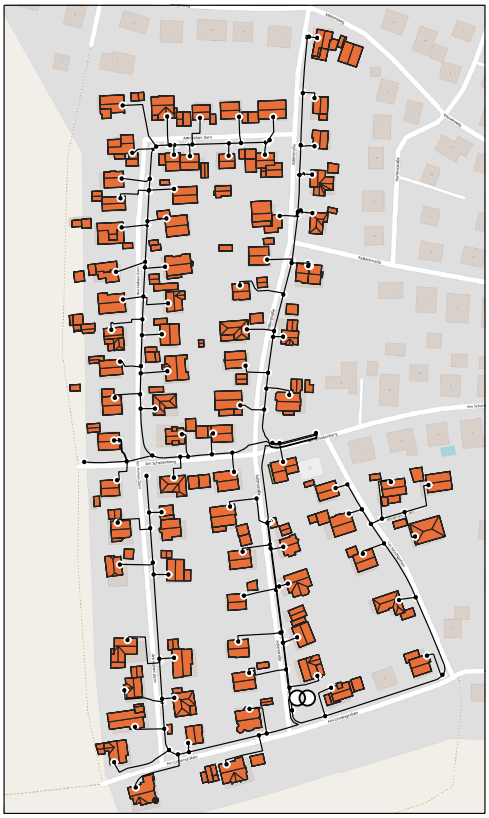

(c) Suburban

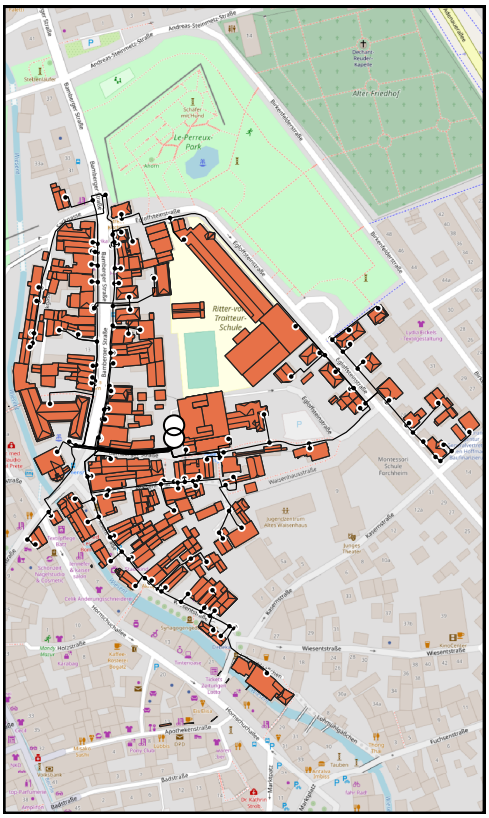

(d) Urban

Figure 3.4: The case study regions with the underlying grid topologies and the supplied buildings. Each building may consist of multiple roof sections, each of which is represented as an individual polygon in the maps.

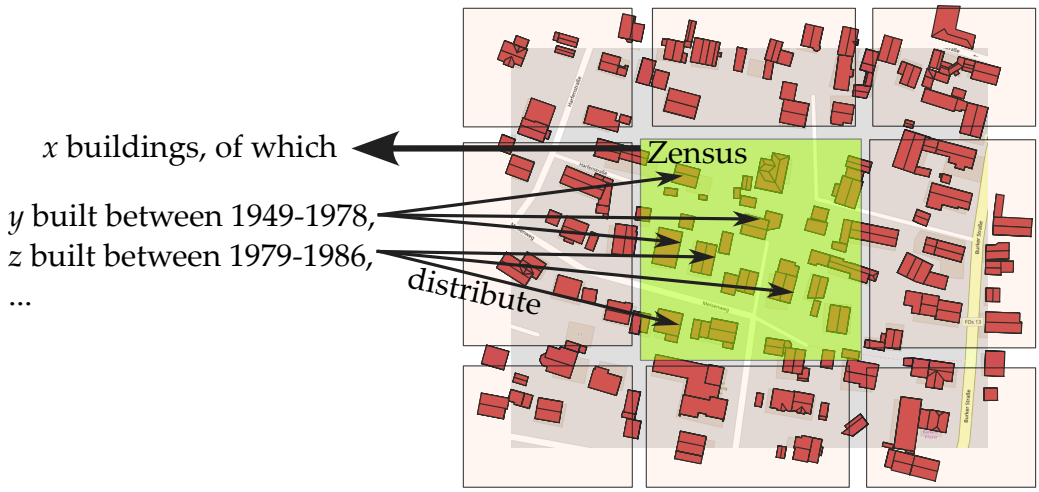

Figure 3.5: Distribution of the aggregated census values for construction years to each building.

to an overestimation of the resultant heat demands. Possible alternative approaches would have been to assign a fixed refurbishment rate in the building stock or to define it as an endogenous decision in the optimization, using an approach similar to [93]. However, these considerations are excluded from the scope of the work for reducing model complexity.

3.3.3 Weather data

The weather characteristics of the investigated regions are an essential factor when deciding on the optimal planning of their energy systems. Low ambient temperatures drive the demand for space heating in buildings as well as influence the efficiency of the heat pumps, and solar irradiation determines the generation potential from the PV systems and the solar gains. For this case study, the Test Reference Year (TRY) data provided by the German Meteorological Service (DWD) has been used as a basis for the weather data. The TRY data contain various meteorological data for every hour of a given year. They represent the typical weather progression for a specific year and climate region. These typical weather characteristics are generated using data from 1995 to 2012 as the baseline [94]. While the dataset also contains an extreme year that incorporates the predicted future climate change effects, the data depicting the current weather properties is used in this study (denoted as TRY 2015).

The first version of the TRY data set was developed in 1985, which divided Germany into 15 climate regions. With the version developed in 2017, now consisting of a data resolution as high as one km^2, local variance in the data can be observed in a highly granular manner.

The parameters included in the data set that are relevant to the study and their uses are the following:

- *Ambient temperature*: The temperature data is used

  1. directly in the one resistance and one capacitance (1R1C) model of the holistic optimization of distribution systems (HOODS) problems,
  2. for calculating the coefficient of performance (COP) of the heat pump systems,
  3. for the generation profiles of the PV systems (higher module temperatures usually yield lower PV efficiencies).

  The basis of the data is measurements from weather stations distributed across the country taken at 2 meters. These are sheltered by Stevenson screens to prevent data distortion

Table 3.2: The building stock contained in each grid region. *Residential buildings also include mixed-use buildings.

		Grids			
		Rural	**Village**	**Suburban**	**Urban**
Number of buildings, total		11	26	79	81
...with use:	**Residential***	8	20	79	66
	SFH	8	17	71	12
	MFH	0	3	6	23
	TH	0	0	2	30
	AB	0	0	0	1
	Commercial	3	2	0	12
	Public	0	2	0	3
	Industrial	0	2	0	0
...with floors	1	8	2	6	2
	2	3	13	45	16
	3	0	11	28	57
	4	0	0	0	6
...with construction year	**before 1919**	0	0	0	43
	1919-1948	9	0	0	10
	1949-1978	2	19	64	22
	1979-1986	0	2	1	0
	1987-1990	0	0	0	3
	1991-1995	0	2	14	0
	1996-2000	0	3	0	3
Number of dwellings		11	33	123	158
Number of occupants		16	57	278	292
Average footprint area (m^2)		173	193	148	251
Average $U + V$ value (kW/K)		1.03	0.78229	0.666	0.98
Average C value (10^7 J/K)		7.9237	8.8519	7.2890	8.9798

due to irradiance. Using additional topographical and land use data, phenomena such as vertical temperature gradients and urban heat island effects are also incorporated.

- *Beam and diffuse irradiances on the horizontal surface:* These are used for calculating the buildings' solar gains and the PV systems' generation profiles. The basis for these data is weather stations and satellites.

For more details regarding the methodology of the TRY data calculation, the reader is referred to the data manual [94].

Some key figures from the high-resolution TRY 2015 data are given in Table 3.3. Although each km^2 corresponds to distinct data points for each of the four grid regions, only minor differences are observed between the regions due to their proximity. Average temperatures are the same, apart from a slightly lower value for the suburban model. The urban model, on the other hand, has a very slightly lower total global horizontal irradiance (the sum of the horizontal direct and diffuse irradiances) over the year, possibly due to increased shading by higher and more densely located buildings.

Table 3.3: Key figures of the DWD TRY weather data for each grid region.

	Grids			
	Rural	**Village**	**Suburban**	**Urban**
Temperature				
Average	9.3	9.1	9.3	9.3
Min	-10.6	-13.2	-10.8	-11.4
Max	33.2	33.2	33.4	35.1
Global Horizontal Irradiance				
Total (kWh/m^2.year)	1,127	1,127	1,127	1,090
Peak (W/m^2)	944	945	925	942
Direct Horizontal Irradiance				
Total (kWh/m^2.year)	555	565	558	517
Peak (W/m^2)	828	825	811	823
Diffuse Horizontal Irradiance				
Total (kWh/m^2.year)	573	562	569	573
Peak (W/m^2)	453	480	486	457

3.3.3.1 Calculating the PV capacity factors using the *gsee* library

The weather data is then used to generate normalized capacity factor time series $cf^{\mathrm{PV}}_{i,r,t}$ for PV units. For this processing step, the *Global Solar Energy Estimator (gsee)*[3] is employed. *gsee* is an open-source Python library that can be used to model solar PV systems and contains a set of submodules to simulate their performances. Its functions are also used in the backend of the *renewable-ninja* tool[4]. Using this library, the technical characteristics of a given PV system can be externalized, as the generation profile can be simplified into a series of normalized capacity factors. These capacity factors can then be used in the optimization framework in a linear fashion (recall equation (2.1)).

For every building i, the capacity factor time series are generated for each of its roof sections $r \in \mathcal{R}^i$. To reduce model complexity and exclude roof sections that are less suitable for PV installations, a cut-off value of at least 25 m^2 of roof section area is chosen. Assuming an area factor of 0.15 m^2 per kW, this cutoff corresponds to 3.75 kW[5]. Then, to generate roof section-specific capacity factor data, the `gsee.pv.run_model()` function is used for each roof section larger than this cutoff value, with the following arguments:

- *weather data* consisting of the ambient temperature, global horizontal irradiance (simple sum of the direct and diffuse components), and the diffuse fraction of the irradiance (ratio between the diffuse and the global irradiance),
- *coordinates* of the building in latitude and longitude,
- *tilt angle* of the roof section,
- *azimuth* of the roof section,
- *tracking* set as zero (fixed PV),

[3]The repository of *gsee* can be found here: `https://github.com/renewables-ninja/gsee/` and the paper elaborating on the methodology can be found in [95]

[4]`https://renewables.ninja/`

[5]This is considered a reasonable cutoff, as only around 15% of the registered rooftop PV (<30 kW) units in Germany had a smaller capacity than this rating according to the Core data registry (*Stammdatenregister* published by the German Federal Network Agency

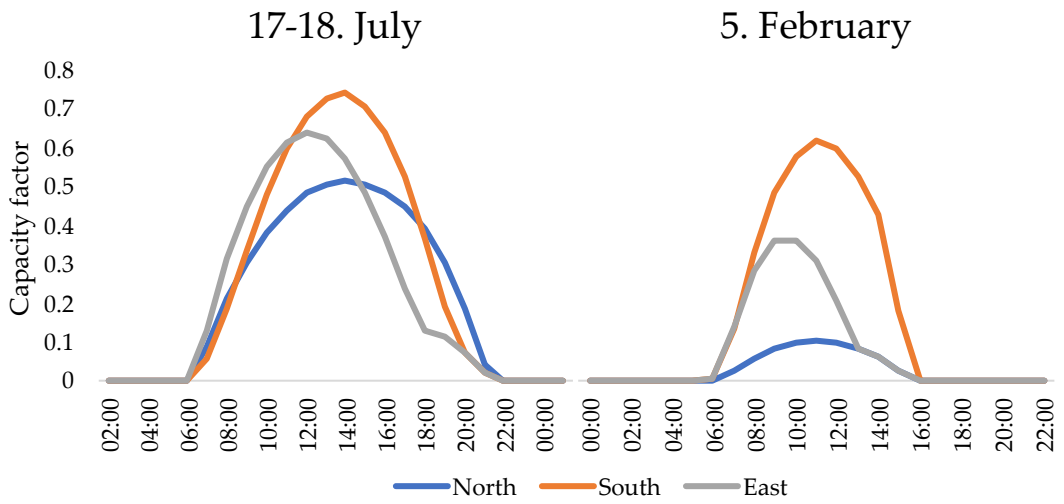

Figure 3.6: Exemplary capacity factor curves for PV systems facing different directions.

- *module type* set as c-Si (crystalline silicon),
- *system losses* set as 10%, and
- *module capacity* set as 1 W to generate normalized profiles.

The function utilizes trigonometric relations between the coordinates, irradiance components, solar angles, and the angles of the PV unit to calculate the aperture area of the module that receives the in-plane irradiance (see [95]). Then, it uses the methodology of [96] for determining the temperature- and irradiance dependence of the module efficiencies around the standard test conditions for temperature and irradiance defined at $25°C$ and $1,000 W/m^2$ respectively. With these parameters, the normalized electricity generation from the PV system can be calculated as follows:

$$cf^{\text{PV}}_{i,c,t} = \frac{\text{irradiance } (\frac{W}{m^2}) \cdot \text{aperture area } (m^2) \cdot \text{efficiency}}{1W}. \tag{3.1}$$

Figure 3.6 illustrates exemplary capacity factor curves calculated using the *gsee* module. These curves represent the solar generation for clear-sky days during two distinct seasons–summer and winter. They are given for panels with three different orientations: facing south, west, and north, and a standard tilt angle of approximately 30°C.

The yearly full load hours that result from these orientations are 1040 h/a for south-facing panels, 815 h/a for west-facing panels, and 733 h/a for north-facing panels. During the winter, north-facing panels experience a substantial reduction in generation, whereas the south-facing panels maintain a relatively high and consistent output. Panels facing east have overall lower capacity factors than those facing south, but their generation curve is partially shifted to early morning hours, which may benefit self-consumption.

Figure 3.7 illustrates an ordered cumulative step plot for the distribution of the capacity potentials and the full load hours of each roof section in the respective grid regions. Here, each region is depicted in a different color. Depending on the angles of a roof section, the full load hours can vary between approximately 500 and 1,100 hours. These full load hours apply in various proportions to potential PV installations in each grid. The rooftop PV potentials depend on the available roof space in each grid and range from 400 kW_p for the rural grid to 3,800 kW_p for the urban grid. Consequently, the maximum generation potential of PV, which would be the case if all roof sections were utilized, ranges from two to three times

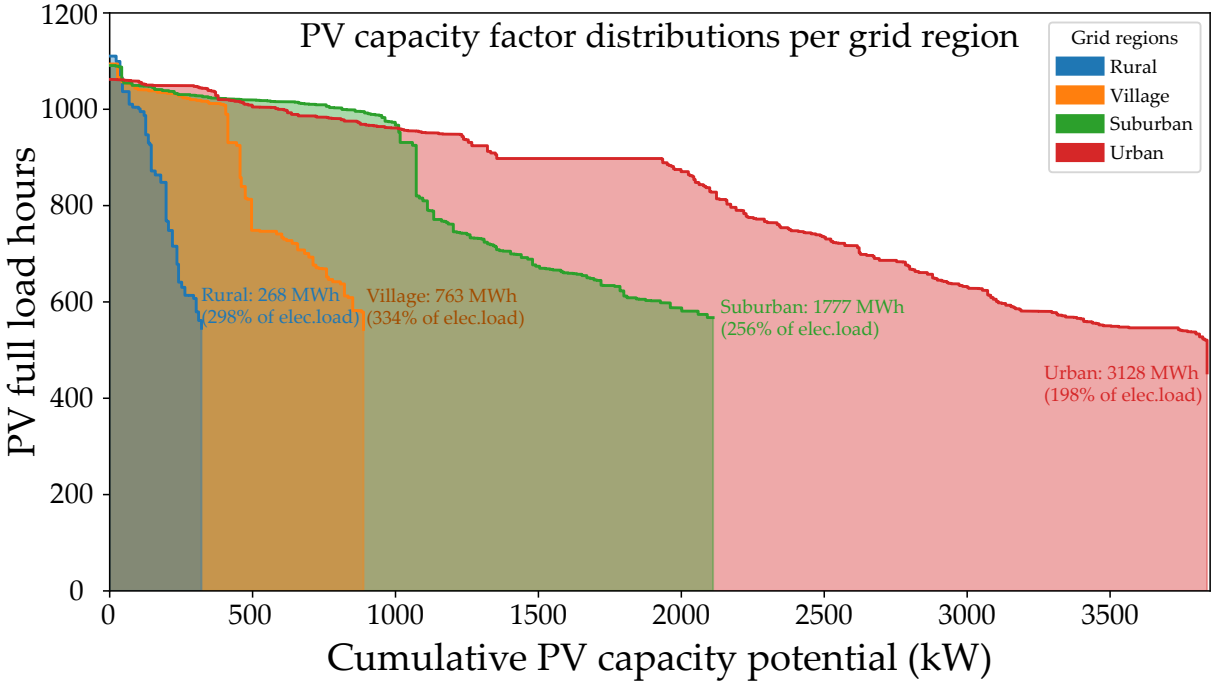

Figure 3.7: PV capacity factor distributions per grid region, given in cumulative step plot. The x-axis gives the cumulative PV capacity potentials above a specific full load hour (y-axis). The numbers on the plot depict the total generation potentials; the percentage values compare this to the total electrical load for each grid region.

the electrical load in the regions. Of course, not all of this generation can be integrated for self-consumption, and the additional demands of the heat pumps and battery electric vehicle (BEV)s are not included yet.

3.3.3.2 Calculating the heat pump coefficients of performance (COPs) using the *When2Heat* methodology

Another set of weather-dependent parameters playing an important role in the optimal planning of DER capacities is the coefficients of performance (COPs) $cop^{\mathrm{HP}}_{i,t}$ of the heat pump units. This parameter acts as the conversion factor between the electrical input to the heat pump and the heat generation, as presented in the HOODS model equation (2.16a).

The methodology to calculate hourly COP values is based closely on the approach of [53], which was developed for deriving the *When2Heat* data set. While the *When2Heat* project dealt with average COP values at the national level for 28 European countries, its bottom-up character makes it suitable for application on the individual heat pump level. This methodology will be described in this Section.

While the COP is connected to the cycle temperature differential through thermodynamic relations, namely the Carnot efficiency, empirical regressions based on manufacturer data yields usually more realistic results. Correspondingly, the basis for the *When2Heat* methodology has been the depiction of the COP using an empirical quadratic regression function of the temperature differential $\Delta\vartheta^{\mathrm{HP}}_{i,t}$ as proposed by [97]. Specifically for air-source heat pump, the COP is described with the following polynomials for space heating and domestic hot water,

respectively:

$$cop_{i,t}^{\text{HP,sh}} = 6.08 - 0.09K^{-1} \cdot \Delta\vartheta_{i,t}^{\text{HP,DHW}} + 0.0005K^{-2} \cdot \left(\Delta\vartheta_{i,t}^{\text{HP}}\right)^2, \tag{3.2}$$

$$cop_{i,t}^{\text{HP,DHW}} = 6.08 - 0.09K^{-1} \cdot \Delta\vartheta_{i,t}^{\text{HP,DHW}} + 0.0005K^{-2} \cdot \left(\Delta\vartheta_{i,t}^{\text{HP,DHW}}\right)^2, \tag{3.3}$$

where the temperature differential of the heat pump is defined as the difference between the sink and source temperatures ($\vartheta_{i,t}^{\text{HP,sink}}$, $\vartheta_{i,t}^{\text{HP,source}}$) of the heat pump:

$$\Delta\vartheta^{\text{HP,sh}} = \vartheta_{i,t}^{\text{HP,sink,sh}} - \vartheta_{i,t}^{\text{HP,source,sh}}, \tag{3.4}$$

$$\Delta\vartheta^{\text{HP,DHW}} = \vartheta_{i,t}^{\text{HP,sink,DHW}} - \vartheta_{i,t}^{\text{HP,source,DHW}}. \tag{3.5}$$

It follows from the equation (3.3) that the smaller the temperature differential, the higher the COP of a heat pump (hence a more cost-efficient operation). Yet, these temperatures are tightly constrained by the heat pump's operational conditions. The source temperature is defined as the temperature of the medium from which the heat pump sources the heat. For air-source heat pumps, the type considered in this case study, the source temperature corresponds to the ambient air temperature ϑ_t^{amb} directly:

$$\vartheta_{i,t}^{\text{HP,source}} = \vartheta_t^{\text{amb}}. \tag{3.6}$$

The heat sink temperature, in turn, refers to the temperature of the medium where the heat pump is releasing the heat. The required heat sink temperature of a heat pump depends on various factors, for instance, the use of the heat. For space heating, the sink temperature $\vartheta_{i,t}^{\text{HP,sink,sh}}$ has an inverse relationship with the surface area of the heat distribution system. For radiator-based distribution systems, the heat transfer surface area is limited. This necessitates a higher sink temperature in order to dissipate a given amount of heat to a building's rooms. In contrast, buildings with floor heating enable more expansive heat transfer surfaces, which allows for the utilization of lower sink temperatures. Moreover, the sink temperature required for adequate heating depends on the ambient temperature. On colder days, a higher sink temperature is often needed to offset the increased heat lost and ensure thermal comfort in the building. This relationship is described by the so-called "heating curve" of the heat pump system. In the adopted methodology, heating curves are linearized and parametrized using an average of the literature values from [97], [98] as follows:

$$\vartheta_{i,t}^{\text{HP,source,sh}} = \begin{cases} 40°C - \vartheta_t^{\text{amb}} & \text{if radiator,} \\ 30°C - 0.5 \cdot \vartheta_t^{\text{amb}} & \text{if floor heating.} \end{cases} \tag{3.7}$$

For domestic hot water supply, different temperature constraints apply. The *When2Heat* methodology sets a water temperature of 50°C, based on a field trial conducted in Germany for heat pump operation in single-family houses [99]. However, the German Environmental Agency recommends heating domestic hot water up to 60°C to prevent the formation of legionella bacteria [100], as their growth persists up to 55°C. While high water circulation rates may reduce this risk for smaller residential buildings like single-family houses and terrace houses, for residential buildings of larger size classes and non-residential buildings, this higher temperature is set:

$$\vartheta_{i,t}^{\text{HP,source,wh}} = \begin{cases} 50°C & \text{if building } i \in \{\text{SFH, TH}\}, \\ 60°C & \text{else.} \end{cases} \tag{3.8}$$

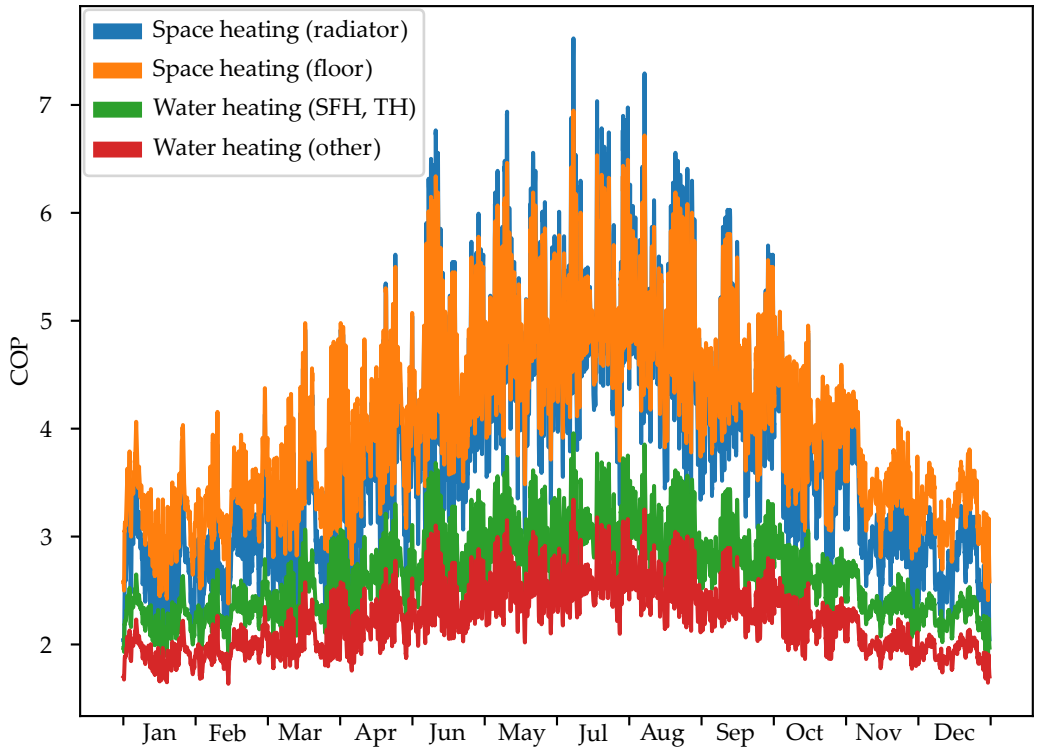

Figure 3.8: The course of heat pump coefficients of performance (COP) for various heat use in the suburban grid region.

Finally, to account for the deviations arising from non-ideal operation conditions and part-load behavior in practice, a fixed correction factor of 0.85 is introduced to all calculated COP values.

Figure 3.8 shows the exemplary COP values for the suburban grid region resultant from the above-described approach. The COP values for space heating vary between above 2 for cold winter days up to 7 for warmer days. While the extremely high COP values up to 7 directly result from very small temperature differentials, they are indeed too high for realistic heat pump operation. Nevertheless, the impact of these values on the overall electrical behavior of the system is minimal, as they occur during warm weather conditions when the space heating demand for heat pumps is minor.

As the HOODS model does not distinguish between the COP values for space heating and domestic hot water production, a single value has to be constituted. This is done by conducting an ex-ante simulation of the space heating and domestic hot water (DHW) demand with the *UrbanHeatPro* tool using the R and C values of each building, along with the set lower temperature limit given in Section 3.3.4.3. This way, a single COP value $cop_{i,t}^{\mathrm{HP}}$ for each model time step can be generated using a simple weighted average—for the time steps where DHW demand exists, the effective COP will experience a decrease below the COP for the space heating.

$$cop_{i,t}^{\mathrm{HP}} = \frac{d_{i,t}^{\mathrm{SH,sim}} \cdot cop_{i,t}^{\mathrm{HP,SH}} + d_{i,t}^{\mathrm{DHW,sim}} \cdot cop_{i,t}^{\mathrm{HP,DHW}}}{d_{i,t}^{\mathrm{SH,sim}} + d_{i,t}^{\mathrm{DHW,sim}}}. \tag{3.9}$$

Note that the space heating demand profiles simulated for this step ($d_{i,t}^{\mathrm{SH,sim}}$) are not used in the HOODS model, where the satisfaction of this demand is instead optimized under the given set of temperature limits as per (2.15). The optimized behavior would indeed lead to a different effective COP behavior in turn. However, this deviation is predicted to be not

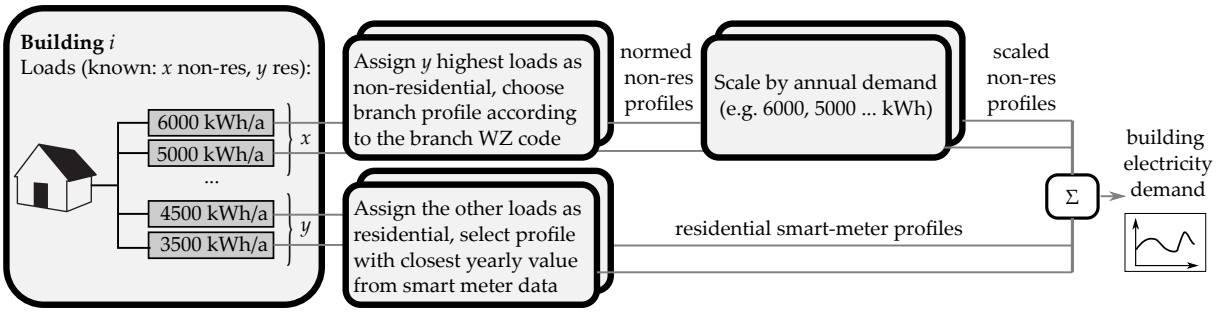

Figure 3.9: The assignment procedure of active power demand profiles to each building.

significant—the significantly higher volume of the space heating demand will usually yield an effective COP profile very close to the COP for space heating.

3.3.4 Demand data

Next, the energy demand profiles associated with each building are defined. The HOODS framework deals with three modes of demand: 1) electricity, 2) heating, and 3) mobility. This step aims to generate a coherent demand dataset that aligns with the characteristics of the specific building stock at hand.

3.3.4.1 Electricity demand

The basis for the electrical demand for each dwelling of the buildings, whether residential or non-residential, is the annual load data provided by the DSO of Forchheim as part of the grid data. The yearly electricity demands for each load bus within the buildings are available for three consecutive years (2019, 2020, 2021). To ensure conservative planning, the highest value among these three years is selected as the individual load's electricity demand.

These annual demands have to be temporally disaggregated into suitable hourly profiles in the next step, before getting aggregated over each dwelling again to constitute a building's collective electrical demand profile. The process is illustrated in Figure 3.9. For this, two data sources are used depending on the type of the load. The number of residential and non-residential loads for each building are known through the inspection as described in Section 3.3.2. Since the information regarding which loads belong to which unit is unavailable, the buildings' largest loads are assumed to be the non-residential units, and the remaining loads are assigned as the residential units. Then, suitable profiles are generated in the next step for each individual load and its use.

Residential loads To allocate electrical load profiles to the residential units of each building, a pool of real smart meter data is used as a basis. These data are sourced from a set of smart meters installed in private households as part of a pilot project in 2011. The data set comprises over 2,700 profiles at a 15-minute resolution, with annual electricity demands reaching up to 19,000 kWh. They consist solely of the electrical consumption of conventional household appliances and do not include any consumption from heat pumps or wall boxes. In the case study, a post-processed version of this data, obtained through the diploma thesis by Vogt [101], and the *lemlab* model [6] are employed.

Figure 3.10 compares a random subset of this smart meter data, consisting of up to 1000 profiles, with the German Federal Association of Energy and Water Industries (BDEW)

[6] https://github.com/tum-ewk/lemlab

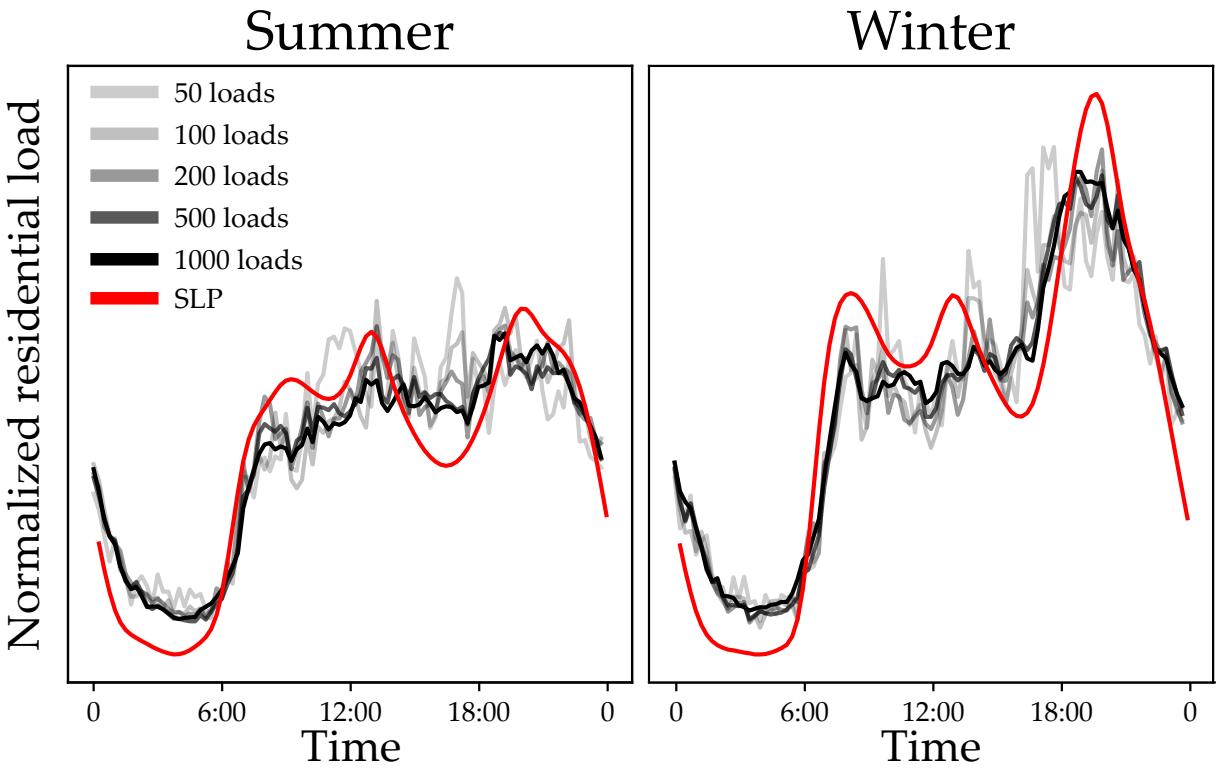

Figure 3.10: The comparison of aggregate smart meter loads with the standard load profiles.

standard load profile (SLP) for households (SLP-H0) [102], for both a winter day and a summer day. In both selected periods, a qualitative approximation to the standard load profiles is evident at around 1,000 samples. However, it is observed that the SLPs underestimate the loads during the night hours and overestimate the loads during the evening peak.

For each load classified as residential, the goal is to match it with a smart meter profile with the closest annual consumption. To accomplish this, a series of data-cleaning steps were necessary. For instance, some units had unrealistically high loads, likely due to the heating load values falsely interpreted by the DSO as electrical load in the data set. Correspondingly, any load exceeding 9,000 kWh per year is substituted with a random value between 8,000 and 10,000 kWh, generated uniformly. By assigning such a high yet still plausible value for these loads, a conservative approach to grid planning is achieved. The random selection within the given range promotes the choice of non-identical profiles for each such load, thus avoiding an unrealistic simultaneity of demands. Additionally, in the rare instances where the annual demand information is missing for a given dwelling, the available load data with the closest demand, preferably within the same building, is adopted as the most probable value. To avoid assigning identical profiles to these loads, i.e., an unrealistic 100% simultaneity within the same building, a minor deviation of 100 kWh/year is incorporated.

Non-residential loads For non-residential loads, open data for synthetic non-residential load profiles from the *synGHD* project is used [103]. These profiles improve over the daily standard load profiles developed by the German Association of Electricity Industry (VDEW) [102] in several ways. Instead of three representative days, they consist of quarter-hourly demand profiles for all years between 2009 and 2018, making them suitable for this case study. Furthermore, they offer a more detailed breakdown of branch profiles, encompassing 32 distinct non-residential sectors. This way, the variations in demand profiles between sectors can be better represented. To each sector, a profile with a distinct industry branch (WZ) (*de:*

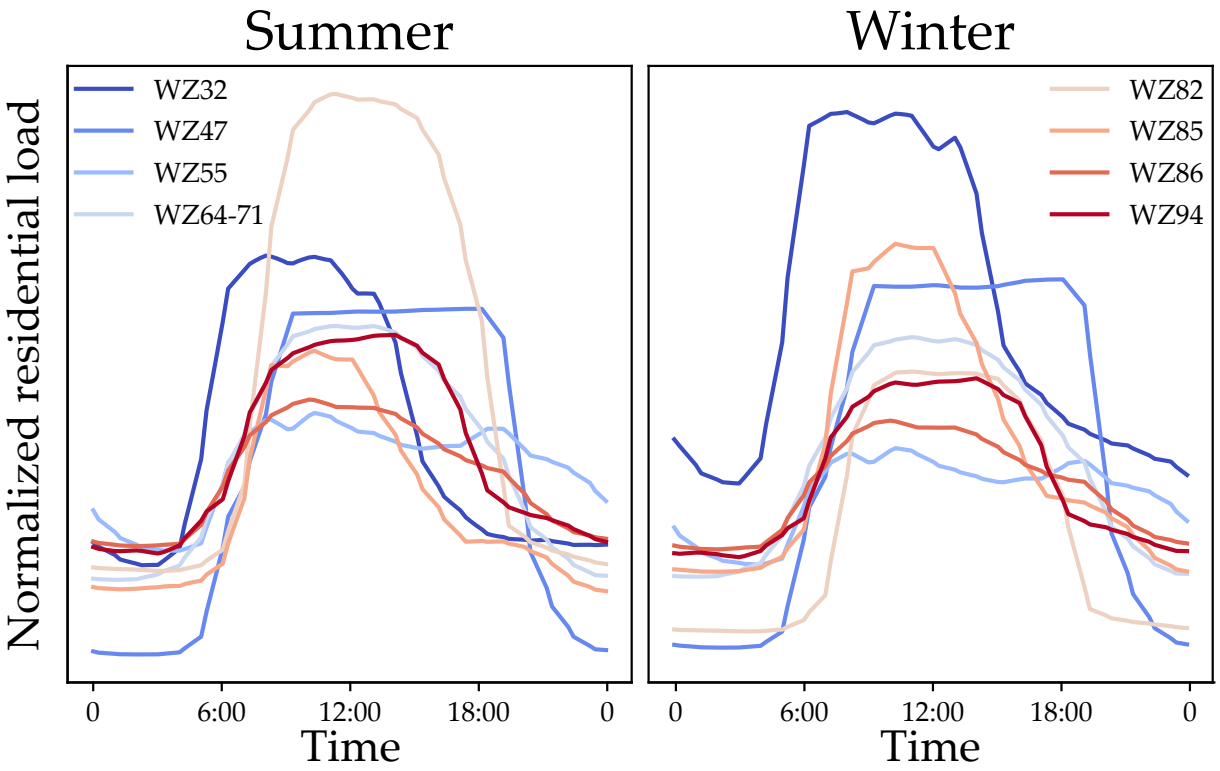

Figure 3.11: Selected non-residential load profiles from [103].

Wirtschaftszweig) code is associated. An exhaustive list of all the sectors associated with their WZ codes can be found in [104]. The particular branches located in the investigated grid regions are given in Table 3.4.

Table 3.4: The non-residential branches observed in the considered grid regions. *While this WZ corresponds primarily with economic services for individuals, it was found to be the most relevant one for the activities marked with an asterisk (*).

WZ code	WZ definition	Examples in the grid region
WZ32	Production of various goods	workshop
WZ47	Retail	retail store, market
WZ55	Lodging	hotel, bar, restaurant, cafe
WZ64-71	Office operations	office
WZ82	Services	hairdresser*, massage parlour*
WZ85	Education and teaching	school
WZ86	Healthcare	clinic, physiotherapy practice
WZ94	Interest groups	church, community center

Figure 3.11 illustrates these profiles in exemplary weeks for summer and winter. Here, seasonal variations are visible—for educational (WZ85) and production (WZ32) branches, higher demands in winter are observed, whereas the services branch (WZ82) has increased demands in summer.

These non-residential profiles are assigned to the buildings in the following manner: first, the highest loads within each building are assigned the normed profile corresponding to their respective branches. Subsequently, these profiles are scaled up to align with the annual demand of the load. This way, a consistent allocation is achieved. However, there is a shortcoming in using these profiles for individual loads: similar to the SLPs, these profiles represent

the *average* consumption behavior of a large number of non-residential units belonging to a particular branch. As a result, they do not accurately reflect the peak demands that one would expect from an individual unit. Indeed, this could lead to underestimating their contribution to the grid peaks. Nonetheless, these profiles are used in the case study due to the lack of reliable data for individual non-residential units.

Ultimately, the total active power demand from a building consists of the sum over all residential and non-residential units it contains:

$$d^{\text{elec}}_{i,t} = \sum_{u \in \text{res. units}} d^{\text{elec}}_{i,u,t} + \sum_{u \in \text{non-res. units}} d^{\text{elec}}_{i,u,t}. \qquad \forall i \in \mathcal{I}^b \qquad \forall t \in \mathcal{T}_m \tag{3.10}$$

Note that it has not been possible to match the underlying household activities leading to the electricity demand profiles assigned in this step to the activity routines simulated by the *UrbanHeatPro* workflow as introduced in Section 3.3.4.3, as the used time series are based on independent measurement data (for residential units) or aggregated profiles (for non-residential units).

Reactive power demand As each electrical appliance in a household operates at a different power factor (PF) [105], the overall power factor of the household load depends on the usage profiles of these devices. However, as the used electricity demand profiles lack information regarding the exact scheduling of the appliances, a constant PF value is set for simplicity. The set value of 0.9 (lagging) corresponds to a Q/P ratio of around $\cos^{-1}(0.9) \approx 0.48$. This is on the higher end compared to usual household operation—indeed, a reduction of the Q/P ratios has been observed in recent years due to the introduction of new devices [105] (see [106] for an example in the United Kingdom). However, this effect is not considered as conservative planning is desired for the case study. This leads to the following definition of the reactive power demand:

$$d^{\text{elec,q}}_{i,t} = \tan(\cos^{-1}(0.9)) \cdot d^{\text{elec}}_{i,t}. \qquad \forall i \in \mathcal{I} \qquad \forall t \in \mathcal{T}_m \tag{3.11}$$

3.3.4.2 Mobility demand using *emobpy*

The BEV charging demand profiles are generated using the open source Python library *emobpy*[7] [107]. *emobpy* is a suitable tool for this case study, as it can generate BEV-specific charging profiles, allowing for a customized parametrization of the driving routines and a flexible temporal scope and resolution. As Figure 3.12 illustrates, the *emobpy* workflow consist of four steps:

- depending on the type of the driver and her driving preferences, a *driving schedule* is synthesized, which consists of time series information regarding the duration and distance of the routes and the BEV location during its idling hours,
- this driving schedule is combined with the technical properties of the BEV, weather, and road condition to generate a *discharge* time series of the vehicle battery,
- to compensate for this consumption, the BEV has to be charged at available charging locations. Depending on the charging capacities at each type of location and the probabilities that these locations are available for charging at a given moment, a time series for the *available charging locations and their capacities* is generated, and

[7] https://gitlab.com/diw-evu/emobpy/emobpy

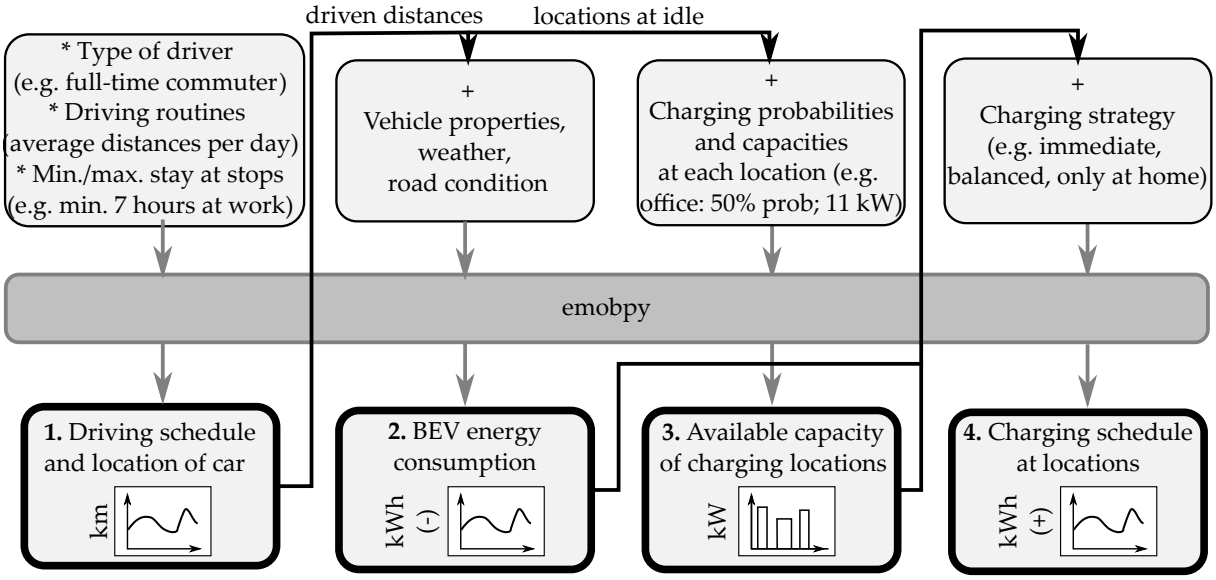

Figure 3.12: The *emobpy* workflow, which is used to generate BEV charging profiles (adapted from [107]).

- under a given charging strategy of the BEV, e.g., an immediate strategy that leads to charging wherever an available station is present or one that only allows charging at specific locations, the *BEV charging schedule* is simulated.

In essence, *emobpy* is a simulation tool that yields a charging behavior of a BEV over a year, including the locations where each of these charging instances occurs. In practice, these charging locations, such as home and workplace, correlate with different grid nodes, which may or may not be part of the LV grids under investigation. Therefore, to simplify the analysis, only the BEV usage associated with residential units will be considered, allowing for a direct association of the charging that took place at home with the corresponding building node. Consequently, the charging instances that occur in other locations (e.g., in the workplace or public charging) will be presumed to be outside of the LV grid and are therefore excluded from the analysis. These at-home charging amounts will be defined in the HOODS problem as the mobility demand, denoted by $d^{\mathrm{BEV}}_{i,c,t}$, which can then be satisfied flexibly by utilizing the vehicle's battery.

For this, the number of BEVs allocated to each building has to be determined for each grid region. Then, a suitable choice of the *emobpy* parameters has to be made to generate the charging profiles for each car. Statistical data provides a valuable starting point.

***Mobility in Germany* survey** To determine the number of cars and their usage in the grid regions, the country-wide statistics provided by the study *Mobility in Germany (de: Mobilität in Deutschland - MiD 2017)* [108] is used as a basis. The MiD 2017 study consists of a nationwide survey to characterize the mobility behavior of the German population. The survey results are based on around a million driving routes reported by over 300,000 interviewees. The questionnaire includes aspects such as:

- the mobility rate, i.e., the ratio of the population that leaves their home at least once a day,
- the time spent mobile per day,
- the number and length of stops per day,

- the modal split, i.e., the favored modes of transportation,
- the ownership of private vehicles per household, and
- the use of private vehicles.

Depending on the regions where each interviewee resides in, the responses for these statistics are categorized into the RegioStaR 7 typology classes [91], to represent the varying preferences of the population living in more and less densely populated areas. To reflect this diversity also in the considered grid regions, the rural and village grid regions are deemed to be located in a *a village-type space, in a rural area (class 77)*, and the suburban and urban grid regions in a *medium-sized city, in a rural area (class 76)*.

According to the MiD 2017 study, households within these regions have car ownership characteristics as depicted in Table 3.5.

Table 3.5: Car ownership in regions based on MiD 2017 [108].

Grid regions	Regiostar 7 class	no car ($prob_0$)	1 car ($prob_1$)	2 cars ($prob_2$)	3 cars or more ($prob_3$)
Rural, Village	76	15%	56%	24%	5%
Suburban, Urban	77	11%	52%	31%	6%

As seen in this Table, residents of rural regions tend to own more cars as the commute distances are longer and public transportation options are more limited.

To allocate the number of vehicles for each building to conform with these ownership ratios, a simple Monte-Carlo-like method is applied for each residential unit (household) within the buildings, as illustrated in Figure 3.13.

The algorithm is performed as follows: the number of occupants in each household gives an upper limit on the number of cars the household owns. Then, a random number is generated for each household to be compared with the (cumulative) car ownership probabilities, yielding the number of cars allocated to this household. Then, for the whole grid region, it is checked whether the total number of vehicles in the grid region at least corresponds to the expected average number of cars ($prob_1 + 2 \cdot prob_2 + 3 \cdot prob_3$ per household). If not, the car ownership probabilities are adjusted by a small amount, and the allocation algorithm is repeated until this condition is satisfied.

An important factor that determines the driving profile of a private vehicle is its use, i.e., whether the car is used for commuting or free-time purposes. In their Germany-wide case study, Gaete Morales et al. assume a split of 62% and 38% [107] between commuters and non-commuters, respectively. To consider the regional differences, these ratios are adjusted for each grid region, depending on the relative differences of the shares of private vehicle use in the overall modal split at each region, as reported in MiB 2017 [108], page 47. To distinguish between full- and part-time commuters, the same source as in the study of Gaete Morales et al. [107] is adopted—22% of all commuters working part-time, from the OECD labor statistics for Germany [109]. Combined with the number of cars calculated in the previous step, these ratios yield a usage breakdown of the allocated private vehicles in each region as given in Table 3.6.

Generating candidates *emobpy* is a non-deterministic tool, as it uses probability distributions for the moment, occurrence, and duration of each route taken by the vehicles. To produce candidate profiles for each of these vehicles, *emobpy* was run with the three driver configurations

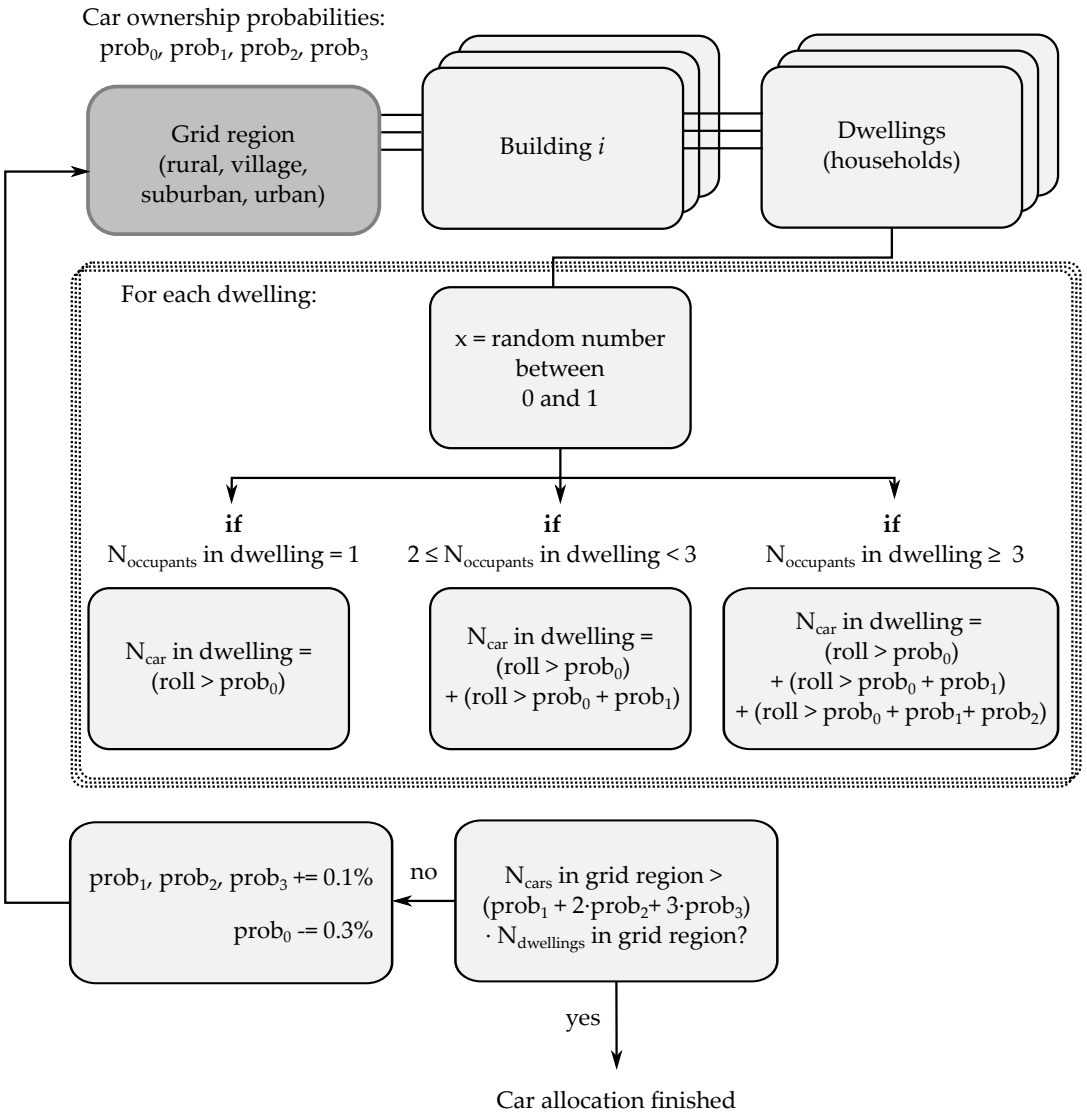

Figure 3.13: The car allocation algorithm for each building.

Table 3.6: Private vehicle allocation with their use within each grid region.

	Grid regions			
	Rural	**Village**	**Suburban**	**Urban**
Dwellings	8	33	123	158
Number of cars	11	42	160	191
Full-time commuter	5	20	83	99
Part-time commuter	1	6	24	29
Leisure	5	18	53	63

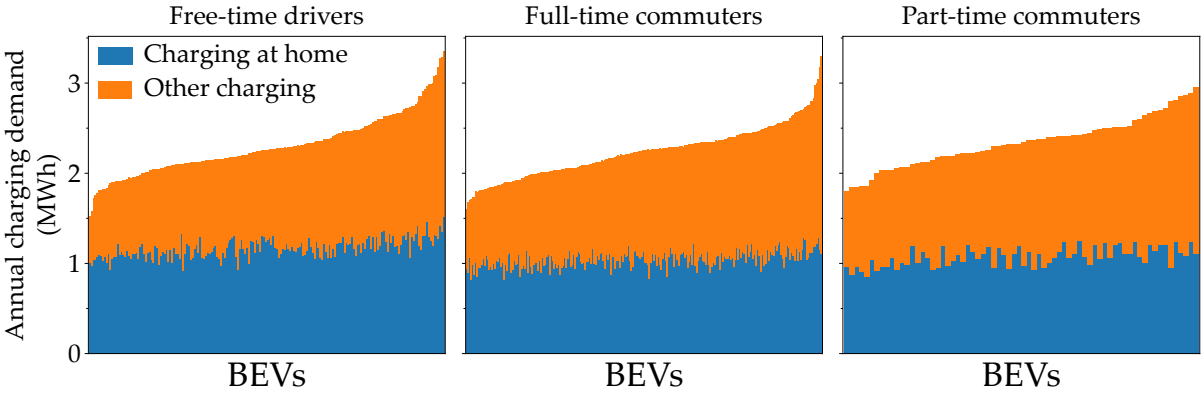

Figure 3.14: The candidate charging profiles generated with *emobpy*. Each plot stands for a different driver type (free-time, full-time, and part-time commuters). Each bar gives the annual consumption of an individual BEV, which are sorted in ascending order and divided into their at-home and public charging portions.

(full-, part-time, free-time (leisure)), with two different BEV models, up to a total of 500 times. A charging strategy of *immediate* was selected, i.e., the BEV decides to be charged wherever a charging station is available. This way, the charging occurrences made in the various locations (e.g., in the workplace, at home, or public charging stations) are determined. The parameter configurations for these simulations can be found in Appendix B.1.

Figure 3.14 presents the annual charging demands for each simulated BEV, differentiated between the types of drivers and the charging locations. Due to the non-determinism mentioned above, each of these profiles yields a different yearly consumption. The resultant annual demands vary between 1.6 and 3 MWh, with an average of slightly above 2 MWh. These values lie close to a statistical estimate of 2,35 MWh, which considers an average yearly driving distance of 14,700 km by private vehicles in Germany and an average BEV energy consumption of 15.96kWh/100km [110]. Given that charging options included not only at-home charging but also at the workplace and public charging stations, over half of the charging demands were met at these alternative locations, leaving the at-home charging demand around 1 MWh.

Out of these candidates, the profiles with the highest yearly consumptions were selected for each grid region based on the number and types listed in Table 3.6. As noted earlier, only the charging segments occurring at home are included in the model, as the rest are assumed to fall outside the optimization scope.

3.3.4.3 Heat demand

As mentioned in Section 2.3.2, the heating demand of buildings comes in two types: a) space heating and b) domestic hot water (DHW) demand.

Space heating demand recap The space heating demand is dictated by the thermal balance of the building and the temperature restrictions of the buildings; recall equations (2.14) and (2.15):

$$d^{\text{sh}}_{i,t} := \gamma^{\text{sh,gen}}_{i,t} = C_i \cdot \frac{\vartheta_{i,t} - \vartheta_{i,t-1}}{\Delta t} + \frac{1}{R_i} \cdot (\vartheta_{i,t} - \vartheta^{\text{amb}}_t) - \gamma^{\text{int}}_{i,t} - \gamma^{\text{sol}}_{i,t}, \quad \forall t \in \mathcal{T}_m \;\; \forall i \in \mathcal{I}^b \tag{2.14}$$

$$\vartheta^{\text{min}}_{i,t} \leq \vartheta_{i,t} \leq \vartheta^{\text{max}}_{i,t}. \qquad \forall t \in \mathcal{T}_m \;\; \forall i \in \mathcal{I}^b \tag{2.15}$$

Assuming known R_i and C_i values from the building stock as described in Section 3.3.2, and the ambient temperature profile ϑ_t^{amb} from Section 3.3.3, the missing parameters to fully define these constraints are as follows:

- the internal gains $\gamma_{i,t}^{\text{int}}$,
- the solar gains $\gamma_{i,t}^{\text{int}}$, and
- the comfort temperature band $\vartheta_{i,t}^{\text{min}}$, $\vartheta_{i,t}^{\text{max}}$.

Internal gains The internal gains $\gamma_{i,t}^{\text{int}}$ are calculated on an hourly basis using the activity model built into the *UrbanHeatPro* tool. This model determines the occupancy profile of the building at each moment, i.e., the number of occupants present in the building at a given moment. Roughly, this process takes place as follows: by taking into account various influencing factors such as the ratio of the working population, their typical absence hours, and the weekday/weekend cycles, a non-deterministic schedule is generated for each occupant of a building. Brought together, these schedules form the occupancy profile of a building. If necessary, this occupancy profile is adjusted to ensure consistency between the driving profiles calculated in the previous Section. This ensures that the number of absent occupants can not be fewer than the number of absent cars. The adjusted occupancy profile is multiplied by a gain factor to calculate the overall internal gains. Analogous to the *UrbanHeatPro* methodology, the gain factor is set to 80 W/occupant between 23:00 and 6:00 and between 100 and 125 W/occupant for the rest of the day.

Solar gains For the calculation of the solar gains $\gamma_{i,t}^{\text{sol}}$, the trigonometric functions provided by the *gsee* tool can be used. Specifically, the function `gsee.trigon.aperture_irradiance` calculates the irradiance received by a surface based on the surface orientation, the horizontal irradiance components, the coordinates of the surface, and the solar elevation angle. Correspondingly, the total solar gains can be calculated as the sum of the aperture irradiance over all the external walls of the building.

Temperature band Through the equations (2.14) and (2.15), the allowable temperature band of a building provides flexibility in the operation of the heat pumps by utilizing the thermal inertia of the building. Specifically, at times when electricity is less expensive or when PV electricity is available, the heat pump can be utilized more intensively to elevate the building's temperature beyond the immediate requirement. This approach would still ensure a comfortable temperature within the building while providing a more efficient use of resources.

For setting the comfort temperature band of buildings, a distinction between residential and non-residential buildings is made. For residential buildings, the Swiss Society of Engineers and Architects (SIA) 382/1 norm of the Swiss Society of Engineers and Architects on the *General Basics and Requirements of Ventilation and Air Conditioning Systems* is taken as a basis. As detailed in [111], this norm includes an ambient temperature-dependent comfort band for building interior temperature, which must be observed when using ventilation and air conditioning systems.

The temperature band correlates positively with the ambient temperature, i.e., as temperatures outside are lower, people usually wear thicker clothing, permitting a lower indoor temperature while still maintaining comfort. Figure 3.15 illustrates this temperature band. For its incorporation into the model, the temperature band is split piece-wise into four segments as follows:

- the daily maximum of the ambient temperature is lower than 16°C,

- the daily maximum of the ambient temperature lies between 16°C and 25°C,
- the daily maximum of the ambient temperature lies between 25°C and 30°C, or
- the daily maximum of the ambient temperature exceeds 30°C.

For each of these segments, the lower and upper-temperature limits $\vartheta_{i,t}^{\min}, \vartheta_{i,t}^{\max}$ are set to be used in the HOODS model.

In addition to this band, during the night, when residents are asleep, it is common practice to set a lower temperature for additional energy saving. Therefore, for half of the residential buildings (precise statistics were not available to the author), the lower limit from SIA 382 is replaced with a *night set-back temperature* of 18°C, applicable between 23:00 and 06:00 (the night set-back period is denoted as $\mathcal{T}^{\text{nsb}}$).

For non-residential buildings, a different temperature band is set depending on the use of the building:

- *Public buildings:* In accordance with the recent energy-saving measures implemented by the German government in 2022 [112], a minimum temperature of 19°C is chosen for public buildings,
- *Commercial buildings:* Through the Work Safety Act (de: *ArbSchG*), The German Federal Ministry of Labour and Social Affairs sets requirements for employers to ensure comfortable working conditions [113]. A minimum temperature of 19°C is set for commercial buildings, adhering to their guideline for predominantly sedentary work with medium intensity. To account for varying employer preferences, a uniform distribution of minimum temperatures between 19-21°C is assigned randomly to each commercial building.
- *Industrial buildings:* The only industrial buildings identified in the grid regions are a mechanical workshop and carpentry in the village grid. The *ArbSchG* guideline is also applied for these buildings, but it corresponds to working conditions that involve walking and medium-intensity tasks, necessitating a minimum temperature of 17°C.

For all of these non-residential buildings, a temperature band of 3.5°C is defined to allow for flexible heat pump operation. This band is selected in line with the minimum width of the SIA guideline for residential buildings to allow a flexibility equivalent for both types of buildings. Thereby, an equivalent level of thermal flexibility is allowed for both residential and commercial buildings.

Note that the model does not define specific *heating periods*. This means the heat pumps are operated whenever the ambient temperature falls below the set minimum temperature. regardless of the season. This might differ from the real-world operation of some building heating systems that are deactivated in the summer period. Nevertheless, this approach allows for a worst-case scenario in terms of the overall electricity consumption of the heat pumps.

Domestic hot water (DHW) demand The DHW demand for buildings is calculated using the *UrbanHeatPro* tool. *UrbanHeatPro* combines the previously mentioned activity model with DHW-consuming events to calculate the DHW demand of each building. Based on a temporal probability distribution, each occupant of a residential building is likely to engage in DHW-consuming events as outlined by Jordan and Vajen [114]. These events include a) taking a shower, b) bathing, or c) small or medium draw-offs. To meet these demands, a DHW tank within the building is heated up during a single daily heating event. This approach can cause unrealistic peak demands, especially in multi-family buildings with many residents. To

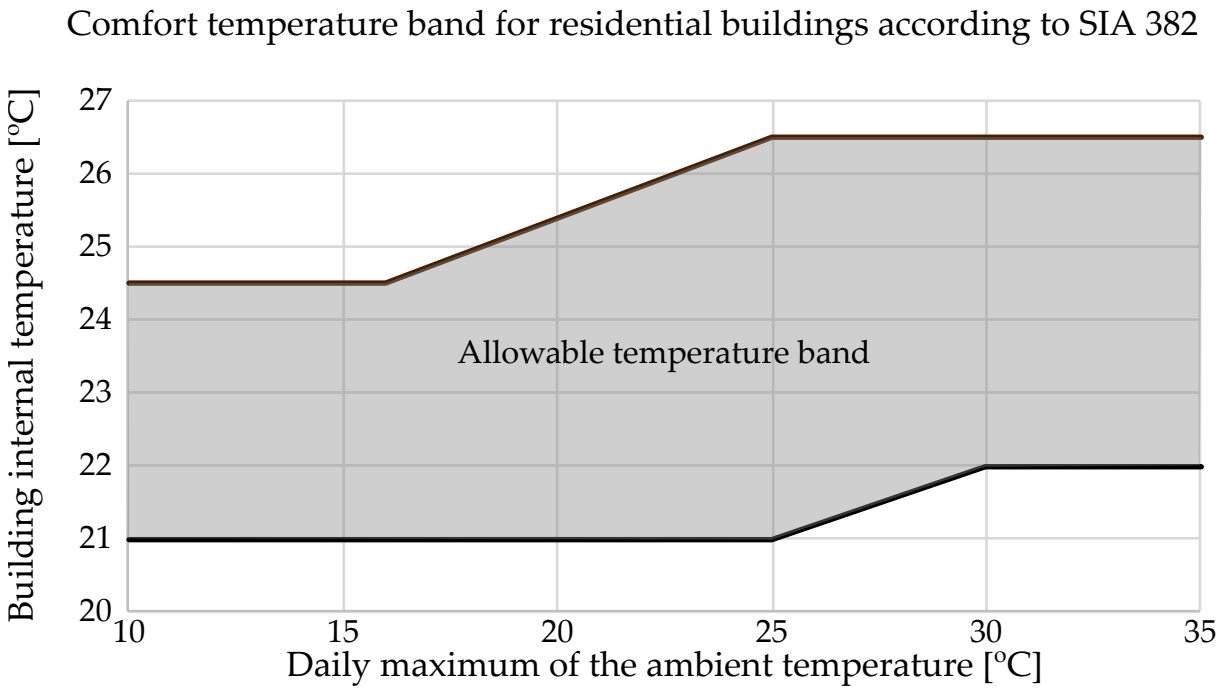

Figure 3.15: The definition of the allowable temperature band for the residential buildings according to SIA 382 norm, adapted from [111].

rectify this, a post-processing step distributes the daily DHW demand over multiple hours within the day, depending on the number of dwellings in the building. For example, a daily DHW demand of 20 kWh for a building with two dwellings would be divided into two distinct hours chosen at random, and for each hour, a DHW demand would be set at 10 kWh.

As DHW usage in non-residential buildings can not be characterized easily and is highly dependent on the specific use of the building, it is left outside the scope of the case study.

With this, the demand characterization for the investigated grid regions is complete. The next step involves elaborating on the techno-economic data concerning the operation of the energy system components, including the distributed energy resources (DERs), which will be used to meet these demands.

3.3.5 Techno-economic energy system data

The techno-economic energy system data involve a) the (non-weather dependent) technical parameters of the system components, such as the efficiencies and lifetimes of DERs, and b) economic data, such as the cost components that each DER or grid component is associated with. This Section will present summary tables for these parameters and briefly describe their data sources.

3.3.5.1 Prosumer-side data

Table 3.7 lists the techno-economic data associated with the prosumers used in the case study. The column *Source* contains either the dataset where the corresponding parameter is sourced from, an indication of the author's own assumption (OA), or a description index, each elaborated below the Table.

Table 3.7: The prosumer-side techno-economic data used within the case study.

	Parameters	Symbol	Value	Unit	Source
PV	Investment costs, fixed	$c^{\text{PV,inv,fix}}$	5,438	€	A [115]
	Investment costs, variable	$c^{\text{PV,inv,var}}$	1,668	€/kW$_p$	
	WACC	x^{PV}	0.027	-	B [116]
	Lifetime	N^{PV}	20	a	[117]
	Minimum PF	$\tan\left(\phi^{\text{PV}}_{\text{min}}\right)$	$\pm$0.95	-	C
	Roof area use factor	U_A	0.15	kW$_p$/m^2	OA
HP (main)	Investment costs, fixed	$c^{\text{HP,inv,fix}}$	4,125	€	D [118]
	Investment costs, variable	$c^{\text{HP,inv,var}}$	3,750	€/kW$_{\text{el}}$	E [118]
	WACC	x^{HP}	0.02	-	[119]
	Lifetime	N^{HP}	18	a	[117]
HP (aux)	Investment costs, fixed	$c^{\text{HP,aux,inv,fix}}$	5,924	€	F [117]
	Investment costs, variable	$c^{\text{HP,aux,inv,var}}$	150	€/kW$_{\text{el}}$	
	WACC	$x^{\text{HP,aux}}$	2%	-	G
	Lifetime	$N^{\text{HP,aux}}$	18	a	
	Efficiency	$\eta^{\text{HP,aux}}$	100%	-	[117]
Wall box	Charging capacity	κ^{WB}	11	kW/WB	H [120]
	Charging efficiency	η^{WB}	1	-	OA
Battery	Investment costs	$c^{\text{bat,inv,var}}$	1,000	€/kWh$_{\text{el}}$	I [121]
	Roundtrip efficiency	$\eta^{\text{bat,ch}} \cdot \eta^{\text{bat,dch}}$	96%	-	[122]
	WACC	x^{bat}	2%	-	[119]
	Lifetime	N^{bat}	20	a	[122]
	Energy-to-power ratio	etp^{bat}	3		OA
Ther. storage	Investment costs	$c^{\text{TS,inv,var}}$	200	€/kWh$_{\text{th}}$	J
	Roundtrip efficiency	$\eta^{\text{TS,ch}} \cdot \eta^{\text{TS,dch}}$	90%	-	OA
	WACC	x^{TS}	2%	-	[123]
	Lifetime	N^{TS}	30	a	[123]
Exchange	Electricity price (fixed)	$c^{\text{imp}}_{\text{spec},t}$	0.4	€/kWh$_{\text{el}}$	K [124]
	Feed-in tariff	$c^{\text{feed-in}}_{\text{spec}}$	0.062	€/kWh$_{\text{el}}$	L

A For estimating the fixed and capacity-dependent investment cost portions of PV, a linear

regression of PV system having sizes varying between 5.5 and 13 kW is made, using the data from [115].

B The weighted average cost of capital (WACC) of rooftop PV systems is approximated by the WACC of utility-scale PV systems for Germany as provided by [116].

C The minimum power factor of the PV systems is set according to the VDE-AR-N 4105 norm.

D As the fixed investment costs of the main heat pump system, the upper limit of the installation costs as given in [118] is taken, on top of which a 25% rebate is applied as per the state participation program (BAFA).

E As the capacity-dependent investment costs of the main heat pump system, the upper limit of the procurement costs as given for a 7 kW_{th} unit in [118] is taken, on top of which a 25% rebate is applied as per the state participation program (BAFA). Per kW_{el} cost is then calculated using a minimum COP value of two.

F For estimating the fixed and capacity-dependent investment cost portions of the auxiliary heating unit of the heat pump, a linear regression of direct heating units having sizes varying between 2 kW and 7 kW is made using the data from [117].

G The heat pump and its auxiliary unit are assumed to be integrated into a single system. Therefore, the auxiliary unit is assigned the same lifetime as the main unit.

H The wall box charging capacities are pre-defined as 11 kW, in line with the federal funding for installing controllable charging stations [120].

I As the specific investment costs of the batteries, an average value of the costs stated in [121] is taken.

J Corresponds to the specific price of a commercial product from WOLF GmbH of 1,800€ with 400 lt volume, assuming a temperature difference between in- and out-take of 20°C.

K As of the writing of this thesis, electricity prices are undergoing strong volatility due to the Russo-Ukrainian War. As this makes it challenging to establish a representative price for the model, the price brake set by the German government for 2023 is used instead [124].

L The German Renewable Energy Act of 2023 (*de: EEG 2023*) sets the feed-in tariff between 6.2 and 9.6 *cents* per kWh, depending on the size of the PV units (the larger the unit, the lower the feed-in tariff). Since the installed PV capacities are not determined ex-ante, a worst-case scenario using the lower limit of the feed-in tariff is assumed.

3.3.5.2 Grid-side data

Analogously, techno-economic data associated with the grid components is shown in Table 3.8. Additionally, a detailed elaboration of the cost parameters is provided in this Section. To establish a consistent case study, the benchmark cost data provided by the distribution grid operator of Forchheim is taken as a basis. As of the writing of this thesis, the grid component costs, especially for the transformers, undergo extreme volatility due to increased demand and material and personnel shortages. For instance, the DSO reports a tripling of the transformer costs between 2019 and 2023 and an increase of 22% in the cabling costs between 2019 and 2022. The most recent cost benchmarks that the DSO reported are the following:

- A 630 kVA aluminum-type transformer: 31,000€ (2023),
- A complete transformer station (which includes the transformer, the housing, LV&MV connections, and the instrumentation): 180,000€ (2023)
- Low-voltage distribution cabling: 305€ per meter (2022).

To derive the voltage regulating distribution transformer (VRDT) installation costs across all size classes and the various cabling cost components, the following assumptions are further made:

- An upgrade price of 7,000€ is assumed for VRDTs, leading to a total cost of 38,000€ for a 630 kVA VRDT,
- In order to set the costs of VRDTs with ratings other than 630 kVA (namely 160, 250, 400, 630, 800, 1,000, 1,250, 1,600, and 2,000 kVA), the amount 38,000€ is scaled with the same relative cost differences as given in [125],
- Drawing from the grid operator's experience, it is assumed that if a transformer is replaced with another rated 1,000 kVA or higher, a replacement of the transformer station becomes necessary, thus incurring the associated additional costs.
- the same material-to-installation cost ratio of 1:9 as in [125] is further applied to 305€/m, yielding a cable material cost of 30.5€/m and installation cost of 274.5€/m.

The weighted cost of capital for all grid components is set at 6%, as per [126]. According to [127], the lifespan of the cables is set at 40 years. For the VRDTs, the lifetime is set at 30 years, the average of its primary unit's 40-year lifespan and its secondary unit's 20-year lifespan.

Table 3.8: The grid-side techno-economic data used within the case study. *Transformer costs above 1000 kVA include the replacement of the transformer station.

	Parameters	Symbol	Value	Unit
VRDT	Inv. costs, 160 kVA	$c_{160}^{\text{VRDT,inv}}$	25,197	€
	Inv. costs, 250 kVA	$c_{250}^{\text{VRDT,inv}}$	31,012	€
	Inv. costs, 400 kVA	$c_{400}^{\text{VRDT,inv}}$	34,694	€
	Inv. costs, 630 kVA	$c_{630}^{\text{VRDT,inv}}$	38,000	€
	Inv. costs, 800 kVA	$c_{800}^{\text{VRDT,inv}}$	40,315	€
	Inv. costs, 1,000 kVA*	$c_{1000}^{\text{VRDT,inv}}$	191,447	€
	Inv. costs, 1,250 kVA*	$c_{1250}^{\text{VRDT,inv}}$	196,099	€
	Inv. costs, 1,600 kVA*	$c_{1600}^{\text{VRDT,inv}}$	200,557	€
	Inv. costs, 2,000 kVA*	$c_{2000}^{\text{VRDT,inv}}$	206,178	€
	O&M costs	$c_o^{\text{VRDT,O\&M}}$	1%	of Capex/a
	WACC	x^{VRDT}	6%	-
	Lifetime	N^{VRDT}	30	a
Cables	Installation costs	c_{ins}	274.5	€/m
	Material costs	c_{mat}	30.5	€/m
	WACC	x^{line}	6%	-
	Lifetime	N^{line}	40	a

3.4 Dimension 2: Electrification scenarios

To investigate various states of grid loading, a set of electrification scenarios with multiple degrees of DER penetration are examined in the case study. These consist of a zero electrification scenario followed by a low, medium, and extreme rate of electrification.

3.4.1 Zero electrification scenario

The zero electrification scenario assumes no adoption of PV, heat pump, and BEV units by any prosumer within the grid regions. Correspondingly, the only electrical loads in the grid are those of the common electrical appliances, as defined in Section 3.3.4.1. This scenario acts as a baseline to evaluate the current capacities of the LV grid, reflecting the conditions likely considered during conventional grid planning. It can be viewed as the current state, or the status quo, of the LV grid, offering a reference point against which the electrification scenarios can be compared or related.

3.4.2 Low (25%) electrification scenario

The medium electrification scenario assumes that a quarter of the buildings adopt heat pumps and BEVs. Additionally, it is assumed that the roofs of every four buildings are available for PV investments. For each type of DER, a randomly selected subset of buildings is chosen to adopt the DERs, with the selection randomized separately for each type of DER. This way, the effects of a low degree of electrification can be analyzed, allowing to quantify the short-term requirements for grid reinforcement.

3.4.3 Medium (50%) electrification scenario

The medium electrification scenario is similar to the low electrification scenario, but instead, the DERs are adopted by half of the buildings in the grid region, which is randomly selected again. This way, the effects of a moderate degree of electrification can be investigated, thereby quantifying the medium-term requirements for grid reinforcement.

3.4.4 Extreme (100%) electrification scenario

The third scenario posits total electrification in the grid regions so that all residential mobility use is electrified and, apart from a few exclusions, all buildings switch to electrical heating with heat pump systems. Buildings excluded from electrified heating are elderly care facilities, schools, and kindergartens, as these buildings are considered excluded from the 65% renewable energy mandate of the Building Energy Act.

To contextualize the electrification rates considered in these scenarios with respect to the actual course of the German energy transition, Figure 3.16 compares these rates with the adoption targets mentioned in the Introduction Chapter (Figure 1.1). The percentage values for these targets are based on a total of 21 million buildings [128] and 48.2 million private vehicles in Germany as of 2021. For simplicity, these values are considered to stay constant. Accordingly, the 2030, 2037, and 2045 targets translate into adoption percentages spanning from 30% to 80% depending on the year. Therefore, for reference, the low (25%) scenario depicts a probable state anticipated short before 2030, the medium (50%) scenario between 2030 and 2037, and the extreme scenario goes beyond the adoption targets of 2045.

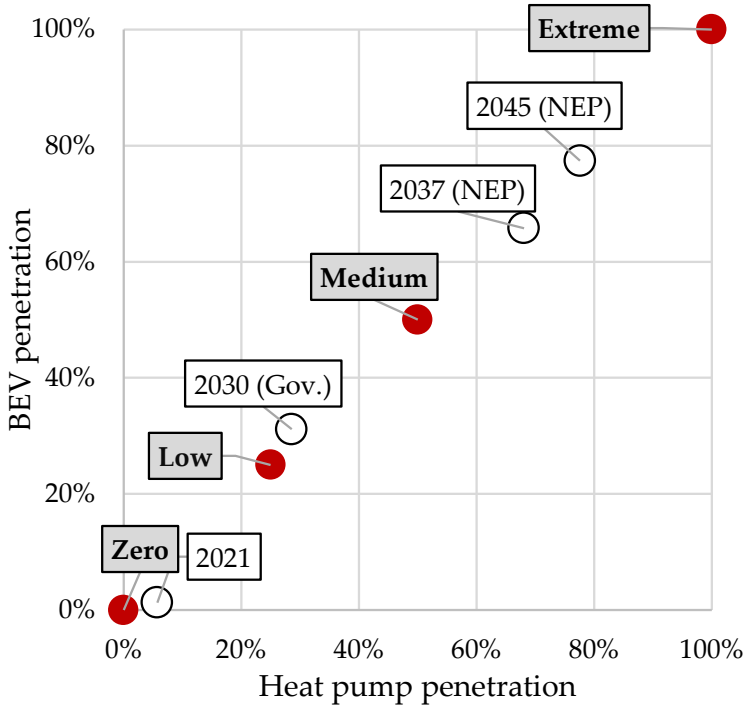

Figure 3.16: The transformation timeline for heating and mobility electrification. The 2030 values correspond to the targets of the current German government, and 2037/2045 are the scenarios *B* posited for the German Network Development Plan.

3.5 Dimension 3: Paradigm definition

One of the research questions of this thesis is to assess the impact of the prosumer-side flexibilities and various grid relief measures on the system costs and the grid reinforcement needs. In this, a best-case assuming complete system-wide coordination has to serve as a benchmark to compare against the suboptimal but more realistic cases. The various paradigms considered in the scenario generation are illustrated in Figure 3.17 and described in this Section.

3.5.1 *Best-Case* paradigm

The *Best-Case* paradigm leverages total coordination of the low-voltage distribution system by a single decision-maker. Here, the HOODS-Sys model formulation is employed, where all prosumers and the DSO collaborate seamlessly to harness their flexibilities and exchange surplus energy among each other, with the common aim of minimizing system costs to the largest extent possible. As total coordination between DSO-prosumer is assumed, no additional grid-relief measures (e.g., capacity/variable tariffs or § 14a regulation) are considered. In contrast, all the following paradigms assume an uncoordinated operation of the LV system.

3.5.2 *Inflexible (InFlex)* paradigm

The *Inflexible (InFlex)* paradigm allows no flexibility options within the buildings. Hence, the prosumer models deal only with the dimensioning of the heat pump system and the PV units to cover a rigid demand.

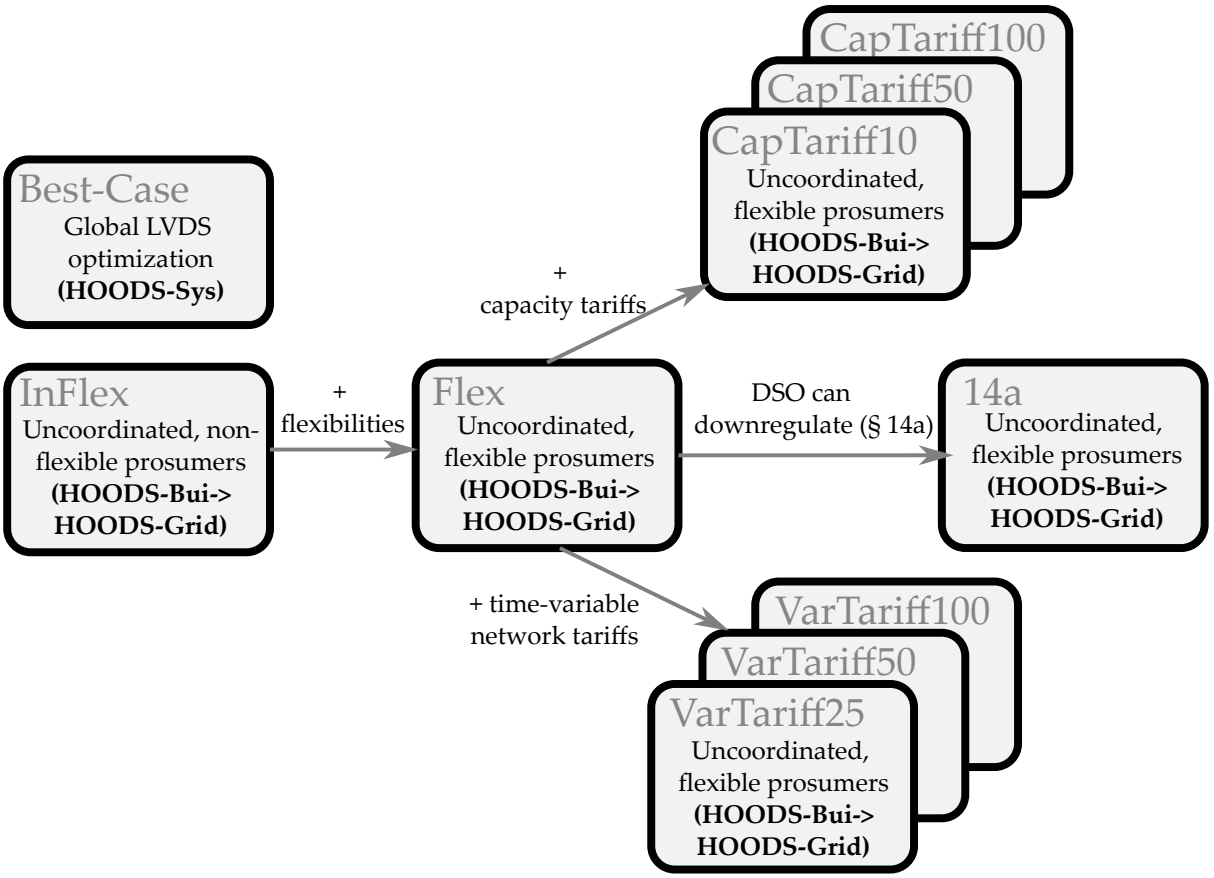

Figure 3.17: The paradigms which are part of the case study.

The exclusion of any flexibility by the prosumers is achieved by

1. setting the capacities of all storage units in the HOODS-Bui models to zero:

$$\kappa_i^{\mathrm{bat,c}} = \kappa_i^{\mathrm{TS,c}} = 0, \qquad \forall i \in \mathcal{I}^b \tag{3.12}$$

$$\kappa_{i,c}^{\mathrm{BS,c}} = 0, \qquad \forall c \in \mathcal{C}^i \qquad \forall i \in \mathcal{I}^b \tag{3.13}$$

2. and preventing the flexible pre-heating of buildings. This is achieved by fixing the building temperature to the minimum temperature

$$\vartheta_{i,t} = \vartheta_{i,t}^{\min}. \qquad \forall i \in \mathcal{I}^b \qquad \forall t \in \mathcal{T} \setminus \mathcal{T}^{\mathrm{nsb}} \tag{3.14}$$

   Note that this constraint does not apply to buildings that utilize night set-back temperatures during their set-back hours. This exception prevents an unrealistically large demand for ventilation at the beginning of the set-back hours.

3.5.3 *Flexible (Flex)* paradigm

All following paradigms, starting from the *flexible (Flex)* paradigm, allow the prosumers to harness their flexibilities for a more cost-efficient operation. For this, the flexibility measures, such as battery and thermal storage, can be installed parallel to the generation components and utilized (e.g., by a home energy management system–HEMS) to minimize the building energy costs. The thermal inertia of the buildings and intelligent BEV charging also serve as additional flexibility options.

In the *HEMS* paradigm, no capacity-based or time-variable tariffs are applied. Correspondingly, the main benefit of using the flexibilities is maximizing the self-consumption of PV electricity. As the retail electricity prices are exceedingly above the feed-in tariffs in many countries, the prosumers will aim to shift their loads to make the most use of their PV electricity. Only when no storage options are available for the excess PV generation, will it be fed into the grid to collect the feed-in revenues.

All the following paradigms will assume a flexible use of DERs as defined in the *HEMS* paradigm, introducing individual grid-relief measures on top of it. Note that while, in reality, a combination of these measures might exist, the purpose of the scenario generation has been to assess the distinct effects of each measure on the system operation.

3.5.4 *Capacity tariff (CapTariff)* paradigm

A series of capacity tariffs are introduced in the *capacity tariff (CapTariff)* paradigms to investigate the individual effect of capacity pricing on the flexible prosumer behavior. The capacity tariff paradigms consist of three price levels:

- 10 €/kW.a (*CapTariff10*) to analyze the effect of a small capacity component in the electricity price. This price level is predicted to incentivize the usage of low- or no-cost load-shifting capabilities, such as through smoother charging of BEVs,
- 50 €/kW.a (*CapTariff50*) to analyze the effect of a moderate and realistic capacity component in the electricity price. This price level is the closest to the current prices in Belgium, which lies around 40€/kW per year as of 2023 [24],
- 100 €/kW.a (*CapTariff100*), where the capacity component will play a more significant role for the prosumers. The predicted price level is expected to impact the ideal sizing of the DERs to achieve an even flatter consumption profile.

3.5.5 *Variable tariff (VarTariff)* paradigm

Alternative to capacity tariffs, the *variable tariff (VarTariff)* paradigm introduces a time-variable network tariff for the prosumers, in line with the latest draft for an amendment to Section 14a of the German Energy Industry Act [22] to come into effect by the beginning of 2024. According to the guidelines, each DSO has to offer time-variable network tariffs to their customers, and each customer can voluntarily opt into these tariffs. The time-variable tariff structure should consist of three price levels: a) a standard tariff (ST), b) a high tariff (HT), and c) a low tariff (LT). The ST should correspond to the regular network tariff for low voltage-level consumers who do not have a dynamic load measurement device. The HT can be up to 100% higher than the ST, while the LT should be set within a range of 10% to 80% of the ST. The HT should apply at least during a period of two hours per day.

As long as these requirements are satisfied, DSOs are free to define their individual tariff windows and the prices of these tariffs in their respective grid region. An example time window is provided by the German Federal Network Agency, which can be found in the report of e.on, which details their response to the policy draft in the consultation round [129]. It consists of the following price levels: a) ST between from 5:00 to 17:00 and from 20:00 to 23:00, b) HT (+100% of ST) from 17:00 to 20:00, and c) LT (-50% of ST) from 23:00 to 05:00. This tariff structure serves well to promote peak reducing behavior under the current electrical load patterns. However, in this case study, a modified structure is defined in an ad-hoc manner based on the loads emerging in a heat pump-dominated system. Figure 3.18 gives the overall grid loading depending on the ambient temperature for the suburban grid

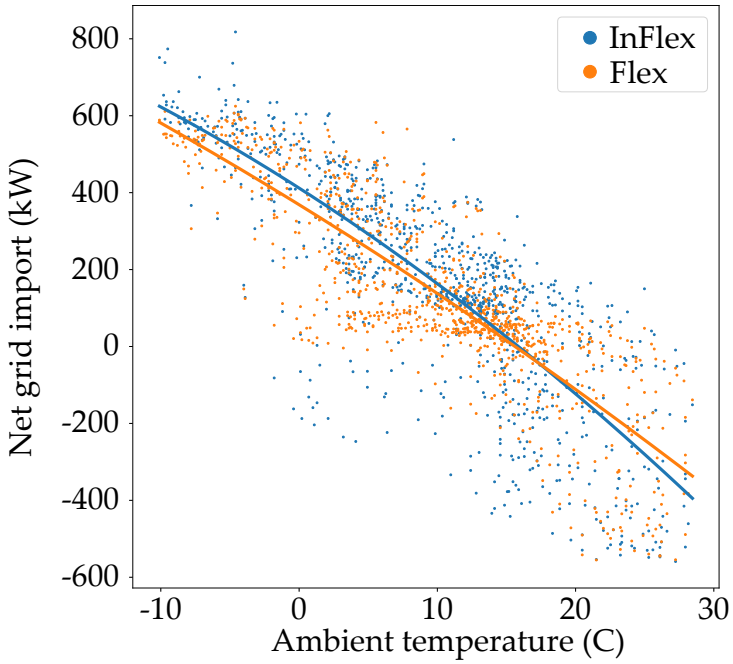

Figure 3.18: The correlation between the ambient temperature and the net grid load for the suburban grid under 100% electrification (load values in the *InFlex* and *Flex* scenarios are given in different colors. The data are depicted as scatter plots, while the lines represent the polynomial fits of each data set).

under 100% electrification. A negative correlation is evident–lower ambient temperatures drive high electrical consumption from heat pumps, increasing the overall loading in the grid. Therefore, the ST is modified to apply to the night hours when temperatures are lower, rather than the noon hours, to promote shifting the heat pump operation to these hours instead, yielding a smoothened load profile. Moreover, an additional HT period in the early morning hours is added, i.e., between 5:00-8:00. This change is implemented in response to the observed simultaneous heating behavior of prosumers during these morning hours, a pattern driven by the night set-back temperature application which triggers an abrupt increase above the setback temperature at the end of the setback. An HT during these peak hours should promote shifting a portion of this coincident heating load to the subsequent hours, resulting in a smoother load profile.

Each grid operator in Germany is obligated to announce their network tariffs every year as part of the grid transparency guidelines set by the Federal Network Agency [130]. In line with the network tariff announced by the DSO of Forchheim applicable to LV customers without digital measurement systems for 2022, the standard tariff is set to 6.75 ct/kWh [131]. This ST, combined with the aforementioned HT and LT periods and the non-network tariff portion of the electricity price, results in the price profile shown on the right-hand side of Figure 3.19. This electricity price profile will be applied to the prosumers who opt for the variable network tariff scheme.

Indeed, time-variable tariffs target expected peak hours with higher prices, incentivizing consumers to shift their loads to achieve an overall smoothened load profile. However, this measure might not always yield the desired outcome. In particular, the literature makes the case for the so-called *avalanche* or *herd phenomenon*, which may lead to an overall increased peak behavior within the grids [132], [133]. When a large proportion of prosumers engage in demand shifting in response to time-variable tariffs, the collective outcome is usually that the peaks are not avoided but rather are shifted in a more concentrated form to another time

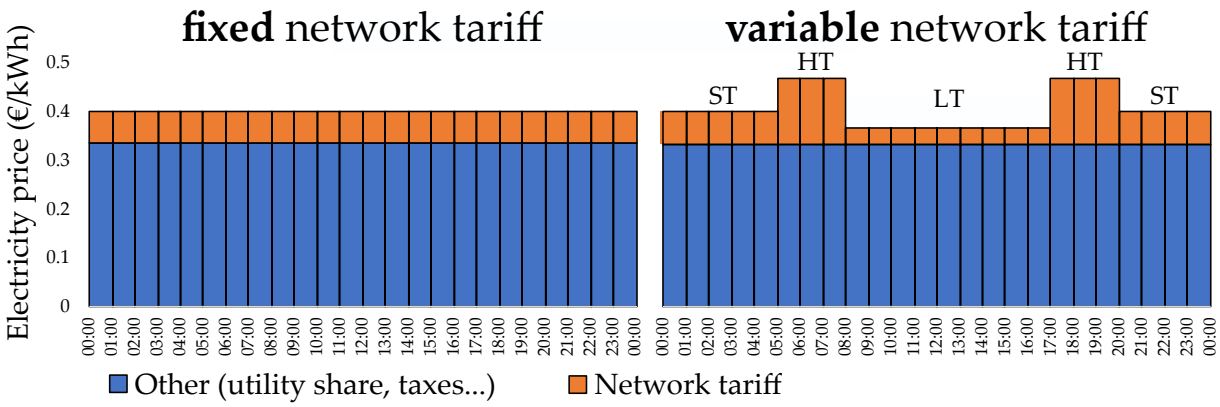

Figure 3.19: The electricity prices in case of fixed or variable network tariff schemes.

point where the low tariff applies. Nevertheless, at least in the short- to medium-term, it is not realistic that all prosumers within a given region will participate in the time-variable tariff schemes. Indeed, an overall peak-reducing behavior may be observed in settings where only a portion of the consumers shift their loads. In this spirit, the possible influences of the time-variable network tariffs on the LV system are investigated in three scenarios, which assume their adoption by a random subset of 25% (*VarTariff25*), 50% (*VarTariff50*), and 100% (*VarTariff100*) of the prosumers respectively.

3.5.6 *14a* paradigm

Finally, the § 14a downregulation is incorporated as an active measure at the disposal of the DSO, with the workflow described in Section 2.7.

This concludes the scenario space developed for the case study of this work. The following Section will elaborate on the time series aggregation method used to implement a tractable model without losing the major characteristics of the temporal scope.

3.6 Time series aggregation using *tsam*

One aspect to consider during the development of the optimization framework and the corresponding case study is the computational tractability of the underlying problems. The mixed-integer linear programming (MILP) formulation employed for the DER investments allows for more realistic investment cost structures. Likewise, the integer implementation of the grid reinforcement measures allows for representing practical discrete decisions, such as replacing a transformer and variable impedance effects through parallel cable reinforcement. However, these formulations usually do not scale well numerically. It can be computationally demanding, even with commercial solvers like Gurobi or CPLEX, as the number of modeled time steps, buildings, and the size of the LV grid increases.

To reduce the computational complexity of the model, an aggregation of the model time series is employed. The time series aggregation is achieved by using the *Time Series Aggregation Module (tsam)*. *tsam*[8] is a *Python* package, which generates reduced (aggregated) time series based on a set of input time series, using various heuristics and machine learning algorithms [134]. For this, it aims to maximize the resemblance of the generated time series to the underlying time series. This way, a significant reduction of the model complexity can be achieved without sacrificing details such as daily, weekly, and seasonal cycles that exist within the temporal scope of energy system models. This complexity reduction leads to improved

[8] https://github.com/FZJ-IEK3-VSA/tsam

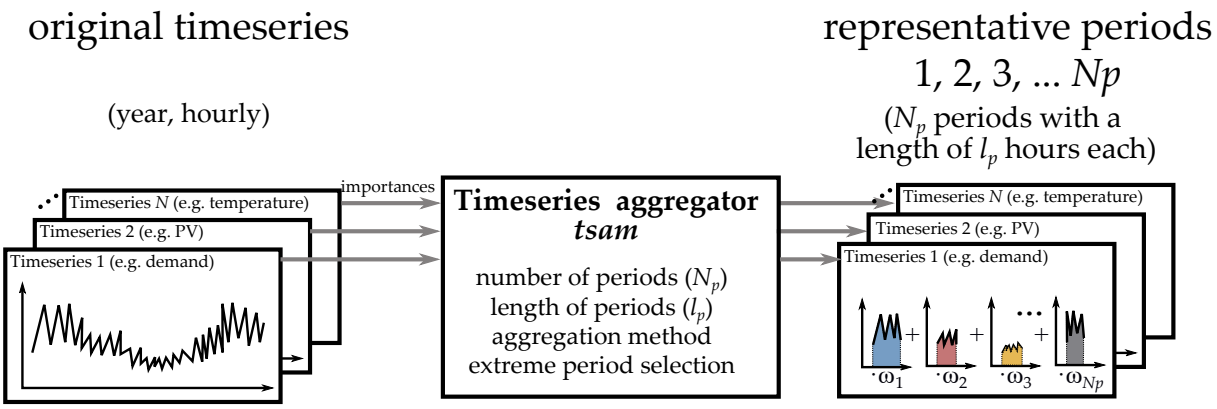

Figure 3.20: Concept of time series aggregation.

runtime and memory usage when solving models with high temporal, spatial, and technical resolution.

The time series parameters of the model were introduced in the preceding Sections, and these include demand, heat pump COP, and ambient temperature. Figure 3.20 illustrates the time series aggregation process as implemented by the *tsam*:

- First, individual *importance factors* are assigned to each time series by the user, depending on how big of an influence they should have on choosing the representative periods,
- Second, the time series data are input to the specified aggregation algorithm,
- Third, the user specifies the number N_p and length l_p of each generated representative period, along with the option of including *extreme periods* for any given time series as an additional representative period
- Finally, as an output, the time series aggregator generates N_p representative periods with a length of l_p hours each, with individual weights ω_t associated with each hour within those weeks. The weights ω_t signify the number of occurrences of each week within the year. This way, the operational costs attached to weeks that occur more often can be correspondingly weighted more in the cost function. In case aspects such as seasonal storage are also to be analyzed in the energy system model, the output also includes the order of occurrence for each representative period. However, as this may introduce more periods to be considered in the model (e.g., the same periods happening in different months of the year), this information is omitted for the application in the framework. Niche solutions for seasonal storage in buildings, e.g., in the form of hydrogen storage in off-grid settings, are indeed recently proposed [135]. However, such applications are beyond the scope of the work.

For a more detailed description of the *tsam* workflow and its algorithms, the reader is referred to the module documentation, [136], or [137]. This Section will explain the specific application of *tsam* in the HOODS framework.

3.6.1 Setting the importance factors

As mentioned, to each time series (denoted as TS) can be assigned an importance factor (denoted as $r(\text{TS})$) to be considered by the aggregator. This can be interpreted as the weighting factor of the aggregation algorithm, which in essence aims to minimize an objective function

that represents the deviation between the sequence of the representative periods and the original time series (say f_{dev}). This can be illustrated in a stylized way as follows:

$$\min \sum_{\text{TS} \in \text{all time series}} r(\text{TS}) \cdot f_{\text{dev}}(\text{TS}), \tag{3.15}$$

In an energy system modeling setting dealing with the optimal planning of DERs such as PV and heat pump units, the aggregator must capture their seasonal properties as accurately as possible. Correspondingly, the importance factors are set to each of the following types of time series:

1. ambient temperature ϑ_t^{amb},
2. capacity factors of PV units, and
3. the COP values of the heat pumps $cop_{i,t}^{\text{HP}}$.

In order to assign equal importance to each of these types, their respective importance factors are divided by the number of these time series that are present in the model:

$$r(\vartheta_t^{\text{amb}}) = 1, \tag{3.16}$$

$$r(cf_{i,r,t}^{\text{PV}}) = \frac{1}{\sum_{i \in \mathcal{I}^b} |\mathcal{R}^i|}, \tag{3.17}$$

$$r(cop_{i,t}^{\text{HP}}) = \frac{1}{|\mathcal{I}^b|} \tag{3.18}$$

Since the remaining time series are less correlated with weather phenomena or are already indirectly influenced by these time series, a negligible importance factor of 10^{-6} is assigned to these.

3.6.2 Choice of the clustering algorithm

tsam has a variety of clustering algorithms at its disposal, such as a) *averaging*, b) *k-means*, c) *exact k-medoids*, and d) *hierarchical*. Due to its advantages of yielding actual periods from the original time series, computational efficiency, and reproducibility through its deterministic nature [136], the *hierarchical clustering* algorithm is chosen in this application.

3.6.3 Determining the length and number of the representative periods via assessment of the flexibility potentials

tsam allows for a flexible choice of number and length of the representative periods. The specific choice here is not obvious—indeed, given fixed computational resources, a trade-off exists between a large number of periods and their length. For the length of the periods, a broad choice is possible. It is more common to use at least daily periods to capture diurnal demand and weather cycles and to investigate storage usage. On the other hand, the usage of weeks extends the ability of the model to consider the weekday/weekend behavior. The choice regarding the number of periods is, therefore, usually a function of the computational capacities—one has to consider as many periods as possible to cover the seasonal variety while maintaining the tractability of the model. It is often challenging to find the optimal selection regarding the length and number of representative periods ex-ante [138].

In order to determine the representative period length that incorporates flexibilities sufficiently, a pre-analysis of flexibility potentials is made for the heat pump and BEV operation. This analysis is stylistically depicted in Figure 3.21, for an example of six hours-long shifting

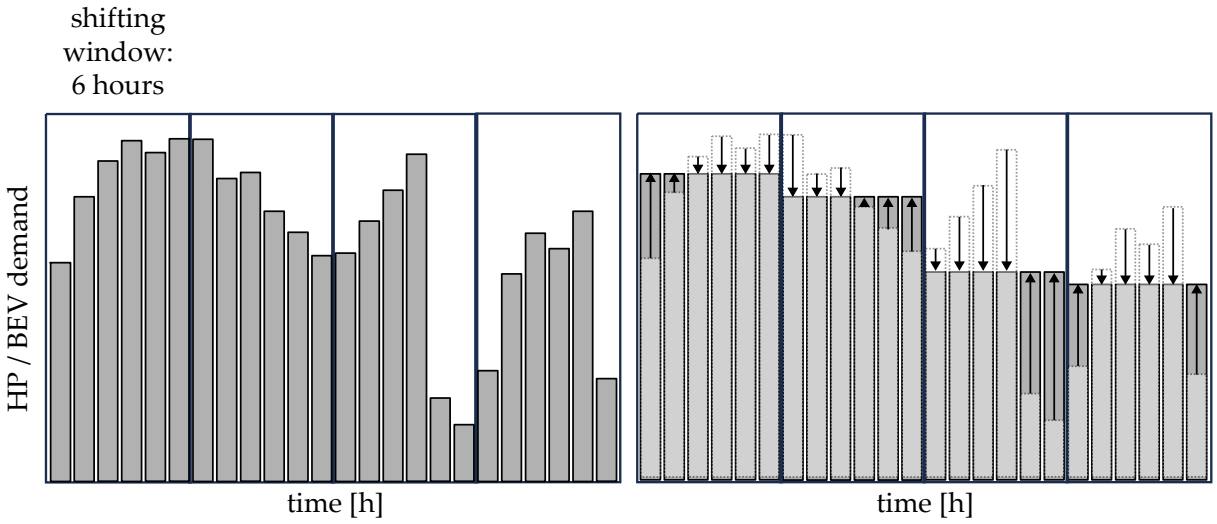

Figure 3.21: The concept of load shifting windows for assessing flexibility potentials, with an example of six hours shifting windows.

windows. In this, the heat pump or BEV loads are smoothened within every window to a level that corresponds to the average consumption in that window. Thereby, the influence of time windows where flexibilities can be applied on the peak demand can be assessed.

Figures 3.22 and 3.23 illustrate the results of this assessment for heat pump and BEV consumptions for a selected scenario, respectively. The light gray line in Figure 3.22 depicts the heat pump operation in the *InFlex* scenario under 100% electrification for the village grid, with respect to the ambient temperature (light blue). The darker lines show a potential shifting of this heat pump operation by distributing them uniformly over longer *shifting windows*, ranging from 6 to 168 hours, with the case for 168 hours–a week–depicted in green for clarity. An intelligent shifting of the load over a period longer than a week is assumed to be impractical due to the accumulation of energy losses and excessive thermal storage volumes (heat storage of 1-2 weeks is found to usually require high-temperature media [139]). For calculating the uniform shifted loads of the heat pump within each window, the total consumption over a shifting window is divided by the length of the period. Note that, for simplicity, this pre-analysis neglects the energy losses between hours, by assuming that the hourly heat pump operation can be shifted freely over the shifting periods while still maintaining thermal comfort, e.g. avoiding temperatures below the minimum or above the maximum comfort temperatures. The left-hand figure depicts the original heat pump operation in each hour of the year, while the right-hand figure shows the temporally sorted lines to facilitate identifying the changes in the peak behavior.

While the total consumption of the heat pumps stays constant regardless of the shifting of the heat pump load, the patterns vary considerably. Without any shifting of the operation allowed, an instantaneous operation of around 500 kWh_{th} occurs throughout the year, more frequently in the winter period. These moments cater to heating the buildings up to the daily comfort temperature at the end of the night setback period. In the wintertime, this amount is exceeded frequently, reaching a maximum of around 770 kWh in the extreme cold period. As the shifting windows are introduced, this peak can be reduced by between 16% (for a shifting over six hours) and 40% (for a shifting over a week).

Similarly, Figure 3.23 illustrates the potential for flexible charging of BEVs under various shifting windows in the village grid scenario with complete electrification of mobility. The approach for determining the demands with shifting windows is similar to that used for heat pumps. The key distinction is that for each BEV, the allocation of demand is restricted to time

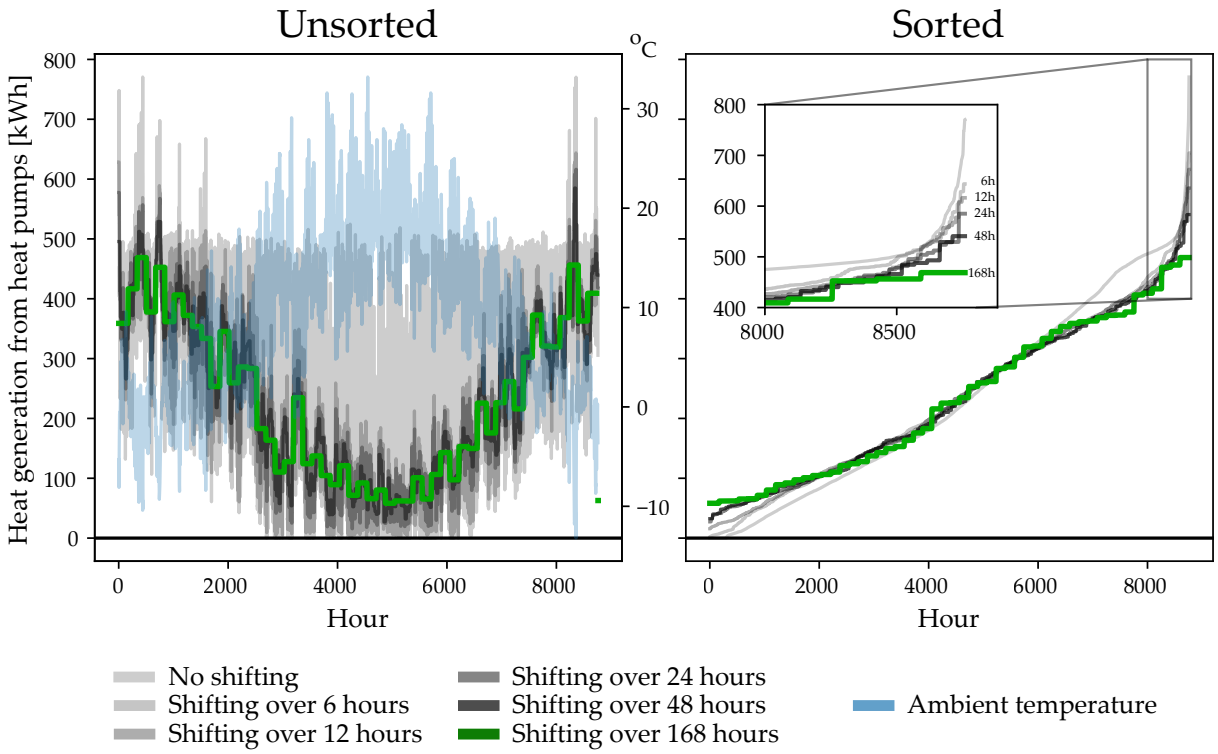

Figure 3.22: Heat pump shifting potential for the village grid under 100% electrification. No-shifting operation corresponds to the *InFlex* paradigm. The different color tones illustrate the heat pump (HP) operation in various shifting periods. The left-hand figure depicts the unsorted operation curve, while the right-hand figure shows the sorted operation curve.

intervals when the vehicle is present at the premises.

The peak consumption from BEVs at the LVDS level is minor compared to heat pumps, limited at 67 kW_{el}. Further, the BEV demand shows weaker temperature dependence, i.e., seasonal variation. Nevertheless, the flexibility potential from BEVs is significantly higher than the heat pumps–the application of shifting periods between six hours and a week reveals a potential of peak reduction ranging from 9% and 83%.

Considering the presented potential of a weekly load shifting for reducing system peaks both for heat pumps and BEVs, the decision was made to focus on *typical weeks* as a basis for analysis. The choice of the number of representative periods was then constrained by the available computational resources. To keep the analysis of the largest grid–the urban grid–within the holistic paradigm manageable, it was feasible to include only six representative periods[9]. Therefore, six representative weeks have been aggregated for each scenario of the case study, ensuring comparability. The adequacy of this approach in terms of accuracy is then evaluated in the Results Chapter (Section 4.1.1).

3.6.4 Inclusion of extreme periods

Besides generating typical periods that represent the yearly profiles as precisely as possible, *tsam* also allows the option to include *extreme* periods for a set of time series chosen by the user. This yields additional time periods where these particular time series' yearly maximum or minimum occurs. Including extreme periods is common practice in energy system modeling, as the sizing of generation technologies has to cater to the moments when demand peaks

[9]For this model, this approach leads to an optimization problem with 12,366,377 constraints and 8,654,898 variables, out of which 1101 are integers.

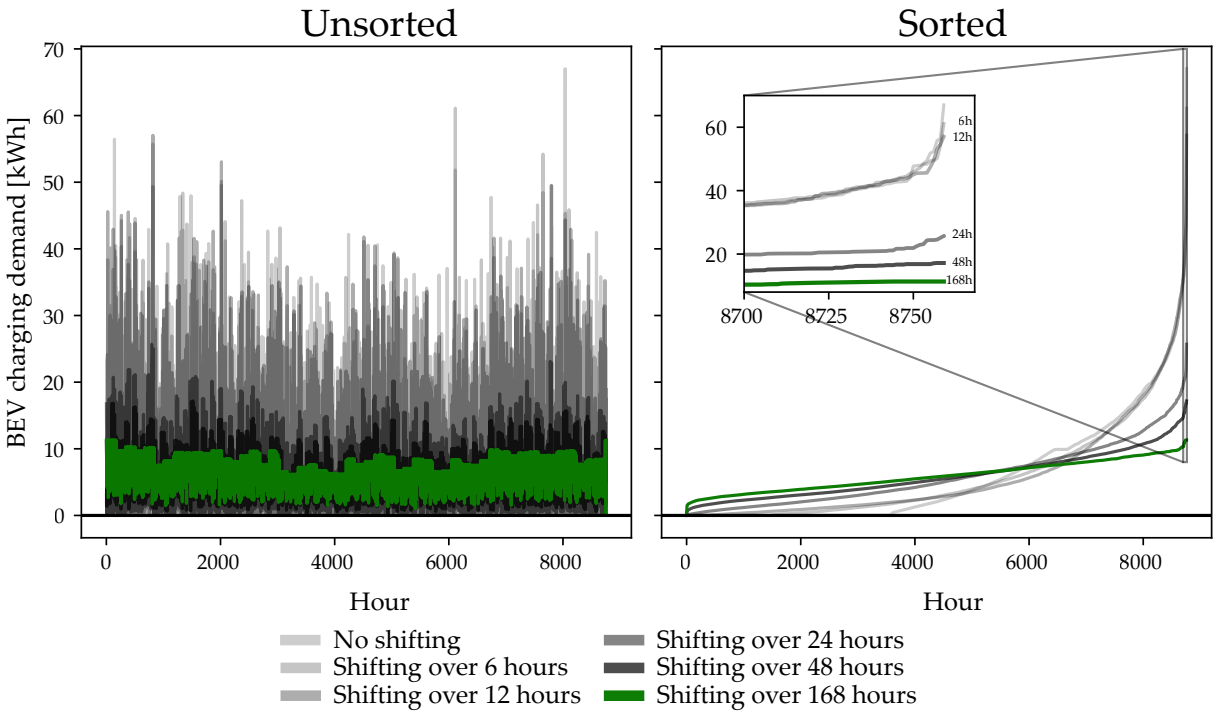

Figure 3.23: BEV shifting potential for the village grid under 100% electrification. The different color tones illustrate the BEV operation in various shifting periods. The left-hand figure depicts the unsorted operation curve, while the right-hand figure shows the sorted operation curve.

occur [136]. A necessary usage of extreme periods in the following case study is for the ambient temperature. Regardless of the average temperature course throughout the year, the heat pumps have to be dimensioned at a sufficient rating to cover the periods with the lowest temperatures. Therefore, one representative week is replaced with the week that contains the *average minimum ambient temperature*. The week to be replaced is chosen as the one that has the closest resemblance to this extreme week.

After deriving the representative weeks, the storage cyclicity equations given in (2.5e), (2.19e), and (2.23e) are re-defined to apply between the starting and ending time steps of each week, instead of the whole year.

3.7 How to achieve 100% open data for this analysis?

The data acquisition workflow illustrated in Figure 3.2 and described in this Chapter is based mostly on open data and open-source tools. However, proprietary data is partially used to enhance the validity of the case study, namely for

1. the grid models,
2. the annual electricity consumption of the buildings, and
3. the pool of residential load profiles.

An alternative approach would be to replace these data with open-source alternatives. These alternatives would render the case study methodology applicable to a broader choice of regions, possibly extending to the whole of Bavaria or even Germany. Moreover, they would promote transparency and reproducibility. Compared to using real data, these sources would

bring additional approximations. Still, they can serve as a starting point for a model, which can be extended by proprietary data by the users for their region of interest. Thanks to the rapidly expanding open-source ecosystem in energy system modeling, largely driven by the *open energy modeling (openmod)* initiative[10], many open alternatives for generating data exist. In this Section, a brief discussion regarding such alternatives will be made.

3.7.1 Synthetic grid generation

As mentioned in Section 3.3.1, synthetic grid data generation is one alternative to using real grid data for a region of choice. For this, within the scope of this thesis, the open-source Python tool *pylovo*[11] (**py**thon tool for **lo**w-**vo**ltage distribution grid generation) is co-developed by the author. *pylovo* generates synthetic low-voltage distribution grids for an arbitrary choice of locations. As a basis, it takes

- the building stock data using OSM (for geometry[12] and use) and Census (for an approximate number of occupants and dwellings per building). The acquisition of this building stock data is introduced in Section 3.3.2,
- the street network data from OSM as candidates for cable routing, and
- a choice of candidate cable and transformer types, along with their electrical parameters.

With this information, *pylovo* emulates the decision-making process of a distribution grid planner regarding the topologies and the capacities of the LV grids in a given region. Its documentation can be found in `https://pylovo.readthedocs.io/en/latest/` and the methodology is described in detail in [140] .

The grid synthesis procedure of *pylovo* roughly consists of the following steps, as also illustrated in Figure 3.24:

1. A flexible choice of an input area (e.g., a postal code area) is given by the user, within which the LV grids are to be synthesized,
2. For each building within this area, a peak load is estimated as a basis for the planning. This corresponds to fixed values for residential dwellings (e.g., 30 kW per dwelling, as proposed in [86]) and empirical area-dependent values for non-residential buildings as proposed in [103].
3. A postal code area is usually too large to have only a single LV grid. Therefore, a two-step building clustering method is employed to derive reasonably sized LV grids fed by a single transformer each. In this process, each cluster's maximum size (i.e., the maximum number of buildings) is limited by an assumed rating of the largest transformer a grid planner has at its disposal and an assumed simultaneity factor for the loads.
4. For each generated LV grid, the transformer is positioned at the node with the smallest power distance, i.e., located in the grid's electrical center.
5. By using a multi-level routing algorithm that considers the simultaneous loads and thermal capacities of available cables, cables are dimensioned for each grid branch.

[10] The manifesto of the *openmod* initiative can be found in `https://openmod-initiative.org/manifesto.html`

[11] `https://github.com/tum-ens/pylovo`

[12] As the Bavarian LOD2 data for building geometries has not been published during the development of the tool, these geometry data is not used by *pylovo* as of the writing of the thesis.

Figure 3.24: The *pylovo* workflow illustrated in multiple steps. A: postcode area selection, B: building clustering, C: transformer positioning, D: topology generation and cable dimensioning.

Following this procedure, a complete grid model consisting of the grid topology and the electrical parameters of each grid component can be generated for any given location where the building stock and street network data exist. This grid model is generated in the standardized *pandapower* format and can be integrated directly into the data workflow illustrated in Figure 3.2.

3.7.2 Annual electricity consumption of buildings

The real annual consumption data, which were part of the provided real grid models in Forchheim, can be replaced with average consumption values for typical dwellings of various sizes and types. For residential units, the German non-profit organization *co2online* conducts the Electricity Mirror for Germany (*de: Stromspiegel für Deutschland*) study every two years, which assigns efficiency ratings for a given electricity consumption for households of various sizes, types, and heating systems [141] (See Table 3.9). The basis of this classification is real consumption data submitted by households (for the 2022 version, data from 362,888 households was used). Depending on the design of a case study, the mean or highest consumption values from this table can be assigned to each dwelling in the investigated region to represent an average or a worst-case scenario, respectively.

Table 3.9: The Electricity Mirror (*Stromspiegel*) for Germany, adapted from [141].

	Electric	Nr. of	Electricity consumption (kWh) per year up to						
Building type	DHW	occupants	A	B	C	D	E	F	G
House	No	1	1,400	1,800	2,200	2,600	3,400	4,500	4,500
		2	2,000	2,500	2,800	3,100	3,500	4,300	4,300
		3	2,500	3,000	3,500	3,900	4,400	5,200	5,200
		4	2,800	3,500	3,900	4,300	5,000	6,000	6,000
		5+	3,200	4,000	4,500	5,200	6,000	7,600	7,600
	Yes	1	1,500	2,000	2,500	3,000	4,000	5,500	5,500
		2	2,400	2,900	3,300	3,800	4,500	6,000	6,000
		3	3,000	3,600	4,100	5,000	6,000	7,500	7,500
		4	3,500	4,200	5,000	5,700	7,000	8,900	8,900
		5+	4,000	5,000	6,000	7,000	8,200	10,800	10,800
Apartment flat	No	1	800	1,000	1,300	1,500	1,700	2,100	2,100
		2	1,400	1,700	2,000	2,300	2,500	3,000	3,000
		3	1,700	2,100	2,500	2,900	3,300	3,800	3,800
		4	1,800	2,300	2,600	3,000	3,600	4,400	4,400
		5+	1,500	2,100	27,00	3,400	4,100	5,500	5,500
	Yes	1	1,100	1,400	1,600	1,900	2,200	2,800	2,800
		2	1,900	2,300	2,600	3,000	3,500	4,000	4,000
		3	2,500	3,000	3,500	4,000	4,500	5,500	5,500
		4	2,500	3,400	4,000	4,500	5,000	6,400	6,400
		5+	2,000	3,000	4,000	5,000	6,000	7,500	7,500

A, B: significantly lower than the average,
C, D: slightly lower than the average.
E, F: above the average,
G: highest 15% percentile.

For non-residential loads, values around the mean sector and area-dependent annual electricity consumption benchmarks can be applied to each load. These benchmarks were devel-

oped as a result of the *synGHD* project [103], based on real data from various non-residential units of different sectors (See Table 3.10). Hourly profiles for these loads can be generated with the same methodology for non-residential units, as described in Section 3.3.4.1.

Table 3.10: Annual consumption benchmarks from the *synGHD* project, adopted from [103]

		Electricity consumption (kWh) per square meter				
	Nr. of samples	Mean	Median	Max.	Min.	SD
Retail store	82	227	193.4	666.7	4.8	186.5
Education	64	29.4	18.8	204.8	2.9	36
Hotels	35	164.8	161.7	383.1	19.8	89.3
Other lodging	37	160.3	151.2	366.8	20	66.4
Public	22	155.7	102.2	528.2	17.3	151.7
Offices	35	94.5	110	161.6	14.7	39.6
Health	18	197.1	177	589.1	2.8	146
Commercial	10	245.7	217.7	544.9	1.2	168.8

3.7.3 Open data for residential load profiles

There is a multitude of open-source software that can be used to generate synthetic electrical load profiles for residential units–some examples are LoadProfileGenerator (LPG) [142], RAMP [143], and Artificial Load Profile Generator (ALPG) [144]. Once the annual consumptions are estimated using the reference values presented in the previous step, suitable load profiles generated by these tools can be assigned to each residential unit considered. These tools, primarily based on stochastic activity models, probabilistically allocate electricity-consuming household activities, such as cooking, watching television, or doing laundry, to each occupant of the residential unit at different moments of the day. As a result, they may additionally require a complete definition of the household, including the list of appliances and the age of the occupants, to determine the possible events that may occur. Such in-depth knowledge of all the residential units in the region is not realistic for a distribution system-level analysis.

Nevertheless, the LPG tool, for instance, has a predefined pool of 60 households, validated to represent German residential units [142]. While initially developed in C#, a Python binding also exists[13], allowing easy integration into the Python-heavy data workflow described in 3.2. Therefore, it could be a suitable choice for implementing an open-source approach to generate residential electrical profiles for a case study in case real data is lacking.

By enhancing the presented data acquisition framework with these open data sources and tools, a first estimation of the LVDS parameters in an arbitrary region can be made. This way, case studies similar to those presented in this dissertation for the four Forchheim grids can be extended to these regions, aiding the decision-making process by the corresponding stakeholders.

[13] https://github.com/FZJ-IEK3-VSA/pylpg/tree/main

Chapter 4

Results of the case study

Now that the data used to define the case study scenarios are detailed in the previous Chapter, this Chapter is devoted to the presentation and discussion of the case study results. The Chapter has the following structure—first, a validation of the approximations employed in the holistic optimization of distribution systems (HOODS) model will be presented (Section 4.1). Second, the influence of the additional loads on the existing grids in each electrification scenario will be investigated (Section 4.2). In the Sections following (Sections 4.3 to 4.6), the potential analysis of the flexibilities and various techno-economic measures on alleviating the grid reinforcement needs will be made. This analysis will be complemented with a comparison of the system cost breakdown in each scenario (Section 4.7). An overall discussion of the results and policy implications will be provided in the Conclusion Chapter.

4.1 Validation of the model approximations

Before delving into the scenario results, a brief look is taken at the accuracy of the approximation methods employed in the optimization framework.

4.1.1 Results of time series aggregation

While the exact choice of the typical periods and their occurrences can be found in Appendix C, Figure 4.1 showcases the results of the time series aggregation method applied to the modeled time series as detailed in Section 3.6. The Figure illustrates significant model time series, including

- ambient temperature, the coefficient of performance (COP) of heat pumps (averaged over each building),
- electricity demand (averaged over each building), and
- capacity factors of the photovoltaics (PV) units (averaged over each roof section).

For each time series, the yearly course of the original time series is depicted first, followed by the representative time series generated by *tsam*. While the exact order of the typical weeks has no significance for the HOODS model as seasonal storages are neglected, it is taken into account here for illustration purposes. Each column in the figure stands for a grid region.

The time series aggregation achieves overall high accuracy, with Pearson correlation coefficients (Rs) ranging from 0.75 to 0.9. Notably, the annual ambient temperature time series is well represented, boasting R values higher than 0.87 for all grid regions. This precision translates well to the COP values, owing to their direct dependence on temperature. Although the

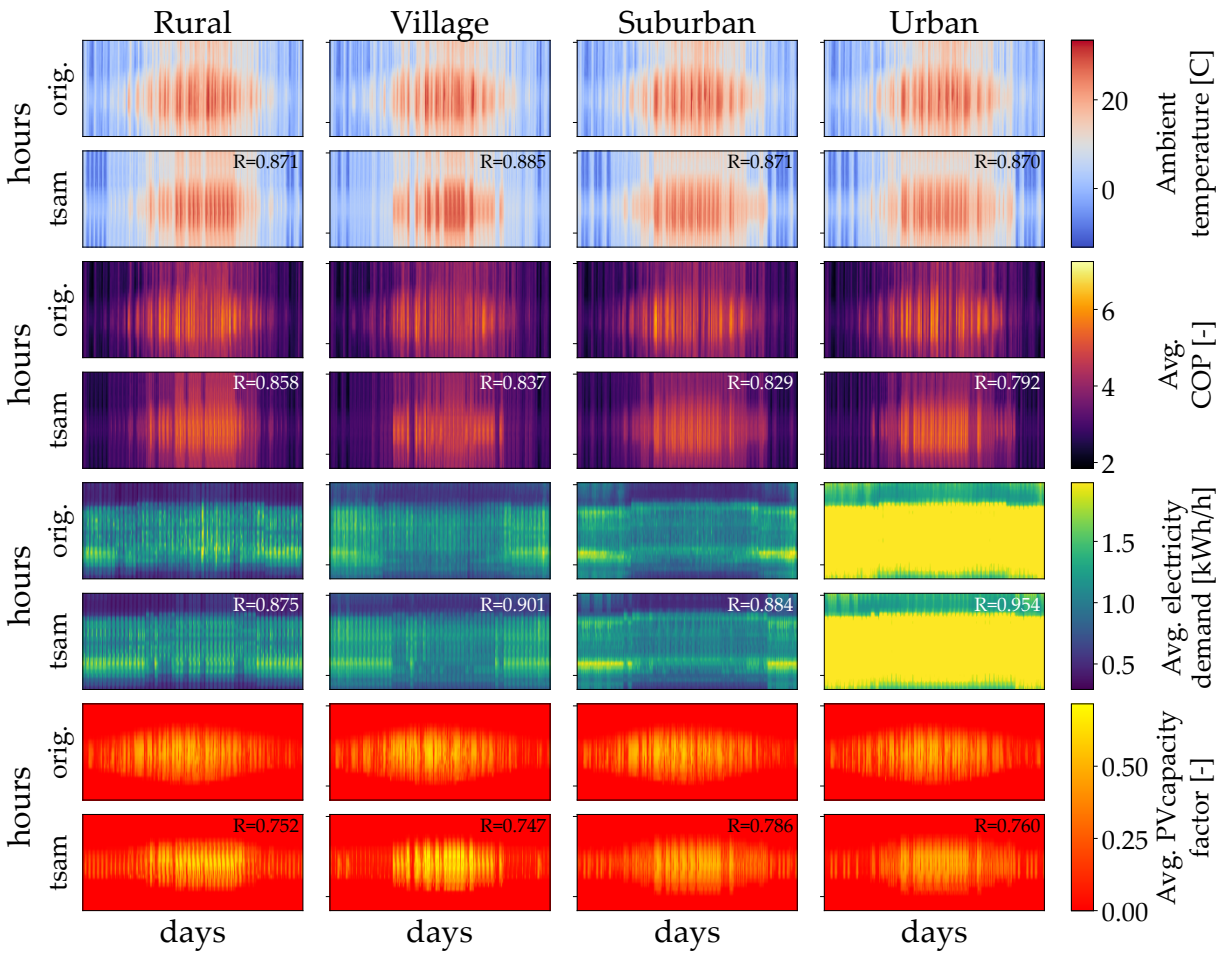

Figure 4.1: Results of the time series aggregation for the various types of modeled time series. The depicted COP and electricity demand time series are averaged across each building, and the PV capacity factors are averaged across each roof section.

aggregation criteria did not consider the electricity demand curves, the typical periods reflect their original trends well. This parameter even achieved R values up to 0.95.

Relative to the other time series, the representation of the PV capacity factors is the lowest. This could be due to two reasons. As the capacity factors differ for each roof section due to their varying angles, their importance factor was scaled down during the aggregation procedure to balance their total importance against the other time series. Second, the PV capacity factors show greater unpredictability compared to ambient temperature, mainly due to cloud cover effects that can lead to variations within short periods. These reasons may explain why a yearly representation of the PV capacity factors by a few typical periods is more challenging than that of temperature.

Regardless, these results demonstrate the applicability of time series aggregation methods for residential low-voltage distribution systems, especially in this case study where seasonal storage is not expected to be a feasible option. Naturally, the exact yearly course of the system cannot be captured. However, one must consider whether a comprehensive representation of a year is worth the significant increase in computational complexity. By reducing the time steps by up to an order of magnitude, a more intricate formulation of the system components can be afforded within the given computational limitations. Incorporating an extreme week, i.e., the period from 15 to 21 January with the lowest average temperature, allows for reliable dimensioning of distributed energy resource (DER) capacities to cover worst-case scenarios. At the same time, the appropriate weighting of typical weeks contributes to an accurate rep-

resentation of the system's overall operational behavior.

4.1.2 Accuracy of *LinDistFlow*

The following validation step involves quantifying the approximation errors resulting from neglecting the quadratic loss terms in the *LinDistFlow* formulation. Figures D.1 and D.2 in the Appendix provide a comparison of i) the bus voltages and ii) the power flow through the transformer for all considered scenarios. In both figures, the x-axes of the subplots represent the parameter values approximated by the *LinDistFlow* model, and the y-axes show either the voltage parameter calculated by the post-optimization non-convex AC power flow model or the relative power loss percentage as neglected by the *LinDistFlow* model. The validation results can be summarized as follows:

- As the absolute losses are quadratically correlated with the power flow, the relative power loss percentages (loss divided by the flow) show a linear correlation with the flow.
- The relative system losses do not exceed 10% at any operation point. For all scenarios except the rural grid with 100% electrification, the losses even stay well below 5%. The rural grid scenarios exhibit higher losses due to the grid having longer distances and no cable reinforcement taking place (resulting in larger impedances).
- As these grid losses have to be compensated by the distribution system operator (DSO), they result in additional costs (analyzed in the Cost Section 4.7).
- Similarly, bus voltages exhibit small variations between *LinDistFlow* and the non-convex power flow model. In no scenario, do the actual voltage variations calculated by the non-convex model lead to a violation of the voltage band restrictions.

In summary, *LinDistFlow* serves as a reliable model for the given use case, as the voltage deviations and losses remain at an acceptable level.

4.2 Impact of rigid electrification on the existing grids

The first analysis following the validation is an assessment of the existing grid capacities to carry the additional loads resulting from the electrification of heating of mobility. For this, an analysis of the transformer loading and bus voltages is made. As a starting point, it is assumed that no flexibilities are employed by the prosumers at this stage (the *InFlex* paradigm)–the heating and mobility demands are satisfied in a rigid manner.

4.2.1 Loading of the transformer

Figure 4.2 sets the total net grid loads emerging from the electrification of heating and mobility in relation to the existing transformer capacities for each grid. For clarity, only the extreme week is investigated since the electrical load is highest in this period due to the highest utilization of the heat pumps.

In terms of loading, the transformers were significantly oversized before the electrification of heating and mobility. All grids can support the loads arising from the low (25%) electrification scenario–only in the urban grid does an overload of 108% occur once. The medium (50%) electrification scenario slightly brings the suburban grid to its loading limits and causes significant overloading for the urban grid. In the extreme (100%) electrification scenario, the violation of the transformer capacities is likewise experienced by the village grid. The rural

grid is notable, where the transformer capacity lies well above the loading limits even under extreme electrification, experiencing a maximum loading of only 32%.

4.2.2 Bus voltages

Figure 4.3 illustrates a similar analysis investigating the over- and undervoltages at the load buses with respect to the main busbar voltage (the voltage differential) under increasing electrification. Here, the x-axis represents the different load buses in the respective grids, sorted by their mean values throughout the year. Black lines depict the average voltage differential for each node throughout the year, and the gray areas with different tones illustrate the ranges for various deciles. The red dashed lines represent the voltage limitations allotted for the LV grid without the use of voltage regulating distribution transformers (VRDTs) ($[-5\%, +3\%]$ p.u.), as introduced in Section 2.5.2.2.

Similar to transformer loading, conventional electrical loads do not cause any voltage violation, with the 25% electrification scenario only causing occasional undervoltages in the suburban grid. This changes under the medium (50%) electrification scenario–the load buses in rural, village, and suburban grids experience significant undervoltages at this rate. While the loading in the rural grid is the lowest compared to the others, the longer electrical distances between its buses result in significant voltage drops. Despite the high density of loads in the urban grid, having these distributed among a large number of branches alleviates the nodal voltage deviations there– 50% electrification causes barely any violation in the voltages. In the 100% electrification, substantial violations of the voltage band take place throughout all grids, with the urban grid affected the least.

In summary, for the 25% electrification scenario, only the suburban and urban grids require a transformer replacement to remedy the occasional voltage and loading violations described above. On the other hand, under higher electrification rates, especially above 50%, a more significant need for grid reinforcement is evident. Among the investigated grids, it is not possible to trace a single source for the reinforcement requirement. While both voltage and loading limitations are experienced in the village and suburban grids, the main drivers for grid reinforcement in the rural and urban grids are the voltage and loading restrictions, respectively. This observation underscores the importance of analyzing each grid individually to identify the specific bottlenecks. Still, one can draw the following general conclusions: i) large electrical lengths per grid branch, typical in rural areas, often lead to critical voltage conditions, and ii) a grid characterized by a high density of tall buildings, typical in urban settings, can lead to loading levels that push the transformers to their limits.

To remedy these violations of the grid capacities, the optimal reinforcement configuration decided by the DSO in the *InFlex* paradigm is illustrated by Figure 4.4. It is observed that there is not a one-size-fits-all solution–both reinforcement options of VRDT installations and parallel cabling are usually present for most grids. While VRDTs increase the total carrying capacity and voltage band of the overall grid, cable reinforcement is used as a localized solution if the violations are restricted to specific regions of the grids. In the rural grid, the voltage violations are prevented by impedance reduction through parallel cabling localized near the substation in the 50% electrification scenario. At the same time, a VRDT installation is preferred instead, as the voltage deviations are further increased at 100% electrification. For the rest of the grids, a suitable combination of VRDT installation and cable reinforcement has been deemed cost-optimal for the grid planner.

The following Sections will analyze the techno-economic measures part of this study, starting with the effects of flexible DER operation in the following Section. Note that each building and grid will exhibit varying behavior according to their individual characteristics. However, from here on, not every scenario combination is explored in detail for the sake of brevity.

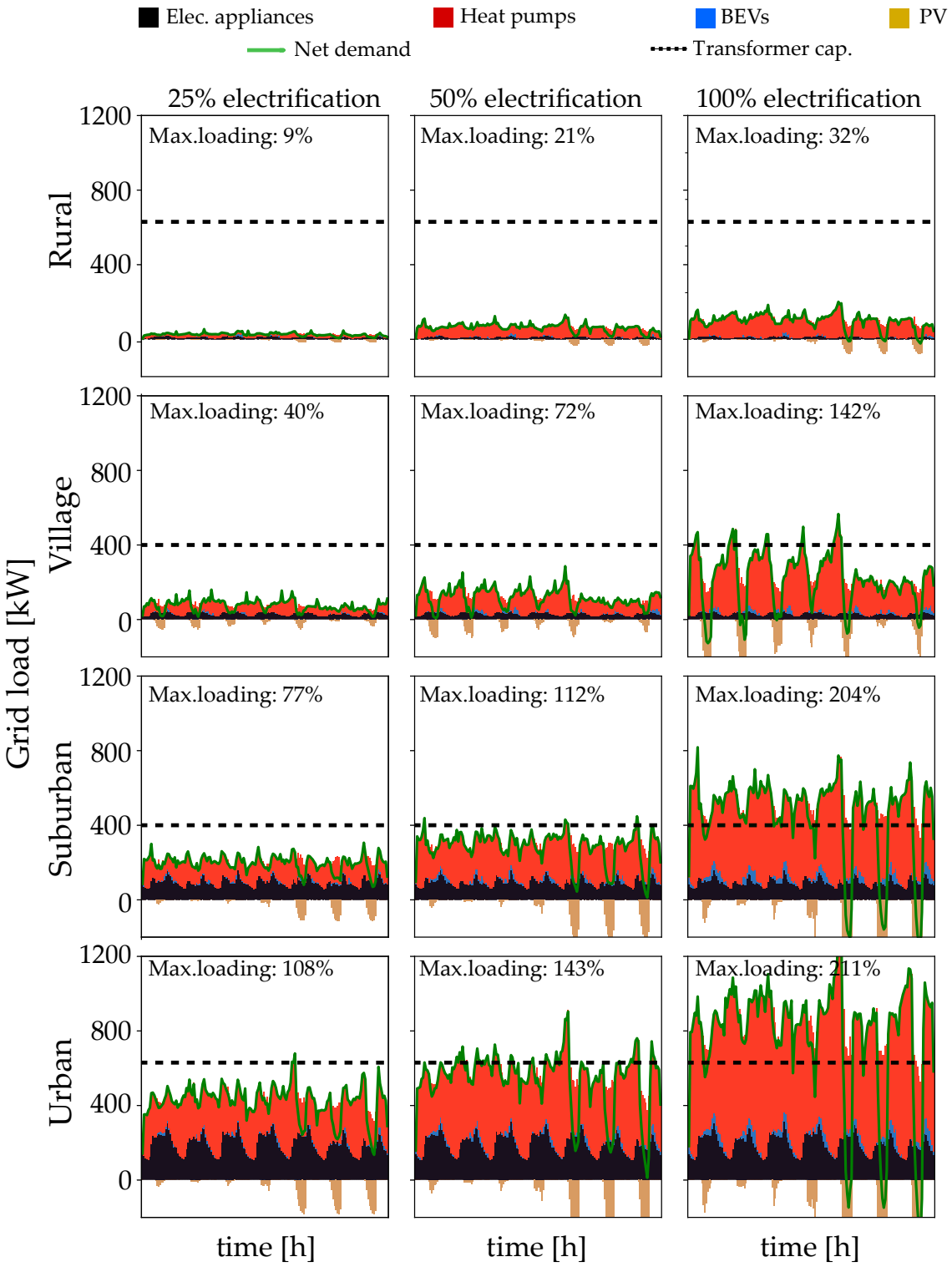

Figure 4.2: The influence of the electrification of heating and mobility on the electrical loading at the transformer in the extreme week.

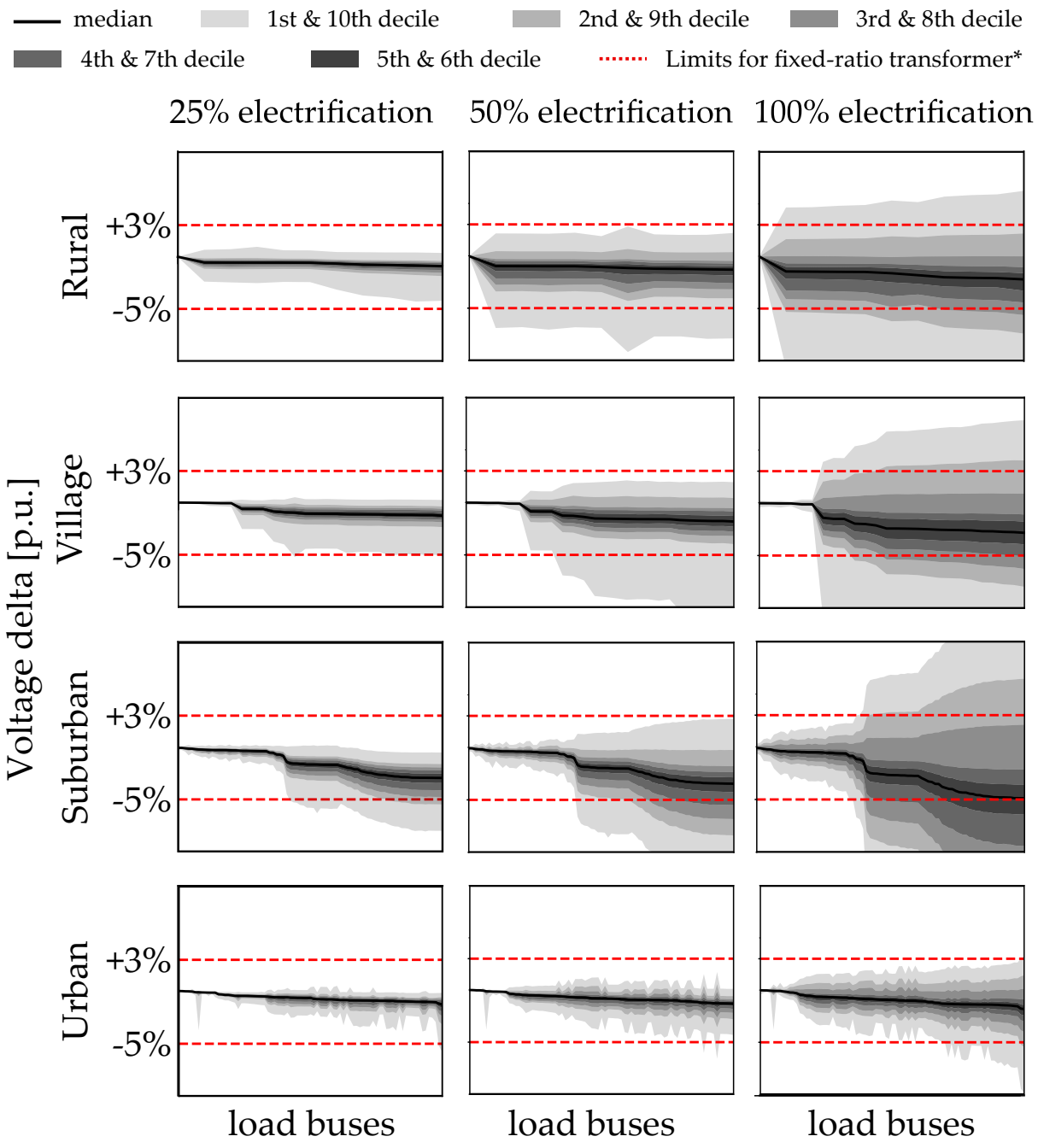

Figure 4.3: The influence of the electrification of heating and mobility on the load bus voltages.

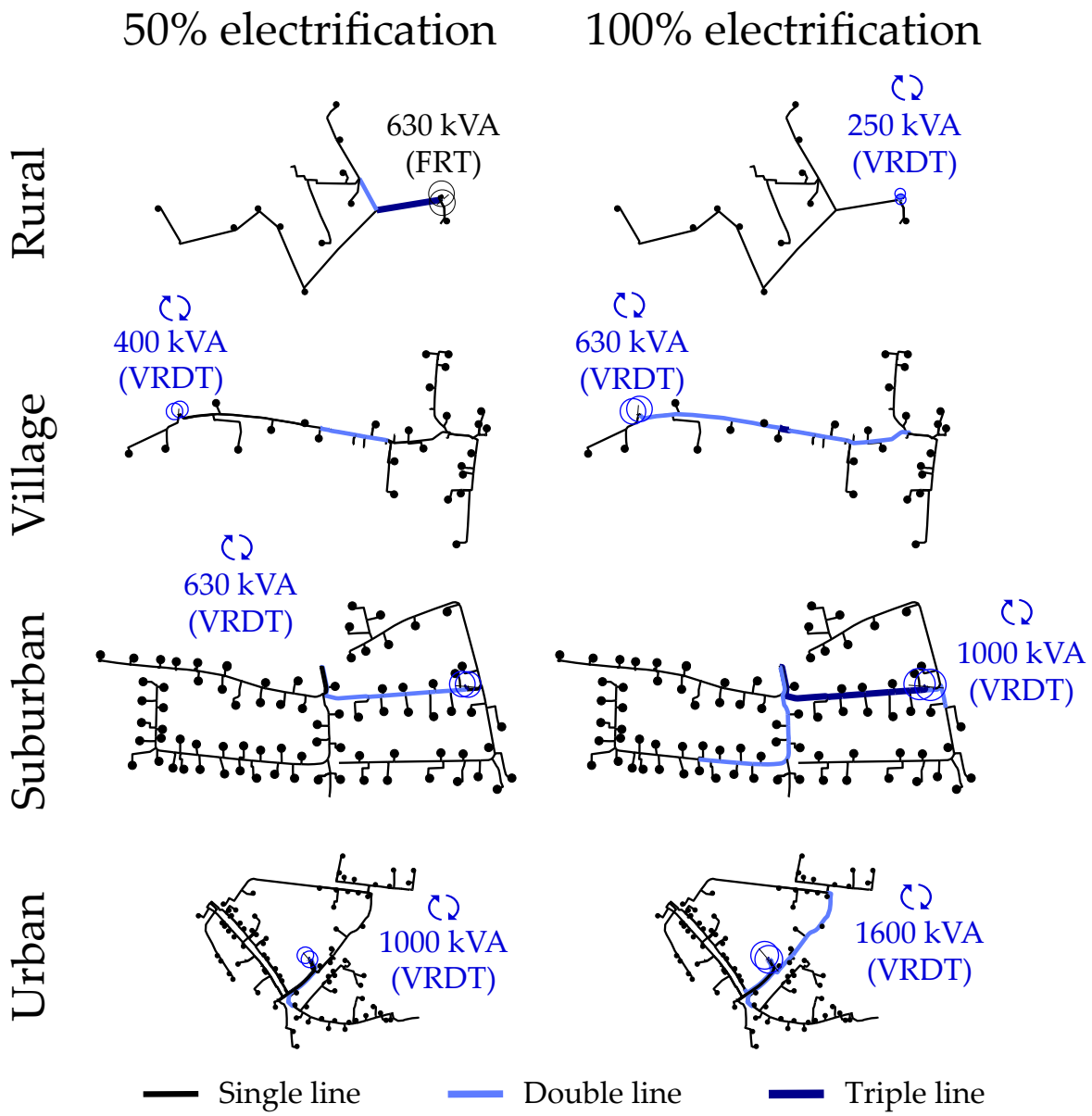

Figure 4.4: The optimal grid reinforcement configurations in the *InFlex* paradigm.

Instead, the corresponding effects are qualitatively described using exemplary buildings and grids, especially where the respective measures lead to a reduced grid reinforcement level. Then, in each Section, the peak reduction effects of each paradigm will be quantitatively summarized for each grid and electrification scenario. Having finally established an understanding of the system effects of the investigated measures, Section 4.7 will return to a cross-scenario analysis regarding the resulting costs, with the goal of deriving generalized statements from the case study.

4.3 Influence of the flexibilities on the prosumer and grid behavior

4.3.1 Flexible prosumer behavior

As previously mentioned, prosumer flexibilities come in the form of leveraging electrical and thermal storage systems, utilizing the thermal inertia of buildings, and employing intelligent battery electric vehicle (BEV) charging strategies. The potential of these flexibilities varies depending on the seasonal conditions. For example, during the summer, overproduction from PV can be better integrated, while the flexible operation of heat pumps becomes crucial in winter due to significant heating demand. Consequently, the following will examine prosumer behavior with and without flexibilities, in an exemplary summer and winter week.

Flexibilities in the summertime Figure 4.5 illustrates the summertime operation of an exemplary building in the suburban grid under 100% electrification. The upper plot shows the electrical balance in the building, with positive and negative values standing for power in- and outflows, respectively. The lower plot illustrates the temperature profiles–the building temperature drawn in blue, minimum and maximum temperatures in orange and green, respectively, and the ambient temperature in red. Comparing the inflexible and flexible behaviors, the following observations are made:

A By taking advantage of the building's thermal inertia, the heat pump operation is shifted to the noon hours, where excess PV production takes place,

B This shifting increases the building temperature above the minimum requirements,

C Likewise, the BEV charging is shifted to the high PV hours.

D No explicit electrical or thermal storage units are installed and utilized, as the thermal inertia is treated as a "free-of-charge" flexibility source.

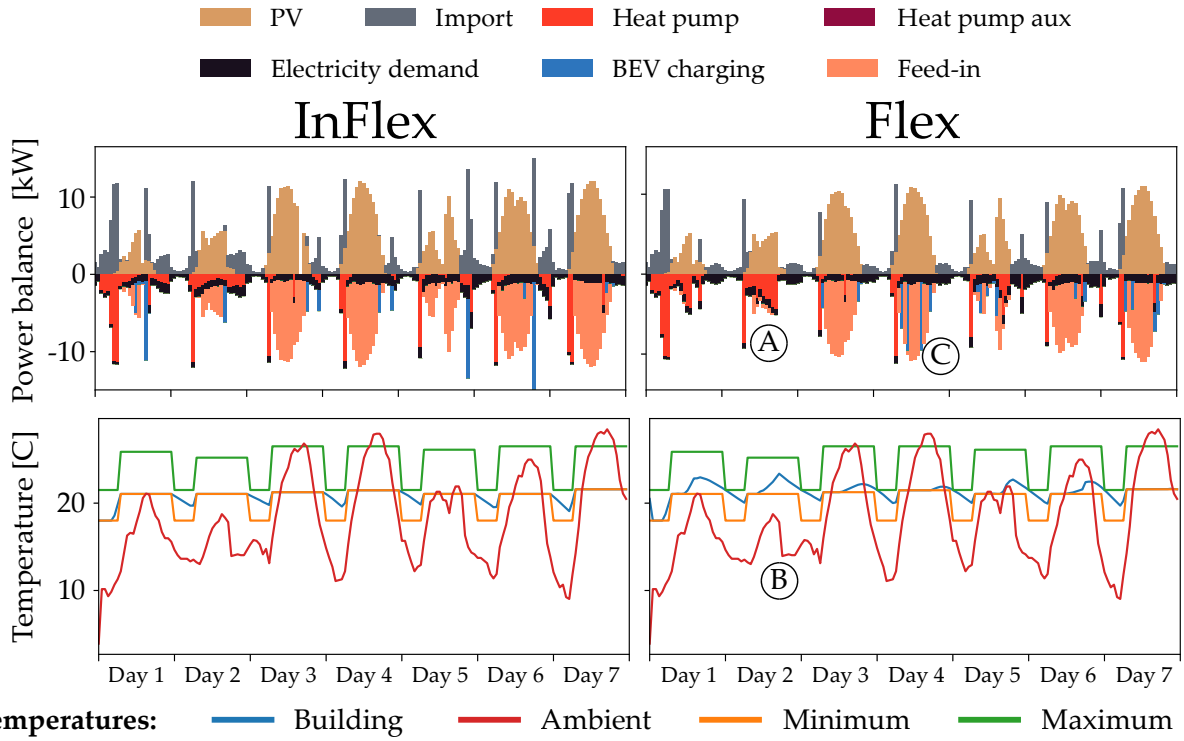

Figure 4.5: Prosumer power balance of an exemplary building in the suburban grid under 100% electrification (summertime).

Simply put, the flexibilities in the summer periods are mainly employed to increase the self-consumption of the excess PV electricity, which would have been fed into the grid otherwise. In turn, the imported amount of grid electricity and the feed-in is reduced. Through intelligent BEV charging, the peak imports are partially reduced as a side benefit.

Flexibilities in the wintertime Figure 4.6 gives an analogous depiction of the wintertime prosumer behavior. Without excess PV generation, its integration cannot be enhanced through flexibilities in this period. Instead, the thermal inertia of the building is used to reduce the required capacities of the heat pump units. With more flexibility regarding when to heat the building, primary and auxiliary heat pump units of lower ratings can be employed at higher full-load hours to meet a given weekly heating demand. This reduction is slight for the main heat pump unit but considerable for the auxiliary unit. As a result, the investment costs for the heat pump units can be decreased. Moreover, the large import peaks caused by the auxiliary heating unit are also reduced (A).

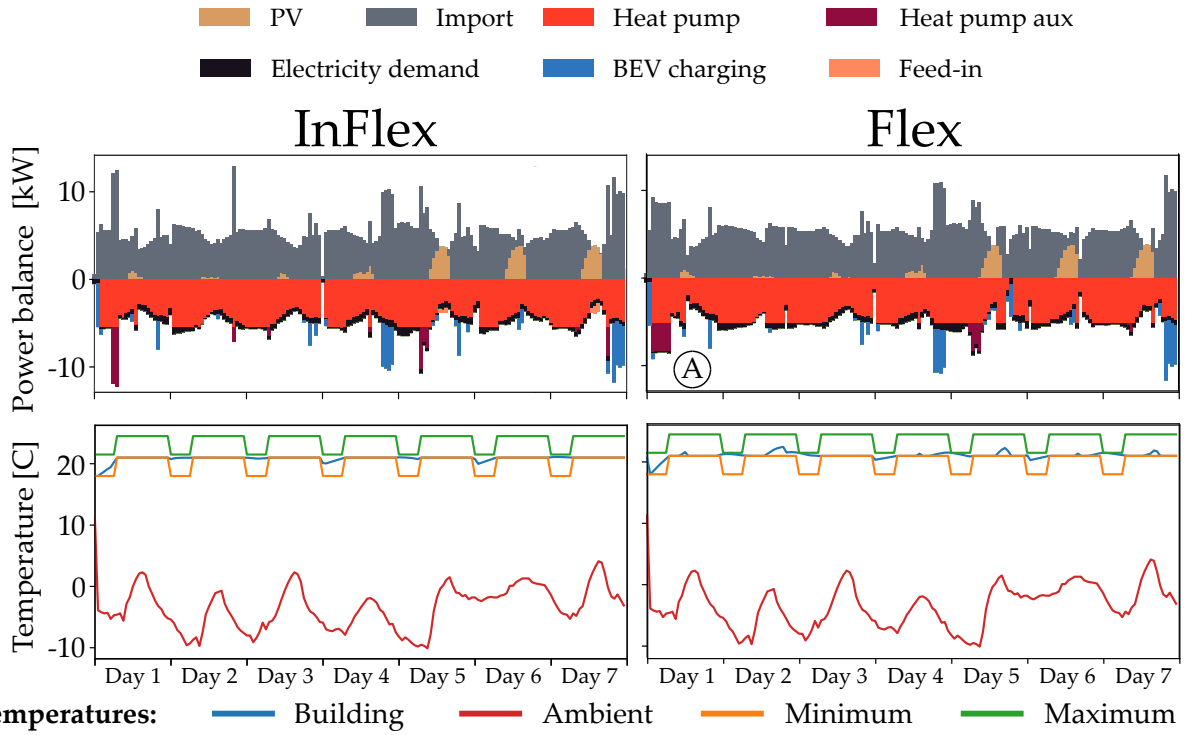

Figure 4.6: Prosumer power balance of an exemplary building in the suburban grid under 100% electrification (extreme winter week).

4.3.2 Grid state with flexible prosumers

Figure 4.7 illustrates the collective impact of the flexibility-driven prosumer behavior described above on the overall load state of the suburban grid. Notably, the individual reductions in prosumer import peaks, resulting from flexible operation, lead to a maximum transformer power peak of around 600 kVA. This allows for installing a lower rating VRDT (630 kVA), as opposed to the 1,000 kVA required in the inflexible paradigm.

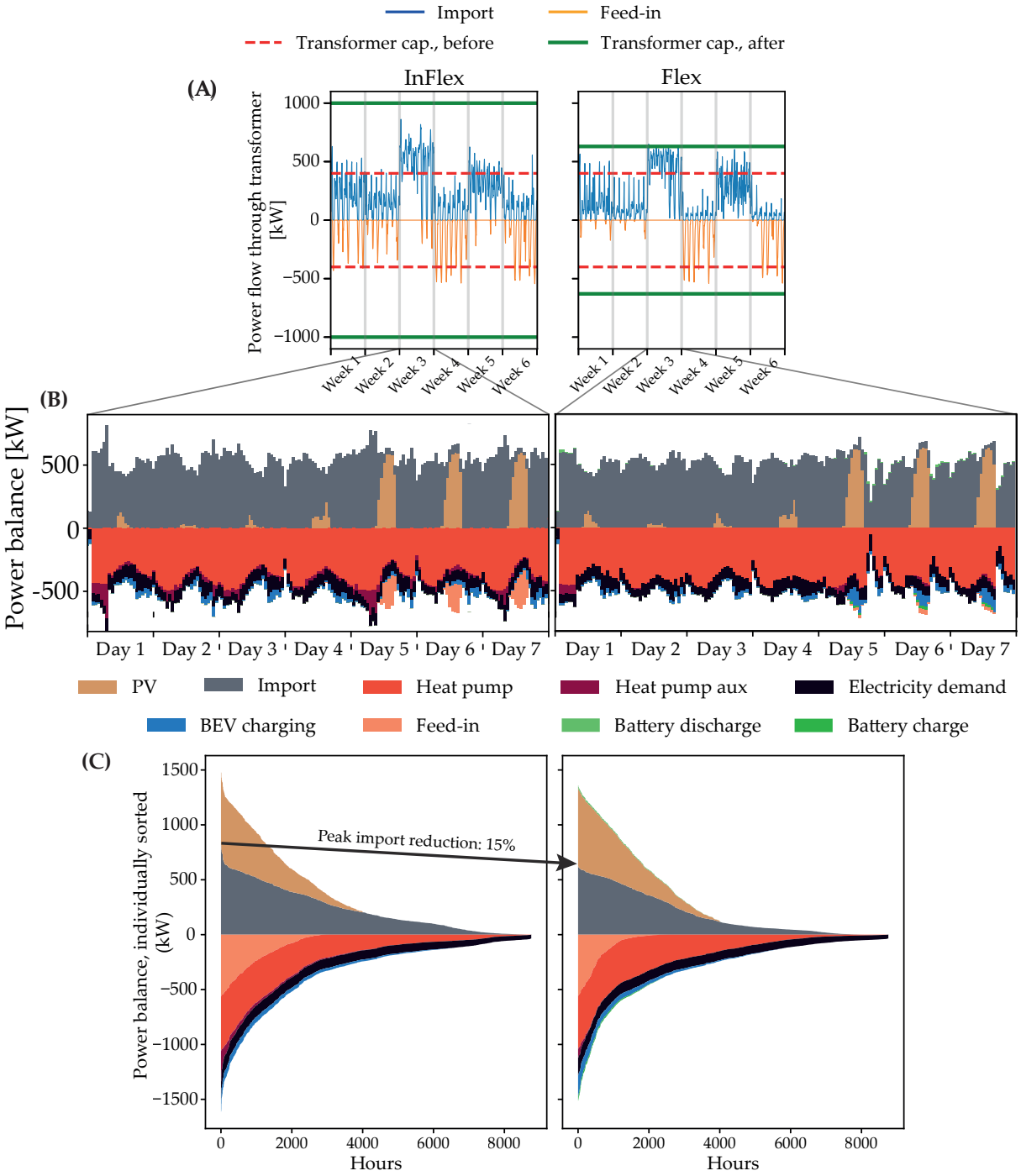

Figure 4.7: Operational comparison between *InFlex* and *Flex* paradigms of the suburban grid under 100% electrification. (A) Grid loading state for the village region under 100% electrification. (B) Prosumer power balance of all buildings in the village grid under 100% electrification (extreme winter week). (C) Individually ordered duration curve of each power balance component throughout the year.

Table 4.1 shows the reduction in peak grid loading through flexible DER operation across all grids and electrification scenarios. Overall, peak reductions between 15% and 32% are achieved. This finding is notable—even in the absence of prosumer-DSO coordination or any explicit incentive for the prosumers to reduce their peaks, their sole goal of increasing the self-consumption of PV through flexibilities yields a more grid-friendly behavior, alleviating the need for grid reinforcement.

Table 4.1: The relative peak grid loading for each *Flex* scenario (*InFlex* paradigm: 100%).

Rural		Village		Suburban		Urban	
50%	100%	50%	100%	50%	100%	50%	100%
79.9%	80.3%	67.9%	80.8%	84.70%	76.4%	78.3%	79.6%

Regardless, the need for a certain level of grid reinforcement motivates the introduction of further grid-relieving measures, the results of which will be described in the following sections.

4.4 Measure 1: capacity pricing

4.4.1 Prosumer behavior under capacity pricing

As outlined in Section 2.3.4, capacity pricing encourages prosumers to minimize their peak import and feed-in power exchange with the grid, thereby reducing their capacity payments. A consistent observation across all scenarios is that these peaks occur during the extreme winter. In order to analyze the reaction of a single prosumer to capacity pricing, Figure 4.8 portrays the behavior of an exemplary multi-family home in the village grid without a night setback temperature, before and after applying the defined set of capacity prices (€10 to €100/kW.a) during the extreme winter week. Without any capacity pricing, a yearly peak of 31.2 kW is observed when the almost base-load operation of heat pumps is combined with auxiliary heating and/or the charging of BEVs (A).

A modest capacity price of €10/kW.a is sufficient to incentivize the prosumer to utilize zero-cost, "low-hanging" flexibility options, such as shifting BEV charging to off-peak heating hours when only the main heat pump unit is in operation (A). This results in a one-third reduction of the peak import to 21.2 kW. As the capacity price increases, the prosumer is further encouraged to decrease the peak electrical consumption of the whole heat pump system. This means that to meet a certain heating demand, the capacity of the auxiliary heat pump unit (which has a lower COP) is reduced at the expense of an increased capacity of the main unit (B). The main heat pump unit is then operated with a higher utilization rate, making more use of the thermal of the building as the capacity price increases (C). While this leads to a deviation from the original optimal capacity configuration of the heat pump system, it enables the prosumers to minimize their peak loads. However, the further reduction in peaks achieved by a capacity tariff of €100/kW.a is marginal at around 15%, compared to €10/kW.a. With the given investment and running cost characteristics, it makes little economic sense for the prosumer to further exchange the auxiliary heat pump capacities with the main unit.

4.4.2 Grid state under capacity pricing

Figure 4.9 shows the collective impact of capacity-price-driven prosumer behavior described above on the overall load state of the village grid. Similarly, Figure 4.10 shows the ordered

duration curves of the grid loading[1].

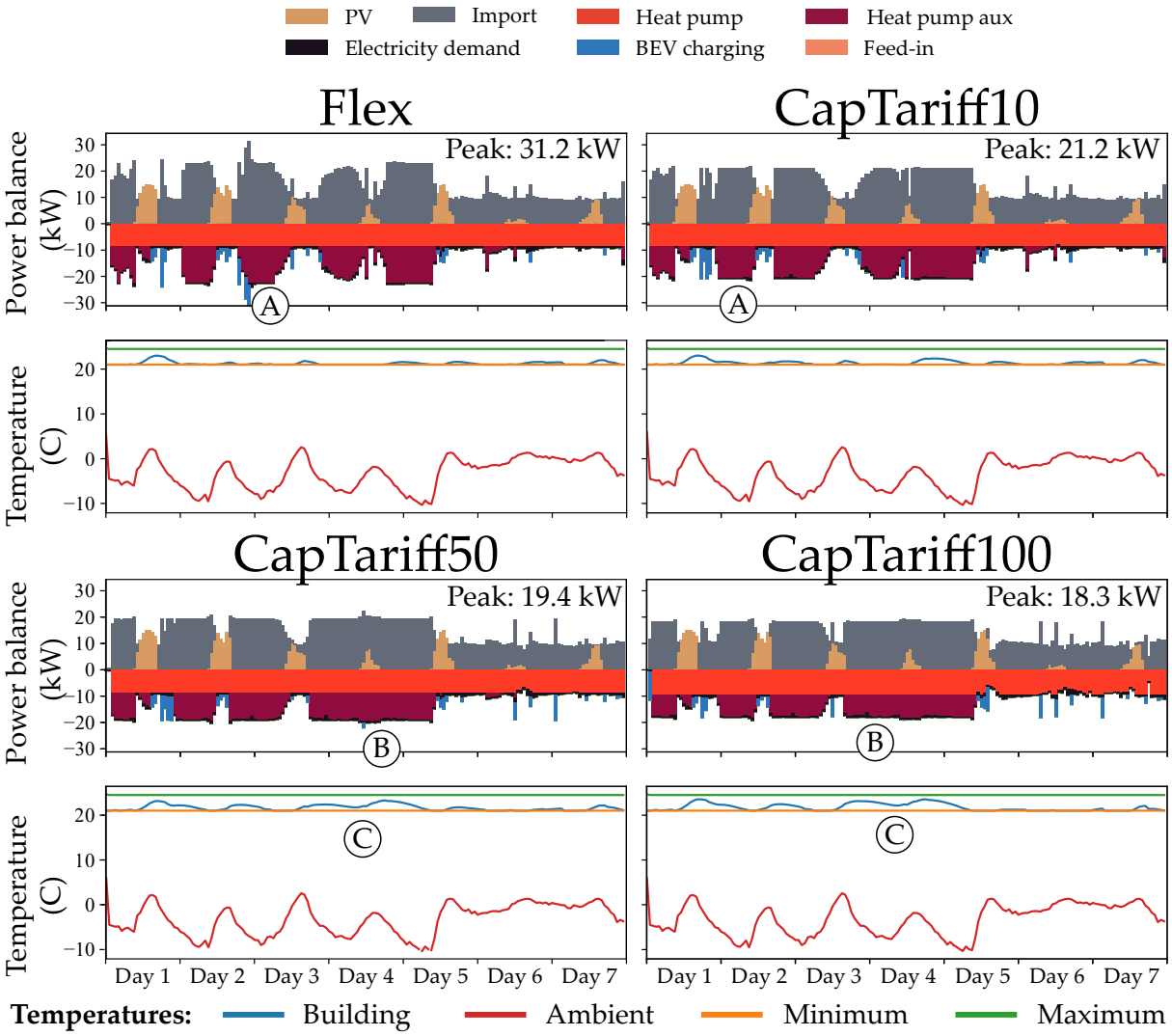

Figure 4.8: Winter operation of a multi-family home in the village grid under 100% electrification, without and with capacity prices of various degrees.

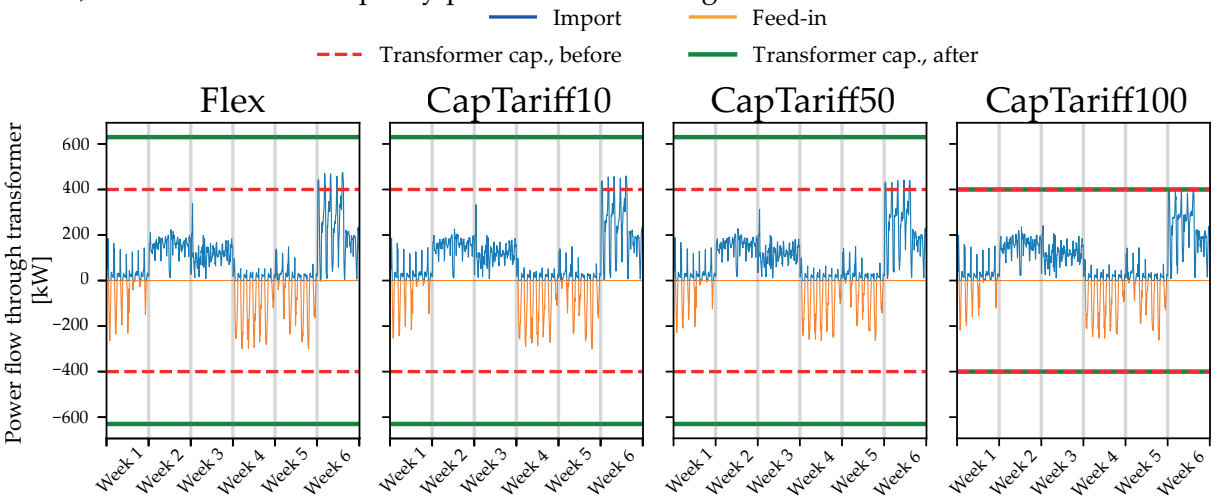

Figure 4.9: Village grid loading state under 100% electrification, without and with capacity prices of various degrees.

[1]In the ordered duration curves, a yearly depiction is achieved by repeating the load values at each representative week as many times as their number of occurrences before ordering them.

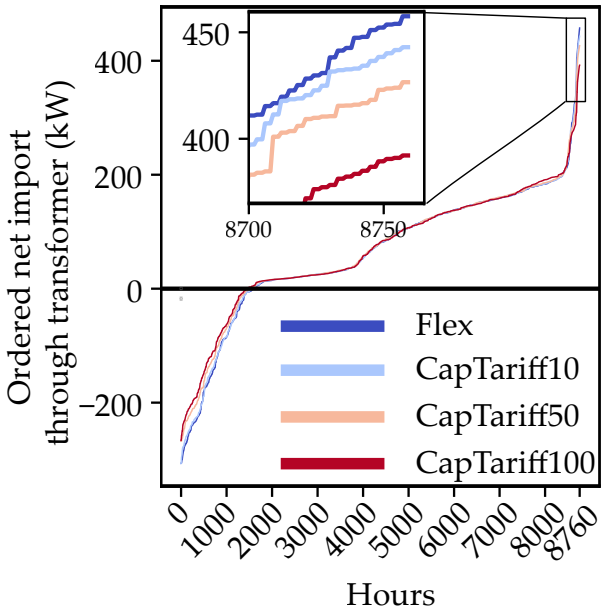

Figure 4.10: Ordered load curve of the village grid under 100% electrification, without and with capacity prices of various degrees.

Through the introduction of a capacity price of 10€/kW.a, 50€/kW.a, and 100€/kW.a, reductions in the overall grid load peaks of around 3%, 7%, and 15% were achieved, respectively. In the latter case–under a capacity pricing of €100/kWa–the peak reduction was substantial enough to avert the need for upgrading the transformer to a VRDT of 630 kVA. This pattern of peak reduction contrasts that of the individual building presented above, where the most significant decrease resulted from introducing a small capacity tariff. This can be explained as follows: the individual peak reductions through the shifting of BEV charging, prompted already by a minimal capacity tariff, tend to occur at different hours, thus having little influence on the overall grid load. Conversely, the consistent reduction of the heat pump base load across all prosumers, driven by significant levels of capacity tariffs, adds to a notable decrease in the overall grid load.

Table 4.2 illustrates the incremental peak grid loading reduction by introducing capacity pricing for all grids and electrification scenarios, compared to the *Flex* paradigm. Depending on the scenario, a capacity pricing at €10, €50, and €100/kW.a results in further peak reductions of up to approximately 5%, 10%, and 20%, respectively. Of particular interest are the scenarios where a price of 10€/kW.a is applied to the village grid under 50% electrification and the suburban grid under 100% electrification. In these cases, the overall peak experiences a minor increase compared to the paradigm without capacity prices. This suggests a potential unintended effect: while the capacity pricing reduces the peak imports per prosumer, the smoothened BEV and heating loads exhibit a higher simultaneity across prosumers, increasing the aggregate peak the grid experiences.

Table 4.2: The relative peak grid loading for each capacity tariff (*CapTariff*) scenario (*Flex* paradigm: 100%)

	Rural		Village		Suburban		Urban	
Capacity price	50%	100%	50%	100%	50%	100%	50%	100%
10€/kW.a	94.8%	93.7%	**101.2%**	96.8%	99.5%	**100.3%**	96.2%	94.9%
50€/kW.a	89.4%	86.5%	98.5%	93.2%	95.0%	96.7%	94.2%	91.5%
100€/kW.a	80.6%	78.9%	91.6%	85.7%	93.0%	93.4%	93.5%	90.2%

4.5 Measure 2: Time-variable tariffs

4.5.1 Prosumer behavior under time-variable tariffs

The time-variable grid tariffs, as outlined in Section 3.5.5, aim to incentivize prosumers to shift their loads away from the peak heating periods, primarily towards the noon hours where the net system demand is low due to high ambient temperatures and PV generation. Figure 4.11 illustrates the winter-time power balance of a building in the rural grid as it adopts the time-variable network tariff, consisting of a standard, a high, and a low tariff (ST, HT, and LT). Major observations are the following:

A Variable tariffs promote the installation and utilization of the battery storage units in a valley-filling manner under varying electricity prices. In this, the grid import is increased in the LT noon hours, with the surplus energy being stored in the batteries for later operating the heat pump. This way, grid import in the HT and ST hours can be reduced to a large extent, reducing the overall electricity costs of the prosumer.

B Auxiliary heat pump units are operated in the night and early morning hours when temperatures are lower, and HT and ST are introduced to. In contrast, the main heat pump unit is utilized throughout the day, thus they can make use of the LT period. Therefore, as variable tariffs are introduced, the economics of the auxiliary heating unit worsens. Instead of installing these units, the main heat pump unit is dimensioned slightly larger to account for the covering of their share of the heat supply. The building inertia combined with the batteries facilitates a highly flexible operation of the heat pump unit.

C The operation under variable tariffs does not guarantee a reduction in the peak import of the individual building, as the BEV charging periods can be wholly shifted to LT hours as well, possibly leading to heightened peaks.

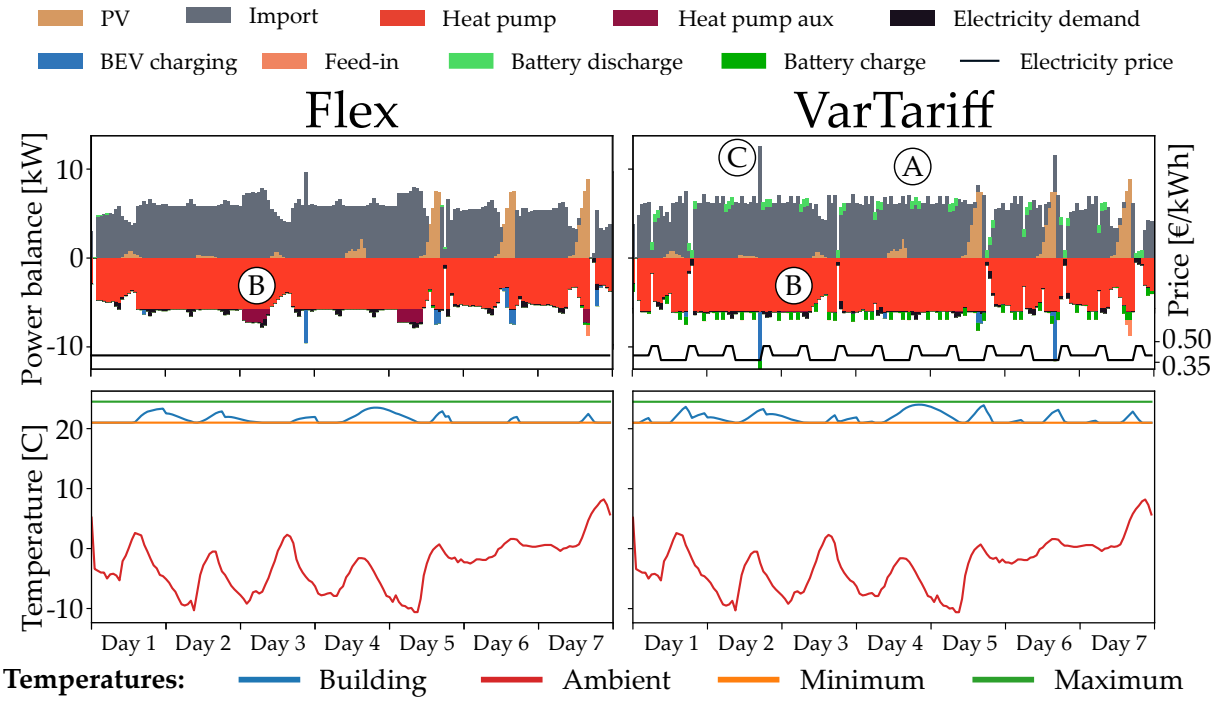

Figure 4.11: Prosumer power balance of a building in the rural grid under 100% electrification, without and with various degrees of participation in variable network tariffs (extreme winter week). The time-variable electricity price is depicted in the above plots, and their values are given in the secondary y-axis.

4.5.2 Grid behavior under time-variable tariffs

To examine the collective influence of the time-variable tariffs on the grid state, the overall energy balance of all buildings within the rural grid during the extreme winter week is presented in Figure 4.12. A minor reduction (up to 4%) in peak imports is observed when up to 50% of prosumers adopt the variable grid tariffs, compared to the *Flex* paradigm. However, the situation turns around as the adoption rate meets 100%. At this point, the avalanche effect becomes evident–the simultaneous charging of heat pumps, BEVs, and batteries during the LT periods results in collective peaks that exceed those seen before the introduction of variable tariffs. Absent any heterogeneous price signal, the distribution of charging and heat demands previously exhibited a smoother pattern. A similar observation can be made when comparing the ordered load curves of the net grid import, as illustrated in the inset of Figure 4.13.

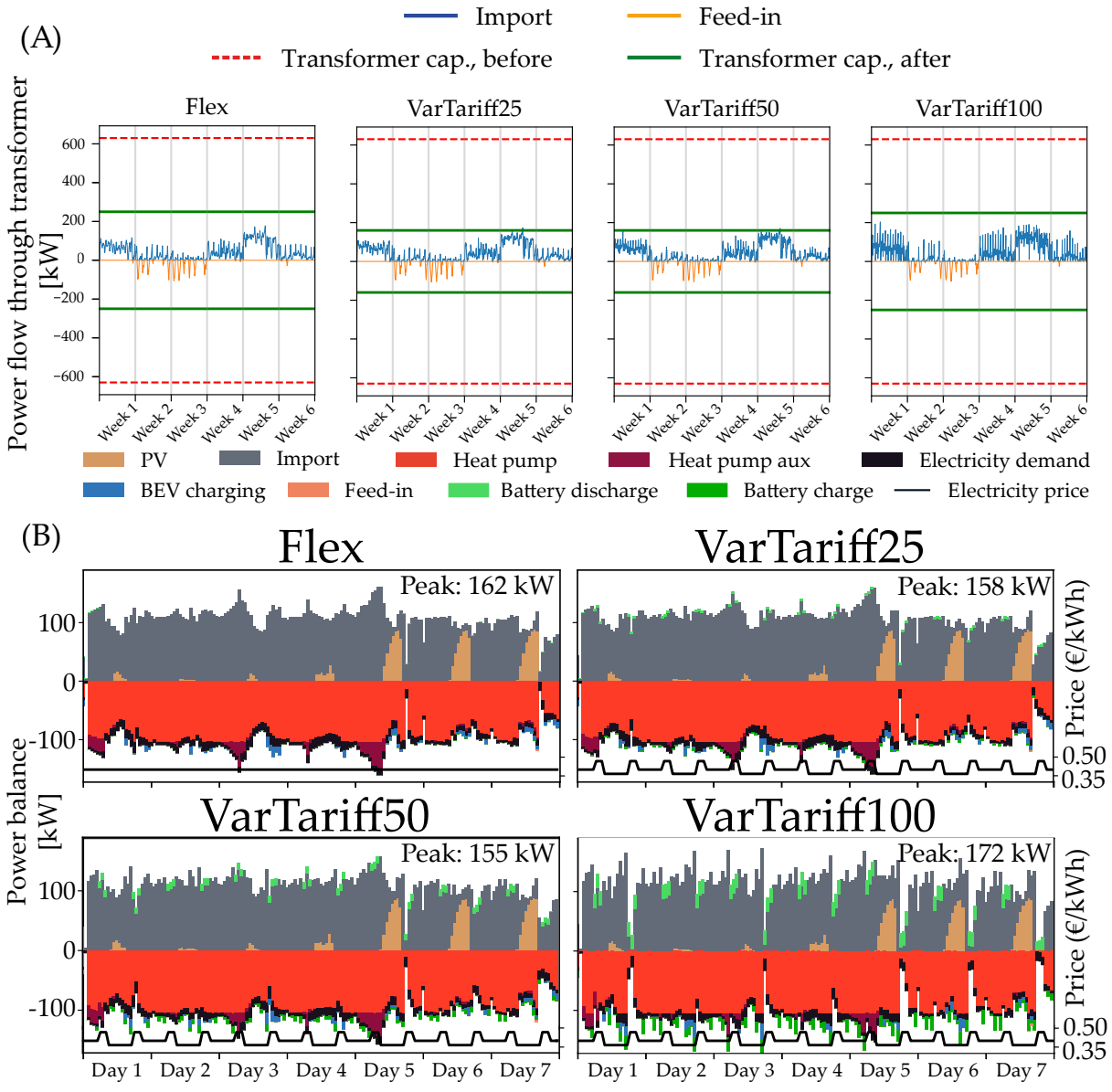

Figure 4.12: (A) Grid loading state in the rural region under 100% electrification, without and with various degrees of participation in variable network tariffs. (B) Prosumer power balance of all buildings in the rural grid under 100% electrification, without and with various degrees of participation in variable network tariffs (extreme winter week).

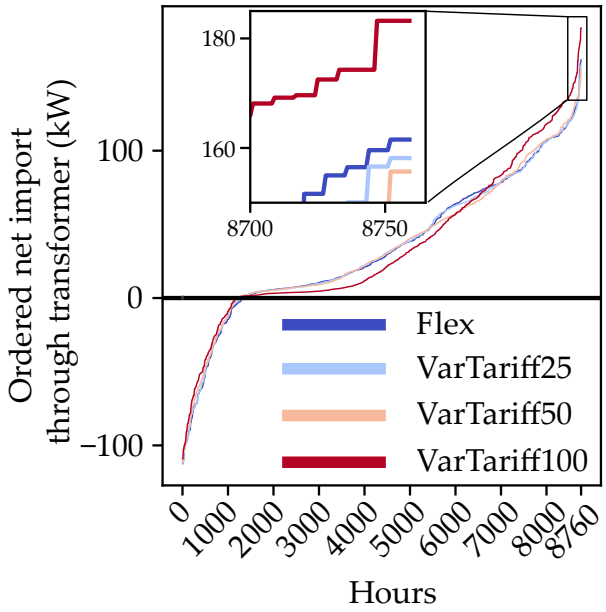

Figure 4.13: Ordered load curve of the rural grid under 100% electrification, without and with variable grid tariffs of various participation rates.

Table 4.3 presents the changes in the grid peaks under different adoption rates of time-variable tariffs for all investigated grid regions and electrification scenarios, compared with the *Flex* scenario. The avalanche effect is apparent for all grid regions, becoming noticeable for village and urban grids even at an adoption rate of 25%. At its most extreme, it results in peak increases of up to 50% (in the case of the suburban grid with 100% electrification and 100% adoption rate), while the best improvement is a modest reduction of 4% (as in the scenario explored above). These findings indicate the potential requirement for implementing network tariffs with time windows dependent on specific zones or branches instead of a uniform one. However, such schemes would inherently require greater implementation effort and bring about transparency issues.

Table 4.3: The relative peak grid loading for each time-variable network tariff (*VarTariff*) scenario (*Flex* paradigm: 100%)

Time-variable	Rural		Village		Suburban		Urban	
tariff adoption	50%	100%	50%	100%	50%	100%	50%	100%
25%	97.3%	97.9%	**100.4%**	**102.5%**	98.4%	99.9%	**103.5%**	**101.2%**
50%	**101.4%**	96.4%	**105.6%**	**107.0%**	**113.0%**	**108.4%**	**109.2%**	**110.9%**
100%	**110.6%**	**113.4%**	**112.7%**	**114.4%**	**133.2%**	**147.5%**	**127.7%**	**139.7%**

4.6 Measure 3: § 14a regulation

While the flexible prosumer behavior, with or without the above-presented, grid relieving pricing measures, helps reduce the system peaks, their contribution is insufficient to eliminate the need for reinforcement under the electrification scenarios above 50%. Moreover, the question stands as to how much a DSO can depend on such a dynamic in their planning process without direct control over these flexibilities.

Therefore, the final measure analyzed in this case study is the potential impact of the § 14a regulation (DSO-side downregulation) on further mitigating the grid reinforcement requirements. Recall that under the § 14a regulation scheme, the DSOs are entitled to downregulate the controllable consumption devices such as heat pumps and wall boxes up to a minimum of 4.2 kW per device whenever their operation above that level would lead to critical grid conditions otherwise, i.e., by violating the loading limits or the voltage band.

4.6.1 Prosumer behavior before and after downregulation

To assess the impact of the DSO-side downregulation on diverse building settings, Figure 4.14 presents the winter-time operation of two distinct buildings within the urban grid, a) a terrace house (TH) without night setback temperature and a total annual heating demand of 88 MWh and b) a multi-family home (MFH) with night setback temperature and a total annual heating demand of 118 MWh.

The terrace house undergoes a moderate downregulation of its heat pump, restricting its operation to 4.2 kW for 19 hours during the winter week. The building compensates for this by shifting (or *rebounding* of) the heat pump operation towards the non-regulated hours, as much as the heat pump capacity and the thermal inertia of the building allow. Nevertheless, occasional reductions in the building temperature up to 2°C below the minimum allowed temperatures are observed (A).

Comparably, the multi-family house is affected by the down-regulation more significantly. Despite its higher heating requirement (around 15 kW base load in winter), the multi-family house faces the same 4.2 kW limitation as per regulation. This leads to the curtailment of a significant portion of the heat pump operation. Trying to adapt, the building likewise shifts the heat pump operation to the unregulated hours. Additionally, it employs the auxiliary heating unit when necessary (Point C) to retain as much thermal comfort as possible. Nevertheless, the building temperature drops to around 10 degrees on multiple days (B). The constraints from the downregulation, combined with narrow unregulated time windows and an inadequate heat pump capacity, make it challenging for the building to maintain its desired temperature.

These observations suggest that the limits imposed by the § 14a regulation should be tailored to the anticipated heating needs of individual buildings. Given the vast differences in heat pump capacities across various buildings, setting a one-size-fits-all limit may result in unfair curtailment effects. Such disparities not only deviate from the regulation's intended fairness but also pose challenges in terms of social acceptance.

To assess the frequency and severity of the thermal comfort losses within the urban grid across all buildings over the year, the following inspection is made. For each modeled hour, the most severe violation of the thermal comfort (represented by the minimum value of the negative $\vartheta_i - \vartheta_i^{\min}$ across all buildings $\mathcal{I}^b$) is depicted in Figure 4.14. Here, each representative week is ordered corresponding to their occurrences. The Figure shows that the thermal comfort losses reach 10°C (corresponding to the MFH example above). Notably, these deficits are confined to the wintertime when heat demand and the associated heat pump loads are at their peak, and the capacities of the heat pumps are dimensioned to meet this demand.

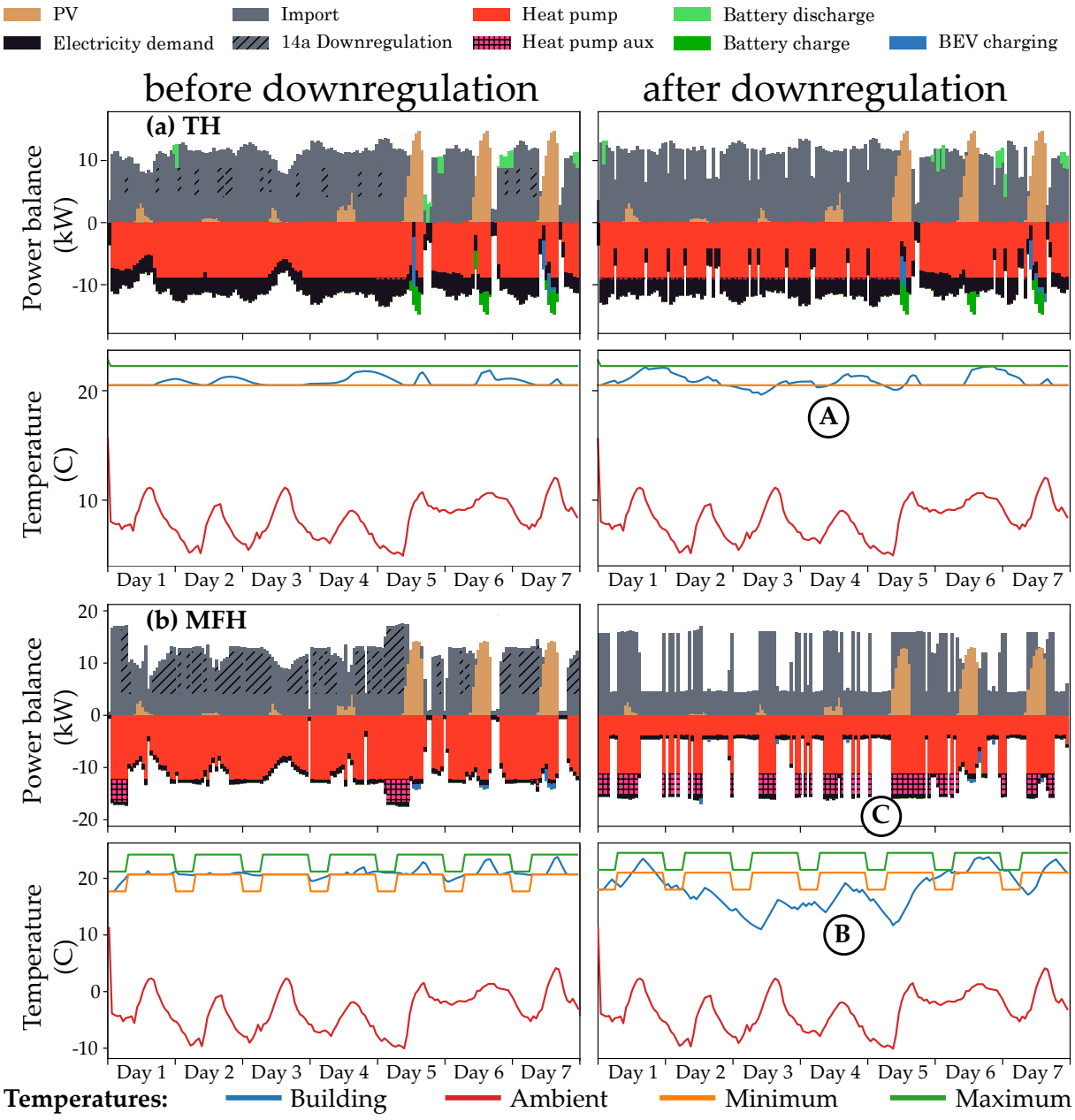

Figure 4.14: Winter operation of two buildings in the urban grid under 100% electrification, before and after the DSO-side downregulation takes place. (A) A terrace house (TH) with a total yearly heating demand of 88 MWh. (B) A multi-family house (MFH) with a total yearly heating demand of 118 MWh.

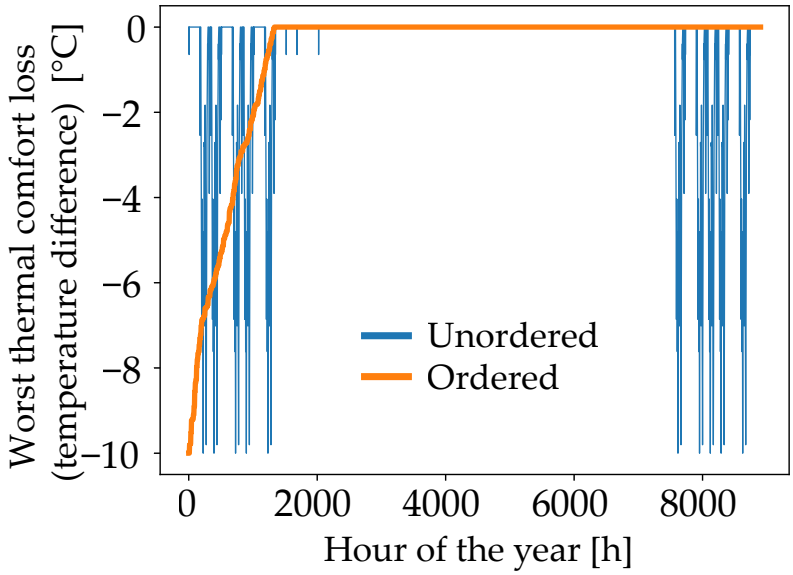

Figure 4.15: The worst thermal comfort losses at each modeled hour across all buildings in the urban grid, given in an unordered and ordered manner. The thermal comfort loss is calculated as the difference between the building and minimum temperature, whenever this yields a negative value.

4.6.2 Grid state with § 14a regulation

Figure 4.16 illustrates the potential of the DSO downregulation to reduce the grid loading in each representative week for the urban grid. By employing the downregulation measures primarily in the winter week, the grid operator could achieve a significant reduction in the grid peaks of up to 13%, despite the rebounding effect illustrated earlier. With this alleviation of loads, installing a transformer of a smaller power rating (1,000 kVA instead of 1,200 kVA) and reduced cabling has been possible (see Section 4.7).

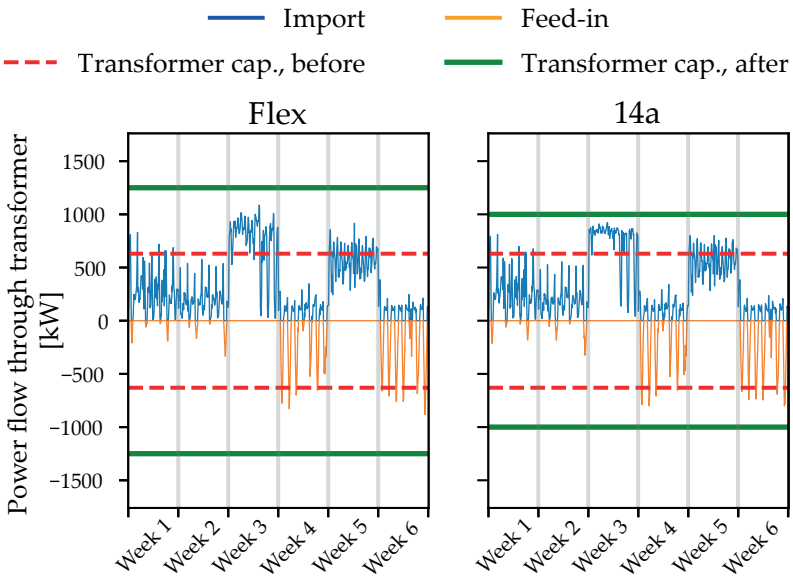

Figure 4.16: Urban grid loading state under 100% electrification, without and with § 14a regulation.

Table 4.4 shows the peak reduction potential of the § 14a regulation in all investigated grid regions and electrification scenarios, compared with the *Flex* scenario. Two types of peak reductions are given: before and after the rebound effect (the prosumers shifting heat-pump load). The former is relevant for the grid reinforcement decision, as this is the operation that the DSO optimizes in the HOODS-Grid-14a problem, unaware of the reaction of the prosumers to the downregulation schedule. Even after the rebound effect, peak reductions between 5% to 23% were observed in the investigated scenarios.

Table 4.4: The relative peak grid loading under the § 14a regulation, before and after the rebound effect (*Flex* paradigm: 100%)

	Rural		Village		Suburban		Urban	
14a paradigm	50%	100%	50%	100%	50%	100%	50%	100%
Before rebound	76.7%	52.3%	81.6%	54.6%	94.1%	94.6%	89.0%	75.4%
After rebound	86.6%	77.0%	86.4%	87.3%	95.1%	95.4%	91.9%	87.0%

The discrepancy between the peaks present before and after the reaction of the prosumers to the downregulation is the highest for the village grid (54.6% vs. 87.3%)—Figure 4.17 shows the load behavior for this scenario along with the DSO's decision for the transformer reinforcement. Indeed, the rebound effect leads to a single-time violation of the transformer limits in the winter week (A). In all other scenarios, loading violations due to rebound were either absent or even less severe.

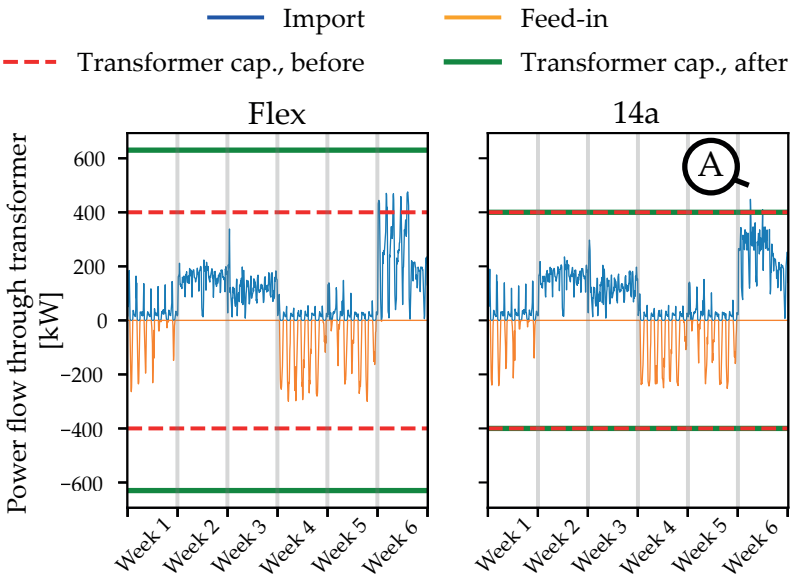

Figure 4.17: Village grid loading state under 100% electrification, without and with § 14a regulation, where a rare violation of the transformer limits occurs.

4.7 Cross-scenario analysis and costs

In this Section, a comparison of the annualized costs across the investigated scenarios is made, first for the overall system costs, followed by a breakdown of the grid costs.

4.7.1 Resultant system costs

Figure 4.18 summarizes the annualized system costs across all grids, electrification scenarios, and paradigms. Here, each column corresponds to a given electrification scenario, each row stands for a grid region, and the individual bars within each subplot represent the particular paradigm. The costs are shown in relative terms between 0% and 100% for each grid region, where the reference value of 100% corresponds to the costs occurring in the *InFlex* paradigm under 100% electrification, where they are the highest. The absolute value of this reference cost level is depicted within each subplot. As the *14a* paradigm does not always yield thermal comfort-ensuring results for the prosumers, it is not included in the cost comparison.

Parallel to Section 2.3.4, the system costs depicted by the plots are the following:

- *Net elec., kWh*: The net volumetric electricity costs for prosumers, i.e., the import costs of electricity minus the revenues collected by PV feed-in (costs in each week scaled by the corresponding *tsam* weight)
- *Cap. tariff:* The total capacity tariff costs paid by the prosumers,
- *PV:* The annualized investment costs paid for the PV systems,
- *Heat pump:* The annualized investment costs paid for the heat pump systems (including the main and auxiliary unit),
- *Battery:* The annualized investment costs paid for the battery units,
- *Heat storage:* The annualized investment costs paid for the thermal storage units, and
- *Grid costs:* The total grid-related costs (to be further broken down in Subsection 4.7.2).

Note that as the goal of this case study is not to evaluate the profitability of electrification per se, the costs related to non-electrified shares of the heating and mobility demands, e.g., the respective fuel costs, are not considered in this analysis.

The major findings from the system cost analysis are as follows:

1. *Electricity costs dominate:* A significant proportion of system costs are attributed to the electricity import costs across all scenarios. These correspond to 71-87%, 67-81%, and 61-72% for the scenarios with low, medium, and high electrification rates—as the rate of electrification increases, the additional investment costs incurred for the DERs overweigh the additional electricity procurement costs.
2. *Flexibilities bring the highest benefits:* Connected to the previous point, the prosumers see considerable benefits from leveraging their flexibilities, especially when PV electricity is optimally integrated. The relative cost improvements between the *Flex* and *InFlex* paradigms are higher as the DER penetration increases, as more prosumers become able to leverage their flexibilities. Depending on the grid region, they correspond to 8%-15% compared to 3%-8% for high and low electrification scenarios, respectively,

3. *Need for storage investment is minor:* The installation of explicit storage systems, i.e., batteries and thermal storage, are not deemed profitable by the prosumers. Instead, the inherent thermal inertia of buildings serves as a more economical source of flexibility. These explicit storage options become more appealing only in scenarios with capacity and variable tariffs as additional load-shifting capabilities are promoted through these tariff schemes. Even then, their contribution to the overall system costs is limited at 2% maximum.

4. *Capacity tariff influences are minor:* The impact of capacity tariffs on the resultant prosumer costs is relatively minor. Even in the highest capacity tariff setting at 100€/kW, these tariffs account only for between 7-13% of the total electricity expenses. One reason is that, in scenarios with capacity tariffs, the volumetric cost portion is adjusted to ensure consistent total electricity expenses for prosumers. Such a revised tariff structure could prove practical to motivate prosumers to reduce their peaks while keeping their total electricity costs virtually constant.

5. *Variable tariffs reduce electricity costs slightly:* Likewise, the influence of a variable tariff structure in the system costs is minor. Nevertheless, up to 6% savings in electricity costs could be achieved for prosumers through intelligently managed electricity imports favoring low-tariff hours. However, these savings are partially offset by the costs associated with the explicit storage units that have to be installed to take advantage of the tariff scheme.

6. *Deviations from the global optimum are low:* Recall that the *Best-Case* paradigm allows a holistic planning and operational procedure within the LV system, including the exchange of excess electricity between prosumers and promoting a grid-friendly prosumer behavior. Yet, the cost reductions observed in these benchmark paradigms compared to the uncoordinated *Flex* paradigms are limited at 1% to 7%. These cost improvements are more pronounced in the lower electrification scenarios (3% to 7% compared to 1% to 3% in the high electrification scenarios). One reason is the following: in the low and medium electrification scenarios where only a limited share of the prosumers own PV systems, there is a more significant potential for exchanging the excess production with the prosumers lacking PV systems. This even leads to a larger dimensioning of these PV systems installed to generate the excess to be shared. However, in a 100% electrification setting, where every prosumer has the option to install PV, the excess energy is available for each prosumer at the same time. Consequently, the advantages of a coordinated electricity exchange are minor. A further reason of limited system benefits from holistic planning is the comparatively small proportion of grid-related costs relative to the total system costs (between 0.3% to 3.3%). While the *Best-Case* approach facilitates a grid-compatible operation for the DERs within the system, the limited contribution of grid costs to overall expenses means that improvements derived from this approach are inherently limited.

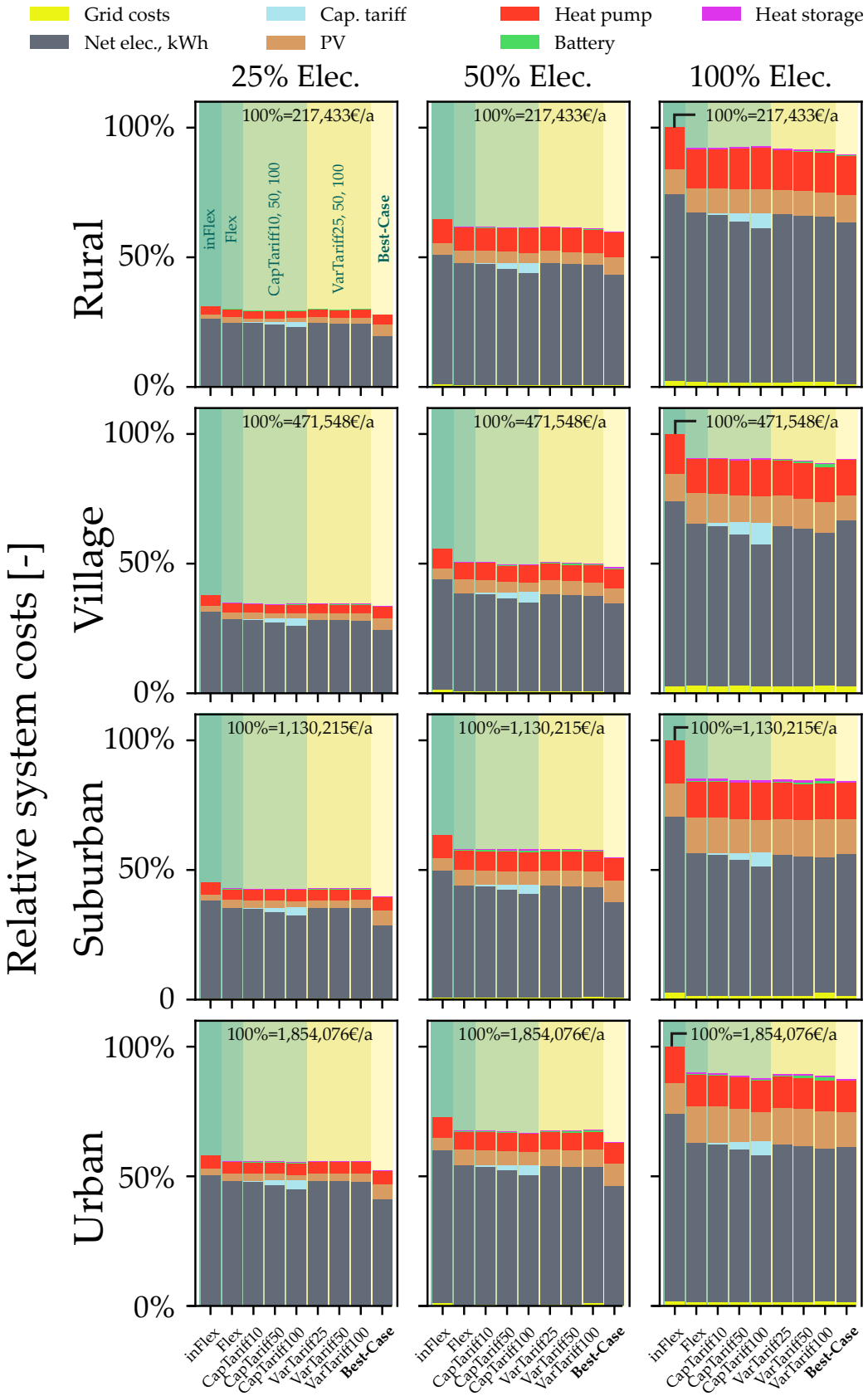

Figure 4.18: Breakdown of the total system costs, given in relative terms (100% represents the most expensive *InFlex* paradigm for 100% electrification for each grid region.)

4.7.2 Resultant grid costs

A detailed view of the emergent annualized grid costs is provided by Figure 4.19, with a layout analogous to the previous Figure. Again, the costs are given in relative terms, with the costs in the *InFlex* paradigm under the 100% electrification scenario set as the reference value for each grid. In contrast to the system costs breakdown, the *14a* paradigm is also included in this Figure to illustrate the corresponding reductions of the grid reinforcement under this regulation. Additionally, the share of the grid costs in the overall system costs is given above each bar, except for the *14a* paradigm.

The grid-side costs consist of the following:

1. *Cables:* The annualized investment costs of parallel line reinforcement,
2. *Transformer:* The annualized investment costs of replacing the transformer with a voltage-regulated distribution transformer,
3. *Loss compensation:* The costs of compensating for the active power losses within the grid,
4. *Q compensation:* The costs of reactive power compensation,
5. *Grid curtailment:* The payments made by the DSO to the PV owners for the remote curtailment of their generation.

The major observations regarding the grid-side measures and the corresponding costs are as follows:

- *Minor reinforcement needs on the short-term:* In the short-term scenario with 25% electrification, the rural, village, and urban grids required either no or minimal grid reinforcement. Only the suburban grid necessitated a switch to VRDTs for a widened voltage band, complemented by localized line reinforcement to address overloading.
- *On the long term, grid reinforcement becomes essential:* As electrification reaches 50%, grid reinforcement in the form of both parallel cabling and transformer replacement becomes relevant across all grids, making up a considerable share of the grid-related costs. As 100% electrification is achieved, the grid-related costs are dominated mainly by the reinforcement costs.
- *Grid-side costs make up 3% of the system costs at most:* Nevertheless, the grid-side costs make up 2.5%, 3.2%, 3.3%, and 2.0% of the total system costs for the rural, village, suburban, and urban grids respectively. They increase along with electrification not only due to the resultant need for grid reinforcement but also partially due to the increasing amount of active power losses that have to be compensated by the DSO.
- *Costs of grid loss compensation are relevant:* The costs associated with compensating for the grid losses, while not being considered in the optimization as *LinDistFlow* omits their corresponding terms, make up a substantial share of the grid costs. They are most pronounced in the rural grid due to the relatively larger electrical lengths of the cables within the grid. Besides, a notable relationship between the line reinforcement and the power losses is observed. A more prominent reinforcement of the lines in a grid decreases their effective impedances, leading to reduced power losses. This dynamic is evident in the *CapTariff100* paradigm of the village grid under 100% electrification. In this scenario, a more optimal grid planning is realized through a more significant reinforcement of the cables to maintain the voltage band rather than opting for the

transformer replacement. This leads to a reduction of not only the hardware costs but also the grid losses.

- *Capacity and variable tariffs alone do not suffice in preventing grid reinforcement:* As discussed in Section 4.3.2, the prosumer flexibilities usually lead to a smoothening of the grid peaks, reducing the need for reinforcement. In contrast, even with substantial capacity pricing, the maximum reduction achieved in peak grid loading was 20%, with results highly dependent on the specific grid region. As mentioned earlier, this can be attributed to the restricted flexibilities of the heat pumps during winter, which predominantly sets the grid reinforcement needs. The adoption of the variable grid tariffs, on the other hand, not only fails to reduce grid loading consistently but, at high adoption rates, even accentuates the peaks compared to fixed tariffs. These scenarios often result in the highest grid reinforcement requirements.
- *§ 14a regulation allows deferring grid reinforcement:* Through implementing the § 14a downregulation of heat pumps and battery electric vehicles, a robust reduction in the grid reinforcement could be achieved across all scenarios. This came, however, at the cost of occasional violations of the thermal comfort in buildings (up to 10°C), occurring mostly in the extreme wintertime.
- *Remote curtailment of PV is disfavored:* The DSO rarely resorted to PV curtailment, as it is associated with high compensation costs. This is an encouraging result, as the PV curtailment leads to the loss of otherwise usable, zero-marginal cost energy. Only in the scenario with the *14a* paradigm in the rural grid was used in combination with the heat pump/BEV downregulation to avoid a significant amount of grid reinforcement. The costs that emerged from the curtailment were minor in this case.

4.8 Discussion of the results

The case study results will be revisited in the Conclusion Chapter to provide answers to the main research questions of the dissertation after the following Chapter.

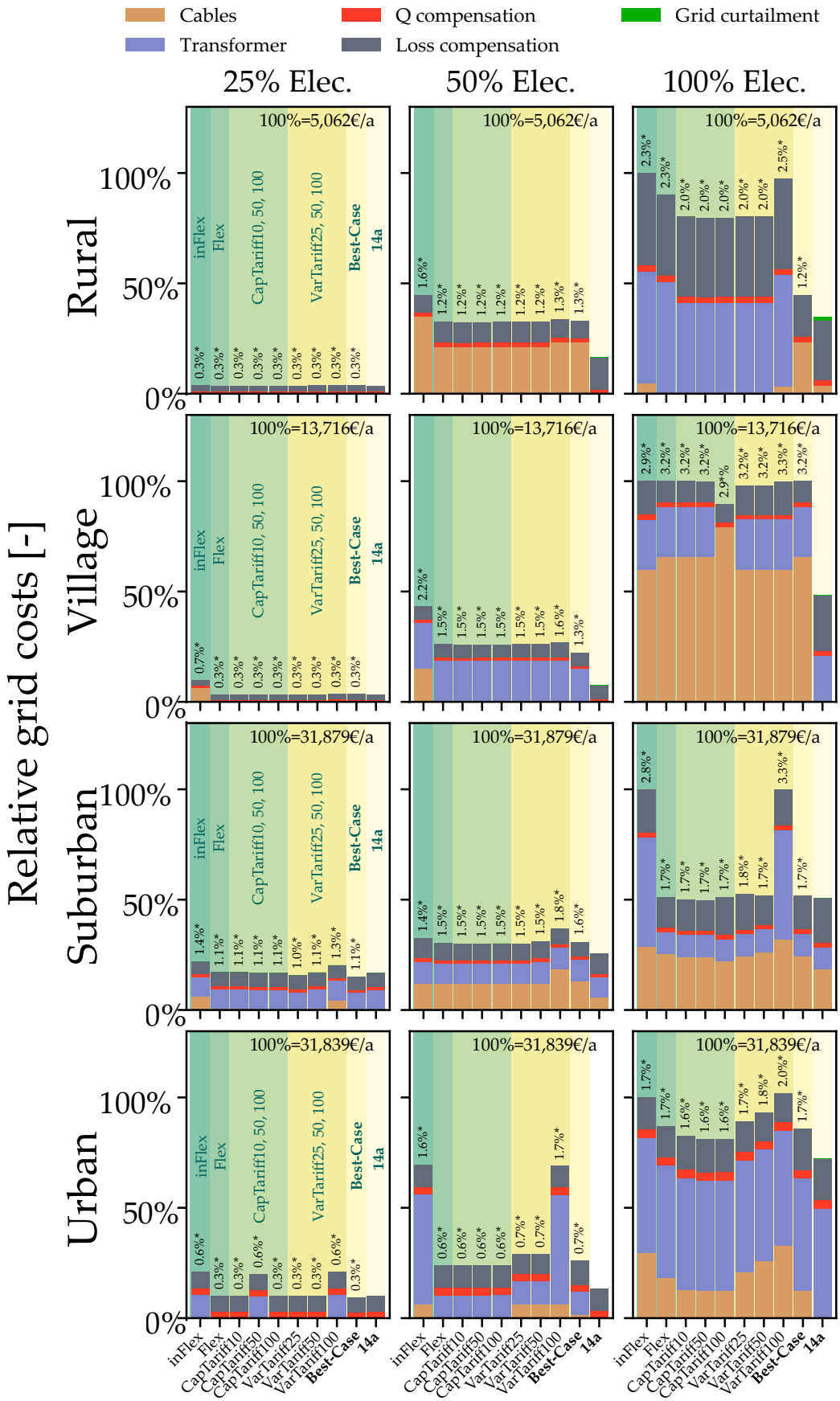

Figure 4.19: Breakdown of the grid costs, given in relative terms (100% represents the most expensive *InFlex* paradigm for 100% electrification for each grid region.
*The share of the grid costs in the total system costs.

Chapter 5

Scaling up: Essay on methods for extending LVDS optimization to large-scale energy system modeling

This Chapter serves as an essay, briefly presenting the additional work conducted by the author, with an aim to explore methods for integrating the localized low voltage distribution system (LVDS) optimization framework—central to this dissertation—into larger-scale energy system models.

Large-scale energy system modeling is a very established practice for supplementing optimal decision-making as energy systems evolve under varying technical, economic, and political requirements (refer to [44] for a review consisting of 75 large-scale energy system modeling frameworks). However, these models conventionally focus on the transmission systems, with the distribution systems simplified as static demand profiles with little consideration of underlying distribution grid topologies, distribution system-level heterogeneities, and detailed representation of the corresponding flexibility options. An insufficient representation of distribution-level dynamics in a model may lead to misinterpretation of their energy requirements and the emergent costs. In contrast, an integration of LVDS models into a large-scale transmission-level model would allow for a detailed assessment of the interactions between these levels. Such a model could encompass, for instance, an entire country, comprising thousands of interconnected LVDSs linked to high-voltage transmission systems. Figure 5.1 illustrates such a model coupling idea. One coupling approach between the distribution and transmission systems is the so-called *soft coupling*, where the outputs of the LVDS submodels serve as an input for the large-scale transmission system model sequentially. Through soft coupling, the load profiles of prosumers, reacting according to various pricing schemes as investigated in this dissertation, can be incorporated into the large-scale model in an aggregated form. This way, the optimal transformation scenarios for the large-scale power plant, transmission, and storage system portfolios can be assessed ex-post. One step beyond soft coupling is the *hard coupling*, i.e., the co-optimization of the transmission-distribution ensemble, where both systems are optimized holistically. This hard coupling would theoretically lead to the *best-case* operation of the entire energy system across levels, where the capacity planning and system operation across levels is set in a manner that minimizes the total system costs encompassing all stakeholders of the energy system such as the prosumers, grid, and power plant operators. To achieve this mathematically, the merit order of the energy system is set within the optimization procedure endogenously, where the prosumers at the LVDSs *de facto* receive a dynamic electricity tariff depending on the merit order condition in the upstream system.

Besides the low availability of granular data, limited computational resources are a sig-

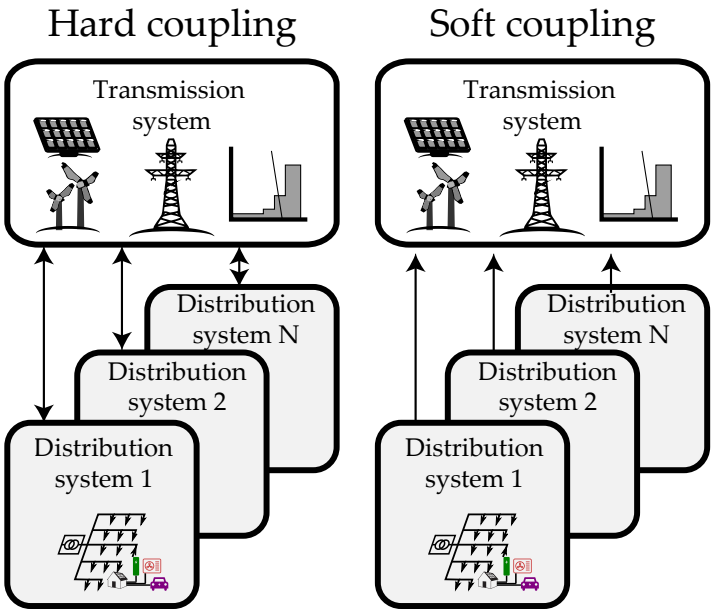

Figure 5.1: Hard and soft coupling between transmission and distribution system models.

nificant obstacle against this pursuit of coupling transmission and distribution-level models. For instance, handling such large models often faces problems in terms of limited computer memory (RAM). The matrix elements stored in the problem models mostly increase quadratically for an increased model size (assuming the number of constraints somewhat correlates with the number of variables, which is usually the case for energy system models). Even if the RAM limitations can be averted, models with higher scales may experience superlinear increases in runtime.

Most countries consist of thousands of LVDSs, and each LVDS may consist of up to hundreds of buses, rendering a single-go integrated solution impossible. Non-conventional methods are necessary to achieve tractability. The following Sections will present three different approaches to that end.

5.1 Hard coupling by representative LVDS integration

One approach for establishing a tractable transmission-distribution level optimization framework is to use representative LVDSs instead of modeling each LVDS separately (see Figure 5.2). In this vein, the author has co-developed a holistic optimization framework that groups LVDSs in two groups: *urban* and *suburban* LVDSs, and applied this framework to a case study dealing with a decarbonized German energy system. These representative LVDSs are "plugged" into each transmission-level node of the large-scale model, i.e., the sixteen federal states of Germany. To represent the multitude of these typical LVDSs in each federal state, the energetic interactions (electricity flows) are scaled up by the "pre-analyzed number of typical LVDS modules", taking each federal state's distinct demographics into account. Compared to depicting thousands of distribution systems, the model complexity is reduced by multiple orders of magnitude through typification. Combined with the time series aggregation presented in this dissertation, and a reduction of each LVDS down to a single branch, a co-optimization of both transmission and distribution systems could be achieved in a computationally tractable manner.

Within the study, a comparison between a rigid and a fully flexible LVDS operation and its influences on the upstream energy system is made. Major findings include notable sys-

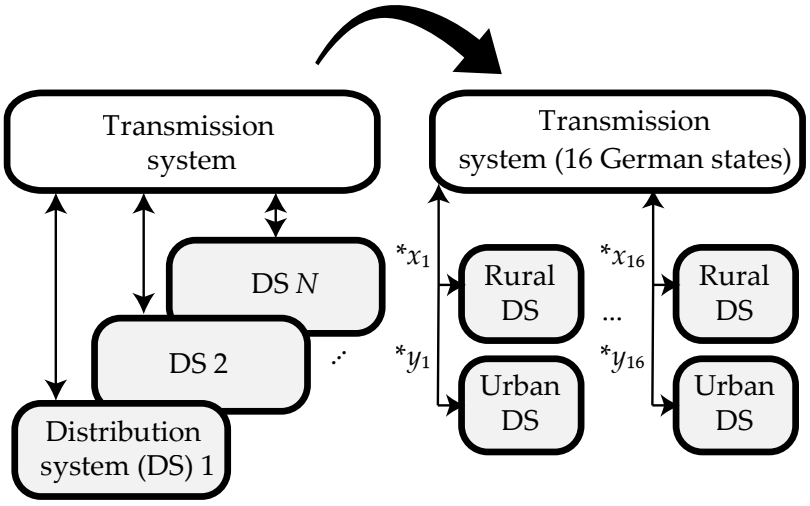

Figure 5.2: Hard coupling scheme for transmission-distribution system integration by representative LVDSs [145].

tem benefits through flexible prosumer operation, corresponding to up to 10% cost reduction between the two scenarios, as

1. higher self-consumption of locally produced PV electricity leads to an alleviation of the transmission grid expansion requirements,
2. smoothened electrical loads of heat pumps and wall boxes along with better integration of local PV electricity reduce the other capacity needs in the upstream, such as peak-load (gas-& H_2-fired) power plants, offshore wind plants, and electrolyzers, and
3. in summer times, the excess PV generation from households can be used to support covering the electrified industry demands.

The work consisting of the representative LVDS-based co-optimization framework and the corresponding case study is published in *Renewable and Sustainable Energy Systems (Elsevier)*:

- Reveron Baecker, Beneharo; Candas, Soner. **Co-optimizing transmission and active distribution grids to assess demand-side flexibilities of a carbon-neutral German energy system**. *Renewable and Sustainable Energy Reviews 163*, 112422, 2022. DOI: `https://doi.org/10.1016/j.rser.2022.112422` [145]

Although the methodology mentioned above allows for a tractable formulation without sacrificing hard coupling, using a limited number of LVDS types and simple scaling of the power flows assumes an unrealistic homogeneity in the configuration and operation of LVDSs of the same type. In particular, the upstream grid observes an overestimation of the peak injection and withdrawals as if a 100% simultaneity governs all the LVDSs within a group. This may lead to unrealistically oversized peak-plant capacities compared to the real-life requirements and motivates alternative methods that address the LVDS heterogeneity more sufficiently.

5.2 Hard coupling by mathematical decomposition

One solution to introduce a more heterogeneous depiction of LVDSs is to increase the number of representative LVDSs until their diversities are represented adequately and the simultaneities reach a realistic level. However, this can quickly bring the model complexity to an intractable level again. To counteract this, mathematical decomposition methods can be

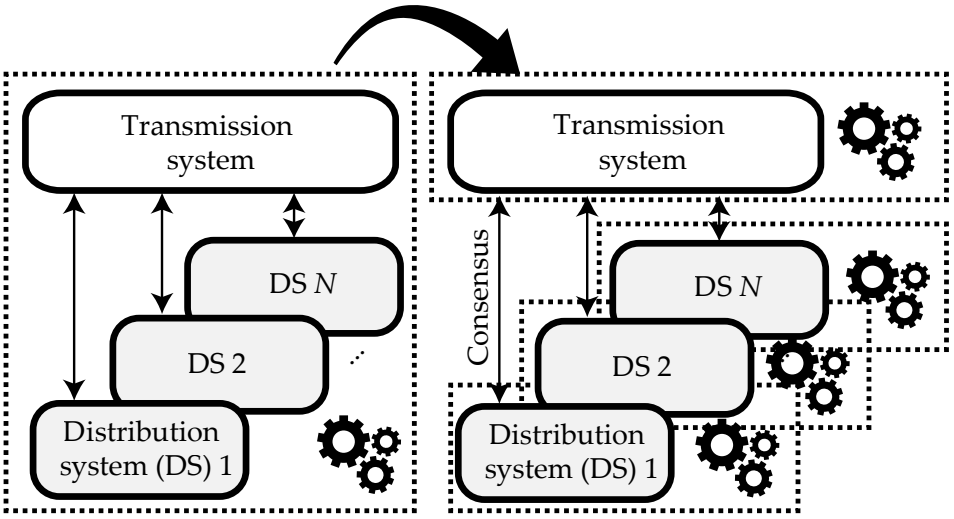

Figure 5.3: Hard coupling scheme for transmission-distribution system integration by mathematical decomposition.

employed. These methods reformulate the optimization problem into multiple "subproblems" that can be solved independently. Through the application of decomposition in various schemes, the aforementioned computational challenges can be tackled:

- if the runtime is the bottleneck: these subproblems can be solved in parallel by making use of a large number of available processors,

- if the RAM is the bottleneck: the subproblems can be solved sequentially, thereby having to contain only a subset of the original problem in the working memory at a time.

Mathematical decomposition offers a structured approach to tackling the co-optimization of transmission-distribution systems (see Figure 5.3). Within this context, each representative LVDS can be treated as an independent subproblem that can be solved using the HOODS framework. In parallel, the transmission system itself stands as another distinct subproblem. Of course, inherent coupling elements interlink these subproblems, such as the power flows between each LVDS and its affiliated transmission system bus. A consensus between subproblems regarding these coupling elements has to be achieved at the solution. Methods such as Benders decomposition or the alternating direction method of multipliers (ADMM) can be utilized to achieve this consensus.

The author has published two works on the potentials and challenges of mathematical decomposition methods in energy system modeling. The first presents a deep dive into the topic, while the second compares the suitability of various decomposition methods for solving optimal power flow problems. They can be found at [146] and [147], respectively. On a discouraging note, no net improvement has been observed through decomposition over a non-decomposed approach in both studies due to many required iterations and communication overheads. Nevertheless, the quantitative results of the studies indicate that decomposition frameworks become increasingly effective as the models scale up well beyond conventional scales, suggesting a potential use for the holistic optimization of transmission-distribution systems.

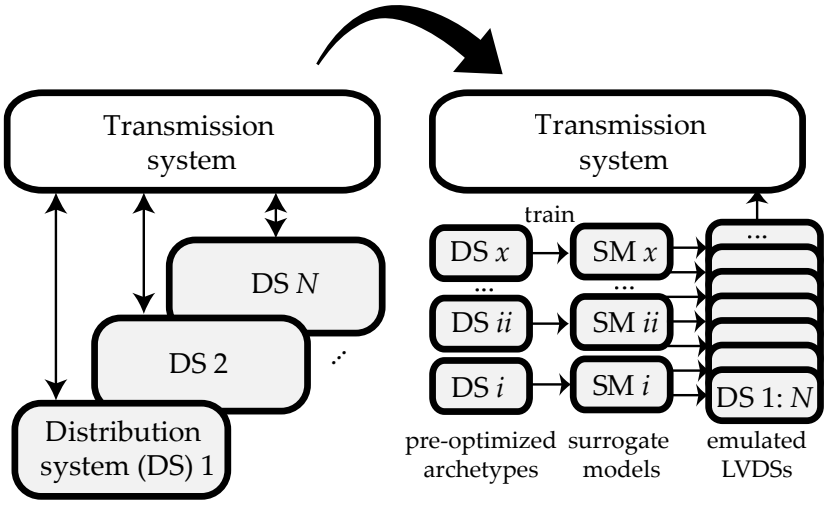

Figure 5.4: Soft coupling scheme for transmission-distribution system integration using surrogate models.

5.3 Soft coupling by machine learning-based surrogate models

AI-based surrogate models might offer an extremely scalable solution in the pursuit of integrating a greater number of LVDSs of varying properties. Surrogate models, in the context of machine learning, function as input-output models that mimic the behavior of an underlying engineering model with significantly less computational time [148]. In this case, the optimal solution of the corresponding HOODS problem. The process is illustrated in Figure 5.4 and can be described as follows:

1. As inputs, the surrogate models consider time series data, like demands, and scalar data, such as the optimized DER capacities,

2. A generously sized LVDS portfolio is established for the specific region of interest, possibly encompassing up to thousands of LVDSs. In the absence of real grid data–often the case–these LVDSs can be synthesized using a method similar to that presented in Section 3.7.1.

3. A subset of these LVDSs (the "archetypes") are optimized conventionally, providing training data for the correspondent surrogate models. After being trained with a series of optimization results on this subset of models, the goal of these surrogate models is then to emulate, for all of the LVDSs, the interaction with the upstream grid, i.e., the net import flows.

4. As the predictions of a surrogate model usually take orders of magnitude less time than solving the equivalent optimization problem, this is a tractable procedure in terms of runtime. This way, thousands of net import time series can be derived to serve as inputs, i.e., in a soft coupled manner, for the upstream transmission-level model.

A publication co-written by the author, which elaborates on this procedure in detail and presents an application on the *HOODS* framework using various neural network architectures, is under submission process as of the writing of this dissertation:

- Mohapatra, Anurag; Candas, Soner; Schulze, Max; Hamacher, Thomas. **Neural network surrogates for large-scale energy system studies of Active Distribution Grids**.

Chapter 6

Conclusion

In this dissertation, an optimization framework has been developed to examine the transformation of low voltage distribution systems (LVDSs), with an emphasis on the assessment of reinforcement requirements for existing grid capacities. A data acquisition framework mainly based on open data has been implemented to ensure a realistic case scenario. With this data suite, regions of the grid being investigated were parametrized consistently.

In this Chapter, the research questions of the dissertation will be revisited. Following this, the limitations associated with the methodology and data will be outlined, motivating future improvements.

6.1 Revisiting the research questions

The case study results presented in Chapter 4 help answer the research questions of this thesis. These questions are revisited in the following.

- *How are the load profiles of an optimally dimensioned, highly electrified low-voltage distribution system altered?*
  As heating and mobility get electrified within an LVDS, interactions between different energy carriers and flexibilities gain importance. Moreover, the resultant load profiles deviate from the conventionally adopted standard load profiles due to the following effects:

  - The adoption of optimally sized heat pumps leads to significantly elevated, largely base-load electrical demands in the winter time for heating. To supplement these heat pumps, auxiliary heating units are utilized throughout to cover peak heating demands occurring in the extreme winter periods,
  - The adoption of optimally-sized photovoltaics (PV) systems leads to significant feed-in periods in the summertime,
  - The adoption of battery electric vehicles introduces temporally distributed peaks throughout the year.

  In the investigated scenarios, these effects lead to an increase in the electrical peaks within the grid up to five times, as heating and mobility are completely electrified (see Figure 4.2).

- *What is the extent of the LV distribution grid reinforcement requirements emerging from various electrification rates?*

In most of the investigated scenarios, the peak loading of the grids was caused by the simultaneous operation of heat pumps during the extreme winter periods. The peak PV feed-ins during the summer resulted in comparable peaks, albeit slightly lower. These peak flows, for which the existing grids were not designed, lead to significant voltage and loading violations depending on the distributed energy resource (DER) penetration. With a 25% penetration of DERs, reinforcement requirements were minor and confined to the suburban and urban grids. However, as the electrification reaches 50% and above, thorough grid reinforcement becomes inevitable for all the grids to ensure a safe grid operation.

- *How do the transformation costs (split into the prosumer- and grid-side costs) stand in relation to one another?*

  Reinforcing their grids invariably results in added costs for distribution grid operators. Grid operators often estimate these costs as extremely high, viewing them as a last resort after all other measures for grid relief have been explored. However, since these costs are ultimately passed on to consumers via the network tariff scheme established by the incentive regulation, a comparison of the grid-related and non-grid-related costs becomes reasonable. In the case study, the grid-related costs constituted at most 3% of the total system costs to be paid by the prosumers. Indeed, grid reinforcement might be infeasible in the short term due to supply shortages and cost volatility. However, in the long term, it is not only the most reliable method for maintaining grid stability but also presents itself as an economically viable option.

- *How much do uncoordinated prosumer optimization paradigms deviate from the global optimum of the LVDS?*

  To quantify the associated welfare losses, the proposed optimization framework facilitated not only a holistic, social-planner-based optimization of the entire LVDS but also more realistic paradigms where coordination between prosumers and the distribution system operator (DSO) is absent. Nevertheless, the suboptimality caused by uncoordinated operation was limited, reaching at most 7%. This can be attributed to two primary reasons:

  – Since the grid-side costs were found to be relatively minor, reducing them through coordinated operation does not yield significant benefits.
  – As more prosumers adopt PV systems, the simultaneity of their excess production limits the potential for significant energy exchange between them.

  These findings underscore the value of prioritizing prosumer-side flexibility over broader grid-wide energy flow management via smart-grid or local energy market-based solutions, especially when the objective is to minimize the overall system costs. The most significant economic benefits from flexible DER operation are reducing electricity costs by integrating PV electricity better for BEV charging (via intelligent charging) and for the heat pump (by leveraging thermal inertia).

  Another implication of these findings is related to the computational aspect. Faced with computational constraints, a communal planner may opt for a sequential optimization of highly detailed building models in their region with subsequent grid planning, instead of holistic optimization models that would require more simplifications for tractability. Using this approach would allow for a more detailed analysis and the inclusion of a larger number of buildings, while the welfare losses associated with a non-holistic consideration would still be minimal.

- *How do the proposed financial incentives and technical measures influence the need for grid reinforcement in the medium and long term?*

  This work evaluated a range of financial incentives, such as capacity and variable tariffs, along with a technical load alleviation measure, the DSO-side downregulation (§ 14a), to assess their impact on the grid state. The need for grid reinforcement was predominantly triggered by the almost base-load operation of heat pumps during winter. Given this, the flexibility of prosumers to adjust their heating loads proved to be minimal in these times.

  This led to the following behavior: on the one hand, the financial incentives had a limited effect in preventing grid reinforcement. Rather, the widespread adoption of variable tariffs by the prosumers even increased the simultaneity of loads that are concentrated during off-peak tariff hours, necessitating even greater grid reinforcement. Nevertheless, by modifying the tariff time windows, such as expanding the LT time window, a reduction of the system peaks might have been achieved by shifting the flexible loads over a broader period.

  On the other hand, the DSO-side downregulation (§ 14a) consistently reduced the peak loads in the grid, establishing itself as a viable tool for DSOs to delay the grid reinforcements. However, to ensure public acceptance, the § 14a regulation must guarantee thermal comfort in buildings without bias. In its present design (downregulation up to a lower limit of 4.2 kW per heat pump), multi-family dwellings with fewer but larger heat pump systems face disproportionate impacts. In order to alleviate these comfort losses for larger buildings, the author proposes that this lower limit be tailored in an adaptable manner, basing it either on the overall heat demand of the building or the rated capacity of the heat pump. Indeed, in the final decision of the regulation, a rated capacity-dependent lower limit using a scaling factor of 0.4 is set for heat pumps larger than 11 kW_{el} instead of a static limit. Of course, this modification may lead to permitting higher electrical consumption for these buildings, in turn reducing the grid-relieving potential of the § 14a regulation below the levels identified in this case study.

- *Can generalized statements regarding these research questions be derived systemically, or is a case-specific approach necessary?*

  To derive generalizable conclusions, the case study encompassed a variety of scenarios, each consisting of different grid regions and levels of DER penetration. Apart from the aspects highlighted above, some further variations of note are:

  - *Grid reinforcement needs:* Depending on the specific grid, either the voltage or the overloading issues might lead to the need for grid reinforcement. Across the considered scenarios, this led to a differing mix of the distinct reinforcement solutions for each grid (some opting for a more thorough parallel cabling and some prioritizing a voltage regulating distribution transformer (VRDT) installation).
  - *Influence of grid-relief measures*: Overall, the influence of the financial incentives was minor across all grid regions. Yet, the exact capacity price levels and variable tariff adoption rates that stimulated a reduction (or an increase in the case of the latter) in grid reinforcement did depend on the grid region.

6.2 Limitations and outlook

Owing to limited resources, some limitations in the presented work have been inevitable. These can be grouped into two: a) limitations in the methodology and b) in the data.

6.2.1 Limitations of the methodology

Various simplifications were made in the developed LVDS optimization framework to maintain a computationally tractable model formulation. These will be briefly listed here.

Rational prosumer behavior with perfect forecast In the modeling framework presented, the prosumers employ their flexibilities in a way that assumes a perfect forecast. In reality, uncertainties are inevitable, such as those in loads and weather conditions. Thus, the flexibility capabilities of the prosumers, as represented in this framework, should be treated as an upper bound to a realistic operation. This highlights the need for a robust energy management system that integrates these uncertainties into its scheduling strategy. Such uncertainties can be accounted for in decision-making through techniques like model-predictive control and stochastic or robust optimization methods.

Besides the uncertainties, the prosumer operation assumes fully rational, cost-minimizing behavior. This assumption can be brought closer to reality by defining various user preferences in the problem formulation of the energy management system, such as operational strategies prioritizing the supply of security under the *§ 14a* regulation.

Level of DER and temporal detail Moreover, the technical accuracy of the model could also be improved by incorporating further features such as the load-dependent coefficient of performance (COP) of heat pumps, the aging behavior of batteries, or a more detailed thermal building model. Additionally, a finer temporal resolution, such as 15-minute intervals, can provide a more accurate reflection of system peaks. However, it is essential to weigh the value of the accuracy achieved through these refinements against the accompanying computational complexity. In a model addressing the sizing of DERs, the yearly course of the time series must be adequately considered. This might motivate a split of the prosumer models into two levels: a) one dealing with the DER dimensioning and b) one dealing with their scheduling, each with a different level of complexity.

Long-term network tariff interaction between the prosumers and the distribution grid operator The dynamic interaction between energy consumers and the grid operator concerning the formation of network charges, as described in the Introduction Chapter, has not been included in the optimization framework. In practice, if consumers adopt behaviors that promote reinforcement, this can lead to increased costs for the DSO. Ultimately, these costs would be passed on to the consumers. Such dynamics could be integrated into the optimization framework through a multi-level or potentially iterative model. This would allow the potential increase in network tariffs to influence and possibly change the optimal behavior of prosumers. Nevertheless, given that grid costs are a minor component of the total system costs, the impacts of these dynamics would be possibly minor.

Refurbishment as an investment decision Besides investments in DERs as outlined in the optimization framework, prosumers might also consider investing in retrofitting measures to reduce their energy costs. Retrofitting effectively lowers the space heating demand of a building, facilitates a more efficient use of the heat pump, and enhances the use of building thermal inertia due to decreased thermal losses. While there are mixed-integer formulations that incorporate retrofitting decisions into energy optimization problems, they entail additional computational complexity. As these, however, bring additional computational load, and the concrete choice of the optimal heating systems is beyond the scope of this research, they have been omitted from the presented optimization framework. However, retrofitting is a crucial measure in the current energy landscape as energy efficiency becomes increasingly important due to concerns about energy security. It should not be overlooked in a more holistic approach to building energy system design.

6.2.2 Limitations of data

Despite the integrated data acquisition suite presented in Chapter 3, there is potential to enhance the data used in the case study. Avenues for data improvement are listed here.

Enhanced data for case-specific analyses The multi-energy nature of local energy systems necessitates a highly diverse data set for a plausible estimation of energetic demands and potentials within a region. The data suite offered in this study represents an approach to producing a consistent set of data for defining each LVDS, relying predominantly on open data. However, it should be viewed as a foundational estimate to facilitate the operation of the optimization framework rather than a decisive data set tailored for a specific region. With the current state of open data, achieving such precision is simply insufficient for an arbitrary region. However, this might change in the future. In the wake of the digitalization of energy systems, the widespread adoption of metering and measurement data collected from buildings and grids can be utilized by local decision-makers to accurately characterize their specific supply region in terms of the building stock, weather, and demand profiles. With this information, the presented framework can be employed more accurately, enabling a detailed examination of the impact of the proposed measures and grid reinforcement needs with even greater precision.

More grid regions for general analysis To enhance the validity of the conclusions drawn from the case study, four real grids in a medium-sized town were considered. These grids were selected to cover a diverse range of characteristics. Through this approach, differences between sparsely and densely populated settings were identified. Nonetheless, the number of grids studied is not substantial enough to make a robustly generalizable statement regarding the need and significance of grid reinforcement. The effort required to generate data influenced the decision not to study more grids. Although the data suite presented in Chapter 3 ensures a consistent definition of each LVDS, the process was not 100% automated, resulting in a suboptimal procedure for the scenario generation. This, combined with the significant optimization runtimes required for all scenarios of each grid region, restricted the assessment of a larger number of regions within the scope of this work. As a next step, with increased data availability, a wider variety of grids might be integrated into the assessment framework to validate the general applicability of the conclusions derived in this work.

More weather years In the conducted case study, weather data was limited to a single representing year, reflecting long-term average weather patterns. However, the diverse range of weather phenomena might impact the optimal solutions. In particular, years with extreme weather conditions, e.g. years involving extreme cold periods leading to more intensive operation of heat pumps, could be critical for a robust distribution grid planning. To have a more reliable understanding of the distribution systems' evolution pathways, future work should include weather data from multiple years, capturing a broader range of weather variations.

6.3 Concluding remarks

The work presented in this dissertation provided an analysis framework for putting low-voltage distribution systems on a computational test bench. This had the goal of enhancing the understanding of the emerging challenges and potentials posed by increasingly electrified systems in the forthcoming years. The featured case study showcased its possible application areas and delivered preliminary insights. These included some findings that were not immediately obvious, such as the significant potential of prosumer-centric flexibilities on reducing grid loading, the relatively small share of grid costs in the system, or limited benefits through the holistic operation and planning of the system. Moreover, the heterogeneity of the results between scenarios and regions further emphasizes the importance of transparent frameworks that facilitate adaptable use. It is thus the author's aspiration for this framework to serve as an initial basis for an analytical approach, aiding in the discourse and potentially being incorporated into the planning processes of these systems by the relevant stakeholders.

Appendix A

Optimization problem formulations

A.1 Formulation of the prosumer optimization problem (HOODS-Bui)

The full formulation of the HOODS-Bui(i) model for a given prosumer i is given below.

$$
\begin{aligned}
\min_{\boldsymbol{\kappa}_i, \boldsymbol{\epsilon}_i} \quad & c_i^{\mathrm{HP}} + c_i^{\mathrm{PV}} + c_i^{\mathrm{bat}} + c_i^{\mathrm{TS}} + c_i^{\mathrm{sto},\epsilon} + c_i^{\mathrm{imp}} + c_i^{\text{feed-in}} + c_i^{\mathrm{cap}} = \\
& af^{\mathrm{HP}} \cdot \left(c^{\mathrm{HP,inv,fix}} \cdot \beta_i^{\mathrm{HP}} + c^{\mathrm{HP,inv,var}} \cdot \kappa_i^{\mathrm{HP}} \right) \\
+ \quad & af^{\mathrm{HP,aux}} \cdot \left(c^{\mathrm{HP,aux,inv,fix}} \cdot \beta_i^{\mathrm{HP,aux}} + c^{\mathrm{HP,aux,inv,var}} \cdot \kappa_i^{\mathrm{HP,aux}} \right) \\
& + \sum_{r \in \mathcal{R}_i} af^{\mathrm{PV}} \cdot \left(c^{\mathrm{PV,inv,fix}} \cdot \beta_{i,r}^{\mathrm{PV}} + c^{\mathrm{PV,inv,var}} \cdot \kappa_{i,r}^{\mathrm{PV}} \right) \\
& + af^{\mathrm{bat}} \cdot c^{\mathrm{bat,inv,var}} \cdot \kappa_i^{\mathrm{bat,e}} + af^{\mathrm{TS}} \cdot c^{\mathrm{TS,inv,var}} \cdot \kappa_i^{\mathrm{TS,e}} \\
& + c_{\mathrm{spec}}^{\mathrm{sto},\epsilon} \cdot \sum_{t \in \mathcal{T}} \omega_t \cdot \left(p_{i,t}^{\mathrm{bat,dch}} + p_{i,t}^{\mathrm{bat,ch}} + \gamma_{i,t}^{\mathrm{TS,dch}} + \gamma_{i,t}^{\mathrm{TS,ch}} + \mu_{i,t}^{\mathrm{VMS,dch}} + \mu_{i,t}^{\mathrm{VMS,ch}} \right) \\
& + \sum_{t \in \mathcal{T}} \left(\omega_t \cdot c_{\mathrm{spec},t}^{\mathrm{imp}} \cdot p_{i,t}^{\mathrm{imp}} \right) - \sum_{t \in \mathcal{T}} \left(\omega_t \cdot c_{\mathrm{spec}}^{\text{feed-in}} \cdot p_{i,t}^{\text{feed-in}} \right) + c_{\mathrm{spec}}^{\mathrm{CP}} \cdot p_i^{\mathrm{peak,exch}}
\end{aligned}
$$

$$
\begin{aligned}
\text{s.t.} \quad & p_{i,r,t}^{\mathrm{PV}} + p_{i,r,t}^{\mathrm{PVcurt}} = \kappa_i^{\mathrm{PV}} \cdot cf_{i,r,t}^{\mathrm{PV}} && \forall t \in \mathcal{T}_m \quad \forall r \in \mathcal{R}^i \\
& p_{i,r,t}^{\mathrm{PV}}, p_{i,r,t}^{\mathrm{PVcurt}} \geq 0 && \forall t \in \mathcal{T}_m \quad \forall r \in \mathcal{R}^i \\
& -\tan\left(\phi_{\min}^{\mathrm{PV}}\right) \cdot p_{i,r,t}^{\mathrm{PV}} \leq q_{i,r,t}^{\mathrm{PV}} \leq \tan\left(\phi_{\min}^{\mathrm{PV}}\right) \cdot p_{i,r,t}^{\mathrm{PV}} && \forall t \in \mathcal{T}_m \quad \forall r \in \mathcal{R}^i \\
& 0 \leq \kappa_{i,r}^{\mathrm{PV}} \leq U_A \cdot A_{i,r} \cdot \beta_{i,r}^{\mathrm{PV}} && \forall r \in \mathcal{R}^i \\
& \epsilon_{i,t}^{\mathrm{bat,e}} = \epsilon_{i,t-1}^{\mathrm{bat,e}} + \eta^{\mathrm{bat,ch}} \cdot p_{i,t}^{\mathrm{bat,ch}} - \frac{p_{i,t}^{\mathrm{bat,dch}}}{\eta^{\mathrm{bat,dch}}} && \forall t \in \mathcal{T}_m \\
& 0 \leq p_{i,t}^{\mathrm{bat,dch}} \leq \kappa_i^{\mathrm{bat,p}} && \forall t \in \mathcal{T}_m \\
& 0 \leq p_{i,t}^{\mathrm{bat,ch}} \leq \kappa_i^{\mathrm{bat,p}} && \forall t \in \mathcal{T}_m \\
& 0 \leq \epsilon_{i,t}^{\mathrm{bat,e}} \leq \kappa_i^{\mathrm{bat,e}} && \forall t \in \mathcal{T}_m \\
& \epsilon_{i,0}^{\mathrm{bat,e}} = \epsilon_{i,T_{\mathrm{end}}}^{\mathrm{bat,e}} \\
& \kappa_i^{\mathrm{bat,e}} = \kappa_i^{\mathrm{bat,p}} \cdot etp^{\mathrm{bat}} \\
\sum_{r \in \mathcal{R}^i} p_{i,r,t}^{\mathrm{PV}} + p_{i,t}^{\mathrm{bat,dch}} + p_{i,t}^{\mathrm{imp}} = {} & d_{i,t}^{\mathrm{elec}} + p_{i,t}^{\mathrm{bat,ch}} + \sum_{c \in \mathcal{C}^i} p_{i,c,t}^{\mathrm{WB}} + p_{i,t}^{\mathrm{HP}} + p_{i,t}^{\text{feed-in}} && \forall t \in \mathcal{T}_m
\end{aligned}
$$

$$
\begin{aligned}
& \sum_{r \in \mathcal{R}^i} q_{i,r,t}^{\mathrm{PV}} + q_{i,t}^{\mathrm{imp}} = d_{i,t}^{\mathrm{elec,q}} + q_{i,t}^{\mathrm{HP}} + q_{i,t}^{\text{feed-in}}, && \forall t \in \mathcal{T}_m \\
& d_{i,t}^{\mathrm{sh}} = C_i \cdot \frac{\vartheta_{i,t} - \vartheta_{i,t-1}}{\Delta t} + \frac{1}{R_i} \cdot (\vartheta_{i,t} - \vartheta_t^{\mathrm{amb}}) - \gamma_{i,t}^{\mathrm{int}} - \gamma_{i,t}^{\mathrm{sol}} && \forall t \in \mathcal{T}_m
\end{aligned}
$$

$$
\begin{aligned}
\vartheta_{i,t}^{\min} \leq \vartheta_{i,t} \leq \vartheta_{i,t}^{\max}. & \qquad \forall t \in \mathcal{T}_m \\
\gamma_{i,t}^{\mathrm{HP}} = p_{i,t}^{\mathrm{HP}} \cdot cop_{i,t}^{\mathrm{HP}} & \qquad \forall t \in \mathcal{T}_m \\
q_{i,t}^{\mathrm{HP}} \cdot = p_{i,t}^{\mathrm{HP}} \cdot \tan(\phi^{\mathrm{HP}}) & \qquad \forall t \in \mathcal{T}_m \\
0 \leq p_{i,t}^{\mathrm{HP}} \leq \kappa_i^{\mathrm{HP}} & \qquad \forall t \in \mathcal{T}_m \\
\gamma_{i,t}^{\mathrm{HP,aux}} = p_{i,t}^{\mathrm{HP,aux}} \cdot \eta^{\mathrm{HP,aux}} & \qquad \forall t \in \mathcal{T}_m \\
0 \leq p_{i,t}^{\mathrm{HP,aux}} \leq \kappa_i^{\mathrm{HP,aux}} & \qquad \forall t \in \mathcal{T}_m \\
0 \leq \kappa_i^{\mathrm{HP}} \leq M \cdot \beta_i^{\mathrm{HP}} & \\
0 \leq \kappa_i^{\mathrm{HP,aux}} \leq M \cdot \beta_i^{\mathrm{HP,aux}} & \\
\gamma_{i,t}^{\mathrm{TS,e}} = \gamma_{i,t-1}^{\mathrm{TS,e}} + \eta^{\mathrm{TS,ch}} \cdot \gamma_{i,t}^{\mathrm{TS,ch}} - \frac{\gamma_{i,t}^{\mathrm{TS,dch}}}{\eta^{\mathrm{TS,dch}}} & \qquad \forall t \in \mathcal{T}_m \\
0 \leq \gamma_{i,t}^{\mathrm{TS,dch}} \leq \kappa_i^{\mathrm{TS,p}} & \qquad \forall t \in \mathcal{T}_m \\
0 \leq \gamma_{i,t}^{\mathrm{TS,ch}} \leq \kappa_i^{\mathrm{TS,p}} & \qquad \forall t \in \mathcal{T}_m \\
0 \leq \gamma_{i,t}^{\mathrm{TS,e}} \leq \kappa_i^{\mathrm{TS,e}} & \qquad \forall t \in \mathcal{T}_m \\
\gamma_{i,0}^{\mathrm{TS,e}} = \gamma_{i,T_{\mathrm{end}}}^{\mathrm{TS,e}} & \\
\gamma_{i,t}^{\mathrm{HP}} + \gamma_{i,t}^{\mathrm{TS,dch}} = \gamma_{i,t}^{\mathrm{TS,ch}} + d_{i,t}^{\mathrm{sh}} + d_{i,t}^{\mathrm{dhw}} + \gamma_{i,t}^{\mathrm{vent}} & \qquad \forall t \in \mathcal{T}_m \\
\mu_{i,c,t}^{\mathrm{WB}} = ava_{i,c,t}^{\mathrm{WB}} \cdot \eta_{i,c}^{\mathrm{WB}} \cdot p_{i,c,t}^{\mathrm{WB}} & \qquad \forall t \in \mathcal{T}_m \quad \forall c \in \mathcal{C}^i \\
p_{i,c,t}^{\mathrm{WB}} \leq \kappa_{i,c}^{\mathrm{WB}} & \qquad \forall t \in \mathcal{T}_m \quad \forall c \in \mathcal{C}^i \\
\mu_{i,c,t}^{\mathrm{BS,e}} = \mu_{i,c,t-1}^{\mathrm{BS,e}} + \mu_{i,c,t}^{\mathrm{BS,ch}} - \mu_{i,c,t}^{\mathrm{BS,dch}} & \qquad \forall t \in \mathcal{T}_m \quad \forall c \in \mathcal{C}^i \\
0 \leq \mu_{i,c,t}^{\mathrm{BS,e}} \leq \kappa_{i,c}^{\mathrm{BS}} & \qquad \forall t \in \mathcal{T}_m \quad \forall c \in \mathcal{C}^i \\
0 \leq \mu_{i,c,t}^{\mathrm{BS,dch}} \leq \kappa_{i,c}^{\mathrm{WB}} & \qquad \forall t \in \mathcal{T}_m \quad \forall c \in \mathcal{C}^i \\
0 \leq \mu_{i,c,t}^{\mathrm{BS,ch}} \leq \kappa_{i,c}^{\mathrm{WB}}, & \qquad \forall t \in \mathcal{T}_m \quad \forall c \in \mathcal{C}^i \\
\mu_{i,c,0}^{\mathrm{BS,e}} = \mu_{i,c,T_{\mathrm{end}}}^{\mathrm{BS,e}} & \qquad \forall c \in \mathcal{C}^i \\
\mu_{i,c,t}^{\mathrm{WB}} = d_{i,c,t}^{\mathrm{mob}} + \mu_{i,c,t}^{\mathrm{BS,ch}} - \mu_{i,c,t}^{\mathrm{BS,dch}} & \qquad \forall t \in \mathcal{T}_m \quad \forall c \in \mathcal{C}^i \\
p_{i,t}^{\mathrm{abs,exch}} \geq \quad p_{i,t}^{\mathrm{imp}} - p_{i,t}^{\mathrm{feed\text{-}in}} & \qquad \forall t \in \mathcal{T}_m \\
p_{i,t}^{\mathrm{abs,exch}} \geq -p_{i,t}^{\mathrm{imp}} + p_{i,t}^{\mathrm{feed\text{-}in}} & \qquad \forall t \in \mathcal{T}_m \\
p_i^{\mathrm{peak,exch}} \geq p_{i,t}^{\mathrm{abs,exch}} & \qquad \forall t \in \mathcal{T}_m
\end{aligned}
$$

A.2 Formulation of the low-voltage distribution grid optimization problem (HOODS-Grid)

The full formulation of the HOODS-Grid model for the distribution grid operator is given below.

$$
\begin{aligned}
\min_{\boldsymbol{\alpha}, f} \quad & c_{\text{DSO}} = c_{\text{DSO}}^{\text{VRDT}} + c_{\text{DSO}}^{\text{line}} + c_{\text{DSO}}^{\text{Qcomp}} + c_{\text{DSO}}^{\text{PVcurt}} = \\
& \sum_{o \in \mathcal{O}} \left((af^{\text{VRDT}} \cdot c_o^{\text{VRDT,inv}} + c_o^{\text{VRDT,O\&M}}) \cdot \alpha_o^{\text{VRDT}} \right) \\
& + \sum_{ji \in \mathcal{L}} \left(\sum_{m \in \{\text{II,III}\}} \left(af^{\text{VRDT}} \cdot c_{ji,\text{spec}}^{\text{line},m} \cdot \alpha_{ji}^{m} \right) \right) \\
& + c_{\text{spec}}^{\text{Qcomp}} \cdot \sum_{t \in \mathcal{T}_m} \left(\omega_t \cdot q_{\text{MBB},t}^{\text{comp}} \right) \\
& + c_{\text{spec}}^{\text{feed-in}} \cdot \sum_{t \in \mathcal{T}_m} \cdot \sum_{i \in \mathcal{I}^b} \left(\omega_t \cdot p_{i,t}^{\text{PV,DSOcurt}} \right)
\end{aligned}
$$

$$
\begin{aligned}
\text{s.t.} \quad & p_{i,t}^{\text{net}} = p_{i,t}^{\text{imp}*} - p_{i,t}^{\text{feed-in}*} && \forall t \in \mathcal{T}_m \quad \forall i \in \mathcal{I}^b \\
& q_{i,t}^{\text{net}} = q_{i,t}^{\text{imp}*} - q_{i,t}^{\text{feed-in}*} && \forall t \in \mathcal{T}_m \quad \forall i \in \mathcal{I}^b \\
& p_{i,t}^{\text{net}} = 0 && \forall t \in \mathcal{T}_m \quad \forall i \in \mathcal{I} \setminus (\mathcal{I}^b \cup \text{MBB}) \\
& q_{i,t}^{\text{net}} = 0 && \forall t \in \mathcal{T}_m \quad \forall i \in \mathcal{I} \setminus (\mathcal{I}^b \cup \text{MBB}) \\
& u_{i,t} = u_{j,t} - 2 \cdot r_{ji} \cdot p_{ji,t} - 2 \cdot x_{ji} \cdot q_{ji,t} && \forall t \in \mathcal{T}_m \quad \forall ji \in \mathcal{L} \\
& p_{i,t}^{\text{net}} - p_{i,t}^{\text{PV,DSOcurt}} + p_{ji,t} = \sum_{k \in N^+(i)} p_{ik,t} && \forall t \in \mathcal{T}_m \quad \forall i \in \mathcal{I}^b \\
& q_{i,t}^{\text{net}} + q_{ji,t} = \sum_{k \in N^+(i)} q_{ik,t} && \forall t \in \mathcal{T}_m \quad \forall i \in \mathcal{I} \\
& \sum_{m \in \{\text{I,II,III}\}} \alpha_{ji}^{m} = 1 && \forall ji \in \mathcal{L} \\
& p_{ji,t} = \sum_{m \in \{\text{I,II,III}\}} p_{ji,t}^{m} && \forall t \in \mathcal{T}_m \quad \forall ji \in \mathcal{L} \\
& q_{ji,t} = \sum_{m \in \{\text{I,II,III}\}} q_{ji,t}^{m} && \forall t \in \mathcal{T}_m \quad \forall ji \in \mathcal{L} \\
& a_y \cdot p_{ji,t}^{m} + b_y \cdot q_{ji,t}^{m} \leq c_y \cdot \kappa_{ji}^{m} \cdot \alpha_{ji}^{m} && \forall m \in \{\text{I,II,III}\} \quad \forall y \in \{1,2,\ldots,8\} \\
& && \forall t \in \mathcal{T}_m \quad \forall ji \in \mathcal{L} \\
& u_{i,t} = u_{j,t} - 2 \cdot \sum_{m \in \{\text{I,II,III}\}} \left(r_{ji}^{m} \cdot p_{ji,t}^{m} + x_{ji}^{m} \cdot q_{ji,t}^{m} \right) && \forall t \in \mathcal{T}_m \quad \forall i \in \mathcal{I} \\
& \alpha^{\text{FRT}} + \sum_{o \in \mathcal{O}} \alpha_o^{\text{VRDT}} = 1 && \\
& p_{\text{MBB},t}^{\text{net}} = p_{\text{MBB},t}^{\text{imp}} - p_{\text{MBB},t}^{\text{feed-in}} && \forall t \in \mathcal{T}_m \\
& q_{\text{MBB},t}^{\text{net}} = q_{\text{MBB},t}^{\text{comp}} && \forall t \in \mathcal{T}_m \\
& a_y \cdot p_{\text{MBB},t}^{\text{net}} + b_y \cdot q_{\text{MBB},t}^{\text{net}} \leq c_y \cdot \left(\alpha^{\text{FRT}} \cdot \kappa^{\text{FLT}} + \sum_{o \in \mathcal{O}} \alpha_o^{\text{VRDT}} \cdot \kappa_o^{\text{VRDT}} \right) && \forall t \in \mathcal{T}_m \quad \forall y \in \{1,2,\ldots,8\} \\
& \frac{u_{i,t}}{(V_{\text{base}})^2} \leq \left((V'_{\text{max}})_i^2 + \sum_{o \in \mathcal{O}} \alpha_o^{\text{VRDT}} \cdot \left((V_{\text{max}})_i^2 - (V'_{\text{max}})_i^2 \right) \right) && \forall t \in \mathcal{T}_m \quad \forall i \in \mathcal{I} \\
& \frac{u_{i,t}}{(V_{\text{base}})^2} \geq \left((V'_{\text{min}})_i^2 + \sum_{o \in \mathcal{O}} \alpha_o^{\text{VRDT}} \cdot \left((V_{\text{min}})_i^2 - (V'_{\text{min}})_i^2 \right) \right) && \forall t \in \mathcal{T}_m \quad \forall i \in \mathcal{I} \\
& 0 \leq p_{i,t}^{\text{PV,DSOcurt}} \leq p_{i,t}^{\text{feed-in}*} && \forall t \in \mathcal{T}_m \quad \forall i \in \mathcal{I}^b \\
& p_{i,t}^{\text{net}} + p_{ji,t} = \sum_{k \in N^+(i)} p_{ik,t} && \forall t \in \mathcal{T}_m \quad \forall i \in \mathcal{I} \setminus \mathcal{I}^b
\end{aligned}
$$

A.3 Formulation of the low-voltage distribution system optimization problem (HOODS-Sys)

The full formulation of the HOODS-Sys model for the whole low-voltage distribution system is given below.

$$
\begin{aligned}
\min_{\boldsymbol{\kappa},\boldsymbol{\epsilon},\boldsymbol{\alpha},f} \sum_{i\in\mathcal{I}^b} \Bigg(& af^{\mathrm{HP}} \cdot \left(c^{\mathrm{HP,inv,fix}} \cdot \beta_i^{\mathrm{HP}} + c^{\mathrm{HP,inv,var}} \cdot \kappa_i^{\mathrm{HP}}\right) \\
& + af^{\mathrm{HP,aux}} \cdot \left(c^{\mathrm{HP,aux,inv,fix}} \cdot \beta_i^{\mathrm{HP,aux}} + c^{\mathrm{HP,aux,inv,var}} \cdot \kappa_i^{\mathrm{HP,aux}}\right) \\
& + \sum_{r\in\mathcal{R}_i} af^{\mathrm{PV}} \cdot \left(c^{\mathrm{PV,inv,fix}} \cdot \beta_{i,r}^{\mathrm{PV}} + c^{\mathrm{PV,inv,var}} \cdot \kappa_{i,r}^{\mathrm{PV}}\right) \\
& + af^{\mathrm{bat}} \cdot c^{\mathrm{bat,inv,var}} \cdot \kappa_i^{\mathrm{bat,e}} + af^{\mathrm{TS}} \cdot c^{\mathrm{TS,inv,var}} \cdot \kappa_i^{\mathrm{TS,e}} \\
& + c_{\mathrm{spec}}^{\mathrm{sto},\epsilon} \cdot \sum_{t\in\mathcal{T}} \omega_t \cdot \left(p_{i,t}^{\mathrm{bat,dch}} + p_{i,t}^{\mathrm{bat,ch}} + \gamma_{i,t}^{\mathrm{TS,dch}} + \gamma_{i,t}^{\mathrm{TS,ch}} + \mu_{i,t}^{\mathrm{VMS,dch}} + \mu_{i,t}^{\mathrm{VMS,ch}}\right)\Bigg) \\
& + \sum_{o\in\mathcal{O}} \left((af^{\mathrm{VRDT}} \cdot c_o^{\mathrm{VRDT,inv}} + c_o^{\mathrm{VRDT,O\&M}}) \cdot \alpha_o^{\mathrm{VRDT}}\right) \\
& + \sum_{ji\in\mathcal{L}} \left(\sum_{m\in\{\mathrm{II,III}\}} \left(af^{\mathrm{VRDT}} \cdot c_{ji,\mathrm{spec}}^{\mathrm{line},m} \cdot \alpha_{ji}^{m}\right)\right) \\
& + c_{\mathrm{spec}}^{\mathrm{Qcomp}} \cdot \sum_{t\in\mathcal{T}_m} \left(\omega_t \cdot q_{\mathrm{MBB},t}^{\mathrm{comp}}\right) \\
& + \sum_{t\in\mathcal{T}} \omega_t \left(c_{\mathrm{spec},t}^{\mathrm{imp}} \cdot p_{\mathrm{MBB},t}^{\mathrm{imp}} - \cdot c_{\mathrm{spec}}^{\mathrm{feed\text{-}in}} \cdot p_{\mathrm{MBB},t}^{\mathrm{feed\text{-}in}}\right)
\end{aligned}
$$

$$
\begin{aligned}
\text{s.t.} \quad p_{i,r,t}^{\mathrm{PV}} + p_{i,r,t}^{\mathrm{PVcurt}} &= \kappa_i^{\mathrm{PV}} \cdot cf_{i,r,t}^{\mathrm{PV}} && \forall t\in\mathcal{T}_m \quad \forall r\in\mathcal{R}^i \quad \forall i\in\mathcal{I}^b \\
p_{i,r,t}^{\mathrm{PV}}, p_{i,r,t}^{\mathrm{PVcurt}} &\geq 0 && \forall t\in\mathcal{T}_m \quad \forall r\in\mathcal{R}^i \quad \forall i\in\mathcal{I}^b \\
-\tan\left(\phi_{\min}^{\mathrm{PV}}\right) \cdot p_{i,r,t}^{\mathrm{PV}} \leq q_{i,r,t}^{\mathrm{PV}} &\leq \tan\left(\phi_{\min}^{\mathrm{PV}}\right) \cdot p_{i,r,t}^{\mathrm{PV}} && \forall t\in\mathcal{T}_m \quad \forall r\in\mathcal{R}^i \quad \forall i\in\mathcal{I}^b \\
0 \leq \kappa_{i,r}^{\mathrm{PV}} &\leq U_A \cdot A_{i,r} \cdot \beta_{i,r}^{\mathrm{PV}} && \forall r\in\mathcal{R}^i \quad \forall i\in\mathcal{I}^b \\
\epsilon_{i,t}^{\mathrm{bat,e}} &= \epsilon_{i,t-1}^{\mathrm{bat,e}} + \eta^{\mathrm{bat,ch}} \cdot p_{i,t}^{\mathrm{bat,ch}} - \frac{p_{i,t}^{\mathrm{bat,dch}}}{\eta^{\mathrm{bat,dch}}} && \forall t\in\mathcal{T}_m \quad \forall i\in\mathcal{I}^b \\
0 \leq p_{i,t}^{\mathrm{bat,dch}} &\leq \kappa_i^{\mathrm{bat,p}} && \forall t\in\mathcal{T}_m \quad \forall i\in\mathcal{I}^b \\
0 \leq p_{i,t}^{\mathrm{bat,ch}} &\leq \kappa_i^{\mathrm{bat,p}} && \forall t\in\mathcal{T}_m \quad \forall i\in\mathcal{I}^b \\
0 \leq \epsilon_{i,t}^{\mathrm{bat,e}} &\leq \kappa_i^{\mathrm{bat,e}} && \forall t\in\mathcal{T}_m \quad \forall i\in\mathcal{I}^b \\
\epsilon_{i,0}^{\mathrm{bat,e}} &= \epsilon_{i,T_{\mathrm{end}}}^{\mathrm{bat,e}} && \forall i\in\mathcal{I}^b \\
\kappa_i^{\mathrm{bat,e}} &= \kappa_i^{\mathrm{bat,p}} \cdot etp^{\mathrm{bat}} && \forall i\in\mathcal{I}^b \\
\sum_{r\in\mathcal{R}^i} p_{i,r,t}^{\mathrm{PV}} + p_{i,t}^{\mathrm{bat,dch}} + p_{i,t}^{\mathrm{imp}} &= d_{i,t}^{\mathrm{elec}} + p_{i,t}^{\mathrm{bat,ch}} + \sum_{c\in\mathcal{C}^i} p_{i,c,t}^{\mathrm{WB}} + p_{i,t}^{\mathrm{HP}} + p_{i,t}^{\mathrm{feed\text{-}in}} && \forall t\in\mathcal{T}_m \quad \forall i\in\mathcal{I}^b \\
\sum_{r\in\mathcal{R}^i} q_{i,r,t}^{\mathrm{PV}} + q_{i,t}^{\mathrm{imp}} &= d_{i,t}^{\mathrm{elec,q}} + q_{i,t}^{\mathrm{HP}} + q_{i,t}^{\mathrm{feed\text{-}in}}, && \forall t\in\mathcal{T}_m \quad \forall i\in\mathcal{I}^b \quad \forall i\in\mathcal{I}^b \\
d_{i,t}^{\mathrm{sh}} &= C_i \cdot \frac{\vartheta_{i,t} - \vartheta_{i,t-1}}{\Delta t} + \frac{1}{R_i} \cdot (\vartheta_{i,t} - \vartheta_t^{\mathrm{amb}}) - \gamma_{i,t}^{\mathrm{int}} - \gamma_{i,t}^{\mathrm{sol}} && \forall t\in\mathcal{T}_m \quad \forall i\in\mathcal{I}^b \\
\vartheta_{i,t}^{\min} &\leq \vartheta_{i,t} \leq \vartheta_{i,t}^{\max}. && \forall t\in\mathcal{T}_m \quad \forall i\in\mathcal{I}^b \\
\gamma_{i,t}^{\mathrm{HP}} &= p_{i,t}^{\mathrm{HP}} \cdot cop_{i,t}^{\mathrm{HP}} && \forall t\in\mathcal{T}_m \quad \forall i\in\mathcal{I}^b \\
q_{i,t}^{\mathrm{HP}} \cdot &= p_{i,t}^{\mathrm{HP}} \cdot \tan(\phi^{\mathrm{HP}}) && \forall t\in\mathcal{T}_m \quad \forall i\in\mathcal{I}^b \\
0 \leq p_{i,t}^{\mathrm{HP}} &\leq \kappa_i^{\mathrm{HP}} && \forall t\in\mathcal{T}_m \quad \forall i\in\mathcal{I}^b \\
\gamma_{i,t}^{\mathrm{HP,aux}} &= p_{i,t}^{\mathrm{HP,aux}} \cdot \eta^{\mathrm{HP,aux}} && \forall t\in\mathcal{T}_m \quad \forall i\in\mathcal{I}^b
\end{aligned}
$$

$$
\begin{aligned}
0 \leq p_{i,t}^{\mathrm{HP,aux}} &\leq \kappa_i^{\mathrm{HP,aux}} && \forall t \in \mathcal{T}_m \quad \forall i \in \mathcal{I}^b \\
0 \leq \kappa_i^{\mathrm{HP}} &\leq M \cdot \beta_i^{\mathrm{HP}} && \forall i \in \mathcal{I}^b \\
0 \leq \kappa_i^{\mathrm{HP,aux}} &\leq M \cdot \beta_i^{\mathrm{HP,aux}} && \forall i \in \mathcal{I}^b \\
\gamma_{i,t}^{\mathrm{TS,e}} &= \gamma_{i,t-1}^{\mathrm{TS,e}} + \eta^{\mathrm{TS,ch}} \cdot \gamma_{i,t}^{\mathrm{TS,ch}} - \frac{\gamma_{i,t}^{\mathrm{TS,dch}}}{\eta^{\mathrm{TS,dch}}} && \forall t \in \mathcal{T}_m \quad \forall i \in \mathcal{I}^b \\
0 \leq \gamma_{i,t}^{\mathrm{TS,dch}} &\leq \kappa_i^{\mathrm{TS,p}} && \forall t \in \mathcal{T}_m \quad \forall i \in \mathcal{I}^b \\
0 \leq \gamma_{i,t}^{\mathrm{TS,ch}} &\leq \kappa_i^{\mathrm{TS,p}} && \forall t \in \mathcal{T}_m \quad \forall i \in \mathcal{I}^b \\
0 \leq \gamma_{i,t}^{\mathrm{TS,e}} &\leq \kappa_i^{\mathrm{TS,e}} && \forall t \in \mathcal{T}_m \quad \forall i \in \mathcal{I}^b \\
\gamma_{i,0}^{\mathrm{TS,e}} &= \gamma_{i,T_{\mathrm{end}}}^{\mathrm{TS,e}} && \forall i \in \mathcal{I}^b \\
\gamma_{i,t}^{\mathrm{HP}} + \gamma_{i,t}^{\mathrm{TS,dch}} &= \gamma_{i,t}^{\mathrm{TS,ch}} + d_{i,t}^{\mathrm{sh}} + d_{i,t}^{\mathrm{dhw}} + \gamma_{i,t}^{\mathrm{vent}} && \forall t \in \mathcal{T}_m \quad \forall i \in \mathcal{I}^b \\
\mu_{i,c,t}^{\mathrm{WB}} &= ava_{i,c,t}^{\mathrm{WB}} \cdot \eta_{i,c}^{\mathrm{WB}} \cdot p_{i,c,t}^{\mathrm{WB}} && \forall t \in \mathcal{T}_m \quad \forall c \in \mathcal{C}^i \quad \forall i \in \mathcal{I}^b \\
p_{i,c,t}^{\mathrm{WB}} &\leq \kappa_{i,c}^{\mathrm{WB}} && \forall t \in \mathcal{T}_m \quad \forall c \in \mathcal{C}^i \quad \forall i \in \mathcal{I}^b \\
\mu_{i,c,t}^{\mathrm{BS,e}} &= \mu_{i,c,t-1}^{\mathrm{BS,e}} + \mu_{i,c,t}^{\mathrm{BS,ch}} - \mu_{i,c,t}^{\mathrm{BS,dch}} && \forall t \in \mathcal{T}_m \quad \forall c \in \mathcal{C}^i \quad \forall i \in \mathcal{I}^b \\
0 \leq \mu_{i,c,t}^{\mathrm{BS,e}} &\leq \kappa_{i,c}^{\mathrm{BS}} && \forall t \in \mathcal{T}_m \quad \forall c \in \mathcal{C}^i \quad \forall i \in \mathcal{I}^b \\
0 \leq \mu_{i,c,t}^{\mathrm{BS,dch}} &\leq \kappa_{i,c}^{\mathrm{WB}} && \forall t \in \mathcal{T}_m \quad \forall c \in \mathcal{C}^i \quad \forall i \in \mathcal{I}^b \\
0 \leq \mu_{i,c,t}^{\mathrm{BS,ch}} &\leq \kappa_{i,c}^{\mathrm{WB}}, && \forall t \in \mathcal{T}_m \quad \forall c \in \mathcal{C}^i \quad \forall i \in \mathcal{I}^b \\
\mu_{i,c,0}^{\mathrm{BS,e}} &= \mu_{i,c,T_{\mathrm{end}}}^{\mathrm{BS,e}} && \forall c \in \mathcal{C}^i \quad \forall i \in \mathcal{I}^b \\
\mu_{i,c,t}^{\mathrm{WB}} &= d_{i,c,t}^{\mathrm{mob}} + \mu_{i,c,t}^{\mathrm{BS,ch}} - \mu_{i,c,t}^{\mathrm{BS,dch}} && \forall t \in \mathcal{T}_m \quad \forall c \in \mathcal{C}^i \quad \forall i \in \mathcal{I}^b \\
p_{i,t}^{\mathrm{net}} &= p_{i,t}^{\mathrm{imp}} - p_{i,t}^{\mathrm{feed\text{-}in}} && \forall t \in \mathcal{T}_m \quad \forall i \in \mathcal{I}^b \\
q_{i,t}^{\mathrm{net}} &= q_{i,t}^{\mathrm{imp}} - q_{i,t}^{\mathrm{feed\text{-}in}} && \forall t \in \mathcal{T}_m \quad \forall i \in \mathcal{I}^b \\
u_{i,t} &= u_{j,t} - 2 \cdot r_{ji} \cdot p_{ji,t} - 2 \cdot x_{ji} \cdot q_{ji,t} && \forall t \in \mathcal{T}_m \quad \forall ji \in \mathcal{L} \\
p_{i,t}^{\mathrm{net}} + p_{ji,t} &= \sum_{k \in N^+(i)} p_{ik,t} && \forall t \in \mathcal{T}_m \quad \forall i \in \mathcal{I} \\
q_{i,t}^{\mathrm{net}} + q_{ji,t} &= \sum_{k \in N^+(i)} q_{ik,t} && \forall t \in \mathcal{T}_m \quad \forall i \in \mathcal{I} \\
\sum_{m \in \{\mathrm{I,II,III}\}} \alpha_{ji}^m &= 1 && \forall ji \in \mathcal{L} \\
p_{ji,t} &= \sum_{m \in \{\mathrm{I,II,III}\}} p_{ji,t}^m && \forall t \in \mathcal{T}_m \quad \forall ji \in \mathcal{L} \\
q_{ji,t} &= \sum_{m \in \{\mathrm{I,II,III}\}} q_{ji,t}^m && \forall t \in \mathcal{T}_m \quad \forall ji \in \mathcal{L} \\
a_y \cdot p_{ji,t}^m + b_y \cdot q_{ji,t}^m &\leq c_y \cdot \kappa_{ji}^m \cdot \alpha_{ji}^m && \forall m \in \{\mathrm{I,II,III}\} \quad \forall y \in \{1,2,\ldots,8\} \\
& && \forall t \in \mathcal{T}_m \quad \forall ji \in \mathcal{L} \\
u_{i,t} &= u_{j,t} - 2 \cdot \sum_{m \in \{\mathrm{I,II,III}\}} \left(r_{ji}^m \cdot p_{ji,t}^m + x_{ji}^m \cdot q_{ji,t}^m \right) && \forall t \in \mathcal{T}_m \quad \forall i \in \mathcal{I} \\
\alpha^{\mathrm{FRT}} + \sum_{o \in \mathcal{O}} \alpha_o^{\mathrm{VRDT}} &= 1 \\
p_{\mathrm{MBB},t}^{\mathrm{net}} &= p_{\mathrm{MBB},t}^{\mathrm{imp}} - p_{\mathrm{MBB},t}^{\mathrm{feed\text{-}in}} && \forall t \in \mathcal{T}_m \\
q_{\mathrm{MBB},t}^{\mathrm{net}} &= q_{\mathrm{MBB},t}^{\mathrm{comp}} && \forall t \in \mathcal{T}_m \\
a_y \cdot p_{\mathrm{MBB},t}^{\mathrm{net}} + b_y \cdot q_{\mathrm{MBB},t}^{\mathrm{net}} &\leq c_y \cdot \left(\alpha^{\mathrm{FRT}} \cdot \kappa^{\mathrm{FLT}} + \sum_{o \in \mathcal{O}} \alpha_o^{\mathrm{VRDT}} \cdot \kappa_o^{\mathrm{VRDT}} \right) && \forall t \in \mathcal{T}_m \quad \forall y \in \{1,2,\ldots,8\} \\
\frac{u_{i,t}}{(V_{\mathrm{base}})^2} &\leq \left((V'_{\mathrm{max}})_i^2 + \sum_{o \in \mathcal{O}} \alpha_o^{\mathrm{VRDT}} \cdot \left((V_{\mathrm{max}})_i^2 - (V'_{\mathrm{max}})_i^2 \right) \right) && \forall t \in \mathcal{T}_m \quad \forall i \in \mathcal{I} \\
\frac{u_{i,t}}{(V_{\mathrm{base}})^2} &\geq \left((V'_{\mathrm{min}})_i^2 + \sum_{o \in \mathcal{O}} \alpha_o^{\mathrm{VRDT}} \cdot \left((V_{\mathrm{min}})_i^2 - (V'_{\mathrm{min}})_i^2 \right) \right) && \forall t \in \mathcal{T}_m \quad \forall i \in \mathcal{I} \\
0 \leq p_{i,t}^{\mathrm{PV,DSOcurt}} &\leq p_{i,t}^{\mathrm{feed\text{-}in}*} && \forall t \in \mathcal{T}_m \quad \forall i \in \mathcal{I}^b
\end{aligned}
$$

A.4 Formulation of the ex-ante prosumer optimization problem under the § 14a regulation (HOODS-Bui-14a)

$$
\begin{aligned}
\min_{\substack{\boldsymbol{\kappa}_i, \boldsymbol{\epsilon}_i, \\ \boldsymbol{p}_{i,t}^{\text{imp,HP}}, \boldsymbol{p}_{i,t}^{\text{imp,WB}}, \\ \boldsymbol{p}_{i,t}^{\text{toHP}}, \boldsymbol{p}_{i,t}^{\text{toWB}}}} \quad & af^{\text{HP}} \cdot \left(c^{\text{HP,inv,fix}} \cdot \beta_i^{\text{HP}} + c^{\text{HP,inv,var}} \cdot \kappa_i^{\text{HP}} \right) \\
+ \quad & af^{\text{HP,aux}} \cdot \left(c^{\text{HP,aux,inv,fix}} \cdot \beta_i^{\text{HP,aux}} + c^{\text{HP,aux,inv,var}} \cdot \kappa_i^{\text{HP,aux}} \right) \\
+ & \sum_{r \in \mathcal{R}_i} af^{\text{PV}} \cdot \left(c^{\text{PV,inv,fix}} \cdot \beta_{i,r}^{\text{PV}} + c^{\text{PV,inv,var}} \cdot \kappa_{i,r}^{\text{PV}} \right) \\
+ & af^{\text{bat}} \cdot c^{\text{bat,inv,var}} \cdot \kappa_i^{\text{bat,e}} + af^{\text{TS}} \cdot c^{\text{TS,inv,var}} \cdot \kappa_i^{\text{TS,e}} \\
+ & c_{\text{spec}}^{\text{sto},\epsilon} \cdot \sum_{t \in \mathcal{T}} \omega_t \cdot \left(p_{i,t}^{\text{bat,dch}} + p_{i,t}^{\text{bat,ch}} + \gamma_{i,t}^{\text{TS,dch}} + \gamma_{i,t}^{\text{TS,ch}} + \mu_{i,t}^{\text{VMS,dch}} + \mu_{i,t}^{\text{VMS,ch}} \right) \\
+ & \sum_{t \in \mathcal{T}} \left(\omega_t \cdot c_{\text{spec},t}^{\text{imp}} \cdot (p_{i,t}^{\text{imp}} + p_{i,t}^{\text{HP,imp}} + p_{i,t}^{\text{WB,imp}}) \right) - \sum_{t \in \mathcal{T}} \left(\omega_t \cdot c_{\text{spec}}^{\text{feed-in}} \cdot p_{i,t}^{\text{feed-in}} \right) + c_{\text{spec}}^{\text{CP}} \cdot p_i^{\text{peak,exch}} \\
+ & c_{\text{spec}}^{\text{conv}} \cdot \sum_{t \in \mathcal{T}} \omega_t \left(p_{i,t}^{\text{toHP}} + p_{i,t}^{\text{toWB}} \right)
\end{aligned}
$$

$$
\begin{aligned}
\text{s.t.} \quad p_{i,r,t}^{\text{PV}} + p_{i,r,t}^{\text{PVcurt}} &= \kappa_i^{\text{PV}} \cdot cf_{i,r,t}^{\text{PV}} && \forall t \in \mathcal{T}_m \quad \forall r \in \mathcal{R}^i \\
p_{i,r,t}^{\text{PV}}, p_{i,r,t}^{\text{PVcurt}} &\geq 0 && \forall t \in \mathcal{T}_m \quad \forall r \in \mathcal{R}^i \\
-\tan\left(\phi_{\min}^{\text{PV}}\right) \cdot p_{i,r,t}^{\text{PV}} \leq q_{i,r,t}^{\text{PV}} &\leq \tan\left(\phi_{\min}^{\text{PV}}\right) \cdot p_{i,r,t}^{\text{PV}} && \forall t \in \mathcal{T}_m \quad \forall r \in \mathcal{R}^i \\
0 \leq \kappa_{i,r}^{\text{PV}} &\leq U_A \cdot A_{i,r} \cdot \beta_{i,r}^{\text{PV}} && \forall r \in \mathcal{R}^i \\
\epsilon_{i,t}^{\text{bat,e}} &= \epsilon_{i,t-1}^{\text{bat,e}} + \eta^{\text{bat,ch}} \cdot p_{i,t}^{\text{bat,ch}} - \frac{p_{i,t}^{\text{bat,dch}}}{\eta^{\text{bat,dch}}} && \forall t \in \mathcal{T}_m \\
0 \leq p_{i,t}^{\text{bat,dch}} &\leq \kappa_i^{\text{bat,p}} && \forall t \in \mathcal{T}_m \\
0 \leq p_{i,t}^{\text{bat,ch}} &\leq \kappa_i^{\text{bat,p}} && \forall t \in \mathcal{T}_m \\
0 \leq \epsilon_{i,t}^{\text{bat,e}} &\leq \kappa_i^{\text{bat,e}} && \forall t \in \mathcal{T}_m \\
\epsilon_{i,0}^{\text{bat,e}} &= \epsilon_{i,T_{\text{end}}}^{\text{bat,e}} \\
\kappa_i^{\text{bat,e}} &= \kappa_i^{\text{bat,p}} \cdot etp^{\text{bat}} \\
p_{i,t}^{\text{HP,imp}} + p_{i,t}^{\text{toHP}} &= p_{i,t}^{\text{HP}} + p_{i,t}^{\text{HP,aux}} && \forall t \in \mathcal{T}_m \\
p_{i,t}^{\text{WB,imp}} + p_{i,t}^{\text{toWB}} &= \sum_{c \in \mathcal{C}^i} p_{i,c,t}^{\text{WB}} && \forall t \in \mathcal{T}_m \\
\sum_{r \in \mathcal{R}^i} p_{i,r,t}^{\text{PV}} + p_{i,t}^{\text{bat,dch}} + p_{i,t}^{\text{imp}} &= d_{i,t}^{\text{elec}} + p_{i,t}^{\text{bat,ch}} + p_{i,t}^{\text{toWB}} + p_{i,t}^{\text{toHP}} + p_{i,t}^{\text{feed-in}} && \forall t \in \mathcal{T}_m
\end{aligned}
$$

$$
\begin{aligned}
\sum_{r \in \mathcal{R}^i} q_{i,r,t}^{\text{PV}} + q_{i,t}^{\text{imp}} &= d_{i,t}^{\text{elec,q}} + q_{i,t}^{\text{HP}} + q_{i,t}^{\text{feed-in}}, && \forall t \in \mathcal{T}_m \\
d_{i,t}^{\text{sh}} &= C_i \cdot \frac{\vartheta_{i,t} - \vartheta_{i,t-1}}{\Delta t} + \frac{1}{R_i} \cdot (\vartheta_{i,t} - \vartheta_t^{\text{amb}}) - \gamma_{i,t}^{\text{int}} - \gamma_{i,t}^{\text{sol}} && \forall t \in \mathcal{T}_m \\
\vartheta_{i,t}^{\min} \leq \vartheta_{i,t} &\leq \vartheta_{i,t}^{\max}. && \forall t \in \mathcal{T}_m \\
\gamma_{i,t}^{\text{HP}} &= p_{i,t}^{\text{HP}} \cdot cop_{i,t}^{\text{HP}} && \forall t \in \mathcal{T}_m \\
q_{i,t}^{\text{HP}} \cdot &= p_{i,t}^{\text{HP}} \cdot \tan(\phi^{\text{HP}}) && \forall t \in \mathcal{T}_m \\
0 \leq p_{i,t}^{\text{HP}} &\leq \kappa_i^{\text{HP}} && \forall t \in \mathcal{T}_m \\
\gamma_{i,t}^{\text{HP,aux}} &= p_{i,t}^{\text{HP,aux}} \cdot \eta^{\text{HP,aux}} && \forall t \in \mathcal{T}_m \\
0 \leq p_{i,t}^{\text{HP,aux}} &\leq \kappa_i^{\text{HP,aux}} && \forall t \in \mathcal{T}_m \\
0 \leq \kappa_i^{\text{HP}} &\leq M \cdot \beta_i^{\text{HP}} \\
0 \leq \kappa_i^{\text{HP,aux}} &\leq M \cdot \beta_i^{\text{HP,aux}}
\end{aligned}
$$

$$\gamma_{i,t}^{\mathrm{TS,e}} = \gamma_{i,t-1}^{\mathrm{TS,e}} + \eta^{\mathrm{TS,ch}} \cdot \gamma_{i,t}^{\mathrm{TS,ch}} - \frac{\gamma_{i,t}^{\mathrm{TS,dch}}}{\eta^{\mathrm{TS,dch}}} \qquad \forall t \in \mathcal{T}_m$$

$$0 \leq \gamma_{i,t}^{\mathrm{TS,dch}} \leq \kappa_i^{\mathrm{TS,p}} \qquad \forall t \in \mathcal{T}_m$$

$$0 \leq \gamma_{i,t}^{\mathrm{TS,ch}} \leq \kappa_i^{\mathrm{TS,p}} \qquad \forall t \in \mathcal{T}_m$$

$$0 \leq \gamma_{i,t}^{\mathrm{TS,e}} \leq \kappa_i^{\mathrm{TS,e}} \qquad \forall t \in \mathcal{T}_m$$

$$\gamma_{i,0}^{\mathrm{TS,e}} = \gamma_{i,T_{\mathrm{end}}}^{\mathrm{TS,e}}$$

$$\gamma_{i,t}^{\mathrm{HP}} + \gamma_{i,t}^{\mathrm{TS,dch}} = \gamma_{i,t}^{\mathrm{TS,ch}} + d_{i,t}^{\mathrm{sh}} + d_{i,t}^{\mathrm{dhw}} + \gamma_{i,t}^{\mathrm{vent}} \qquad \forall t \in \mathcal{T}_m$$

$$\mu_{i,c,t}^{\mathrm{WB}} = ava_{i,c,t}^{\mathrm{WB}} \cdot \eta_{i,c}^{\mathrm{WB}} \cdot p_{i,c,t}^{\mathrm{WB}} \qquad \forall t \in \mathcal{T}_m \quad \forall c \in \mathcal{C}^i$$

$$p_{i,c,t}^{\mathrm{WB}} \leq \kappa_{i,c}^{\mathrm{WB}} \qquad \forall t \in \mathcal{T}_m \quad \forall c \in \mathcal{C}^i$$

$$\mu_{i,c,t}^{\mathrm{BS,e}} = \mu_{i,c,t-1}^{\mathrm{BS,e}} + \mu_{i,c,t}^{\mathrm{BS,ch}} - \mu_{i,c,t}^{\mathrm{BS,dch}} \qquad \forall t \in \mathcal{T}_m \quad \forall c \in \mathcal{C}^i$$

$$0 \leq \mu_{i,c,t}^{\mathrm{BS,e}} \leq \kappa_{i,c}^{\mathrm{BS}} \qquad \forall t \in \mathcal{T}_m \quad \forall c \in \mathcal{C}^i$$

$$0 \leq \mu_{i,c,t}^{\mathrm{BS,dch}} \leq \kappa_{i,c}^{\mathrm{WB}} \qquad \forall t \in \mathcal{T}_m \quad \forall c \in \mathcal{C}^i$$

$$0 \leq \mu_{i,c,t}^{\mathrm{BS,ch}} \leq \kappa_{i,c}^{\mathrm{WB}}, \qquad \forall t \in \mathcal{T}_m \quad \forall c \in \mathcal{C}^i$$

$$\mu_{i,c,0}^{\mathrm{BS,e}} = \mu_{i,c,T_{\mathrm{end}}}^{\mathrm{BS,e}} \qquad \forall c \in \mathcal{C}^i$$

$$\mu_{i,c,t}^{\mathrm{WB}} = d_{i,c,t}^{\mathrm{mob}} + \mu_{i,c,t}^{\mathrm{BS,ch}} - \mu_{i,c,t}^{\mathrm{BS,dch}} \qquad \forall t \in \mathcal{T}_m \quad \forall c \in \mathcal{C}^i$$

$$p_{i,t}^{\mathrm{abs,exch}} \geq \quad p_{i,t}^{\mathrm{imp}} - p_{i,t}^{\mathrm{feed\text{-}in}} \qquad \forall t \in \mathcal{T}_m$$

$$p_{i,t}^{\mathrm{abs,exch}} \geq -p_{i,t}^{\mathrm{imp}} + p_{i,t}^{\mathrm{feed\text{-}in}} \qquad \forall t \in \mathcal{T}_m$$

$$p_i^{\mathrm{peak,exch}} \geq p_{i,t}^{\mathrm{abs,exch}} \qquad \forall t \in \mathcal{T}_m$$

A.5 Formulation of the grid optimization problem under the § 14a regulation (HOODS-Grid-14a)

$$
\begin{aligned}
\min_{\boldsymbol{\alpha}, f} \quad & \sum_{o \in \mathcal{O}} \left((af^{\text{VRDT}} \cdot c_o^{\text{VRDT,inv}} + c_o^{\text{VRDT,O\&M}}) \cdot \alpha_o^{\text{VRDT}} \right) \\
& + \sum_{ji \in \mathcal{L}} \left(\sum_{m \in \{\text{II,III}\}} \left(af^{\text{VRDT}} \cdot c_{ji,\text{spec}}^{\text{line},m} \cdot \alpha_{ji}^{m} \right) \right) \\
& + c_{\text{spec}}^{\text{Qcomp}} \cdot \sum_{t \in \mathcal{T}_m} \left(\omega_t \cdot q_{\text{MBB},t}^{\text{comp}} \right) + c_{\text{spec}}^{\text{feed-in}} \cdot \sum_{t \in \mathcal{T}_m} \cdot \sum_{i \in \mathcal{I}^b} \left(\omega_t \cdot p_{i,t}^{\text{PV,DSOcurt}} \right) \\
& + c_{\text{spec}}^{\text{14a}} \cdot \sum_{t \in \mathcal{T}} \omega_t \left(p_{i,t}^{\text{HP,14a}} + p_{i,t}^{\text{WB,14a}} \right)
\end{aligned}
$$

$$
\begin{aligned}
\text{s.t. } p_{i,t}^{\text{net}} &= p_{i,t}^{\text{imp}*} + p_{i,t}^{\text{HP}*} + p_{i,t}^{\text{WB}*} - p_{i,t}^{\text{feed-in}*} && \forall t \in \mathcal{T}_m \quad \forall i \in \mathcal{I}^b \\
q_{i,t}^{\text{net}} &= q_{i,t}^{\text{imp}*} - q_{i,t}^{\text{feed-in}*} && \forall t \in \mathcal{T}_m \quad \forall i \in \mathcal{I}^b \\
p_{i,t}^{\text{net}} &= 0 && \forall t \in \mathcal{T}_m \quad \forall i \in \mathcal{I} \setminus (\mathcal{I}^b \cup \text{MBB}) \\
q_{i,t}^{\text{net}} &= 0 && \forall t \in \mathcal{T}_m \quad \forall i \in \mathcal{I} \setminus (\mathcal{I}^b \cup \text{MBB}) \\
u_{i,t} &= u_{j,t} - 2 \cdot r_{ji} \cdot p_{ji,t} - 2 \cdot x_{ji} \cdot q_{ji,t} && \forall t \in \mathcal{T}_m \quad \forall ji \in \mathcal{L} \\
p_{i,t}^{\text{net}} - p_{i,t}^{\text{PV,DSOcurt}} + p_{ji,t} &= \sum_{k \in N^+(i)} p_{ik,t} - p_{i,t}^{\text{HP,14a}} - p_{i,t}^{\text{WB,14a}} && \forall t \in \mathcal{T}_m \quad \forall i \in \mathcal{I}^b \\
q_{i,t}^{\text{net}} + q_{ji,t} &= \sum_{k \in N^+(i)} q_{ik,t} && \forall t \in \mathcal{T}_m \quad \forall i \in \mathcal{I} \\
\sum_{m \in \{\text{I,II,III}\}} \alpha_{ji}^{m} &= 1 && \forall ji \in \mathcal{L} \\
p_{ji,t} &= \sum_{m \in \{\text{I,II,III}\}} p_{ji,t}^{m} && \forall t \in \mathcal{T}_m \quad \forall ji \in \mathcal{L} \\
q_{ji,t} &= \sum_{m \in \{\text{I,II,III}\}} q_{ji,t}^{m} && \forall t \in \mathcal{T}_m \quad \forall ji \in \mathcal{L} \\
a_y \cdot p_{ji,t}^{m} + b_y \cdot q_{ji,t}^{m} &\leq c_y \cdot \kappa_{ji}^{m} \cdot \alpha_{ji}^{m} && \forall m \in \{\text{I,II,III}\} \quad \forall y \in \{1,2,\ldots,8\} \\
& && \forall t \in \mathcal{T}_m \quad \forall ji \in \mathcal{L} \\
u_{i,t} &= u_{j,t} - 2 \cdot \sum_{m \in \{\text{I,II,III}\}} \left(r_{ji}^{m} \cdot p_{ji,t}^{m} + x_{ji}^{m} \cdot q_{ji,t}^{m} \right) && \forall t \in \mathcal{T}_m \quad \forall i \in \mathcal{I} \\
\alpha^{\text{FRT}} + \sum_{o \in \mathcal{O}} \alpha_o^{\text{VRDT}} &= 1 \\
p_{\text{MBB},t}^{\text{net}} &= p_{\text{MBB},t}^{\text{imp}} - p_{\text{MBB},t}^{\text{feed-in}} && \forall t \in \mathcal{T}_m \\
q_{\text{MBB},t}^{\text{net}} &= q_{\text{MBB},t}^{\text{comp}} && \forall t \in \mathcal{T}_m \\
a_y \cdot p_{\text{MBB},t}^{\text{net}} + b_y \cdot q_{\text{MBB},t}^{\text{net}} &\leq c_y \cdot \left(\alpha^{\text{FRT}} \cdot \kappa^{\text{FLT}} + \sum_{o \in \mathcal{O}} \alpha_o^{\text{VRDT}} \cdot \kappa_o^{\text{VRDT}} \right) && \forall t \in \mathcal{T}_m \quad \forall y \in \{1,2,\ldots,8\} \\
\frac{u_{i,t}}{(V_{\text{base}})^2} &\leq \left((V'_{\text{max}})_i^2 + \sum_{o \in \mathcal{O}} \alpha_o^{\text{VRDT}} \cdot \left((V_{\text{max}})_i^2 - (V'_{\text{max}})_i^2 \right) \right) && \forall t \in \mathcal{T}_m \quad \forall i \in \mathcal{I} \\
\frac{u_{i,t}}{(V_{\text{base}})^2} &\geq \left((V'_{\text{min}})_i^2 + \sum_{o \in \mathcal{O}} \alpha_o^{\text{VRDT}} \cdot \left((V_{\text{min}})_i^2 - (V'_{\text{min}})_i^2 \right) \right) && \forall t \in \mathcal{T}_m \quad \forall i \in \mathcal{I} \\
0 \leq p_{i,t}^{\text{PV,DSOcurt}} &\leq p_{i,t}^{\text{feed-in}*} && \forall t \in \mathcal{T}_m \quad \forall i \in \mathcal{I}^b \\
p_{i,t}^{\text{net}} + p_{ji,t} &= \sum_{k \in N^+(i)} p_{ik,t} && \forall t \in \mathcal{T}_m \quad \forall i \in \mathcal{I} \setminus \mathcal{I}^b
\end{aligned}
$$

$$
0 \leq p_{i,t}^{\text{HP,14a}} \leq \begin{cases} p_{i,t}^{\text{HP,imp}*} - 4.2 \text{ kW} & \text{if } p_{i,t}^{\text{HP,imp}*} \geq 4.2 \text{ kW} \\ 0 & \text{if } p_{i,t}^{\text{HP,imp}*} < 4.2 \text{ kW} \end{cases} \qquad \forall t \in \mathcal{T}_m \quad \forall i \in \mathcal{I}^b
$$

$$
0 \leq p_{i,t}^{\text{WB,14a}} \leq \begin{cases} p_{i,t}^{\text{WB,imp}*} - 4.2 \text{ kW} \cdot |\mathcal{C}^i| & \text{if } p_{i,t}^{\text{WB,imp}*} \geq 4.2 \text{ kW} \cdot |\mathcal{C}^i| \\ 0 & \text{if } p_{i,t}^{\text{WB,imp}*} < 4.2 \text{ kW} \cdot |\mathcal{C}^i| \end{cases} \qquad \forall t \in \mathcal{T}_m \quad \forall i \in \mathcal{I}^b
$$

A.6 Formulation of the ex-post prosumer optimization problem under the § 14a regulation (HOODS-Bui-React)

$$
\begin{aligned}
\min_{\substack{\boldsymbol{\kappa}_i, \boldsymbol{\epsilon}_i, \\ \boldsymbol{p}^{\text{imp,HP}}_{i,t}, \boldsymbol{p}^{\text{imp,WB}}_{i,t}, \\ \boldsymbol{p}^{\text{toHP}}_{i,t}, \boldsymbol{p}^{\text{toWB}}_{i,t}}} \quad & af^{\text{HP}} \cdot \left(c^{\text{HP,inv,fix}} \cdot \beta_i^{\text{HP}} + c^{\text{HP,inv,var}} \cdot \kappa_i^{\text{HP}} \right) \\
+ \quad & af^{\text{HP,aux}} \cdot \left(c^{\text{HP,aux,inv,fix}} \cdot \beta_i^{\text{HP,aux}} + c^{\text{HP,aux,inv,var}} \cdot \kappa_i^{\text{HP,aux}} \right) \\
+ & \sum_{r \in \mathcal{R}_i} af^{\text{PV}} \cdot \left(c^{\text{PV,inv,fix}} \cdot \beta_{i,r}^{\text{PV}} + c^{\text{PV,inv,var}} \cdot \kappa_{i,r}^{\text{PV}} \right) \\
+ & af^{\text{bat}} \cdot c^{\text{bat,inv,var}} \cdot \kappa_i^{\text{bat,e}} + af^{\text{TS}} \cdot c^{\text{TS,inv,var}} \cdot \kappa_i^{\text{TS,e}} \\
+ & c^{\text{sto},\epsilon}_{\text{spec}} \cdot \sum_{t \in \mathcal{T}} \omega_t \cdot \left(p_{i,t}^{\text{bat,dch}} + p_{i,t}^{\text{bat,ch}} + \gamma_{i,t}^{\text{TS,dch}} + \gamma_{i,t}^{\text{TS,ch}} + \mu_{i,t}^{\text{VMS,dch}} + \mu_{i,t}^{\text{VMS,ch}} \right) \\
+ & \sum_{t \in \mathcal{T}} \left(\omega_t \cdot c^{\text{imp}}_{\text{spec},t} \cdot (p_{i,t}^{\text{imp}} + p_{i,t}^{\text{HP,imp}} + p_{i,t}^{\text{WB,imp}}) \right) - \sum_{t \in \mathcal{T}} \left(\omega_t \cdot c^{\text{feed-in}}_{\text{spec}} \cdot p_{i,t}^{\text{feed-in}} \right) + c^{\text{CP}}_{\text{spec}} \cdot p_i^{\text{peak,exch}} \\
+ & c^{\text{conv}}_{\text{spec}} \cdot \sum_{t \in \mathcal{T}} \omega_t \left(p_{i,t}^{\text{toHP}} + p_{i,t}^{\text{toWB}} \right)
\end{aligned}
$$

$$
\begin{aligned}
\text{s.t.} \quad p_{i,r,t}^{\text{PV}} + p_{i,r,t}^{\text{PVcurt}} &= \kappa_i^{\text{PV}} \cdot cf_{i,r,t}^{\text{PV}} && \forall t \in \mathcal{T}_m \quad \forall r \in \mathcal{R}^i \\
p_{i,r,t}^{\text{PV}}, p_{i,r,t}^{\text{PVcurt}} &\geq 0 && \forall t \in \mathcal{T}_m \quad \forall r \in \mathcal{R}^i \\
-\tan\left(\phi_{\min}^{\text{PV}}\right) \cdot p_{i,r,t}^{\text{PV}} \leq q_{i,r,t}^{\text{PV}} &\leq \tan\left(\phi_{\min}^{\text{PV}}\right) \cdot p_{i,r,t}^{\text{PV}} && \forall t \in \mathcal{T}_m \quad \forall r \in \mathcal{R}^i \\
0 \leq \kappa_{i,r}^{\text{PV}} &\leq U_A \cdot A_{i,r} \cdot \beta_{i,r}^{\text{PV}} && \forall r \in \mathcal{R}^i \\
\epsilon_{i,t}^{\text{bat,e}} &= \epsilon_{i,t-1}^{\text{bat,e}} + \eta^{\text{bat,ch}} \cdot p_{i,t}^{\text{bat,ch}} - \frac{p_{i,t}^{\text{bat,dch}}}{\eta^{\text{bat,dch}}} && \forall t \in \mathcal{T}_m \\
0 \leq p_{i,t}^{\text{bat,dch}} &\leq \kappa_i^{\text{bat,p}} && \forall t \in \mathcal{T}_m \\
0 \leq p_{i,t}^{\text{bat,ch}} &\leq \kappa_i^{\text{bat,p}} && \forall t \in \mathcal{T}_m \\
0 \leq \epsilon_{i,t}^{\text{bat,e}} &\leq \kappa_i^{\text{bat,e}} && \forall t \in \mathcal{T}_m \\
\epsilon_{i,0}^{\text{bat,e}} &= \epsilon_{i,T_{\text{end}}}^{\text{bat,e}} \\
\kappa_i^{\text{bat,e}} &= \kappa_i^{\text{bat,p}} \cdot etp^{\text{bat}} \\
p_{i,t}^{\text{HP,imp}} + p_{i,t}^{\text{toHP}} &= p_{i,t}^{\text{HP}} + p_{i,t}^{\text{HP,aux}} && \forall t \in \mathcal{T}_m \\
p_{i,t}^{\text{WB,imp}} + p_{i,t}^{\text{toWB}} &= \sum_{c \in \mathcal{C}^i} p_{i,c,t}^{\text{WB}} && \forall t \in \mathcal{T}_m \\
\sum_{r \in \mathcal{R}^i} p_{i,r,t}^{\text{PV}} + p_{i,t}^{\text{bat,dch}} + p_{i,t}^{\text{imp}} &= d_{i,t}^{\text{elec}} + p_{i,t}^{\text{bat,ch}} + p_{i,t}^{\text{toWB}} + p_{i,t}^{\text{toHP}} + p_{i,t}^{\text{feed-in}} && \forall t \in \mathcal{T}_m
\end{aligned}
$$

$$
\begin{aligned}
\sum_{r \in \mathcal{R}^i} q_{i,r,t}^{\text{PV}} + q_{i,t}^{\text{imp}} &= d_{i,t}^{\text{elec,q}} + q_{i,t}^{\text{HP}} + q_{i,t}^{\text{feed-in}}, && \forall t \in \mathcal{T}_m \\
d_{i,t}^{\text{sh}} &= \mathrm{C}_i \cdot \frac{\vartheta_{i,t} - \vartheta_{i,t-1}}{\Delta t} + \frac{1}{R_i} \cdot (\vartheta_{i,t} - \vartheta_t^{\text{amb}}) - \gamma_{i,t}^{\text{int}} - \gamma_{i,t}^{\text{sol}} && \forall t \in \mathcal{T}_m \\
\vartheta_{i,t}^{\min} - \vartheta_{i,t}^{\text{slack}} &\leq \vartheta_{i,t} \leq \vartheta_{i,t}^{\max}. && \forall t \in \mathcal{T}_m \\
\gamma_{i,t}^{\text{HP}} &= p_{i,t}^{\text{HP}} \cdot cop_{i,t}^{\text{HP}} && \forall t \in \mathcal{T}_m \\
q_{i,t}^{\text{HP}} &= p_{i,t}^{\text{HP}} \cdot \tan(\phi^{\text{HP}}) && \forall t \in \mathcal{T}_m \\
\gamma_{i,t}^{\text{HP,aux}} &= p_{i,t}^{\text{HP,aux}} \cdot \eta^{\text{HP,aux}} && \forall t \in \mathcal{T}_m \\
0 \leq \kappa_i^{\text{HP}} &\leq M \cdot \beta_i^{\text{HP}} \\
0 \leq \kappa_i^{\text{HP,aux}} &\leq M \cdot \beta_i^{\text{HP,aux}} \\
\gamma_{i,t}^{\text{TS,e}} &= \gamma_{i,t-1}^{\text{TS,e}} + \eta^{\text{TS,ch}} \cdot \gamma_{i,t}^{\text{TS,ch}} - \frac{\gamma_{i,t}^{\text{TS,dch}}}{\eta^{\text{TS,dch}}} && \forall t \in \mathcal{T}_m
\end{aligned}
$$

$$
\begin{aligned}
0 \leq \gamma_{i,t}^{\mathrm{TS,dch}} &\leq \kappa_i^{\mathrm{TS,p}} && \forall t \in \mathcal{T}_m \\
0 \leq \gamma_{i,t}^{\mathrm{TS,ch}} &\leq \kappa_i^{\mathrm{TS,p}} && \forall t \in \mathcal{T}_m \\
0 \leq \gamma_{i,t}^{\mathrm{TS,e}} &\leq \kappa_i^{\mathrm{TS,e}} && \forall t \in \mathcal{T}_m \\
\gamma_{i,0}^{\mathrm{TS,e}} &= \gamma_{i,T_{\mathrm{end}}}^{\mathrm{TS,e}} \\
\gamma_{i,t}^{\mathrm{HP}} + \gamma_{i,t}^{\mathrm{TS,dch}} + \gamma_{i,t}^{\mathrm{slack}} &= \gamma_{i,t}^{\mathrm{TS,ch}} + d_{i,t}^{\mathrm{sh}} + d_{i,t}^{\mathrm{dhw}} + \gamma_{i,t}^{\mathrm{vent}} && \forall t \in \mathcal{T}_m \\
\mu_{i,c,t}^{\mathrm{WB}} &= ava_{i,c,t}^{\mathrm{WB}} \cdot \eta_{i,c}^{\mathrm{WB}} \cdot p_{i,c,t}^{\mathrm{WB}} && \forall t \in \mathcal{T}_m \quad \forall c \in \mathcal{C}^i \\
p_{i,c,t}^{\mathrm{WB}} &\leq \kappa_{i,c}^{\mathrm{WB}} && \forall t \in \mathcal{T}_m \quad \forall c \in \mathcal{C}^i \\
\mu_{i,c,t}^{\mathrm{BS,e}} &= \mu_{i,c,t-1}^{\mathrm{BS,e}} + \mu_{i,c,t}^{\mathrm{BS,ch}} - \mu_{i,c,t}^{\mathrm{BS,dch}} && \forall t \in \mathcal{T}_m \quad \forall c \in \mathcal{C}^i \\
0 \leq \mu_{i,c,t}^{\mathrm{BS,e}} &\leq \kappa_{i,c}^{\mathrm{BS}} && \forall t \in \mathcal{T}_m \quad \forall c \in \mathcal{C}^i \\
0 \leq \mu_{i,c,t}^{\mathrm{BS,dch}} &\leq \kappa_{i,c}^{\mathrm{WB}} && \forall t \in \mathcal{T}_m \quad \forall c \in \mathcal{C}^i \\
0 \leq \mu_{i,c,t}^{\mathrm{BS,ch}} &\leq \kappa_{i,c}^{\mathrm{WB}}, && \forall t \in \mathcal{T}_m \quad \forall c \in \mathcal{C}^i \\
\mu_{i,c,0}^{\mathrm{BS,e}} &= \mu_{i,c,T_{\mathrm{end}}}^{\mathrm{BS,e}} && \forall c \in \mathcal{C}^i \\
\mu_{i,c,t}^{\mathrm{WB}} &= d_{i,c,t}^{\mathrm{mob}} + \mu_{i,c,t}^{\mathrm{BS,ch}} - \mu_{i,c,t}^{\mathrm{BS,dch}} && \forall t \in \mathcal{T}_m \quad \forall c \in \mathcal{C}^i \\
p_{i,t}^{\mathrm{abs,exch}} &\geq \quad p_{i,t}^{\mathrm{imp}} - p_{i,t}^{\mathrm{feed\text{-}in}} && \forall t \in \mathcal{T}_m \\
p_{i,t}^{\mathrm{abs,exch}} &\geq -p_{i,t}^{\mathrm{imp}} + p_{i,t}^{\mathrm{feed\text{-}in}} && \forall t \in \mathcal{T}_m \\
p_i^{\mathrm{peak,exch}} &\geq p_{i,t}^{\mathrm{abs,exch}} && \forall t \in \mathcal{T}_m
\end{aligned}
$$

if $\kappa_i^{\mathrm{HP}*} \leq 4.2$ kW : $\quad 0 \leq p_{i,t}^{\mathrm{HP}} \leq \kappa_i^{\mathrm{HP}} \qquad \forall t \in \mathcal{T}_m$

if $\kappa_i^{\mathrm{HP}*} + \kappa_i^{\mathrm{HP,aux}*} \leq 4.2$ kW : $\quad 0 \leq p_{i,t}^{\mathrm{HP,aux}} \leq \kappa_i^{\mathrm{HP,aux}} \qquad \forall t \in \mathcal{T}_m$

else : $\quad 0 \leq p_{i,t}^{\mathrm{HP,aux}} \leq \begin{cases} p_{i,t}^{\mathrm{HP,aux}*} - p_{i,t}^{\mathrm{HP,14a}*} & \text{if } p_{i,t}^{\mathrm{HP,14a}*} \geq 0 \ \wedge \ \kappa_{i,t}^{\mathrm{HP,aux}*} + \kappa_{i,t}^{\mathrm{HP}*} \geq 4.2 \text{ kW} \\ \kappa_{i,t}^{\mathrm{HP,aux}*} & \text{if } p_{i,t}^{\mathrm{HP,14a}*} = 0 \ \wedge \ \kappa_{i,t}^{\mathrm{HP,aux}*} + \kappa_{i,t}^{\mathrm{HP}*} \geq 4.2 \text{ kW} \end{cases} \qquad \forall t \in \mathcal{T}_m$

else : $\quad 0 \leq p_{i,t}^{\mathrm{HP}} \leq \begin{cases} p_{i,t}^{\mathrm{HP}*} - (p_{i,t}^{\mathrm{HP,14a}*} + p_{i,t}^{\mathrm{HP,aux}*}) & \text{if } \quad p_{i,t}^{\mathrm{HP,14a}*} \geq p_{i,t}^{\mathrm{HP,aux}*} \ \wedge \ \kappa_{i,t}^{\mathrm{HP}*} \geq 4.2 \text{ kW} \\ \kappa_{i,t}^{\mathrm{HP}} & \text{if } 0 \leq p_{i,t}^{\mathrm{HP,14a}*} \leq p_{i,t}^{\mathrm{HP,aux}*} \ \wedge \ \kappa_{i,t}^{\mathrm{HP}*} \geq 4.2 \text{ kW} \end{cases} \qquad \forall t \in \mathcal{T}_m$

$$
0 \leq p_{i,t}^{\mathrm{HP,aux}} \leq \begin{cases} 0 & \text{if } \quad p_{i,t}^{\mathrm{HP,14a}*} \geq p_{i,t}^{\mathrm{HP,aux}*} \ \wedge \ \kappa_{i,t}^{\mathrm{HP}*} \geq 4.2 \text{ kW} \\ p_{i,t}^{\mathrm{HP,aux}*} - p_{i,t}^{\mathrm{HP,14a}*} & \text{if } \quad p_{i,t}^{\mathrm{HP,14a}*} \leq p_{i,t}^{\mathrm{HP,aux}*} \ \wedge \ \kappa_{i,t}^{\mathrm{HP}*} \geq 4.2 \text{ kW} \\ \kappa_{i,t}^{\mathrm{HP,aux}*} & \text{if } \quad p_{i,t}^{\mathrm{HP,14a}*} = 0 \qquad \wedge \ \kappa_{i,t}^{\mathrm{HP}*} \geq 4.2 \text{ kW} \end{cases} \qquad \forall t \in \mathcal{T}_m
$$

$$
0 \leq p_{i,c,t}^{\mathrm{WB}} \leq \begin{cases} \dfrac{\sum_{c \in \mathcal{C}^i} \left(p_{i,c,t}^{\mathrm{WB}*} \right) - p_{i,t}^{\mathrm{WB,14a}*}}{|\mathcal{C}_i|} & \text{if } p_{i,t}^{\mathrm{WB,14a}*} \geq 0 \\ \kappa_{i,c,t}^{\mathrm{WB}} & \text{if } p_{i,t}^{\mathrm{WB,14a}*} = 0 \end{cases} \qquad \forall t \in \mathcal{T}_m \quad \forall c \in \mathcal{C}^i
$$

$\boldsymbol{\kappa}_i = \boldsymbol{\kappa}_i^*$

Appendix B

emobpy parameters

B.1 Driver profiles

In *emobpy*, distinct driving characteristics for various driver types can be defined. These profiles enforce various characteristics, such as the

- *n_trip_out*: The number of outward trips per day,
- *last_trip_to*: The final destination of the trip,
- *at_least_one_trip*: Whether a location has to be visited at least once during a weekday or a weekend,
- *overall_min_time_at*: The minimum enforced duration in a given location during a weekday or a weekend,
- *overall_max_time_at*: The maximum allowable duration in a given location during a weekday or a weekend,
- *min_state_duration*: The minimum duration in a given location, only if it is visited during a trip.

The driver profiles defined for the case study are given in Listing B.1

Listing B.1: Driving profiles defined for *emobpy*

```
{
    "freetime": {
        "weekday": {
            "n_trip_out": [1],
            "last_trip_to": {"home": true},
            "overall_min_time_at": {"home": 9}
        },
        "weekend": {
            "n_trip_out": [1],
            "last_trip_to": {"home": true},
            "overall_min_time_at": {"home": 6}
        }
    },
    "fulltime": {
        "weekday": {
            "n_trip_out": [1],
            "last_trip_to": {"home": true},
            "at_least_one_trip": {"workplace": true},
            "overall_min_time_at": {"home": 9, "workplace": 7.0},
            "overall_max_time_at": {"workplace": 8.0},
            "min_state_duration": {"workplace": 3.5}
        },
        "weekend": {
            "n_trip_out": [1],
            "last_trip_to": {"home": true},
            "overall_min_time_at": {"home": 6, "workplace": 3},
            "overall_max_time_at": {"workplace": 4},
            "min_state_duration": {"workplace": 3}
        }
    },
    "parttime": {
        "weekday": {
            "n_trip_out": [1],
            "last_trip_to": {"home": true},
            "at_least_one_trip": {"workplace": true},
            "overall_min_time_at": {"home": 9, "workplace": 3.5},
            "overall_max_time_at": {"workplace": 4},
            "min_state_duration": {"workplace": 3.5}
        },
        "weekend": {
            "n_trip_out": [1],
            "last_trip_to": {"home": true},
            "overall_min_time_at": {"home": 6, "workplace": 3},
            "overall_max_time_at": {"workplace": 4},
            "min_state_duration": {"workplace": 3}
        }
    }
}
```

Appendix C

Typical weeks *tsam*

Table C.1: The typical weeks generated by the time-series aggregation for each grid region. The period indicated with an asterisk (*) is the period with the minimum average temperature (the extreme winter week).

	Rural		Village		Suburban		Urban	
Typical week	Period	Occurrence	Period	Occurrence	Period	Occurrence	Period	Occurrence
1	26.11-02.12	13	24.09-30.09	13	08.10-14.10	8	15.10-21.10	8
2	10.09-16.09	8	12.11-18.11	13	03.09-09.09	9	03.09-09.09	9
3	20.08-26.08	12	05.11-11.11	12	15.01-21.01*	10	15.01-21.01*	10
4	05.11-11.11	6	30.08-05.08	8	25.06-01.07	11	25.06-01.07	11
5	15.01-21.01*	8	06.05-13.05	3	19.11-25.11	9	19.11-25.11	9
6	24.09-30.09	5	15.01-21.01*	3	04.06-10.06	5	04.06-10.06	5

Appendix D

LinDistFlow validation

D.1 Voltages

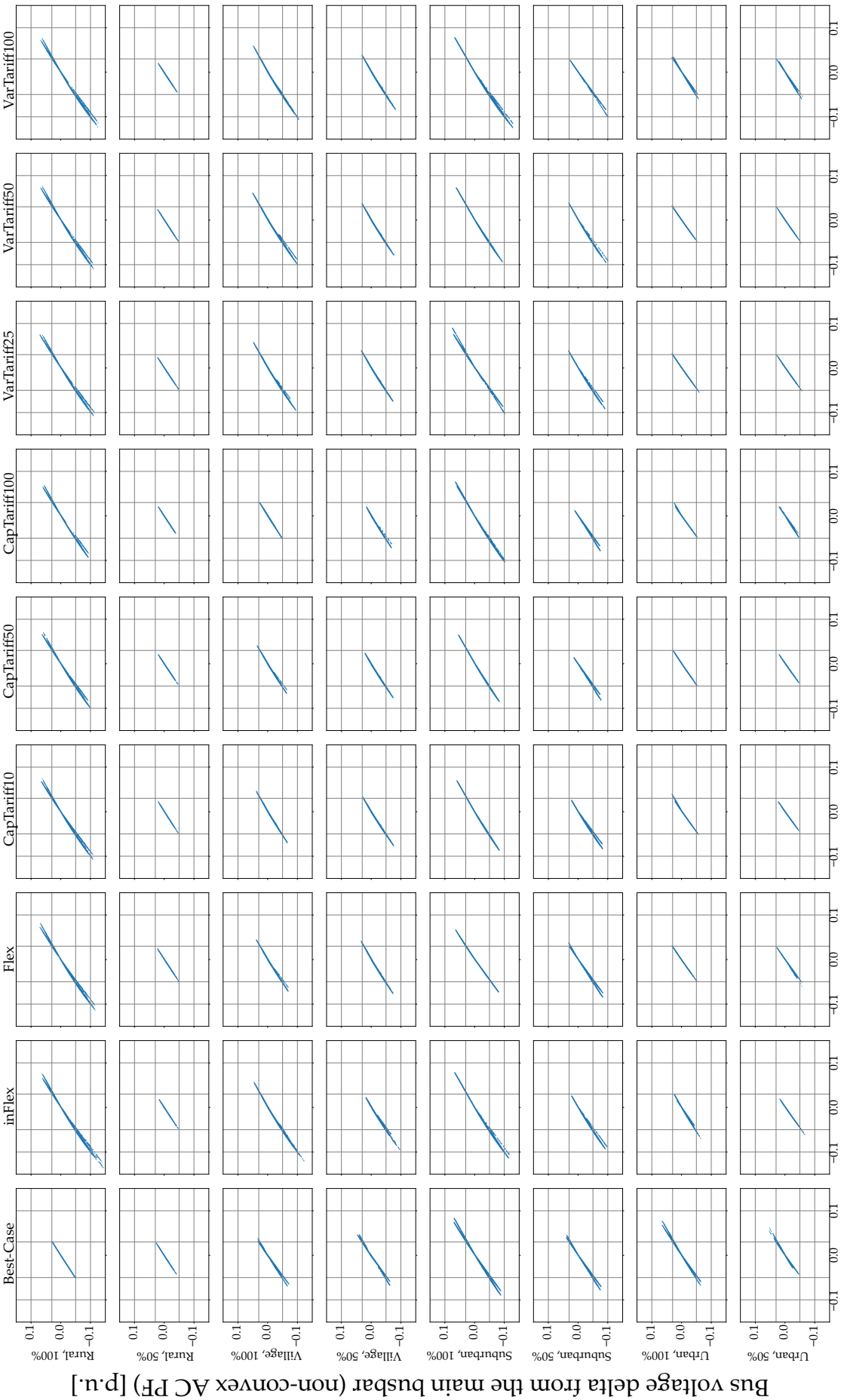

Figure D.1: Comparison between the bus voltages, as calculated by LinDistFlow and non-convex AC power flow.

D.2 Power losses

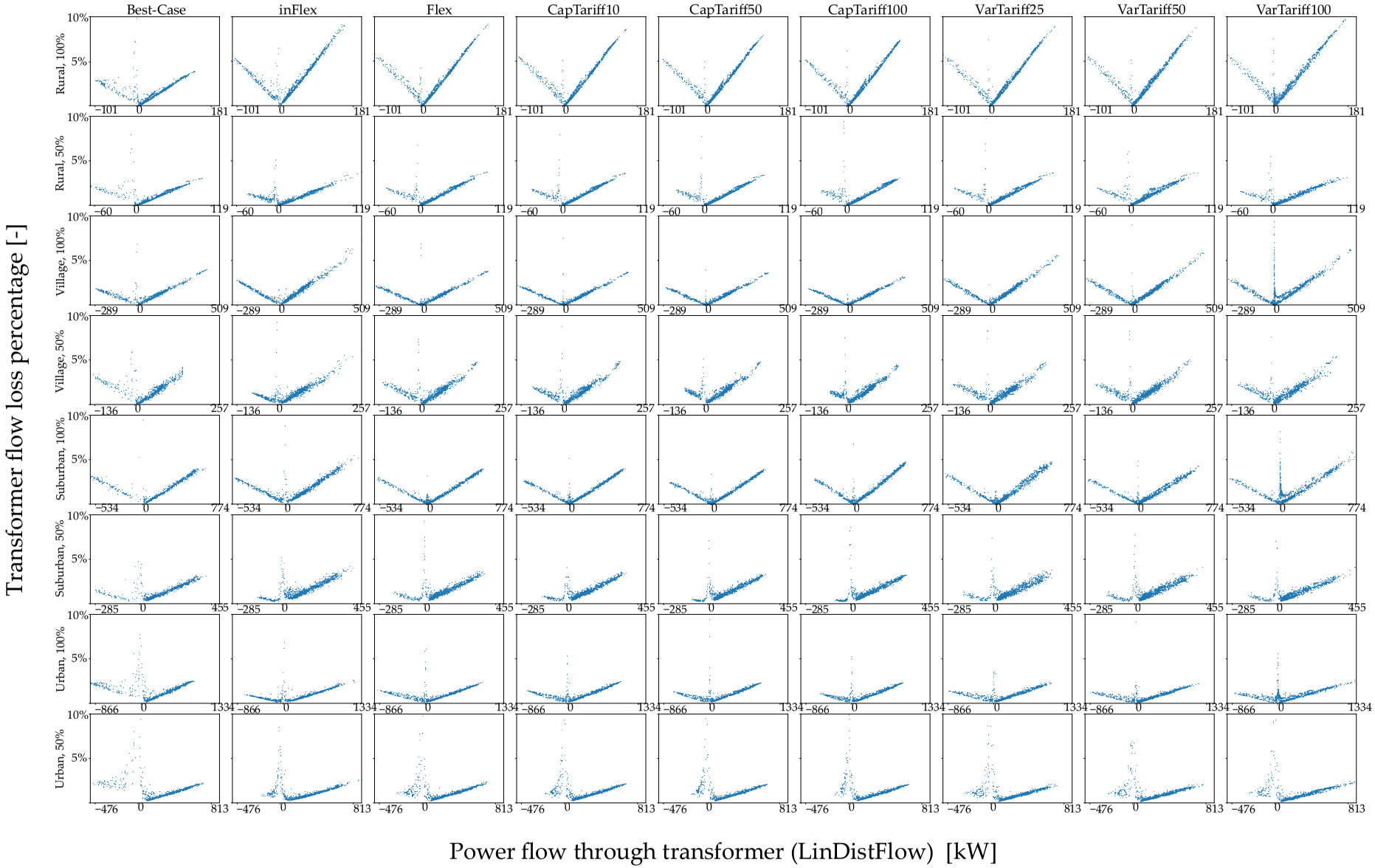

Figure D.2: The share of overall power loss given in percentage of the total transformer flow (import or feed-in), which was neglected by LinDistFlow for each scenario.

Bibliography

[1] Govinda R. Timilsina. "Are renewable energy technologies cost competitive for electricity generation?" In: *Renewable Energy* 180 (2021), pp. 658–672. ISSN: 09601481. DOI: 10.1016/j.renene.2021.08.088. URL: https://www.sciencedirect.com/science/article/pii/S0960148121012568.

[2] Foundation of climate neutrality. *Comparison of the "Big 5" climate neutrality scenarios (de: Vergleich der "Big 5" Klimaneutralitätsszenarien)*. 2022. URL: https://www.stiftung-klima.de/app/uploads/2022/03/2022-03-16-Big5_Szenarienvergleich_final.pdf.

[3] de: Agentur für Erneuerbare Energien. *Graphic dossier: The electricity mix in Germany 2018-2022 (de: Grafik-Dossier: Der Strommix in Deutschland 2018-2022)*. URL: https://www.unendlich-viel-energie.de/mediathek/grafiken/grafik-dossier-strommix-2015-2022.

[4] Prognos, Öko-Institut, and Wuppertal-Institut. "Klimaneutrales Deutschland 2045. Wie Deutschland seine Klimaziele schon vor 2050 erreichen kann (Climate-neutral Germany 2045. How Germany can achieve its climate targets even before 2050): Zusammenfassung im Auftrag von Stiftung Klimaneutralität, Agora Energiewende und Agora Verkehrswend (Summary commissioned by Stiftung Klimaneutralität, Agora Energiewende and Agora Verkehrswend)". In: (2021). URL: https://static.agora-energiewende.de/fileadmin/Projekte/2021/2021_04_KNDE45/A-EW_209_KNDE2045_Zusammenfassung_DE_WEB.pdf.

[5] Federation of German Industry. "Climate pathways 2.0 (de: Klimapfade 2.0): An economy programm for climate and future (de: Ein WIrtschaftsprogramm für Klima und Zukunft)". In: (2021). URL: https://issuu.com/bdi-berlin/docs/211021_bdi_klimapfade_2.0_-_gesamtstudie_-_vorabve.

[6] de: Deutsche Energie-Agentur GmbH. *dena Pilot Study Departure to Climate Neutrality (de: Aufbruch Klimaneutralität)*. 2021. URL: https://www.dena.de/fileadmin/dena/Publikationen/PDFs/2021/Abschlussbericht_dena-Leitstudie_Aufbruch_Klimaneutralitaet.pdf.

[7] Fraunhofer ISI et al. "Long-term scenarios for the transformation of the energy system in Germany (de: Langfristszenarien für die Transformation des Energiesystems in Deutschland)". In: (2022). URL: https://langfristszenarien.de/enertile-explorer-wAssets/docs/LFS3_T45_Webinar_Angebot_Nov_2022_final_webinarversion.pdf.

[8] Kopernikus-Projekt Ariadne. *Ariadne-Report: Germany on the path to climate neutrality in 2045 - Scenarios and paths in a model comparison (de: Deutschland auf dem Weg zur Klimaneutralität 2045 - Szenarien und Pfade im Modellvergleich)*. 2021. DOI: 10.48485/PIK.2021.006.

[9] Kerstine Appunn. *Next German government's key climate and energy plans in 2021 coalition agreement*. 2021. URL: https://www.cleanenergywire.org/factsheets/future-german-governments-key-climate-and-energy-plans-2021-coalition-treaty.

[10] Jessica Bateman. *Heat pump installation plans may overburden Germany's grid - energy industry*. 2023. URL: https://www.cleanenergywire.org/news/heat-pump-installation-plans-may-overburden-germanys-grid-energy-industry.

[11] German Federal Network Agency. *Genehmigung des Szenariorahmens 2023-2037/2045 (Approval of the scenario framework 2023-2037/2045*. URL: https://www.netzausbau.de/SharedDocs/Downloads/DE/2037/SR/Szenariorahmen_2037_Genehmigung.pdf.

[12] German Federal Parliament. "Draft Act on the Amendment of the Building Energy Act and amending the Heating Costs Ordinance and amending the Sweeping and Inspection Ordinance (de: Entwurf eines Gesetzes zur Änderung des Gebäudeenergiegesetzes und zur Änderung der Heizkostenverordnung sowie zur Änderung der Kehr- und Überprüfungsordnung)". In: (2023). URL: https://www.bmwk.de/Redaktion/DE/Downloads/Gesetz/entwurf-geg.pdf?.

[13] European Parliament and Council. *Regulation (EU) 2023/851 of the European Parliament and of the Council of 19 April 2023 amending Regulation (EU) 2019/631 as regards strengthening the CO2 emission performance standards for new passenger cars and new light commercial vehicles in line with the Union's increased climate ambition (Text with EEA relevance)*. URL: https://eur-lex.europa.eu/legal-content/EN/TXT/?uri=celex:32023R0851.

[14] Harry Wirth. *Recent Facts about Photovoltaics in Germany*. 2023. URL: https://www.pv-fakten.de/.

[15] German Federal Network Agency. *Report on the State and Expansion of Distribution Grids 2021 (ger: Bericht zum Zustand und Ausbau der Verteilernetze 2021)*. 2022. URL: https://www.bundesnetzagentur.de/SharedDocs/Downloads/DE/Sachgebiete/Energie/Unternehmen_Institutionen/NetzentwicklungUndSmartGrid/ZustandAusbauVerteilernetze2021.pdf.

[16] Jenny Love et al. "The addition of heat pump electricity load profiles to GB electricity demand: Evidence from a heat pump field trial". In: *Applied Energy* 204 (2017), pp. 332–342. ISSN: 03062619. DOI: 10.1016/j.apenergy.2017.07.026. URL: https://www.sciencedirect.com/science/article/pii/S0306261917308954.

[17] Agora Verkehrswende, Agora Energiewende, and Regulatory Assistance Project. *Distribution grid planning for a successful energy transition – focus on electromobility: Conclusions of a study commissioned by Agora Verkehrswende, Agora Energiewende and Regulatory Assistance Project (RAP)*. 2019. URL: https://static.agora-energiewende.de/fileadmin/Projekte/2018/Netzausbau_Elektromobilitaet/AgoraRAP2019_VerteilnetzausbauElektromobilitaet_EN.pdf.pdf.

[18] Pio Baake, Sebastian Schwenen, and Christian von Hirschhausen. "Local Energy Markets*". In: *The Journal of Industrial Economics* 71.3 (2023), pp. 855–882. DOI: 10.1111/joie.12338.

[19] Hussain Shareef et al. "Review on Home Energy Management System Considering Demand Responses, Smart Technologies, and Intelligent Controllers". In: *IEEE Access* 6 (2018), pp. 24498–24509. DOI: 10.1109/ACCESS.2018.2831917.

[20] Patrick Matschoss et al. "The German incentive regulation and its practical impact on the grid integration of renewable energy systems". In: *Renewable Energy* 134 (2019), pp. 727–738. ISSN: 09601481. DOI: 10.1016/j.renene.2018.10.103. URL: https://www.sciencedirect.com/science/article/pii/S0960148118313090.

[21] Tim Schittekatte, Ilan Momber, and Leonardo Meeus. "Future-proof tariff design: Recovering sunk grid costs in a world where consumers are pushing back". In: *Energy Economics* 70 (2018), pp. 484–498. ISSN: 0140-9883. DOI: 10.1016/j.eneco.2018.01.028.

[22] German Federal Network Agency. *Determination for the implementation of the grid-oriented control of controllable consumption devices and controllable grid connections in accordance with § 14a EnWG (de: Festlegung zur Durchführung der netzorientierten Steuerung von steuerbaren Verbrauchseinrichtungen und steuerbaren Netzanschlüssen nach § 14a EnWG)*. 2023. URL: https://www.bundesnetzagentur.de/DE/Beschlusskammern/1_GZ/BK6-GZ/2022/BK6-22-300/Anlagen_Zweite Konsultation/BK6-22-300_Regelungswerk.pdf.

[23] German Federal Parliament. *Energy Industry Act § 41a Load-variable, time-of-day-dependent or dynamic and other electricity tariffs (de: Energiewirtschaftsgesetz § 41a Lastvariable, tageszeitabhängige oder dynamische und sonstige Stromtarife): EnWG*. URL: https://www.gesetze-im-internet.de/enwg_2005/__41a.html.

[24] Flemish regulator of the electricity and gas market. *How much capacity tariff do you pay for a kilowatt? (nl: Hoeveel capaciteitstarief betaalt u voor een kilowatt?) | VREG*. 2023. URL: https://www.vreg.be/nl/veelgestelde-vragen/hoeveel-capaciteitstarief-betaalt-u-voor-een-kilowatt.

[25] Juan Caballero-Peña et al. "Distributed energy resources on distribution networks: A systematic review of modelling, simulation, metrics, and impacts". In: *International Journal of Electrical Power & Energy Systems* 138 (2022), p. 107900. ISSN: 0142-0615. DOI: 10.1016/j.ijepes.2021.107900. URL: https://www.sciencedirect.com/science/article/pii/S0142061521011133.

[26] Bernd Thormann and Thomas Kienberger. "Evaluation of Grid Capacities for Integrating Future E-Mobility and Heat Pumps into Low-Voltage Grids". In: *Energies* 13.19 (2020), p. 5083. DOI: 10.3390/en13195083. URL: https://www.mdpi.com/1996-1073/13/19/5083.

[27] Mahdi Sedghi, Ali Ahmadian, and Masoud Aliakbar-Golkar. "Assessment of optimization algorithms capability in distribution network planning: Review, comparison and modification techniques". In: *Renewable and Sustainable Energy Reviews* 66 (2016), pp. 415–434. ISSN: 1364-0321. DOI: 10.1016/j.rser.2016.08.027. URL: https://www.sciencedirect.com/science/article/pii/S1364032116304592.

[28] Hedayat Saboori, Reza Hemmati, and Vahid Abbasi. "Multistage distribution network expansion planning considering the emerging energy storage systems". In: *Energy Conversion and Management* 105 (2015), pp. 938–945. ISSN: 0196-8904. DOI: 10.1016/j.enconman.2015.08.055. URL: https://www.sciencedirect.com/science/article/pii/S0196890415008092.

[29] Simon Koopmann et al. "Optimized deployment of storage systems for integration of distributed generation in smart grids". In: *CIRED 2013: Electricity distribution systems for a sustainable future*. IET/CIRED: Institution of Engineering and Technology, 2013, p. 0713. ISBN: 978-1-84919-732-8. DOI: 10.1049/cp.2013.0889. URL: https://digital-library.theiet.org/content/conferences/10.1049/cp.2013.0889.

[30] Iver Bakken Sperstad, Eivind Solvang, and Oddbjørn Gjerde. "Framework and methodology for active distribution grid planning in Norway". In: *2020 International Conference on Probabilistic Methods Applied to Power Systems (PMAPS)*. 2020, pp. 1–6. DOI: 10.1109/PMAPS47429.2020.9183711.

[31] Julio López, Marcos J. Rider, and Javier Contreras. "Electric Distribution Network Planning Under Uncertainty". In: *Handbook of Optimization in Electric Power Distribution Systems*. Ed. by Mariana Resener et al. Cham: Springer International Publishing, 2020, pp. 293–323. ISBN: 978-3-030-36115-0. DOI: 10.1007/978-3-030-36115-0_10.

[32] Boran Morvaj, Ralph Evins, and Jan Carmeliet. "Optimization framework for distributed energy systems with integrated electrical grid constraints". In: *Applied Energy* 171 (2016), pp. 296–313. ISSN: 03062619. DOI: 10.1016/j.apenergy.2016.03.090. URL: https://www.sciencedirect.com/science/article/abs/pii/S0306261916304159.

[33] Boran Morvaj, Ralph Evins, and Jan Carmeliet. "Decarbonizing the electricity grid: The impact on urban energy systems, distribution grids and district heating potential". In: *Applied Energy* 191 (2017), pp. 125–140. ISSN: 03062619. DOI: 10.1016/j.apenergy.2017.01.058. URL: https://www.sciencedirect.com/science/article/abs/pii/S0306261917300661.

[34] Salman Mashayekh et al. "A mixed integer linear programming approach for optimal DER portfolio, sizing, and placement in multi-energy microgrids". In: *Applied Energy* 187 (2017), pp. 154–168. ISSN: 03062619. DOI: 10.1016/j.apenergy.2016.11.020. URL: https://www.sciencedirect.com/science/article/abs/pii/S0306261916316051.

[35] Konstantinos Spiliotis, Ariana Isabel Ramos Gutierrez, and Ronnie Belmans. "Demand flexibility versus physical network expansions in distribution grids". In: *Applied Energy* 182 (2016), pp. 613–624. ISSN: 03062619. DOI: 10.1016/j.apenergy.2016.08.145. URL: https://www.sciencedirect.com/science/article/abs/pii/S0306261916312545.

[36] Matthias Resch et al. "Techno-Economic Assessment of Flexibility Options Versus Grid Expansion in Distribution Grids". In: *IEEE Transactions on Power Systems* 36.5 (2021), pp. 3830–3839. ISSN: 0885-8950. DOI: 10.1109/TPWRS.2021.3055457. URL: https://ieeexplore.ieee.org/document/9339973.

[37] Martin Geidl et al., eds. *The Energy Hub - A Powerful Concept for Future Energy Systems*. 2007. URL: https://research.ece.cmu.edu/electriconf/2007/2007%20Conf%20Papers/Andersson%20Paper%20final.pdf.

[38] Veronika Grimm et al. "Storage investment and network expansion in distribution networks: The impact of regulatory frameworks". In: *Applied Energy* 262 (2020), p. 114017. ISSN: 03062619. DOI: 10.1016/j.apenergy.2019.114017. URL: https://www.sciencedirect.com/science/article/abs/pii/S0306261919317040.

[39] Pio Baake, Sebastian Schwenen, and Christian von Hirschhausen. *Local Power Markets*. Discussion Papers of DIW Berlin, 2020. URL: https://www.diw.de/de/diw_01.c.800474.de/publikationen/diskussionspapiere/2020_1904/local_power_markets.html.

[40] Wolfgang Zander et al. *Gutachten Digitalisierung der Energiewende (Assessment of the digitalization of the energy transition): Topthema 3: Regulierung, Flexibilisierung und Sektorkopplung (Topic 3: regulation, flexibilization and sector coupling)*. 2018. URL: https://www.bmwk.de/Redaktion/DE/Publikationen/Studien/digitalisierung-der-energiewende-thema-2.pdf.

[41] H. von Stackelberg et al. *Market Structure and Equilibrium*. Springer Berlin Heidelberg, 2010. ISBN: 9783642125867. URL: https://books.google.de/books?id=dghH9OH5fDoC.

[42] Roman Bolgaryn et al. "Active Power Curtailment in Power System Planning". In: *IEEE Open Access Journal of Power and Energy* 8 (2021), pp. 399–408. DOI: 10.1109/OAJPE.2021.3118445.

[43] Deutsche Energie-Agentur GmbH (dena) – German Energy. *dena Ancillar Services Study 2030: Security and reliability of a power supply with a high percentage of renewable energy: FInal report*. 2014. URL: https://www.dena.de/fileadmin/dena/Dokumente/Themen_und_Projekte/Energiesysteme/dena-Studie_Systemdienstleistungen_2030/dena_Ancillary_Services_Study_2030.pdf.

[44] Markus Groissböck. "Are open source energy system optimization tools mature enough for serious use?" In: *Renewable and Sustainable Energy Reviews* 102 (2019), pp. 234–248. ISSN: 1364-0321. DOI: 10.1016/j.rser.2018.11.020.

[45] Drury B. Crawley et al. "EnergyPlus: creating a new-generation building energy simulation program". In: *Energy and Buildings* 33.4 (2001), pp. 319–331. ISSN: 0378-7788. DOI: 10.1016/S0378-7788(00)00114-6. URL: https://www.sciencedirect.com/science/article/pii/S0378778800001146.

[46] Anahi Molar-Cruz and Thomas Hamacher. "UrbanHeatPro: A GIS-based gray-box model for the simulation of heat demand profiles at the urban scale: (Submitted with main manuscript)". In: *MethodsX* (2022).

[47] Jimeno Fonseca et al. *architecture-building-systems/CityEnergyAnalyst: v3.32.0*. 2022. DOI: 10.5281/zenodo.7317134.

[48] Institut Wohnen und Umwelt GmbH. *Typology Approach for Building Stock Energy Assessment - Calculation Method*. Darmstadt, 2013. URL: https://www.episcope.eu/downloads/public/docs/report/TABULA_FinalReport_AppendixVolume.pdf.

[49] Samuel F. Fux et al. "EKF based self-adaptive thermal model for a passive house". In: *Energy and Buildings* 68 (2014), pp. 811–817. ISSN: 0378-7788. DOI: 10.1016/j.enbuild.2012.06.016. URL: https://www.sciencedirect.com/science/article/pii/S0378778812003039.

[50] Herie Park et al. "Thermal parameter identification of simplified building model with electric appliance". In: *11th International Conference on Electrical Power Quality and Utilisation*. 2011, pp. 1–6. DOI: 10.1109/EPQU.2011.6128822.

[51] Tobias Loga, Britta Stein, and Nikolaus Diefenbach. "TABULA building typologies in 20 European countries—Making energy-related features of residential building stocks comparable". In: *Energy and Buildings* 132 (2016), pp. 4–12. ISSN: 0378-7788. DOI: 10.1016/j.enbuild.2016.06.094. URL: https://www.sciencedirect.com/science/article/pii/S0378778816305837.

[52] Paula Carroll, Michael Chesser, and Pádraig F. Lyons. "Air Source Heat Pumps field studies: A systematic literature review". In: *Renewable and Sustainable Energy Reviews* 134 (2020), p. 110275. ISSN: 1364-0321. DOI: 10.1016/j.rser.2020.110275. URL: https://www.sciencedirect.com/science/article/pii/S1364032120305621.

[53] Oliver Ruhnau, Lion Hirth, and Aaron Praktiknjo. "Time series of heat demand and heat pump efficiency for energy system modeling". In: *Scientific Data* 6.1 (2019), p. 189. ISSN: 2052-4463. DOI: 10.1038/s41597-019-0199-y.

[54] Martin Kittel and Wolf-Peter Schill. "Renewable energy targets and unintended storage cycling: Implications for energy modeling". In: *iScience* 25.4 (2022), p. 104002. ISSN: 2589-0042. DOI: 10.1016/j.isci.2022.104002. URL: https://www.sciencedirect.com/science/article/pii/S2589004222002723.

[55] Bundesnetzagentur. "Monitoringbericht 2022 gemäß § 63 Abs. 3 i. V. m. § 35 EnWG und § 48 Abs. 3 i. V. m. § 53 Abs. 3 GWB". In: ().

[56] Mesut Baran and Felix Wu. "Network reconfiguration in distribution systems for loss reduction and load balancing". In: *IEEE Transactions on Power Delivery* 4.2 (1989), pp. 1401–1407. DOI: 10.1109/61.25627. URL: https://ieeexplore.ieee.org/document/25627.

[57] Masoud Farivar and Steven H. Low. "Branch Flow Model: Relaxations and Convexification—Part I". In: *IEEE Transactions on Power Systems* 28.3 (2013), pp. 2554–2564. ISSN: 0885-8950. DOI: 10.1109/TPWRS.2013.2255317.

[58] Daniel K. Molzahn et al. "A Survey of Distributed Optimization and Control Algorithms for Electric Power Systems". In: *IEEE Transactions on Smart Grid* 8.6 (2017), pp. 2941–2962. ISSN: 1949-3053. DOI: 10.1109/TSG.2017.2720471.

[59] Mohammad A.A. Al-Jaafreh, Geev Mokryani. "Planning and operation of LV distribution networks: a comprehensive review". In: *IET Energy Systems Integration* Volume 1, Issue 3 (2019), pp. 133–146. URL: https://ietresearch.onlinelibrary.wiley.com/doi/full/10.1049/iet-esi.2019.0013.

[60] Joshua Adam Taylor. *Conic Optimization of Electric Power Systems: Doctoral Thesis*. 2011. URL: https://core.ac.uk/download/pdf/4431974.pdf.

[61] Xiaoqing Bai et al. "Semidefinite programming for optimal power flow problems". In: *International Journal of Electrical Power & Energy Systems* 30.6 (2008), pp. 383–392. ISSN: 0142-0615. DOI: 10.1016/j.ijepes.2007.12.003. URL: https://www.sciencedirect.com/science/article/pii/S0142061507001378.

[62] Kenneth Van den Bergh, Erik Delarue, and William D'haeseleer. *DC power flow in unit commitment models: TME Working Paper*. 2014. URL: https://www.mech.kuleuven.be/en/tme/research/energy_environment/Pdf/wpen2014-12.pdf.

[63] Kyriaki E. Antoniadou-Plytaria et al. "Distributed and Decentralized Voltage Control of Smart Distribution Networks: Models, Methods, and Future Research". In: *IEEE Transactions on Smart Grid* 8.6 (2017), pp. 2999–3008. ISSN: 1949-3053. DOI: 10.1109/TSG.2017.2679238.

[64] Deepjyoti Deka, Scott Backhaus, and Michael Chertkov. "Estimating distribution grid topologies: A graphical learning based approach". In: *2016 Power Systems Computation Conference (PSCC)*. 2016, pp. 1–7. DOI: 10.1109/PSCC.2016.7541005.

[65] Soumya Kundu, Scott Backhaus, and Ian A. Hiskens. "Distributed control of reactive power from photovoltaic inverters". In: *2013 IEEE International Symposium on Circuits and Systems (ISCAS)*. 2013, pp. 249–252. DOI: 10.1109/ISCAS.2013.6571829.

[66] Sicong Tan, Jian-Xin Xu, and Sanjib Kumar Panda. "Optimization of Distribution Network Incorporating Distributed Generators: An Integrated Approach". In: *IEEE Transactions on Power Systems* 28.3 (2013), pp. 2421–2432. ISSN: 0885-8950. DOI: 10.1109/TPWRS.2013.2253564.

[67] Hen-Geul Yeh, Dennice F. Gayme, and Steven H. Low. "Adaptive VAR Control for Distribution Circuits With Photovoltaic Generators". In: *IEEE Transactions on Power Systems* 27.3 (2012), pp. 1656–1663. ISSN: 0885-8950. DOI: 10.1109/TPWRS.2012.2183151.

[68] Ulf Philipp Müller et al. "Integrated Techno-Economic Power System Planning of Transmission and Distribution Grids". In: *Energies* 12.11 (2019). DOI: 10.3390/en12112091. URL: https://www.mdpi.com/1996-1073/12/11/2091.

[69] Benjamin Bayer et al. "The German experience with integrating photovoltaic systems into the low-voltage grids". In: *Renewable Energy* 119 (2018), pp. 129–141. ISSN: 09601481. DOI: 10.1016/j.renene.2017.11.045. URL: https://www.sciencedirect.com/science/article/pii/S0960148117311461.

[70] Zhifang Yang et al. "Optimal power flow based on successive linear approximation of power flow equations". In: *IET Generation, Transmission & Distribution* 10.14 (2016), pp. 3654–3662. DOI: 10.1049/iet-gtd.2016.0547.

[71] Forum Netztechnik/Netzbetrieb im VDE. "Voltage Regulating Distribution Transformer (VRDT) – Use in Grid Planning and Operation: English Translation". In: (2016). URL: https://www.vde.com/resource/blob/1570326/c4c73c2670f47f82071b81eab368b85e/hinweis--ront--download-englisch-data.pdf.

[72] Oytun Babacan, William Torre, and Jan Kleissl. "Siting and sizing of distributed energy storage to mitigate voltage impact by solar PV in distribution systems". In: *Solar Energy* 146 (2017), pp. 199–208. ISSN: 0038-092X. DOI: 10.1016/j.solener.2017.02.047. URL: https://www.sciencedirect.com/science/article/pii/S0038092X17301494.

[73] Holger Ruf. "Limitations for the feed-in power of residential photovoltaic systems in Germany – An overview of the regulatory framework". In: *Solar Energy* 159 (2018), pp. 588–600. ISSN: 0038-092X. DOI: 10.1016/j.solener.2017.10.072.

[74] Maximilian Arnold. "Planungsgrundsätze für Niederspannungsnetze unter Berücksichtigung regelbarer Ortsnetztransformatoren (Planning principles for low-voltage networks considering controllable local network transformers)". Doctoral thesis. Technische Universität Kaiserslautern, 2019. URL: http://nbn-resolving.de/urn:nbn:de:hbz:386-kluedo-55056.

[75] Georg Kerber. *Empfehlung zur Richtlinie zum Anschluss von Erzeugungsanlagen an das Niederspannungsnetz (Recommendation on the guideline for connecting generation plants to the low-voltage grid)*. 2009. URL: https://mediatum.ub.tum.de/doc/683667/683667.pdf.

[76] Gerrit Schlömer. *Planung von optimierten Niederspannungsnetzen: Dissertation*. 2017.

[77] ENTSO-E. *Survey on Ancillary Services Procurement and Electricity Balancing Market Design*. 2016. URL: https://docstore.entsoe.eu/publications/market-reports/ancillary-services-survey/Pages/default.aspx.

[78] Sandra Enkhardt. *EnSiG amendment: Abolition of the 70 percent regulation for new photovoltaic systems up to 25 kilowatts brought forward - small existing systems from 1 January 2023 also without restriction - larger ones only with smart meters (de: EnSiG-Novelle: Abschaffung der 70-Prozent-Regelung für neue Photovoltaik-Anlagen bis 25 Kilowatt vorgezogen – kleine Bestandsanlagen ab 1. Januar 2023 ebenfalls ohne Beschränkung – größere nur mit Smart Meter)*. 2022. URL: https://www.pv-magazine.de/2022/10/11/ensig-novelle-abschaffung-der-70-prozent-regelung-fuer-neue-photovoltaik-anlagen-bis-25-kilowatt-vorgezogen-kleine-bestandsanlagen-ab-1-januar-2023-ebenfalls-ohne-beschraenkung-g/.

[79] German Federal Network Agency. *Discussion paper: Reactive power supply for the grid operation: de: Diskussonspapier - Blindleistungsbereitstellung für den Netzbetrieb*. 2018. URL: https://www.bundesnetzagentur.de/SharedDocs/Downloads/DE/Sachgebiete/Energie/Unternehmen_Institutionen/NetzentwicklungUndSmartGrid/SmartGrid/Blindleistungspapier.pdf.

[80] Adolf Schwab, ed. *Elektroenergiesysteme: Erzeugung, Transport, Übertragung und Verteilung elektrischer Energie*. Berlin, Heidelberg: Springer Berlin Heidelberg, 2009. ISBN: 978-3-540-92227-8.

[81] Bundesnetzagentur. *Verlustenergie (de: Loss energy)*. URL: https://www.bundesnetzagentur.de/DE/Beschlusskammern/BK08/BK8_05_EOG/52_Kostenpruefung/522_Verlustenergie/BK8_Verlustenergie.html.

[82] German Federal Network Agency. *Decision in the determination procedure for the integration of controllable consumption devices and controllable grid connections in accordance with Section 14a of the Energy Industry Act (EnWG) (de: Beschluss in dem Festlegungsverfahren zur Integration von steuerbaren Verbrauchseinrichtungen und steuerbaren Netzanschlüssen nach § 14a Energiewirtschaftsgesetz (EnWG))*. 27.11.2023. URL: https://www.bundesnetzagentur.de/DE/Beschlusskammern/1_GZ/BK6-GZ/2022/BK6-22-300/Beschluss/BK6-22-300_Beschluss_20231127.pdf.

[83] German Federal Network Agency. *Determination of network charges for the application of network-oriented control of controllable consumption devices and controllable grid connections in accordance with § 14a EnWG as per specification of BK6-22-300 (de: Festlegung zu Netzentgelten bei Anwendung der netzorientierten Steuerung von steuerbaren Verbrauchseinrichtungen und steuerbaren Netzanschlüssen nach § 14a EnWG*

gem. Festlegung BK6-22-300). 2023. URL: https://www.bundesnetzagentur.de/DE/Beschlusskammern/BK08/BK8_06_Netzentgelte/68_%C2%A7%2014a%20EnWG/Downloads/BK8-22-010-A_Eckpunktepapier_zweite_Kons.pdf.

[84] Leon Thurner et al. "Pandapower—An Open-Source Python Tool for Convenient Modeling, Analysis, and Optimization of Electric Power Systems". In: *IEEE Transactions on Power Systems* 33.6 (2018), pp. 6510–6521. ISSN: 0885-8950. DOI: 10.1109/TPWRS.2018.2829021.

[85] Wided Medjroubi et al. "Open Data in Power Grid Modelling: New Approaches Towards Transparent Grid Models". In: *Energy Reports* 3 (2017), pp. 14–21. ISSN: 2352-4847. DOI: 10.1016/j.egyr.2016.12.001. URL: https://www.sciencedirect.com/science/article/pii/S2352484716300877.

[86] Georg Kerber. "Aufnahmefähigkeit von Niederspannungsverteilnetzen für die Einspeisung aus Photovoltaikkleinanlagen (Intake capacity of low-voltage distribution networks for feed-in from small photovoltaic systems)". Dissertation. München: Technische Universität München, 2011. URL: https://mediatum.ub.tum.de/doc/998003/998003.pdf.

[87] Joerg Dickert, Max Domagk, and Peter Schegner. "Benchmark low voltage distribution networks based on cluster analysis of actual grid properties". In: *2013 IEEE Grenoble Conference*. 2013, pp. 1–6. DOI: 10.1109/PTC.2013.6652250.

[88] Steffen Meinecke, Leon Thurner, and Martin Braun. "Review of Steady-State Electric Power Distribution System Datasets". In: *Energies* 13.18 (2020). DOI: 10.3390/en13184826. URL: https://www.mdpi.com/1996-1073/13/18/4826.

[89] Lukas Verheggen, Robert Ferdinand, and Albert Moser. "Planning of low voltage networks considering distributed generation and geographical constraints". In: *2016 IEEE International Energy Conference (ENERGYCON)*. 2016, pp. 1–6. DOI: 10.1109/ENERGYCON.2016.7514042.

[90] G. Schlömer, C. Blaufuß, and L. Hofmann. "Modelling of Low-Voltage Grids with the Help of Open Data". In: *NEIS Conference 2016*. Ed. by Detlef Schulz. Wiesbaden: Springer Fachmedien Wiesbaden, 2017, pp. 21–25. ISBN: 978-3-658-15029-7.

[91] Markus Sigismund. *RegioStaR - Regional Statistical Spatial Typology for Mobility and Transport Research*. URL: https://bmdv.bund.de/SharedDocs/DE/Anlage/G/regiostar-raumtypologie-englisch.pdf.

[92] Filip Biljecki, Hugo Ledoux, and Jantien E. Stoter. "An improved LOD specification for 3D building models". In: *Comput. Environ. Urban Syst.* 59 (2016), pp. 25–37. DOI: 10.1016/j.compenvurbsys.2016.04.005.

[93] Ivalin Petkov et al. "MANGOret: An optimization framework for the long-term investment planning of building multi-energy system and envelope retrofits". In: *Applied Energy* 314 (2022), p. 118901. ISSN: 03062619. DOI: 10.1016/j.apenergy.2022.118901. URL: https://www.sciencedirect.com/science/article/pii/S0306261922003269.

[94] German Weather Service. *Locally accurate test reference years from Germany for average, extreme and future weather conditions (de: Ortsgenaue Testreferenzjahre von Deutschland für mittlere, extreme und zukünftige Witterungsverhältnisse): Manual*. 2017. URL: https://www.bbsr.bund.de/BBSR/DE/forschung/programme/zb/Auftragsforschung/5EnergieKlimaBauen/2013/testreferenzjahre/try-handbuch.pdf.

[95] Stefan Pfenninger and Iain Staffell. "Long-term patterns of European PV output using 30 years of validated hourly reanalysis and satellite data". In: *Energy* 114 (2016), pp. 1251–1265. ISSN: 03605442. DOI: 10.1016/j.energy.2016.08.060. URL: https://www.sciencedirect.com/science/article/pii/S0360544216311744.

[96] Thomas Huld et al. "Mapping the performance of PV modules, effects of module type and data averaging". In: *Solar Energy* 84.2 (2010), pp. 324–338. ISSN: 0038-092X. DOI: 10.1016/j.solener.2009.12.002. URL: https://www.sciencedirect.com/science/article/pii/S0038092X0900293X.

[97] David Fischer et al. "Model-based flexibility assessment of a residential heat pump pool". In: *Energy* 118 (2017), pp. 853–864. ISSN: 03605442. DOI: 10.1016/j.energy.2016.10.111. URL: https://www.sciencedirect.com/science/article/pii/S0360544216315572.

[98] Bernhard Hasche Christian Nabe et al. *Potentials of the heat pump for load management in electricity and for grid integration of renewable energies (de: Potenziale der Wärmepumpe zum Lastmanagement im Strom und zur Netzintegration erneuerbarer Energien)*. 2011. URL: https://www.clearingstelle-eeg-kwkg.de/sites/default/files/ecofys_2011_potenziale_der_waermepumpe_zum_lastmanagement_im_strom_und_zur_netzintegration_0.pdf.

[99] Danny Günther et al. *Heat pump monitor- Field measurements of heat pump systems (de: "HP Monitor" Feldmessung von Wärmepumpenanlagen)*. 2014.

[100] German Environmental Agency. *UBA statement - Energy saving in water heating - Compatibility of energy saving and hygiene requirements for drinking water (de: Stellungnahme des UBA - Energiesparen bei der Warmwasserbereitung – Vereinbarkeit von Energieeinsparung und Hygieneanforderungen an Trinkwasser)*. 2011. URL: https://www.umweltbundesamt.de/sites/default/files/medien/419/dokumente/warmwasserbereitung_energiesparen_stellungnahme_uba.pdf.

[101] Christoph Vogt. *Analysis of the influence of smart metering on the electricity demand of private households (de: Analyse des Einfluss von Smart-Metering auf den Strombedarf von privaten Haushalten)*. Diploma thesis, 2011.

[102] Ralph Bitterer. *Representative VDEW load profiles (de: Repräsentative VDEW-Lastprofile)*. 1999. URL: https://www.bdew.de/media/documents/1999_Repraesentative-VDEW-Lastprofile.pdf.

[103] Bernhard Wille-Haussmann et al. "synGHD - Synthetic load profiles for an efficient supply planning for non-residential buildings (de: synGHD - Synthetische Lastprofile für eine Effiziente Versorgungsplanung für nicht-Wohngebäude): Project report". In: (). URL: https://edocs.tib.eu/files/e01fb20/1737777061.pdf.

[104] German Federal Office of Statistics. *Structure of the Classification of Economic Activities, 2008 edition (de: Gliederung der Klassifikation der Wirtschaftszweige, Ausgabe 2008): WZ 2008*. 2008. URL: https://www.destatis.de/DE/Methoden/Klassifikationen/Gueter-Wirtschaftsklassifikationen/Downloads/gliederung-klassifikation-wz-3100130089004.pdf.

[105] Jackson Hannagan et al. "The Impact of Household Appliances and Devices: Consider Their Reactive Power and Power Factors". In: *Sustainability* 15.1 (2023). ISSN: 2071-1050. DOI: 10.3390/su15010158. URL: https://www.mdpi.com/2071-1050/15/1/158.

[106] Christos G. Kaloudas et al. "Assessing the Future Trends of Reactive Power Demand of Distribution Networks". In: *IEEE Transactions on Power Systems* 32.6 (2017), pp. 4278–4288. ISSN: 0885-8950. DOI: 10.1109/TPWRS.2017.2665562.

[107] Carlos Gaete-Morales et al. "An open tool for creating battery-electric vehicle time series from empirical data, emobpy". In: *Scientific Data* 8.1 (2021), p. 152. ISSN: 2052-4463. DOI: 10.1038/s41597-021-00932-9.

[108] Claudia Nobis and Tobias Kuhnimhof. *Mobility in Germany - MiD result report (de: Mobilität in Deutschland - MiD Ergebnisbericht): (de: Studie von infas, DLR, IVT und infas 360 im Auftrag des Bundesministers für Verkehr und digitale Infrastruktur (FE-Nr. 70.904/15))*. 2018. URL: https://www.mobilitaet-in-deutschland.de/archive/pdf/MiD2017_Ergebnisbericht.pdf.

[109] OECD. *OECD Labour Force Statistics 2018*. 2018. DOI: 10.1787/oecd_lfs-2018-en. URL: https://www.oecd-ilibrary.org/content/publication/oecd_lfs-2018-en.

[110] Öko-Institut. "eMobil 2050: Szenarien zum möglichen Beitrag des elektrischen Verkehrs zum langfristigen Klimaschutz". In: (2014). URL: https://www.oeko.de/oekodoc/2114/2014-670-de.pdf.

[111] Arno Dentel and Udo Dietrich. *Thermal comfort in buildings (Thermische Behaglichkeit - Komfort in Gebäuden)*. 2006. URL: https://rom-umwelt-stiftung.de/wp-content/uploads/2006/02/Dokumentation_Thermische_Behaglichkeit.pdf.

[112] de: Bundesregierung Deutschland. *Measures to save energy (de: Maßnahmen zum Energiesparen): Ensuring energy supply (de: Energieversorgung sichern)*. 2023. URL: https://www.bundesregierung.de/breg-de/schwerpunkte/klimaschutz/energiesparmassnahmen-2078224.

[113] Workplace Safety Commissions of the German Federal Ministry of Labour and Social Affairs. *Technical rules for Workplaces (de: Technische Regeln für Arbeitsstätten): Temperature (de: Temperatur)*. 2022. URL: https://www.baua.de/DE/Angebote/Rechtstexte-und-Technische-Regeln/Regelwerk/ASR/pdf/ASR-A3-5.pdf?__blob=publicationFile&v=5.

[114] Ulrike Jordan and Klaus Vajen. "DHWcalc: Program to generate domestic hot water profiles with statistical means for user defined conditions". In: *Proceedings ISES SOlar World Congress, Orlando*.

[115] E.ON Energie Deutschland. *Costs of a photovoltaic system in overview (de: Kosten einer Photovoltaikanlage im Überblick)*. URL: https://www.eon.de/de/pk/solar/photovoltaik-kosten.html.

[116] Bjarne Steffen. "Estimating the cost of capital for renewable energy projects". In: *Energy Economics* 88 (2020), p. 104783. ISSN: 0140-9883. DOI: 10.1016/j.eneco.2020.104783. URL: https://www.sciencedirect.com/science/article/pii/S0140988320301237.

[117] Max Peters et al. *Kommunale Wärmeplanung - Einführung in den Technikkatalog (Communal heat planning - Introduction to the technology catalogue)*. Ed. by KEA Klimaschutz- und Energieagentur Baden-Württemberg GmbH. Stuttgart, 2022. URL: https://www.kea-bw.de/waermewende/wissensportal/kommunale-waermeplanung/technikkatalog.

[118] Bosch. *Heat pump costs: you should expect this (de: Wärmepumpe Kosten: damit müssen Sie rechnen)*. URL: https://www.bosch-homecomfort.com/de/de/wohngebaeude/wissen/heizungsratgeber/waermepumpe/waermepumpe-kosten/.

[119] Quintel Intelligence. *Cost of Capital | Energy Transition Model*. URL: https://docs.energytransitionmodel.com/main/cost-wacc/.

[120] German Federal Ministry for digital and transport. *Öffentlich zugängliche Ladeinfrastruktur für Elektrofahrzeuge in Deutschland (Publicly available charging infrastructure for electric cars in Germany)*. 2022. URL: https://www.bmvi.de/SharedDocs/DE/Artikel/G/foerderrichtlinie-ladeinfrastruktur-elektrofahrzeuge.html.

[121] gruenes.haus. *Electricity storage costs: Prices for PV-storage in 2023 (de: Stromspeicher-Kosten: Preise für PV-Speicher in 2023)*. URL: https://gruenes.haus/stromspeicher-kosten-preise-pv-speicher/.

[122] Steffen Fattler, Jochen Conrad, and Anika Regett et al. *Dynamis Datenanhang – Dynamis – Dynamische und intersektorale Maßnahmenbewertung zur kosteneffizienten Dekarbonisierung des Energiesystems (Dynamic and intersectoral measure assesssment for cost efficient decarbonization of the energy system)*. 2019. URL: https://openaccess.ffe.de/10.34805/ffe-146-19/.

[123] Danish Energy Agency and Energinet. *Technology Data - Energy storage: Technology descriptions and projections for long-term energy system planning*. 2018. URL: https://ens.dk/sites/ens.dk/files/Analyser/technology_data_catalogue_for_energy_storage.pdf.

[124] German Federal Government. *Energy price brakes are entering into effect: Price caps for electricity, gas and heat*. 2022. URL: https://www.bundesregierung.de/breg-en/search/energy-price-brakes-2156430.

[125] Soner Candas et al. "Optimization-based framework for low-voltage grid reinforcement assessment under various levels of flexibility and coordination". In: *Applied Energy* 343 (2023), p. 121147. ISSN: 03062619. DOI: 10.1016/j.apenergy.2023.121147. URL: https://www.sciencedirect.com/science/article/pii/S0306261923005111.

[126] E.ON Group. *Facts & Figures 2018*. 2018. URL: https://www.eon.com/content/dam/eon/eon-com/investors/presentations/facts-and-figures-2018.pdf.

[127] Florian Tobias Samweber. "Systematischer Vergleich Netzoptimierender Maßnahmen zur Integration elektrischer Wärmeerzeuger und Fahrzeuge in Niederspannungsnetze (Systematic Comparison of Network Optimization Measures for the Integration of Electric Heat Generators and Vehicles into Low-Voltage Networks)". Dissertation. München: Technische Universität München, 2018. URL: https://mediatum.ub.tum.de/doc/1379767/1379767.pdf.

[128] Sophie Ballaschk et al. *dena Building Report (de: dena Gebäudereport 2023)*. Ed. by de: Deutsche Energie-Agentur GmbH (dena). 2022. URL: https://www.dena.de/fileadmin/dena/Publikationen/PDFs/2022/dena_Gebaeudereport_2023.pdf.

[129] Simone Rubbert, Matthias Terschüren, and E.ON Energie Deutschland. *Consultation of the Federal Network Agency: Financial incentives regarding the determination of the Section 14 of the Energy Industry Act (de: BNetzA-Anhörung: Wirtschaftliche Anreize i.R. der Festlegung zu §14a EnWG)*. 16. March 2023. URL: https://www.bundesnetzagentur.de/DE/Beschlusskammern/BK08/BK8_06_Netzentgelte/68_%C2%A7%2014a%20EnWG/Downloads/BK8-22-0010-A%20_Vortrag_EON_Energie_Deutschland.pdf.

[130] German Federal Network Agency. *Information for electrical distribution grid operators regarding adjustments to revenue limits and formation of network tariffs for year 2022 (Hinweise für Verteilernetzbetreiber Elektrizität zur Anpassung der Erlösobergrenze und zur Bildung der Netzentgelte für das Kalenderjahr 2022)*. 2021. URL: https://www.bundesnetzagentur.de/DE/Beschlusskammern/BK08/BK8_04_InfoRundschr/42_Hinweise/Download/BK8_Hinweis%20EOG%202022.pdf.

[131] Stadtwerke Forchheim GmbH. *Tariffs for grid access (de: Entgelte für den Netzzugang): Price sheet 2: points of withdrawal without power measurement (de: Preisblatt 2: Entnahmestellen ohne Leistungsmessung)*. URL: https://www.stadtwerke-forchheim.de/fileadmin/public/pdf/pflichtveroeffentlichungen/strom/netzentgelte/Entgelte_fuer_die_Netznutzung_gueltig_ab_01.01.2022.pdf.

[132] Sebastian Gottwalt et al. "Demand side management—A simulation of household behavior under variable prices". In: *Energy Policy* 39.12 (2011), pp. 8163–8174. ISSN: 0301-4215. DOI: 10.1016/j.enpol.2011.10.016. URL: https://www.sciencedirect.com/science/article/pii/S0301421511008007.

[133] Matthias Kühnbach, Judith Stute, and Anna-Lena Klingler. "Impacts of avalanche effects of price-optimized electric vehicle charging - Does demand response make it worse?" In: *Energy Strategy Reviews* 34 (2021), p. 100608. ISSN: 2211-467X. DOI: 10.1016/j.esr.2020.100608. URL: https://www.sciencedirect.com/science/article/pii/S2211467X20301619.

[134] Maximilian Hoffmann, Leander Kotzur, and Detlef Stolten. "The Pareto-optimal temporal aggregation of energy system models". In: *Applied Energy* 315 (2022), p. 119029. ISSN: 03062619. DOI: 10.1016/j.apenergy.2022.119029. URL: https://www.sciencedirect.com/science/article/pii/S0306261922004342.

[135] Dominik Keiner et al. "Seasonal hydrogen storage for residential on- and off-grid solar photovoltaics prosumer applications: Revolutionary solution or niche market for the energy transition until 2050?" In: *Applied Energy* 340 (2023), p. 121009.

ISSN: 03062619. DOI: 10.1016/j.apenergy.2023.121009. URL: https://www.sciencedirect.com/science/article/pii/S0306261923003732.

[136] Leander Kotzur et al. "Impact of different time series aggregation methods on optimal energy system design". In: *Renewable Energy* 117 (2018), pp. 474–487. ISSN: 09601481. DOI: 10.1016/j.renene.2017.10.017. URL: https://www.sciencedirect.com/science/article/pii/S0960148117309783.

[137] Maximilian Hoffmann et al. "A Review on Time Series Aggregation Methods for Energy System Models". In: *Energies* 13.3 (2020). DOI: 10.3390/en13030641. URL: https://www.mdpi.com/1996-1073/13/3/641.

[138] Maximilian Hoffmann et al. "Typical periods or typical time steps? A multi-model analysis to determine the optimal temporal aggregation for energy system models". In: *Applied Energy* 304 (2021), p. 117825. ISSN: 03062619. DOI: 10.1016/j.apenergy.2021.117825. URL: https://www.sciencedirect.com/science/article/pii/S0306261921011545.

[139] John Allison et al. "Assessing domestic heat storage requirements for energy flexibility over varying timescales". In: *Applied Thermal Engineering* 136 (2018), pp. 602–616. ISSN: 1359-4311. DOI: 10.1016/j.applthermaleng.2018.02.104. URL: https://www.sciencedirect.com/science/article/pii/S1359431117370825.

[140] Beneharo Reveron Baecker et al. "Generation of low-voltage synthetic grid data for energy system modeling with the pylovo tool". In: (2022).

[141] co2online. *Stromspiegel (de: Electricity Mirror)*. 2023. URL: https://www.stromspiegel.de/fileadmin/ssi/stromspiegel/Downloads/StromspiegelFlyer_2023_Web.pdf.

[142] Noah Pflugradt et al. "LoadProfileGenerator: An Agent-Based Behavior Simulation for Generating Residential Load Profiles". In: *Journal of Open Source Software* 7.71 (2022), p. 3574. DOI: 10.21105/joss.03574.

[143] Francesco Lombardi et al. "Generating high-resolution multi-energy load profiles for remote areas with an open-source stochastic model". In: *Energy* 177 (2019), pp. 433–444. ISSN: 03605442. DOI: 10.1016/j.energy.2019.04.097. URL: https://www.sciencedirect.com/science/article/pii/S0360544219307303.

[144] Gerwin Hoogsteen et al. "Generation of flexible domestic load profiles to evaluate demand side management approaches". In: *2016 IEEE International Energy Conference (ENERGYCON)*. IEEE, 2016, p. 1279. ISBN: 978-1-4673-8463-6. DOI: 10.1109/ENERGYCON.2016.7513873. URL: http://www.ieee-energycon2016.org/.

[145] Beneharo Reveron Baecker and Soner Candas. "Co-optimizing transmission and active distribution grids to assess demand-side flexibilities of a carbon-neutral German energy system". In: *Renewable and Sustainable Energy Reviews* 163 (2022), p. 112422. ISSN: 1364-0321. DOI: 10.1016/j.rser.2022.112422. URL: https://www.sciencedirect.com/science/article/pii/S136403212200329X.

[146] Soner Candas. *Potentials and challenges of decomposition methods in energy system modelling: Deep-dive report*. URL: https://extremos.ffe.de/pdf/Potentials%20and%20Challenges%20of%20Decomposition%20Methods%20in%20Energy%20System%20Modelling.pdf.

[147] Soner Candas, Kai Zhang, and Thomas Hamacher. "A Comparative Study of Benders Decomposition and ADMM for Decentralized Optimal Power Flow". In: *2020 IEEE Power & Energy Society Innovative Smart Grid Technologies Conference (ISGT)*. 2020, pp. 1–5. DOI: 10.1109/ISGT45199.2020.9087777.

[148] A.T.D. Perera et al. "Machine learning methods to assist energy system optimization". In: *Applied Energy* 243 (2019), pp. 191–205. ISSN: 03062619. DOI: 10.1016/j.apenergy.2019.03.202. URL: https://www.sciencedirect.com/science/article/pii/S030626191930618X.